Université de Toulouse

THÈSE

En vue de l'obtention du

DOCTORAT DE L'UNIVERSITÉ DE TOULOUSE

Délivré par :
Université Toulouse 3 Paul Sabatier (UT3 Paul Sabatier)

Cotutelle internationale avec :

Présentée et soutenue par :
Amanda GOUNOU

Le 27 Janvier 2011

Titre :
Etude des Processus Pilotant les Cycles Diurnes de la Mousson Ouest Africaine
-
The Driving Processes Behind the Diurnal Cycles of the West African Monsoon

---

École doctorale et discipline ou sp cialit :
ED SDU2E : Océan, Atmosphère et Surfaces Continentales

Unité de recherche :
CNRM-GAME (Météo-France - CNRS)

Directeur(s) de Thèse :

Françoise GUICHARD
Fleur COUVREUX

Rapporteurs :

Cyrille FLAMANT
Miguel GAERTNER

Autre(s) membre(s) du jury :

Serge CHAUZY
Jon PETCH
Jean-Luc REDELSPERGER
Christopher TAYLOR

Merci…

Je tiens à remercier tout particulièrement Françoise et Fleur, mes directrices de thèse, pour m’avoir offert la chance de faire cette thèse et pour avoir encadré mon travail tout au long de ces trois années. Leur disponibilité pour répondre à mes questions et leurs conseils avisés m’ont permis de progresser durant toute la durée de ce projet de recherche.

Je tiens également à remercier l'équipe du CEH de Wallingford pour m'avoir accueillie pendant trois mois. L'enthousiasme communicatif et les conseils de Chris, les aides en statistiques et informatiques de Phil et les pauses café avec Richard, Martin, Becky et les autres sympathiques thésards du CEH en ont fait une expérience très enrichissante et agréable!

Je remercie Serge Chauzy pour avoir accepter de présider mon jury de thèse, Cyrille Flamant et Miguel Gaertner pour leur travail de rapporteur, Chris Taylor, Jon Petch et Jean-Luc Redelsperger pour m’avoir fait l’honneur de participer à mon jury et pour leurs retours enrichissants sur mon travail de thèse.

Merci à Florence pour sa précieuse aide pour résoudre les problèmes informatiques et trouver des astuces bien pratiques ! Merci à l’équipe Meso-NH pour toutes leurs contributions qui m’ont permis de répondre rapidement à mes questions en termes de fonctionnement et debugage du modèle. Je remercie également Régine pour son accueil toujours souriant au secrétariat.

Je remercie également les membres de l’équipe Moana, pour l’expérience enrichissante qu’elle m’a fait vivre durant ces années. Merci pour les nombreuses discussions scientifiques et non scientifiques, vos conseils et encouragements! Merci à Cécile, Romain et Vanessa, pour avoir partagé le bureau 133 avec moi dans une atmosphère agréable ! Merci aussi à Abdoul, Aaron, Catherine, Chiel, Daphné, Dominique, Florent, Guylaine, Julien, Laurence, Mathieu, Manu, Philippe et l’équipe EUFAR.

Je tiens à remercier Laurent pour m’avoir conseillé et orienté vers le CNRM lors de mes recherches de sujet de thèse et Jean-Philippe pour m’avoir accueilli au sein de son équipe. Je remercie Robin, mon encadrant de stage de master, qui m'a fait découvrir les problématiques liées à la couche limite atmosphérique et m'a également donné le goût et l’envie de poursuivre dans la recherche.

Merci à mes amis pour m’avoir soutenue, encouragée et aussi permis que je me détendre même pendant les moments les plus difficiles de ma thèse ; un merci tout particulier à Stef, Jeff, Bob, Landry, Arnaud, Rémi, David, Laeti et Patou. Un grand merci à Antoine, pour son admirable soutien quotidien et pour les nombreux encouragements et la super motivation qu’il a su m’insuffler et à mes parents, pour leur aide et leur soutien tout au long de mes études.

Résumé étendu

Les travaux effectués lors de cette thèse s'inscrivent dans le cadre du programme international AMMA (Analyses Multidisciplinaires de la Mousson Africaine) qui a pour objectif d'améliorer la compréhension et la prévision de la Mousson de l'Afrique de l'Ouest (MAO). La MAO est un système complexe directement lié au déplacement vers le nord de la zone de convergence intertropicale pendant l'été boréal. Au cours de cette période, le flux de mousson apporte de l'air frais et humide dans les basses couches de l'atmosphère jusqu'aux marges du Sahara. La convection continentale joue alors un rôle prépondérant dans le transport vertical d'humidité, l'ennuagement et la pluie. L'ensemble de ces processus présente des cycles diurnes marqués qui dépendent fortement du secteur géographique, de la saison et de la période de la mousson considérés. Ces cycles diurnes sont fortement influencés par l'hygrométrie et l'humidité du sol. Ces influences multiples laissent supposer des signatures dynamiques et thermodynamiques différentes pour des régimes atmosphériques secs, humides, précipitants et nuageux. Cependant les connaissances actuelles concernant les facteurs contrôlant ces cycles diurnes et leurs couplages restent qualitatives et partielles. Cette limitation se traduit en termes de modélisation par une représentation des cycles diurnes très approximative et entachée d'erreurs systématiques. Par conséquent, la compréhension du rôle du cycle diurne dans le phénomène de mousson reste à établir.

Ces travaux de thèse s'appuient sur l'analyse des données collectées lors des campagnes de mesures AMMA selon un transect méridien qui s'étend de la côte Guinéen jusqu'aux marges du Sahara et leurs mises en relation avec des résultats de simulation obtenus à partir d'un modèle couplé surface-atmosphère. Le but est d'améliorer la compréhension des processus liés au phénomène de mousson aux échelles diurnes et d'évaluer leurs représentations dans les modèles numériques.

Caractérisation des cycles diurnes

La première phase de cette étude s'est concentrée sur l'analyse d'observations, composées principalement de radiosondages documentant l'atmosphère avec une haute fréquence temporelle (8 par jour), de données de stations sol (météo et flux) et de produits satellites de suivis des systèmes convectifs.

Tout d'abord, l'analyse des mesures de flux de surface a permis de quantifier les bilans énergétiques à la surface le long du transect méridien. Bien que l'on observe un fort gradient méridien du rayonnement solaire reçu à la surface, le rayonnement net ne présente pas de variabilité notable en fonction de la latitude. Le fort gradient d'humidité du sol est responsable d'une redistribution de l'énergie de surface principalement sous forme de chaleur sensible au Nord et de chaleur latente au Sud.

Ensuite, l'analyse des données SYNOP et des radiosondages a permis de caractériser et quantifier les cycles diurnes à la surface et dans les basses couches atmosphériques. De forts contrastes sont observés le long du transect avant le début de la mousson, avec des amplitudes et des phasages différents suivant la latitude. Des différences notables ont été identifiées entre les cycles diurnes à la surface et dans les basses couches atmosphériques en liens avec des développements de couches limites particuliers selon la latitude.
Les comportements des couches limites convectives et nocturnes ont été étudiés via des diagnostics (hauteurs, stabilité, dynamique). On observe notamment des couches limites convectives allant de quelques centaines de mètres d'épaisseurs sur la Côte Guinéenne jusqu'à plus de 5km aux portes du Sahara. Ces développements différents en terme d'altitude sont associés à des propriétés thermodynamiques et dynamiques différentes sur le transect. Des structures nocturnes ont été également mise en évidence telles des couches limites nocturnes sont très fines et stables surmontées de couche résiduelle très peu stable (couche d'air saharien) dans le nord du Sahel et des couches limites nocturnes humides étonnamment mélangées (peu stables) ont été observées dans le sud du Sahel. Des jet nocturnes sont fréquemment observé sur la zone sud de l'ITD. Pendant, la phase active de la mousson, une diminution du rayonnement net à la surface est observée sur la portion sud du transect, en lien avec l'augmentation de l'ennuagement, et une augmentation sur le Sahel Central. L'apport d'humidité dans le sol par les systèmes convectifs au Sahel, augmente considérablement le flux de chaleur latente au détriment du flux de chaleur sensible. Les couches limites convectives sont fortement modifiées avec notamment une réduction drastique des hauteurs de couches limites convectives. Les couches limites nocturnes sont également affectées par l'arrivée de la mousson sur la zone Sahélienne, avec notamment une diminution de la fréquence d'occurrence des jets nocturnes. Des similarités observées entre les régimes des différentes stations le long du transect suivant la période ont permis de distinguer quatre régimes de fonctionnements différents.

Modélisation des cycles diurnes: évaluation des modèles et du rôle des processus

Dans un deuxième temps, un cadre de modélisation basé sur le modèle atmosphérique Méso-NH couplé au modèle de surface ISBA a été développé afin de pouvoir évaluer la capacité du modèle à simuler les cycles diurnes observés dans les quatre régimes identifiés à partir des observations. Les réanalyses ECMWF-AMMA et les résultats de simulations offline d'ISBA sont utilisés pour définir les conditions initiales et limites des simulations poursuivies sur dix jours. Ce cadre de modélisation, au delà de ces limitations, s'avère suffisamment proche des observations pour reproduire, au moins qualitativement, la variabilité synoptique observée. Ces simulations ont permis de mettre en évidence les points forts ainsi que les faiblesses du modèle dans des régimes très contrastés. Dans des conditions sèches où les couches limites convectives sont très développées et surmontées de couches atmosphériques complexes très peu stables, le schéma de turbulence du modèle présente des difficultés dans la conservation des structures délicates séparant la couche limite et la couche d'air Saharien qui la surplombe, la prise en compte des aérosols pouvant également jouer un rôle. Une autre raison semble provenir de la sous-estimation des advections d'air frais et humide notamment lors des pulsations de mousson. Le développement trop important de la couche limite

atmosphérique mène à un assèchement et à un chauffage trop important des basses couches atmosphériques.
Pendant la phase de mousson au Sahel, lorsque l'atmosphère est humide et précipitante, le modèle reproduit trop approximativement le développement des couches limites diurnes. Les nuages non précipitants sont sous représentés par le modèle ce qui conduit à une surestimation du flux solaire incident à la surface. Cette surestimation se traduit par un flux sensible trop important. qui engendre des couches limites convectives trop développées et trop sèches, et ainsi inhibe le développement de convection profonde.
Ces résultats montrent globalement que la modélisation du cycle diurne sur les zones continentales ne se limite pas à un problème de paramétrisation de la convection, mais qu'elle fait également intervenir, suivant les régimes, des interactions complexes significatives entre processus et notamment entre la turbulence et le forçage radiatif des nuages. Ainsi, même si la couverture nuageuse est souvent moindre sur continent que sur océan, son impact sur le bilan énergétique à la surface s'avère probablement plus important sur continent aux échelles de temps diurnes considérées ici.

Liens entre humidité du sol et déclenchement de convection diurne

L'analyse des observations montre une variabilité des basses couches atmosphériques particulièrement forte pendant la journée, qui correspond également à la période privilégiée d'initiation de la convection nuageuse. Plusieurs études récentes suggèrent un couplage important entre l'humidité du sol et l'initiation de convection profonde en Afrique de l'Ouest. Ainsi, dans le cadre de cette thèse, une collaboration a été établie avec une équipe du Centre d'Ecologie and Hydrologie (CEH) de Wallingford (Grande-Bretagne) pour étudier les liens entre l'humidité du sol et le déclenchement de convection profonde à l'échelle diurne à partir de produits satellites. Plus précisément, cette étude a ensuite montré, à l'aide de produits satellites complémentaires documentant la surface, que l'initiation de convection est plus fréquente sur des surfaces chaudes au Sahel en période de pré-mousson à l'échelle de 100km (Gounou et al. 2009). Cette étude repose sur l'utilisation conjointe d'ISIS et de produits de température de surface (LST, produits SEVIRI) et d'humidité du sol (AMSRE).
A plus fine échelle, il a été mis en évidence que ces initiations sont également plus fréquentes suivant des configurations spécifiques d'hétérogénéité de surface. La convection est alors initiée sur une surface chaude en amont d'un gradient de température de surface (suivant le vent de basses couches atmosphériques). Ces résultats suggèrent que l'initiation de la convection dans cette région fait intervenir des circulations de méso-échelle.

Abstract

This thesis work is devoted to the study of diurnal variations in the atmospheric low levels over the Sahel during the West African Monsoon (WAM) season. The AMMA (African Monsoon Multi-disciplinary Analysis) program provided an excellent opportunity to study the diurnal cycles of the WAM thanks to a unique set of measurements gathered during its campaign in 2006 (Redelsperger et al., 2006). In particular, high frequency radiosoundings (8 per day) and surface measurements were carried out during two special observing periods (SOP) (before and after the monsoon onset) at several sites along the meridional transect (from the Guinean coast (Cotonou) to the northern part of the Sahel (Agadez)).

A first part of this work is devoted to a detailed characterisation of atmospheric diurnal cycles based on the measurements made during the two SOPs. A quantification of diurnal cycles is made along the latitudinal transect and throughout the season. The study of dynamic and thermodynamic diurnal cycles at the surface as well as in the lower troposphere reveals very contrasted cycles in terms of amplitude and phasing along the meridional transect. Vertical structures of convective and nocturnal boundary layer are characterised via diagnostics (ie: height, atmospheric stability, monsoon flow thickness). Large contrasts in the structures along the transect are evidenced and quantified. Deep convective boundary layers develop in the Northern Sahel (more than 5km deep) whereas boundary layers remains very shallow on the Guinean coast (less than 500m). After the monsoon start, drastic changes in the dynamic and thermodynamic diurnal cycles are observed: convective boundary layers in the Northern Sahel collapse (1.5-2km deep), the diurnal cycles become closer together in terms of timing and amplitude. This characterisation allowed the distinction between four atmospheric regimes encountered during the WAM: (i) wet and heavily precipitating (ii) moist and cloudy, (iii) dry (iv) wet and cloudy.

A second part of this work focuses on the modelling of the diurnal cycles observed in the four identified atmospheric regimes. The modelling framework is based on a coupled surface-atmosphere model (Meso-NH-SURFEX). The AMMA data are used to initialise, constrain and evaluate the simulations. The modelling framework is idealised but realist enough for simulating the synoptic variability. Distinct strengths and weaknesses of the models are identified for the four atmospheric regimes of the WAM. In a cloudy but not precipitating Guinean monsoon regime, the model has difficulties to handle the stratiform cloud layer; it drifts towards a too cool and dry equilibrium state. In Soudanian monsoon regime, characterised by intense and frequent convective events, the model manages to simulate correctly the precipitation but drifts towards a too cool and dry state. In a Sahelian monsoon regime, daytime low-level cumulus clouds are underestimated, they do not interact strongly enough with the radiation scheme which leads to an overestimation of the surface fluxes. This induces a drift towards a too warm and dry equilibrium state. In the Sahelian dry regime, the turbulence scheme fails in representing the subtle vertical structures observed (a convective boundary layer capped by a slightly stable Sahelian air layer. To sum-up, these results have shown

that a correct modelling of the diurnal cycles over land needs an adequate behaviour of the convection scheme as well as the turbulence and radiation schemes.

The third part of this thesis investigates the links between surface properties and daytime storm initiations over the Sahel based on satellite measurements. Two different sets of satellite-based estimates of surfaces properties are used in this study; surface temperature (LST-MSG) and soil moisture (AMRS-E -AQUA). The daytime storm initiations data come from a convective tracking system (ISIS) which is then refined using a back-tracking method in order to locate more precisely the location of initiation. Combining surface properties with the storm initiations at the meso-scale (100x100km) indicates that storm initiations are favoured over dry soils (+13% more chances) especially during the moistening phase of the WAM and also over soils presenting more variability. The links between surface heterogeneities and storm initiations are also investigated at finer scale with LST estimates. The results suggest that storm initiations are more frequent over zones presenting a strong negative gradient along the wind direction. This corresponds to a warm to cold transition along the wind direction with the initiation located on the warm side of the transition. This study is extended using a 4-year dataset (more than 2000 storm initiations) which gives consistent results. This work provides an observationally based evidence of the links between surface heterogeneities and initiation of deep convection over the Sahel and more precisely, it suggests the importance of mesoscale circulations induced by surface heterogeneities on the triggering of deep convection.

Table of Contents

Chapter 3 Observation of diurnal cycles of the WAM

Chapter 4 Evaluation of Modelled Diurnal Cycles in the atmospheric low levels

Chapter 6 Conclusions and Perspectives

Chapter 1
Introduction

Le cycle diurne correspond à un mode de variabilité climatique qui est induit par les variations du rayonnement solaire sur 24 heures. Ces variations sont liées à la rotation de la Terre autour de son axe, la proportion jour/nuit dépendant de la latitude ainsi que de la saison. Ainsi, l'intensité du rayonnement solaire au sommet de l'atmosphère est maximum dans les Tropiques et diminue en allant vers les Pôles. Ce rayonnement solaire, particulièrement fort au niveau des Tropiques, confère au cycle diurne un rôle prépondérant dans la variabilité climatique de cette zone, l'amplitude des variations diurnes dominant nettement les variations saisonnières. Cette prépondérance s'illustre dans l'expression du climat Sahélien, comme le montre l'imagerie satellitaire qui met clairement en évidence un cycle diurne marqué dans la formation de nuages convectifs.

Ce climat Sahélien présente la particularité de connaître deux saisons annuelles: la saison sèche et la saison humide également appelée Mousson d'Afrique de l'Ouest (MAO) qui se caractérise par un renversement des vents. En effet, alors que pendant la saison sèche l’Harmattan souffle un air sec et chaud sur le Sahel, celui-ci est dominé et repoussé par des vents frais et humides, de sens contraire, provenant du golf de Guinée. Ainsi, la MAO apporte l'essentiel des précipitations sur le Sahel en seulement quelques épisodes pluvieux très intenses regroupés sur une courte période allant des mois de mai à octobre. Lors des dernières décennies, ces épisodes pluvieux se sont caractérisés par une très forte variabilité spatiale et temporelle qui ont vu un retard ou déclin dans les précipitations, selon les secteurs et les années considérées. Ces fluctuations significatives des précipitations reçues au Sahel ont pour conséquence d'importantes crises économiques et alimentaires, reliées à l’alimentation en eau des populations et de leurs cultures. Dans l’optique d’une anticipation et donc d’une meilleure gestion de ces crises Sahéliennes graves et chroniques, des programmes scientifiques ont été mis en place pour améliorer nos connaissances sur les mécanismes d'établissement et de fonctionnement de ce système climatique particulier d’Afrique de l’Ouest.

Cette thèse s'inscrit dans ce cadre et plus précisément dans celui du programme international AMMA (Analyses Multidisciplinaire de la Mousson Africaine). Ce programme a pour but d'améliorer les connaissances et la prévisibilité de la MAO. L’un des objectifs de ce volet consiste à bâtir et alimenter des outils d’aide à la décision et à la gestion des risques liés à la mousson, pour traiter plus particulièrement les enjeux liés à la gestion des ressources en eau ainsi qu'à la maîtrise des épidémies.

Ainsi, la campagne de mesure du programme AMMA a permis de recueillir une quantité d'observations très importante permettant notamment d'étudier le système couplé surface-atmosphère à l'échelle diurne. En effet, des périodes d'observation intensive ont été menées pendant les phases de pré-mousson et de mousson (radiosondages à haute fréquence temporelle, mesures météo et de flux de surface, …). Ces observations constituent une opportunité exceptionnelle pour étudier les cycles diurnes sur la totalité d’un transect méridien allant de Cotonou sur la côte Guinéenne jusqu'à Agadez dans le nord du Sahel et observer les évolutions spatiales et temporelles de la MAO.

Des travaux antérieurs laissaient supposer un impact fort du cycle diurne sur le fonctionnement et les modalités d'expression de la MAO. Le long d'un transect méridien allant de la côte Guinéenne jusqu'aux limites du Sahara, les basses couches atmosphériques sont caractérisées par des cycles diurnes très contrastés mais encore peu documentés. Leur représentation correcte dans les modèles numériques est nécessaire pour pouvoir obtenir une simulation correcte de l'évolution de la mousson sur le continent Africain. En effet, les basses couches atmosphériques, qui subissent les plus fortes variations diurnes, pilotent les gradients méridiens de température et d'humidité et conditionnent ainsi le flux de mousson qui apporte l'humidité sur le continent Africain. Pendant la nuit, un jet favorise la progression vers le nord du flux de mousson et ainsi alimente en humidité les basses couches atmosphériques du Sahel. Pendant la journée, cette humidité est redistribuée sur la verticale par mélange turbulent et convection sèche dans la couche limite convective. A l'échelle diurne, de nombreux processus physiques et dynamiques interagissent à fine échelle: le mélange turbulent, la convection profonde, le rayonnement… L'absence ou la mauvaise prise en compte de ces processus des basses couches peut induire un biais dans la représentation du système de mousson africaine par les modèles numériques à l'échelle diurne ainsi que sur des échelles de temps plus longues.

Aussi, cette thèse s'attache à étudier les cycles diurnes des basses couches atmosphériques observés dans le système de mousson. Elle a pour objectif premier de caractériser plus particulièrement les différents cycles dynamiques et thermodynamiques observés dans cette couche atmosphérique pendant la MOA. Il s'agit ici de mieux comprendre le fonctionnement de ces basses couches notamment les couches limites convectives et nocturnes, et d'identifier le rôle des différents processus régissant ces cycles diurnes. Les principales questions soulevées dans cette thèse sont les suivantes:

Quelles sont les amplitudes et phasages de ces cycles diurnes? Comment varient-ils le long du transect méridien avant et après l'établissement de la mousson? Comment le gradient méridien dans les basses couches atmosphériques est-il modulé sur un cycle diurne?

Quelle est la structure des couches limites atmosphériques observées? quels sont les processus qui pilotent leurs évolutions? Comment les cycles diurnes à la surface sont-ils reliés aux structures verticales des couches limites?

Plus particulièrement, au sein du cycle diurne, la convection profonde est-elle favorisée dans des environnements plus secs ou plus humides? Les hétérogénéités de surface liées aux fortes pluies convectives sur le Sahel, jouent-elles un rôle dans l'initiation de la convection profonde à fine échelle?

Comment les cycles diurnes observés sont-ils représentés dans les modèles numériques? Quels sont les points forts et les faiblesses des modèles suivant les régimes de temps? Comment les biais observés sur les différents régimes peuvent affecter le gradient méridien de température et d'humidité?

Les réponses de cette thèse apportées à ces questions s'organisent en quatre grandes parties. La première partie s'attache à établir un état de l'art approfondi dans le domaine de la connaissance des cycles diurnes, des basses couches atmosphériques et de leur représentation par les modèles.

La seconde phase de l'étude se concentre sur l'analyse d'observations, composées principalement de radiosondages documentant l'atmosphère avec une haute fréquence temporelle (8/jour), de données de stations sol (météo et flux) ainsi que de produits satellites. L'analyse des radiosondages, via des diagnostics, permet de caractériser les couches limites atmosphériques et d'établir une climatologie des différents cycles diurnes observés le long d'un transect méridien en régime de pré-mousson ainsi que pendant la phase de mousson établie.

Dans un troisième temps, un cadre de modélisation idéalisé basé sur le modèle atmosphérique Méso-NH couplé au modèle de surface ISBA a été développé afin de pouvoir évaluer la représentation des différents cycles diurnes et de les confronter aux observations. Il permet de mettre en évidence les points forts ainsi que les faiblesses du modèle dans différents régimes de temps, concernant notamment les représentations des cycles diurnes à la surface, des développements de couches limites atmosphériques, et des déclenchements de convection peu profonde et profonde.

Enfin, la quatrième partie de cette thèse porte sur l'étude plus particulière des couplages entre la surface et l'atmosphère à l'échelle diurne au Sahel. A partir de la combinaison de propriétés de surface avec des données d'initiation de la convection profonde (issues d'observations satellites), l'étude s'attache à mettre en évidence les liens entre les propriétés de la surface (humidité du sol et température de surface) et le développement de la convection profonde à méso-échelle ainsi qu'à des échelles spatiales de l'ordre de la dizaine de kilomètres.

Introduction

The diurnal cycle corresponds to an important mode of climatic variability. It is mainly driven by fluctuations in solar radiation over 24 hours. These variations are linked to the rotational movement of the Earth around its axis. Therefore, the partition between night and day depends on the latitude and season. The solar radiation intensity at the top of the atmosphere is maximised above the Tropics and decreases when moving towards the Poles. In the Tropics, the diurnal cycle is a dominant mode of variability as often, the amplitude of diurnal variations are larger than seasonal variations. This fundamental mode of variability can be clearly observed with the satellite imagery over West Africa where it shapes the timing of convection (Yang and Slingo 2001, Nesbitt and Zipser 2003) which typically displays a strong daytime development. (Slingo et al. 2004, Mohr 2004).

During the course of the year, the West African climate typically experiences two distinct regimes: a dry season and a monsoon season also called the West African Monsoon (WAM) season. This season is characterised by a low-level wind reversal. Indeed, moist and cool winds originating from the Guinean Gulf propagate into the continent and push northwards the established Harmattan which is a dry and warm flow originating from the Saharian region. The boundary between these two air masses is called the Inter-Tropical Discontinuity (ITD). The WAM brings almost all the annual precipitation over the Sahel within only a few months, from June to September. During the past decades, the Sahel experienced a strong decline in precipitation (e.g. Hulme 2001) which led to important economical and humanitarian crisis. Scientific programs were recently organised in order to improve the understanding of the fundamental mechanisms controlling the establishment and the functioning of the WAM.

This thesis work was carried out within the frame of an international program called African Monsoon Multidisciplinary Analyses (AMMA) that was launched in 2004. This program has for main objectives to broaden the knowledge and improve the predictability of the WAM (Redelsperger et al., 2006). Another important goal of this program is to promote the integration of scientific findings into the operational forecasts, decision making and crisis management linked to the WAM activity.

The AMMA program incorporates an important observational campaign which includes several special observing periods carried out in 2006. The AMMA dataset combines a large variety of ground-based, airborne and satellite measurements at multi-spatial and temporal scale. This unprecedented amount of observations allowed in particular to study the coupled surface-atmosphere WAM system at the diurnal time scale from an observationally based perspective. Intensive observing periods were dedicated to the acquisition of observations at high temporal frequency (e.g. radiosoundings launched every 3 hours, surface-flux measurements, radar observations etc..). This provides a unique opportunity to study the diurnal cycles along a latitudinal transect going from the Guinean coast up to the Northern part of the Sahel at different key stages of the WAM; before and after the monsoon start.

Recent studies suggest that the diurnal cycle is an important mode of variability of the WAM system (Parker et al. 2005, Peyrillé and Lafore 2007, Lothon et al. 2008). Along the meridional transect, a strong gradient of climatic properties is observed from the densely vegetated Guinean coast up the limits of the Sahara desert. It is expected to display contrasted diurnal modulations. However, due to the scarcity of observations, our knowledge on this mode of variability remains poor and need to be characterised and studied further. The improvements of our knowledge on the diurnal cycle of atmospheric processes and of their representation into numerical models are likely to result into an improvement of the numerical simulations of the WAM system. Indeed, the atmospheric low levels experience the largest diurnal variations and are important in determining the meridional gradients of temperature and humidity which are known to be of significance to the WAM (e.g. Eltahir and Gong 1996). These gradients partly drive the propagation of the monsoon flow. During nighttime, a nocturnal jet accelerates in the atmospheric low levels favouring the northward propagation of the water vapour into the continent. By contrast, during daytime, water vapour is transported vertically upwards by boundary-layer convective processes. Along the meridional West African transect, one may find distinct diurnal atmospheric regimes which are not well documented. Furthermore, the thermodynamics of the low levels is the main driver of convective instability (Williams and Reno, 1993; Guichard et al, 2008; Koehler et al., 2010). At diurnal timescales, numerous physical and dynamical processes interact in the low levels. The characteristics of the atmospheric boundary layers and the specific features of deep convection involve these strong interactions.

This PhD thesis focuses on the diurnal cycles in the atmospheric low levels during the West African Monsoon. The objectives are to characterise and quantify the thermodynamic and dynamic diurnal cycles observed along the west African meridional transect before the WAM establishment and during the full monsoon period. The main goal is to better understand the mechanisms and physical processes involved in the diurnal cycles and more globally in the functioning of the WAM system and assess their modelling. The main questions addressed in this thesis are:

What are the main characteristics of the atmospheric diurnal cycles along the meridional transect? What are their amplitude and timing? Do they exhibit seasonal variations? Which processes are important in their evolution?

At diurnal time scales, what are the links between surface properties and the triggering of deep convection at mesoscale? Does convection preferentially triggered over dry or wet soil or neither? Do surface heterogeneities play a role on the initiation of convection in the Sahel at fine spatial scale?

How well do numerical models perform in simulating the diurnal cycles? What are the main strengths and weaknesses of the models? Do they perform differently for the distinct regimes observed?

This PhD thesis is organised into four main chapters. The first section (Chapter 2) consists in an overview of the relevant literature on the subject. It includes (i) a brief description of the WAM system, (ii) the main characteristics of the diurnal cycles over land, (iii) a discussion on the current numerical modelling of the diurnal cycles and (iv) a review of past studies on the interactions between the surface and the atmosphere.

The third chapter is dedicated to the analysis of observations made during the AMMA campaign. It makes use of a high-frequency radiosoundings, flux measurements, satellite and radars images to characterise and quantify the observed diurnal cycles in the atmospheric low levels along the meridional transect. The study focuses on two key stages of the WAM (before and after the monsoon onset). Diagnostics characterizing boundary layers, atmospheric stability are defined and applied in order to quantify these diurnal evolutions.

Then, chapter 4 focuses on numerical simulations of the observed diurnal cycles along a climatological transect. A modelling framework is developed based on the atmospheric model Meso-NH coupled to the surface model ISBA. The objective of this section is to evaluate the representation of the atmospheric diurnal cycles by the model and to identify its weaknesses in the different regimes observed along the transect.

Finally, chapter 5 consists in a detailed examination of the links between surface properties and daytime initiation of deep convection over the Sahel. This is a study based on satellite measurements of surface temperature from Meteosat Second Generation and soil moisture estimates from AMSR-E. The convection initiation dataset is based in a first stage on a satellite convective tracking algorithm (Morel et Senesi, 2002). The ECMWF atmospheric analysis is used to document the local environment of the initiation dataset. Two length scales are considered. First, at the mesoscale (100kmx100km), a methodology is developed to investigate whether or not convective systems are triggered over surface displaying specific properties at this scale. Then, the links between deep convection and smaller-scale surface features, on the order of a few tens of km, are explored. Here, the analysis is conducted with some consideration of the low-level atmospheric flow.

Chapter 2
Literature Review

Contents

This chapter aims at providing an overview of the subjects and scientific issues which are central to my PhD work. It is organised as follows; First, an overview of the West African Monsoon system will be presented. Then, the major features of diurnal cycles over land will be discussed including the main mechanisms of boundary-layer developments and their characteristics observed in West Africa. The third section will be on the modelling of diurnal cycles and the difficulties associated with this. Finally, the last section will focus on the interactions between surface and atmosphere at the diurnal timescale.

2.1 The West African Monsoon

2.1.1 Geographical context and overview of the West African climate

West Africa is the westernmost region of the African continent. It includes 15 countries and a total area of 5 millions of square kilometres. It is a continental region in the Tropics characterised by sharp climatic contrasts between the humid tropical Guinean coast and the Saharan desert. West Africa can be divided into the four different climatic zones:

- The Guinean coast, which is the southern part of West Africa. The climate of this region is tropical humid. It is affected by the Inter-tropical Convergence Zone (ITCZ) which brings rains almost all year round (e.g.: Cotonou at 6.5°N has an average annual rainfall of 2000 mm/year).
- The Soudanian zone is a region located between 7°-10°N. It is predominantly savanna, or plains covered with a mixture of tropical or subtropical grasses and woodlands. The region receives less rain than on the Guinean coast and experiences a dry and a wet seasons (e.g. Parakou (9.8°N): 1200mm/year).
- The Sahelien region; this is a semi-arid region where the vegetation is sparse; it is also characterised by two well defined seasons, the dry and the wet seasons. During the dry season, the Harmattan, which is a northerly flow from the Sahara blows warm and dry air. During the wet season, convective systems bring almost the equivalent of mid-latitude annual rainfall in just four months (eg: Niamey(13.5°N): 500-600mm/year).
- The Saharian region; this is a desert arid and dusty region where dusts are uplifted into the atmosphere. This is the primary source of dusts worldwide. This region receives very little precipitation during the monsoon season (e.g.Agadez (16.5°N): 120-130mm/year).

The Atlantic Ocean forms its west and south borders and plays an important role in the climate. In particular, the waters of the Guinean Gulf interact through Sea Surface Temperatures (SST) and advection of cool and moist air. This is known to have a large impact on the West African Climate especially on the monsoon (Caniaux et al., 2010).

The region is characterised by relatively low orography except few mountain ranges like the Cameroon mountain range in the Southeast and the Hoggar in the Northeastern part. A strong meridional gradient of vegetation is observed over West Africa , as illustrated in Fig. 2-1 which shows a map of Normalised Difference Vegetation index (NDVI) [1]. The transect is characterised by progressive change in vegetation going from the equatorial densely vegetated coastal zone (high NDVI) to the bare soils of the Sahara desert region (low NDVI, with vegetation becoming increasingly sparse moving northwards).

[1] This is a numerical indicator derived from satellite measurements that can be used to assess whether the observed target is covered by live green vegetation or not. It is directly linked to the photosynthetic capacity. The NDVI is calculated from measurements of spectral reflectance in the red and the near infrared. It is expressed as follows:

$$NDVI = \frac{(NIR - RED)}{(NIR + RED)}$$

where RED is the reflectance in the red region and NIR in the near infrared region.

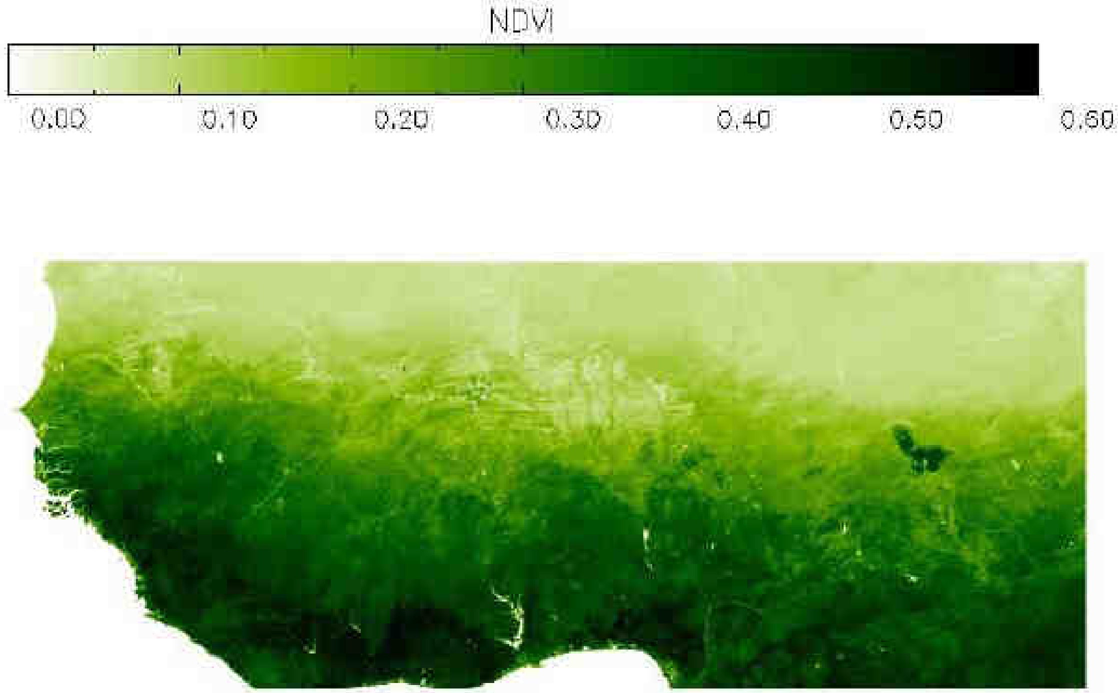

Figure 2-1 : NDVI (Normalised Difference Vegetation Index) derived from MODIS 2005 averaged over May to October. Densely vegetated canopies appear in dark green whereas deserts which have a low reflectance come out in very light green. Courtesy of Johanna Ramarohetra.

As everywhere on Earth, and more critically in the Sahel than in the Guinea region, the amount of rainwater, here brought by the monsoon system, is important to people's life. In this tropical region, rainfall rather than insolation is a major shaping factor for agriculture and breeding, which are the main economical resources in this region (Sultan et al., 2005). Late Springs and Summers are particularly critical periods in this respect. During the monsoon, rainfall can be suppressed for extended periods called dry spells. Such intraseasonal variability of rainfall can ruin crop yields (Banca et al., 2008).

During the second part of the 20th century, a decline in the monsoon activity has been observed in the Sahel corresponding to a strong deficit in rainfall amount (Nicholson, 1980), (Le Barbé et al., 2002; Hulme 1992). A reduction of about 25% of the annual rainfall was found in the 1968-1989 period compared to the 1950-1967 mean at Niamey (Lebel et al., 1995). An index called the Standardized Precipitation Index (SPI) was calculated in order to evaluate the evolution of the monsoon activity (Ali and Lebel, 2009). Figure 2-2 shows the evolution of this index over the 1905-2005 period. It highlights the dryness of the last 40 years compared to the mean over the century. Notably, it corresponds to the most important rainfall trend worldwide, the causes of which are not yet fully understood.

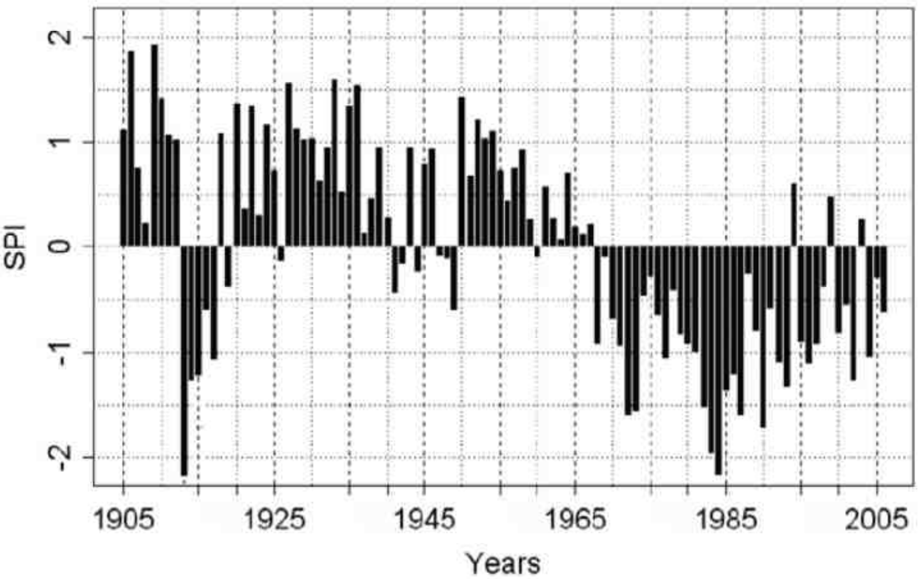

Figure 2-2 : Standardized Precipitation Index (SPI) for the Sahel between1905 and 2006. Index diagnosing whether the Sahelian region can be considered as wet or dry for a given year, it is computed from network rain gage measurements. Figure from Ali and Lebel (2009).

Different theories or hypothesis were proposed to explain this change in precipitation. At first, an important role of deforestation and land use was suggested by Charney (1975). This pioneer study highlights the fact that the land use modification and deforestation lead to an increase in surface albedo in the Sahel. The surface becomes more reflective to solar radiation and hence it reduces the net radiation at the surface. The loss of net radiation translates into less convective heating in the atmosphere, which is compensated by a subsiding air motion that dries up the atmosphere. This would correspond to a positive feedback leading to more desertification. Other studies suggest a more important role of vegetation changes in the Southern Soudanian region (Eltahir and Gong, 1996). These authors argue that they would play a role via their impact on the strength of the monsoon flow, they also emphasise the importance of the SST in the Guinean Gulf and the meridional gradients developing between the Gulf of Guinea and the Northern Sahel. Besides, increasing greenhouse gases in the atmosphere are possibly playing a role in the global augmentation of atmospheric temperature especially in sensitive regions like West Africa (IPCC report, 2007; Paeth et al., 2004, 2005). The climatic projections on the West African monsoon exhibits strong dispersion from one numerical model to the other. A large range of future projections of precipitation is found among the models. Some models forecast a reduction of precipitation in the next century, whereas some models project an increase of precipitation (Cook and Vizy, 2006).

These deficits in rainfall amount have lead to severe droughts causing agricultural, economical and human disasters. The West African societies rely almost solely on rainfall and surface water for agriculture and water resources. Therefore, they are very dependent upon monsoon activity. For example, between 1980 and 1990, a large percentage of cattle died, crops were devastated and rivers were almost dried, leading to widespread poverty. Sahelian floods have also regularly hit the headlines. Indeed, both dry spells and floods are frequent events in the Sahel. From a climatological perspective, numerous scientific reasons indicate the value of an advanced understanding of the West African climate. Moreover, the facts mentioned above also point to the significance of the societal and economical impacts on its fluctuations and evolutions.

Only a few scientific programs were dedicated to better understanding the Sahelian climate in the past. The ECLATS campaign took place in Niamey (Niger) in 1984 to observe and measure atmospheric boundary-layer characteristics (see section 2.2.2 for more details). The Hapex-Sahel program (Goutorbe et al., 1997) was carried out also in Niger to provide observations of the surface energy exchanges with the atmosphere. It aimed at improving the modelling and parameterisations of the surface-atmosphere interactions in the global circulation models. A few years later, the campaign JET2000 was organised to sample the characteristics of the main dynamical structure of the African Easterly Jet using aircraft measurements (Thorncroft et al., 2003).

2.1.2 The AMMA program

The dramatic changes in precipitation observed over the Sahel during the last decades of the 20^{th} century summarised above, as well as the large climatic projection uncertainties, were a major motivation of the AMMA (African Monsoon Multi-disciplinary Analysis) project (web site: http://www.amma-international.org). AMMA is an international program that was launched in 2002 in order to investigate possible mechanisms responsible for the rainfall decline over the West Africa (Redelsperger et al., 2006). It is a project funded in part by a large number of agencies, especially from France, Uk, US and Africa with a large contribution from the European Community. It involves researchers from more than 40 different organisations from Europe, Africa and North America.

The research program aims at studying the mechanisms involved in the monsoon system at different time and space scales. The main challenges are to improve weather and climate forecasts, to maintain environmental monitoring and better manage food security, water resources and public health.

The monsoon system involves interactions between the ocean, the land surface and the atmosphere. Studying these processes over a wide range of scales ranging from micro to global scale, will lead to a better understanding of the monsoon system. A number of issues are still not well understood, notably the mechanisms involved in the onset of the monsoon, its pauses and retreats. Factors involved in the triggering, maintenance and decay of convective systems are not well identified either. There are important efforts underway to strengthen our knowledge of the water cycle. This will help improve our understanding of the monsoon variability, from diurnal to seasonal time periods. It is known that aerosol optical thickness can be particularly high over the region. However, its precise role in the monsoon system has been largely unexplored. The AMMA program devotes a large part of its activities to investigate their role in more depth. Finally, the program aims at understanding the interactions between the monsoon and the global climate from a physical and a chemical perspective and will increase our confidence in the predicted climate changes over the Sahelian region.

The field campaign aimed at observing the atmosphere, the ocean and the surface at different space and time scales (Lebel et al., 2010). The Long term Observing Period (LOP) is concerned with observations of interannual to decadal variability of the WAM. It was operated from 2002 to 2010 over three main mesosites with enhanced measures of rainfall amounts and surface properties.

The Enhanced Observing Period (EOP) was operated from 2005 to 2007 and aimed at documenting the annual cycle of the surface and atmospheric conditions. Extra radiosoundings were launched along the meridional transect, enhanced surface measurements were carried out, ground-based instruments (radars, profilers) were operated at different sites. In addition, oceanic measurements were done on research vessels in the Gulf of Guinea.

The Special Observing Periods (SOP) were devoted to detailed observations of processes taking place at key stages of the WAM with high temporal and spatial resolutions. They were dedicated to the intensive observation of the meridional transect and a large range of instruments (radiosounding stations, flux stations) was deployed (see Fig. 2-3) . There were four SOPs:

- SOP-0 was assigned to the observations of aerosols during the dry season (January-February 2006).

- SOP-1 was carried out during the pre-monsoon/onset phase (15th May - 30th June 2006) to provide diurnal information on the atmospheric low-levels as well as the evolution of oceanic surface layer. This was designed to get enough information to investigate relationships between the regional circulations, and atmospheric /surface water budgets.

- SOP-2 occurred during the full monsoon period (1st July - 14th August 2006) to observe the interactions between the surface/ atmosphere and convective systems when the activity of the WAM is at its maximum.

- SOP-3 was dedicated to the observation of the late monsoon and its withdrawal (15th August-15th September 2006).

In this thesis, the measurements carried out during the SOP-1 (pre-monsoon) and SOP-2 (full monsoon) are explored and analysed for the study of processes driving the diurnal cycles of the monsoon.

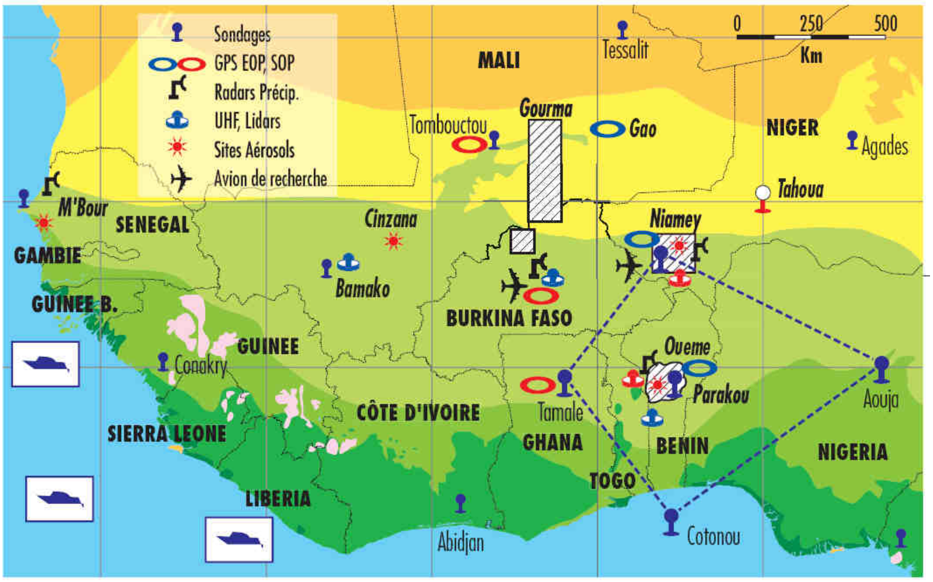

Figure 2-3 : Observing Strategy of the 2006 AMMA Campaign. Instrumentation was emphasized over the meridional transect going through Cotonou (6.5°N, 2.4°E), Parakou (9.4°N, 2.6°E), Niamey (13.5°N, 2.2°E) and Agadez (17°N, 8.0°E) and also over zonal transect via Tamale (9.5°N, 0.8°W) and Abuja (9.0°N, 7.1°E). Radiosoundings were launched at all these sites. Other instruments like radar, lidar, GPS stations were operated at different stations.

2.1.3 The Monsoon System

Monsoon is traditionally defined as a seasonal reversing of the low-level winds, together with important changes in precipitation. West Africa, Southern Asia and South America are the main regions of the world affected by monsoons, as illustrated in Fig. 2-4. The inclusion of other regions like Australia and North America is still a debate, as they do not exhibit a complete wind reversal. It is a phenomenon involving advection of low-level moisture onto the continental regions and generating strong convective systems. In these regions, there are two seasons, a dry season and a wet season corresponding to the monsoon season (Ramage, 1971).

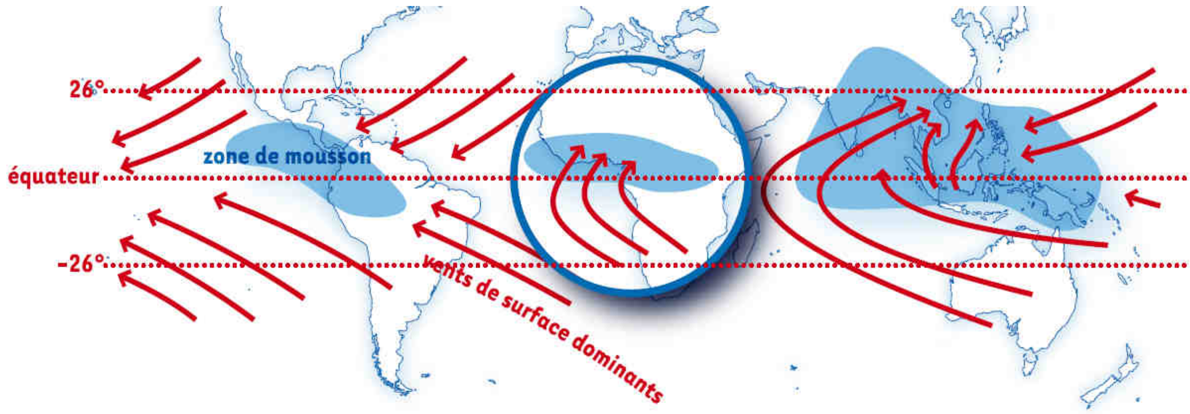

Figure 2-4 : Monsoon location and associated wind directions. Three different monsoons are observed: in South America, West Africa and Southern Asia. It is characterised by a wind reversal in the atmospheric low-levels. Figure from AMMA exhibition.

The African monsoon system is a coupled system involving strong interactions between the land surface, the atmosphere and the ocean. A reversal of the low-level winds from east-northerly to south-westerly announces the end of the dry season. Originating from the strong meridional gradient in temperature and humidity, a low-level flow called the monsoon flow goes from the Gulf of Guinea towards the continent and brings cool and moist air. The circulations associated with the monsoon system involve the monsoon flow as well as four major jets (3 zonal and one meridional jets) :

- The African Easterly Jet (AEJ) represented in yellow in Fig. 2-5, is located at around 700hPa (3-4km)), it is formed in response to the strong meridional gradient of moisture and temperature that creates baroclinicity (Burpee 1972, Thorncroft and Blackburn 1999). This jet is an important feature of the WAM system, as it helps organising the convection and participates in the self-sustained processes. As the monsoon season starts, this jet migrates northward until reaching its northernmost position, located at about 15°N in August.

- The Tropical Easterly Jet (TEJ) shown in green in Fig. 2-5 is located at around 200hPa (12-15km) (Nicholson et al., 2007). This jet is strongly linked to the Asian Monsoon circulation. It migrates during the monsoon season; it is centred around 0°N at the beginning of the monsoon and migrates towards 5-10°N. It extends from the South-East Asia to West Africa (Raman et al., 2009).
- The nocturnal low-level jet is confined in the lower troposphere (at about 300-400m) (not shown in Fig. 2-5, see also p24, 40). It forms in response to the meridional gradient of pressure, which develops between the Saharian heat low and the cooler Guinean coast. This jet accelerates the monsoon flow and hence favours the advection of moisture during night-time (Parker et al. 2005; Lothon et al. 2008; Bain et al 2010).
- The Sub-Tropical westerly Jet (STWJ) (in blue) is a high level jet (12- 15km) located at higher latitude (around 30°N).
-

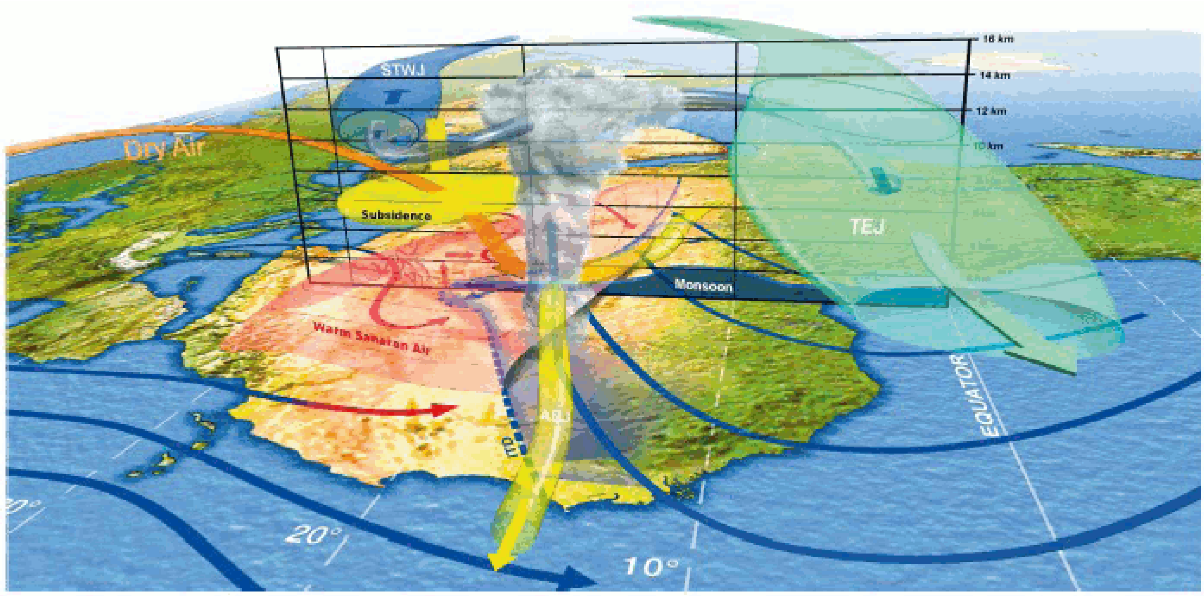

Figure 2-5 : Representation of the main components of the West African Monsoon. In the atmospheric low levels, the ITD (Inter-Tropical Discontinuity) (blue dotted line) is the boundary between the Harmattan flow (in red) and the monsoon flow (blue arrows). In mid-troposphere, the African Easterly Jet appears in yellow. In altitude, the Tropical Easterly Jet (TEJ) is in green, the Sub-Tropical Westerly Jet (STWJ) in blue. Figure from Lafore and Poulain (2010).

The WAM exhibits three main stages including a moistening period, a transition period when the convection ceases over the Soudanian zone, while it starts over the Sahelian region (onset) and the full monsoon period characterised by a strong convective activity over the Sahel. This evolution is illustrated in Fig. 2-6 with the evolution of water vapour mixing ratio (wvmr) at the ground in the Sahel (Niamey) during 2006. The moistening period lasts about 3 months (from May to mid-July) depending on the latitude (and the position of the ITD). The wet season is active until the end of September. Then, a drying period starts, but lasts only a few weeks.

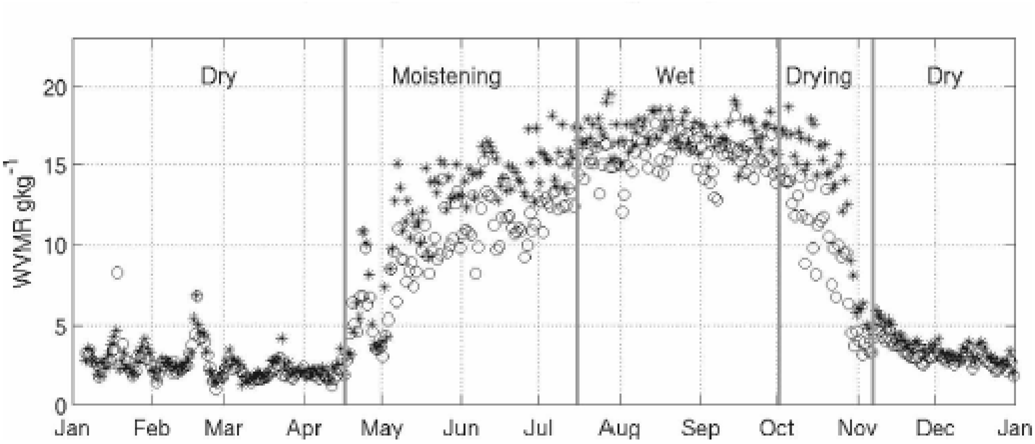

Figure 2-6 : Seasonal evolution of the Water Vapour Mixing Ratio (WVMR) observed at the ground at Niamey (13.5°N) in 2006, with nighttime average from 0000UTC to 0600UTC (asterisks) and daytime average from 1100UTC to 17UTC (circles) Figure from Lothon et al., 2008.

– ***Moistening processes prior to the onset:***

During the boreal summer, the maximum of insolation moves inland. The temperature over the Sahel increases, meanwhile, the temperature of the Gulf of Guinea decreases, due to upwelling of cooler water, which leads to an increase of the meridional gradient of temperature. This creates a northward circulation of moist and cool air called the monsoon flow. In opposite direction to this low-level wind, the previously established Harmattan winds blow warm and dry air from the Sahara towards the West-South/West. The boundary between these two opposite winds is called the Inter-Tropical Discontinuity (ITD) region (see Fig. 2-5). Located at about 10°N in April, it reaches 20°N in August. The moistening phase is a non linear phenomenon, which involves the interplay of atmospheric processes at different timescales:

-At the diurnal timescale: during night-time, water vapour is brought in the atmospheric low-levels by the monsoon flow. The nocturnal acceleration of the flow typically leads to a further northward extension of specific humidity in the lowest levels (e.g. Pospichal and Crewell, 2007). During daytime, specific humidity is redistributed vertically by convective processes within the boundary layer (see section 2.3.2)(Parker et al. 2005; Lothon et al. 2008). As a result, specific humidity can decrease substantially during daytime in the low levels and at the surface, the ITD can become more diffuse and can shift southward by as much as a few hundreds of kilometres. For the atmosphere as a whole in the Sahel, there is no such a clear diurnal cycle of the amount of water vapour during this period, as shown by precipitable water (Bock et al. 2008); this emphasizes the significant convective vertical mixing at that time. Precipitating convection can sometimes play a role in the humidification of the low-levels via rainfall evaporation and the subsequent enhancement of evapotranspiration following rain events in the early monsoon phase (Kohler et al. 2010).

- At the synoptic scale: pulsations of the monsoon flow responding to an enhancement of the Saharan Heat Low with periodicity of about 3-5 days (Couvreux et al., 2010). They are associated with an acceleration of the meridional flow. These pulsations drive strong fluctuations of precipitable water. However, there is no evidence of a progressive moistening of the atmosphere at larger scale when one considers time series of precipitable water.

– ***Onset of the Monsoon: Several Hypothesis***

The onset of the monsoon over the Sahel is defined as the abrupt shift of the ITCZ from 5°N to 10°N (Sultan and Janicot 2000, 2003, Le Barbe and Lebel , 2002). On the basis of a thirty-year rainfall dataset (1968-1990), Sultan and Janicot (2000) estimated that the average date of the monsoon onset is centred on the 24th of June, with a variability of a few days. The convective activity centred around the Guinean coast strongly decreases. Then, after several days to a few weeks during which convection remains suppressed, the convective activity becomes stronger and its centre is shifted about 5°N northwards, as illustrated in Fig 2-7, which shows the mean annual evolution of convective activity through rainfall measurements over West Africa.

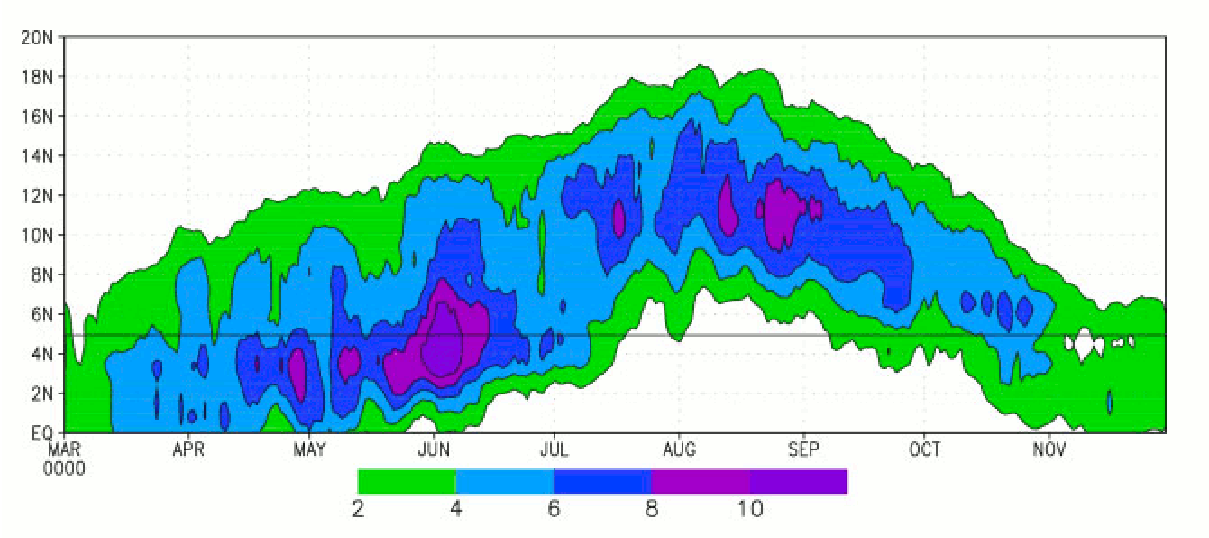

Figure 2-7 : Mean seasonal cycle of rainfall over West Africa through a latitude cross-section. Precipitation values (mm/day) from GPCP satellite-estimated values are averaged over 5°W-5°E and over the period 1997-2006. This illustrates the abrupt shift from 5°N to 15°N of the convection zone at the end of June during the onset period (figure from Janicot et al., 2010).

There is still uncertainty about the precise causes or combination of factors that leads to the triggering of the monsoon onset. Past studies suggest different origins of the onset:

- Effect of Kelvin Waves (Matthews 2004, Zang et al. 2006): the convective activity over the Warm Pool (Pacific) could generate a Kelvin wave that could propagate around the equator and 20 days later trigger convective activity over the Sahel.

- Effect of Sea Surface Temperatures (SST) and Land Surface Temperature (LST) (Janicot 1992, Eltahir and Gong 1996, Grodsky and Carton 2001). Upwelling in the Gulf of Guinea leads to a cooling of the SST in June-July. At the same time, LST increases over the Sahel. This amplifies the meridional gradient of temperature between the overheated Sahara and the cooler Gulf of Guinea. This cooling also inhibits convection over the ocean and favours convection over land.

- Effect of Heat Low (Sultan and Janicot 2003, Ramel et al. 2006): This mechanism involves the reinforcement of the Heat Low dynamics that increases the subsidence north of the ITCZ and also increase convergence in the ITD zone. The subsiding motion accentuates the Convective Inhibition (CIN), the increase in convergence strengthens the monsoon flow that brings the moisture (Peyrillé et al., 2007). This results in an intensification of the convective instability.

– ***The full monsoon: Mesoscale Convective Systems and African Easterly Waves***

The West African monsoon brings most of the annual rainfall over the Sahel region (Mathon et al., 2002). This rainfall is generated by intense precipitating convective systems called Mesoscale Convective Systems (MCS). They are long-lived and well organised systems travelling from East to West. There are several types of MCS; squall lines are linear types of MCS (Lafore and Moncrieff, 1989), Mesoscale Convective Complexes (MCC) are organised in a circular shape (Maddox, 1980), and Organised Convective Systems (OCS) are very long-lived systems (sometimes more than two days). Their tops can reach up to the tropopause (about 18km) and sometimes even overshoots can overcome the stability of this layer and intrude the stratosphere. Their horizontal dimensions extent up to several hundred kilometres. Their structures are complex. A MCS is composed by one or several main convective cells with strong ascending updrafts, a cool downdraught that propagates at the front (density current) and uplifts air that contributes to feed the system. The organisation of a MCS is closely linked to the AEJ dynamics and in particular, they interact with African Easterly Wave (AEW) activity. AEW are disturbances in the AEJ with a periodicity of about 3 to 5 days (Burpee, 1972). Their origins are still not well known. Some studies suggest that strong convection over the Tchad region could initiate these waves (Hall et al., 2006; Leroux et al., 2009). AEWs play an important role in the development of deep convection over West Africa at synoptic scales. At smaller scale, deep convection is strongly modulated by the diurnal cycle. This is discussed in more details within the following section, specifically focused on the diurnal cycles over land.

2.2 Diurnal Cycles over Land

The diurnal cycle is a mode of variability that comes from the Earth rotation around its axis in 24 hours. This rotational movement around itself induces variability in the intensity of solar radiation received at a specific point of the Earth, which results in alternation of night and day. The daytime intensity depends on the latitude and the position of the Earth on its orbit around the sun.

Under clear-sky conditions, a large portion of the incoming solar radiation at the top of the atmosphere reaches the surface. Then, over the ocean, solar heating is mainly absorbed by the semi-transparent upper waters and only a small fraction is retransmitted to the atmosphere. The ocean heat capacity further damps the diurnal cycle at the surface and in the low levels. By contrast, over land, a large amount of the surface incoming solar radiation is transferred back to the atmosphere within minutes, which makes the diurnal cycle an important mode of variability over land.

2.2.1 Importance of Diurnal Cycle and issues

This diurnal cycle of solar radiation drives the diurnal cycles of many elements in the atmosphere. It is an important mode of variability of weather and climate systems over land. A significant control on temperature, humidity, cloudiness and precipitation is imposed by the solar diurnal cycle. This mode of variability is often dominant compared to the seasonal cycle in the Tropics, whereas in the Mid-latitudes the seasonal cycle dominates. This is illustrated in Fig 2-8 (Hastenrath, 1995) which shows the evolution of 2m temperature as a function of daytime and month at two locations, one in the mid-latitudes (Berlin) and one in the Tropics (Quito). In Berlin, the seasonal variation (ΔT=20°C) is much larger than the diurnal variation (maximum of ΔT=6°C), whereas in Quito, almost no seasonal variation exists (ΔT=1°C) and the diurnal cycle is the main mode of variability (ΔT=12°C).

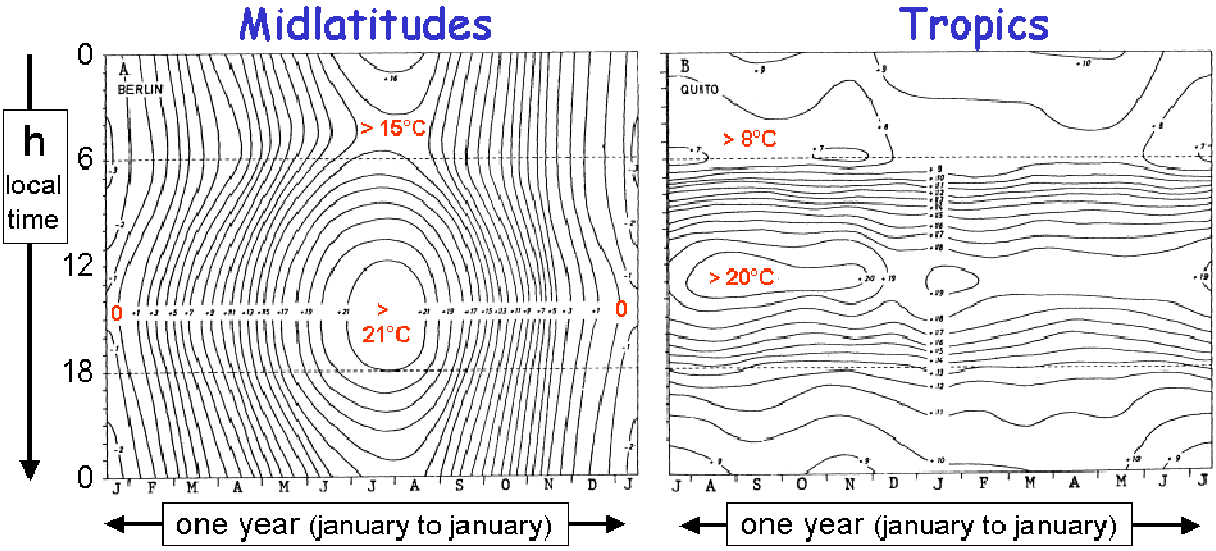

Figure 2-8 : Hovmöller diagrams of the temperature at 2m above the ground at Berlin (left) and Quito (right). The diurnal variability can be estimated from the vertical axis and the seasonal variability from the horizontal axis (figure from Hastenrath, 1995).

The Diurnal Temperature Range (DTR) is defined as the difference between the minimum and maximum surface temperatures. The DTR is an important climatic parameter, humans are directly sensitive to it, in particular to minimum temperatures (IPCC report 2007). It also has large impacts on ecosystems. The DTR varies from less than 4°C over the ocean up to 20°C over the continent as illustrated on Fig 2-9 which shows a geographic distribution of DTR over the globe in winter and summer periods from Dai et al. (1999). Weaker seasonal variations are observed in the Tropics compared to the mid-latitudes, except in monsoon regions (i.e. West Africa, India), where the DTR are larger during the dry season. Cloud cover, soil moisture and water vapour are significant local forcings on DTR (Trenberth and Shea, 2005). Strong correlations between soil moisture and DTR have been found especially over semi-arid regions. Others factors can contribute to shape the DTR, such as aerosols, which are especially important in the Sahel (Slingo et al., 2006) or East Asia (Huang et al., 2006), but also advections, which contribute to decrease the DTR in coastal regions.

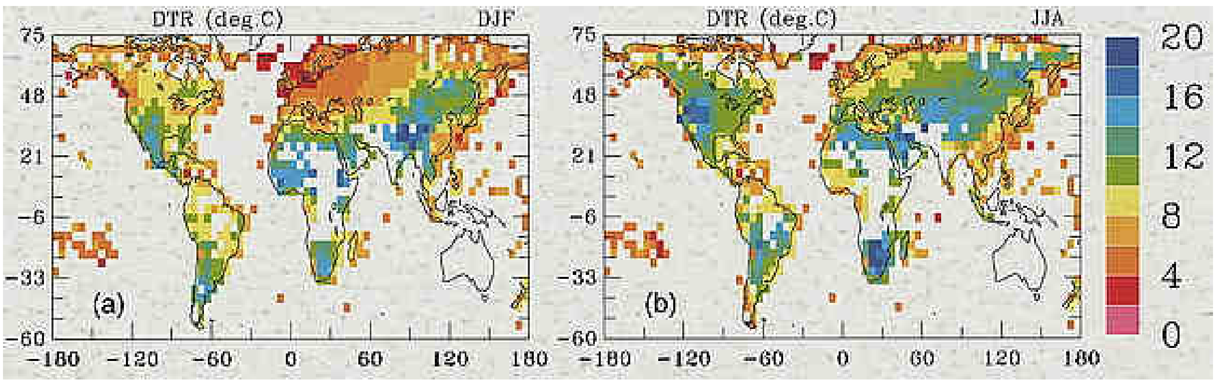

Figure 2-9 : Geographic distributions of the mean DJF and JJA DTR (°C) averaged over the 1980-91 period. Figure from Dai et al. (1999).

The Intergovernmental Panel on Climate Change (IPCC) report (2007) highlights the uncertainties in climatic projections of DTR changes. They report that on average, minimum temperatures are increasing at about twice the rate of maximum temperatures (0.2 versus 0.1°C/decade). They mention that this decrease in continental temperature range coincides with an increase in cloud amount, precipitation and total water vapour.

A study of the climatic projection of daily maximum and minimum land surface temperatures shows a global decrease in diurnal temperature range (Easterling et al, 1997; Stone and Weaver, 2002; Braganza et al., 2004; Karoly and Braganza, 2005). Global warming appears to be associated with a change in DTR, with, in particular, a significant increase in mean minimum temperatures. However, in some parts of the world, model dispersion associated with diurnal temperature range is too large to be taken into account, thus, this highlights the necessity of improving the knowledge of diurnal cycles.

The climatic diurnal cycle is mainly driven by solar variations and more precisely by the energy budget at the surface. As solar energy strikes the earth's surface, a thin layer of air (2-3cm) is heated by conduction. Atmospheric instabilities/stabilities are generated via the position of this warm layer underneath a cooler layer. The energy is transported upwards by turbulent processes.

Figure 2-10 presents the diurnal cycle of a radiative budget at the surface. The diurnal cycle is primarily driven by solar (shortwave) radiation received at the surface (SWin, in red on the figure). A part of this received radiation is reflected by the surface (SWup, yellow curve). The amount of reflected radiation depends on the surface albedo. White surfaces reflect more radiation (albedo of 0.8-0.9) than dark surface (albedo of ~0.1). The surface also receives infrared (longwave) radiation from the atmosphere (LWin, in dark blue) and emits back longwave radiation to the atmosphere (LWup, in light blue). The intensity emitted by the surface is proportional to the fourth power of its temperature. The LWin depends on the vertical profile of temperature and its content of water vapour (and other greenhouse gases) and clouds (greenhouse warming). It has a far less pronounced diurnal cycle. The net radiation budget (Rnet) is the sum of incoming minus outgoing radiation. It is given by:

$$Rnet = SWin - SWup + LWin - LWup$$

Rnet is positive during daytime and can become slightly negative during night time, longwave upward flux is often larger than the downward.

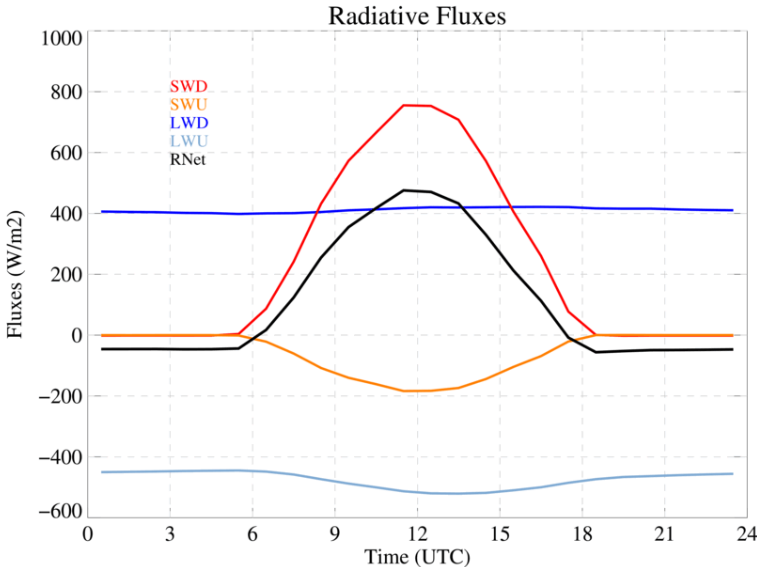

Figure 2-10 : Radiative budget at the surface: Downwelling and upwelling shortwave and longwave radiation as well as the net radiation.

This energy is then partitioned into latent heat flux (LE) and sensible heat flux to both the atmosphere (H) and ground (G). The nature of this partition strongly depends on surface/soil properties as illustrated in Fig. 2-11. Over the desert, the availability of water is low, so the partitioning of the energy goes into sensible and ground heat flux. On the other hand, in the tropical forest where water is largely available, the energy goes mainly into latent heat flux and the sensible heat flux is very small. At the sea surface, the behaviour is very different, as a large part of the net radiation is absorbed by the water. The rest of the energy which is not absorbed by the waters goes primarily into latent flux.

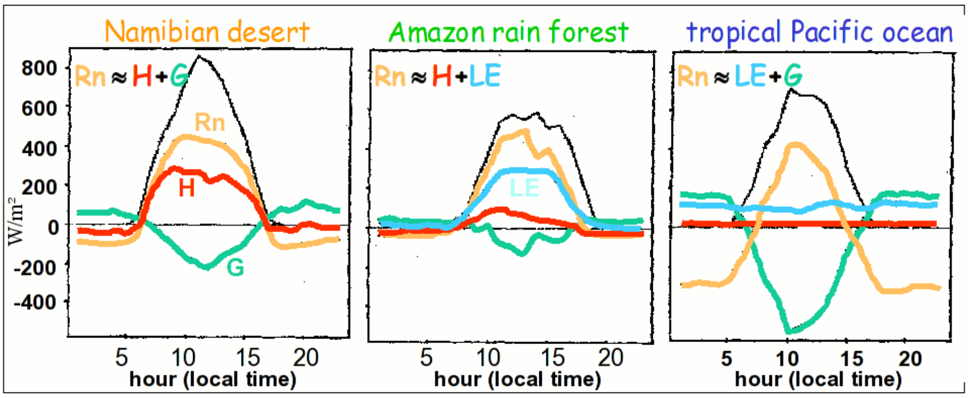

Figure 2-11 : Examples of partitioning of net radiative energy (Rn) into turbulent fluxes(sensible (H) and latent (LE)) and ground fluxes (G); over the Namibian desert (left plot), over the Amazonian rain forest (middle plot) and the TRopical Pacific Ocean (right plot) from Garstang and Fitzjarrald (1988).

These turbulent fluxes then partly control the properties of a relatively thin layer of the atmosphere (few hundred metres up to a few kilometres) called the atmospheric boundary layer.

The term of boundary layer in aerodynamics was first introduced by Prandtl (1905) who referred to the flow of a low viscosity fluid along a solid boundary. In atmospheric sciences, this interface layer is called the atmospheric boundary layer. This is the layer of the atmosphere directly influenced by the surface through turbulent fluxes at a timescale of one hour or less (Stull, 1988). The Earth's surface involves frictions, surface heating and cooling as well as fluxes of moisture.

2.2.2 Contrasts in daytime and nightime atmospheric boundary layers

Atmospheric boundary layers extend vertically from approximately 100m during night-time when the atmosphere is stratified up to several kilometres during daytime, when the boundary layer is convective. The atmospheric boundary layer exhibits a strong diurnal variation and it is an important zone of energy, humidity and materials (aerosols, pollutants) exchanges between the surface and the free atmosphere above. It has a crucial role in mediating changes in surface behaviour to larger scale weather and climate patterns (Stull, 1988; Garrat, 1992).

– ***Convective boundary layers***

A Convective Boundary Layer (CBL) is characterised by a positive buoyancy flux at the surface. Buoyancy is the dominant mechanism driving turbulence within a convective boundary layer. The turbulence is organised into identifiable vertical structures called thermals. Within a convective atmospheric boundary layer, thermodynamic properties (potential temperature in particular) are well mixed, this is why a linear decrease of temperature with altitude is observed. A constant profile is observed when considering the potential temperature (θ) which considers the decrease in temperature for a rising air parcel due to air expansion. The expression of θ is given by:

$$\theta = T(\frac{P_o}{P})^{rd/cp}$$

with T and P the temperature (K) and pressure (Pa) of the air parcel, P_o the surface pressure, rd the gas constant of air and cp the constant capacity of air at constant pressure.

The properties of this layer depend on atmospheric conditions, surface properties and the net radiative budget at the surface. During daytime, the convective boundary layer with a depth Zi, is composed by distinct sub-layers as illustrated in Fig 2-12:

- The surface layer (5-10% of Zi): this layer is also known as the constant flux layer; in this layer the temperature, wind and humidity vary rapidly with altitude. This is a well observed layer as measurement towers sample this layer.

- The mixed layer (70-80% of Zi): the properties of this layer are well mixed throughout the depth, where small scale turbulence and thermals act to mix momentum, potential temperature (θ) and water vapour mixing ratio (rv) and all tracer species. The increase of relative humidity is due to the decrease in temperature throughout the boundary-layer depth.

- The capping inversion also called entrainment zone (10-20% of Zi): this is a stable layer which corresponds to the top of the convective boundary layer. This zone is often characterised by large gradients in potential temperature, water vapour mixing ratio, wind.. and constitutes a buffer zone between the boundary layer and the free troposphere.

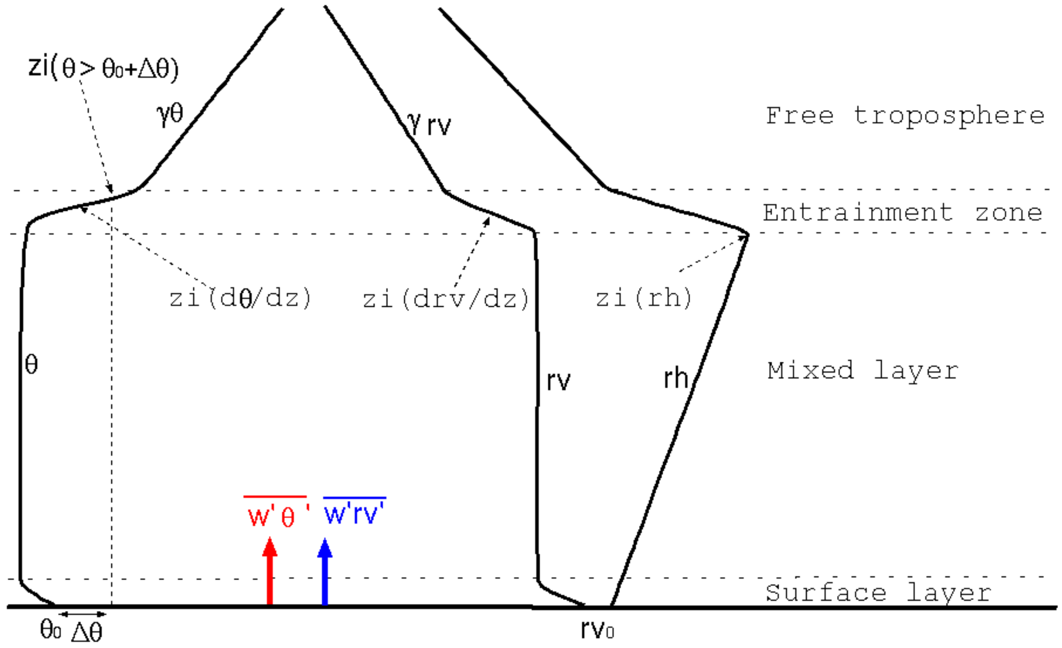

Figure 2-12 : Profiles of potential temperature (θ), water vapour mixing ratio (rv) and relative humidity (rh) in the boundary layer. The surface layer, the mixing layer, the entrainment zone and the free troposphere are indicated on the figure.

The boundary-layer depth can be determined according to different diagnostics that correspond to different levels as illustrated in Fig 2-12:

- The maximum of potential temperature gradient.
- The maximum of water vapour mixing ratio gradient.
- The maximum of relative humidity.
- The level where $\theta=\theta_{surf}+\Delta\theta$ with $\Delta\theta$=0.5K.

When analysing the radiosounding data, we have evaluated these different diagnostics. The last one is used in the following sections to determine the boundary-layer height.

The daytime boundary-layer growth is mainly controlled by surface buoyancy fluxes. The dynamical turbulence generated by wind shear can also play a role, but is generally of second order (Pino et al., 2003). The growth of boundary layer by buoyancy and wind shear is known as the encroachment process. Thermals originating from the surface layer are due to inhomogeneities in the surface properties (hills, surface with lower albedo...). They are rising plumes of warm air that travel towards the top of the convective boundary layers. When they acquire enough speed to slightly overcome the inversion layer, they entrain air back from the free troposphere to the convective boundary layer. This is known as the entrainment process. The typical mixing time is in the order of 30-60mins. The boundary layer height is directly related to maximum height reached by the thermals.

Observations of boundary layers can be carried out using radiosoundings to obtain vertical profiles of thermodynamic and dynamical properties at a particular point (as used in this PhD thesis). Measurements using sodar, lidars or radar allow to obtain a spatial view of the structures. This is illustrated in Fig 2-13, where different sequences of radar measurements onboard an aircraft capture the structures of thermals in a growing CBL.

Through the morning growth, thermals become stronger, taller and more sparsely spread over space. Intrusion of dry and warm air from the free troposphere called dry intrusion are also organised structures that play a role in the humidity transport (Couvreux et al., 2007, Canut et al., 2010). They can reach down to the Earth's surface.

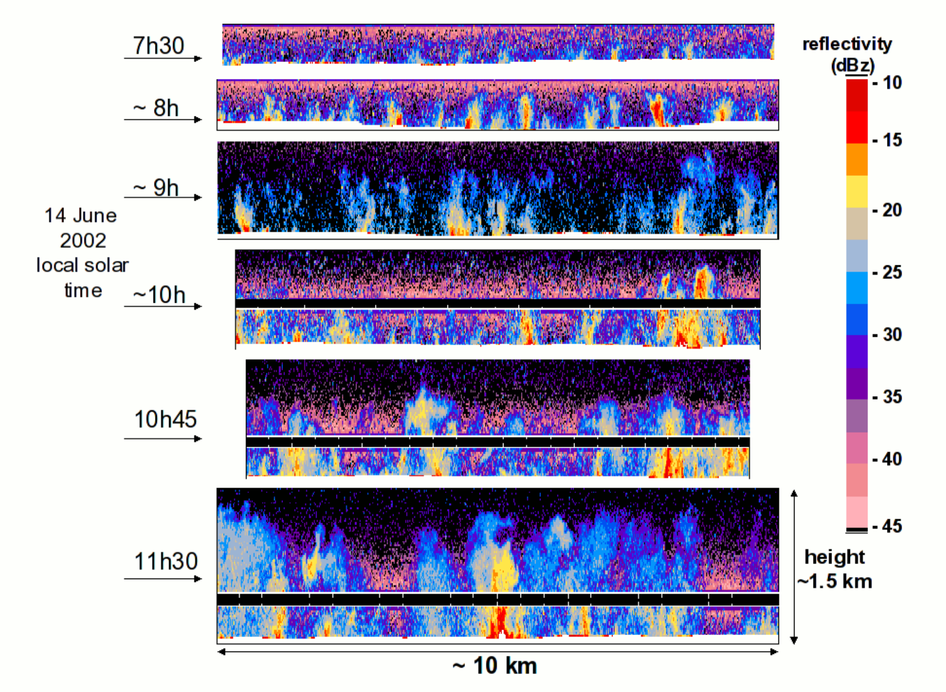

Figure 2-13 : Reflectivity of the convective boundary layer at different times of its development from radar measurement onboard on aircraft (Courtesy B. Geert) .

The dry and warm air from the free troposphere entrained into the CBL reduces the amount of water vapour within the CBL, whereas the surface latent heat flux tend to increase it. The balance between these two processes is subtle and can sometimes be positive corresponding to a humidification and sometimes negative (drying) like observed in the Sahel during the pre-monsoon season (Van Heerwaarden et al., 2010, see appendix A).

– ***Nocturnal boundary layers***

At sunset, solar radiation stops heating the surface, the surface net radiation becomes negative and the surface starts cooling down via emission of longwave radiation. The thermals cease rapidly and turbulence diminishes. The atmosphere becomes stratified with colder air at the surface than above, which gives a stable temperature profile, as illustrated in Fig 2-14. A stable boundary layer is topped by a residual layer corresponding to the decaying convective mixed layer. The intensity of the cooling rate depends mainly upon the energy budget at the surface. The more negative Rnet is, the strongest the cooling is. The atmospheric water content and the cloud cover have a strong influence on the longwave budget, as they have a large greenhouse effect.

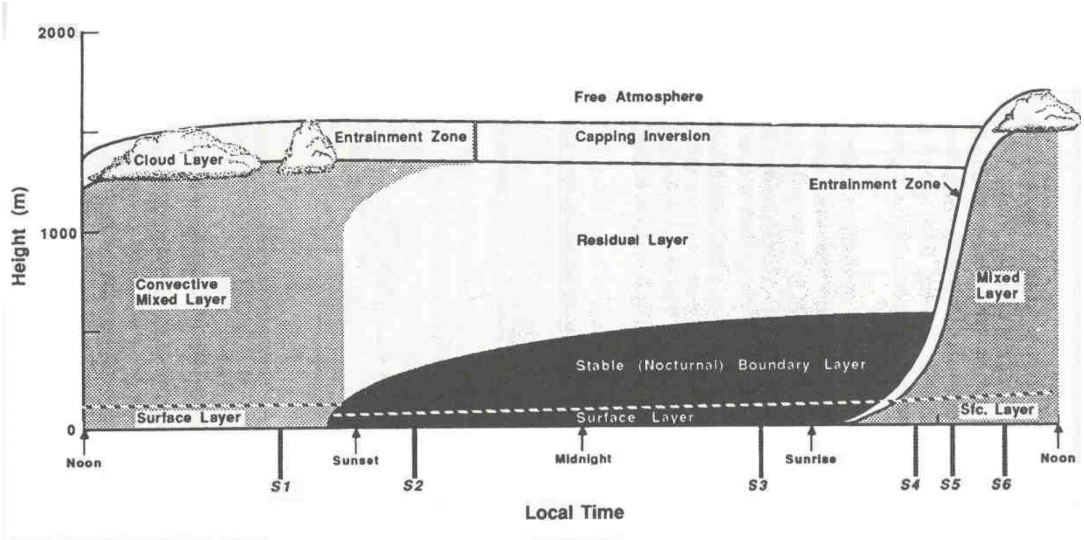

Figure 2-14 : Schematic of diurnal evolution of atmospheric boundary layer from Stull, 1988.

The stratification stabilise the flow, the turbulence and vertical mixing tend to quickly be suppressed. Turbulence occurs sporadically due to wind shear depending on the Richardson number of the flow. Gravity waves can also occur and propagate on the nocturnal layer generating also disturbances. A strong cooling of the atmospheric low-levels can lead to the decoupling of the surface with the layer above; due to this decoupling the formation of a nocturnal jet can be observed (Blackadar, 1975; Thorpe, 1977; Garrat, 1994) as illustrated in Fig. 2-15. A nocturnal jet is defined as an acceleration of the low-level flow, which can sometimes be greater than the geostrophic flow. Some conditions are found in the literature in the definition of a nocturnal jet like the minimum wind speed (greater than $5 m.s^{-1}$), the thickness and the clockwise rotation with time.

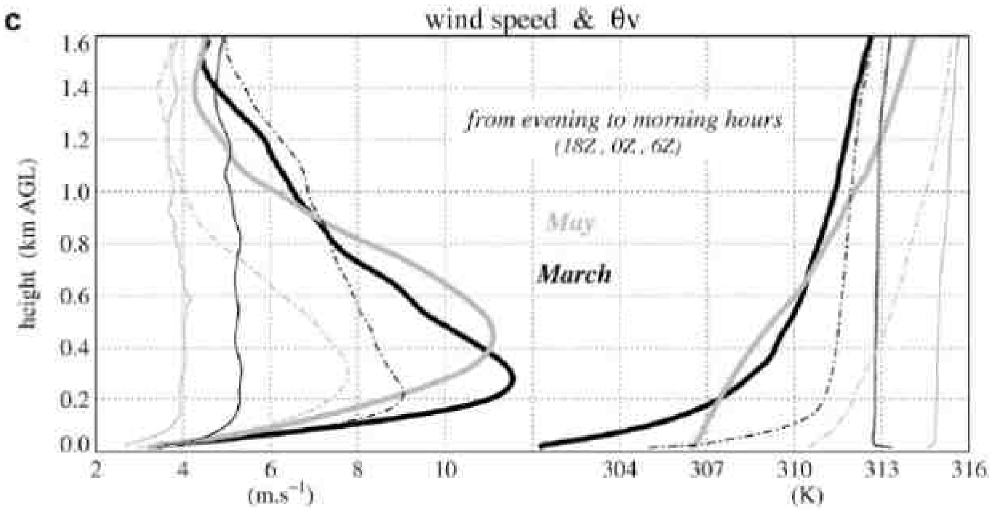

Figure 2-15 : Evolution of dynamic and thermodynamic structures of the nocturnal jet at 18Z (thin full lines), at 0Z (dash dotted lines) and 6Z (thick full lines) in March and May at Agoufou (Mali) from Guichard et al.(2009).

2.2.3 Shallow and deep convection diurnal modulations

In strongly convective boundary layers cumulus clouds can form at the top of the mixed layer. On the other hand, in nocturnal or weakly convective boundary layers, stratiform clouds can exist within or at the top of the boundary layer. Before going into further details, a few convective indexes are introduced below (see also Fig 2-16).

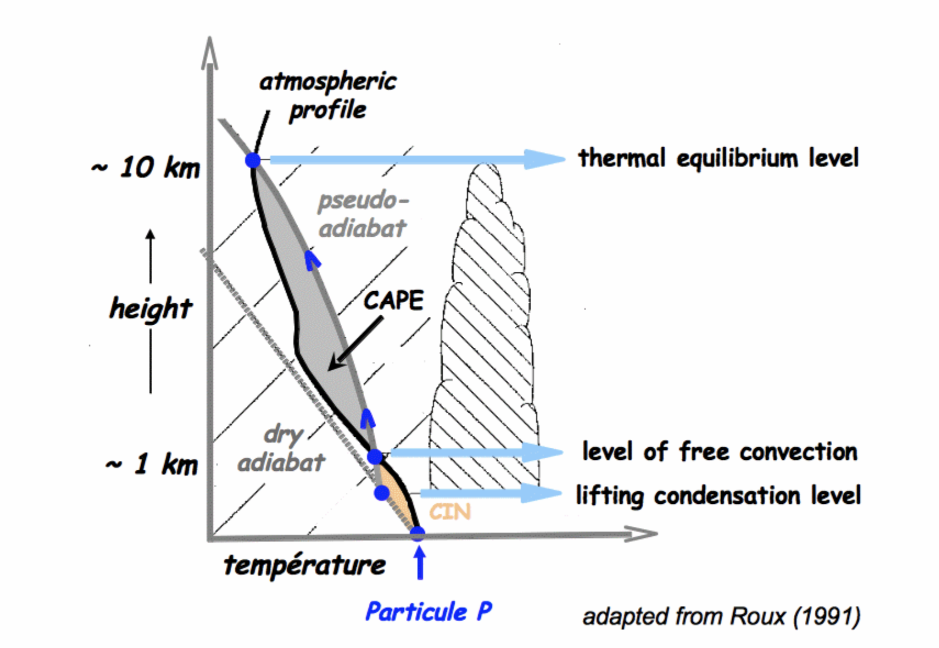

Figure 2-16 : Representation of Convective Available Potential Energy (CAPE, in grey) and Convective Inhibition (CIN, in pinky beige) on a tephigram. The atmospheric profiles (black), the dry and pseudo adiabats (in grey lines) for a particle P are represented on the tephigram.

As a thermal rise through the convective boundary layer, the air cools down and the relative humidity of the air parcel increases (cf Fig. 2-12). If it reaches the Lifting Condensation Level (LCL), a cumulus cloud forms at the top of the mixed layer. The energy released by condensation helps the cloud to develop (Zhu 2002), while it also stabilises the atmosphere above and stops the boundary-layer growth.

Boundary-layer clouds are important for the energy budget at the surface as they absorb and reflect a large part of the incoming solar radiation (see Fig 2-17 for illustration). Significant feedbacks can be found in the atmospheric boundary layer properties, such as a decrease in sensible and latent heat fluxes.

As a P surface air parcel rises following the dry adiabat (see Fig. 2-16), it reaches saturation at a level called the Lifting condensation Level (LCL). If it carries on rising following the pseudo-adiabat (as the air parcel condensates), when it becomes warmer than its environment, it reaches the Level of Free Convection (LFC). At this point, the air parcel can freely rise until the Level of Neutral Buoyancy (LNB) where the air parcel temperature is equal to its environment.The Convective Available Potential Energy (CAPE) corresponds to the positive area between the pseudo-adiabat of a surface air parcel and its environment.

This is the amount of energy a parcel of air would have if it was lifted vertically through the atmosphere. CAPE is effectively the positive buoyancy of an air parcel and is an indicator of atmospheric instability, which makes it valuable in predicting mesoscale convective systems. It is expressed as follows:

$$CAPE = \int_{Z_{LFC}}^{Z_{LNC}} g \frac{\{Tv_{par}(z) - Tv_{env}(z)\}}{Tv_{env}(z)} dz$$

The Convective Inhibition (CIN) is the energy needed for a parcel to overcome the stability and reach the level of free convection (see Fig. 2-17 for illustration).

$$CIN = \int_{Z_{LCL}}^{Z_{LFC}} g \frac{\{Tv_{par}(z) - Tv_{env}(z)\}}{Tv_{env}(z)} dz$$

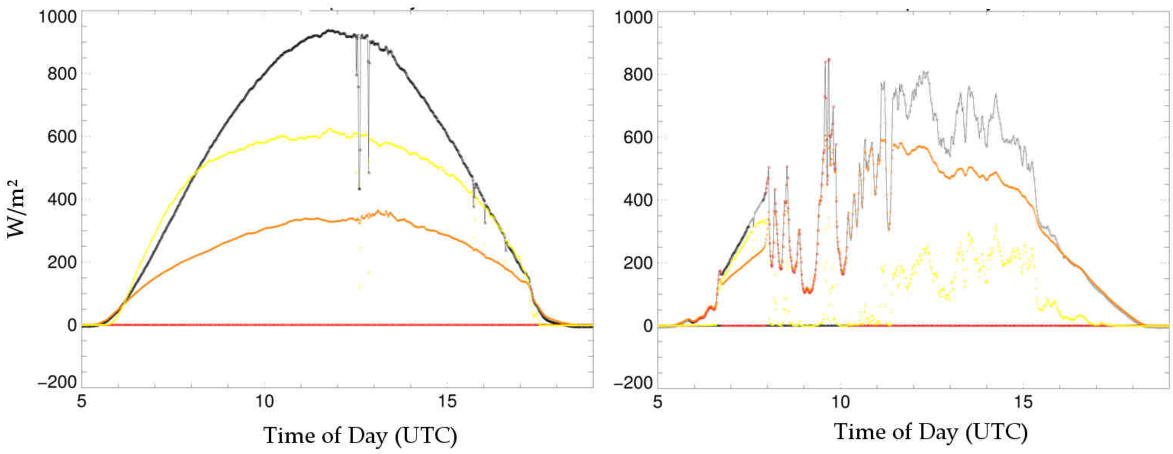

Figure 2-17 : Total (black), direct (yellow) and diffuse (orange) incoming shortwave flux measurements at the surface, ARM site (Niamey - Niger) in clear sky conditions (21 June 2006, left plot) and partly cloudy conditions (30June 2006, right plot).

Shallow (cumulus, stratocumulus) and deep convection are strongly modulated by the solar diurnal cycle (Betts et al., 1996; Yang and Slingo, 2001; Dai et al., 2001; Machado et al., 2002; Nesbitt and Zipser, 2003; Mohr, 2004; Rickenbach 2004). A maximum in deep convection is typically observed in in the afternoon over continental regions, whereas over the ocean, a weaker diurnal variation is observed with a tendency to develop preferentially in the morning (see Fig. 2-18).

Over West Africa, shallow cumulus clouds form during daytime and sometimes develop into mesoscale convective systems. This typically occurs in the late afternoon or early evening and can last few hours up to more than 24 hours. The decaying phase also exhibits a diurnal modulation. Houze (2004) suggested that the nocturnal stabilisation of the lower troposphere could inhibit the spatial extension of mesoscale convective systems. However, over West-Africa, the convection tends to be suppressed in the late morning, when the convective boundary layer are already quite developed. This highlights the complexity of convective mechanisms and the need for improving the knowledge and understandings on these issues.

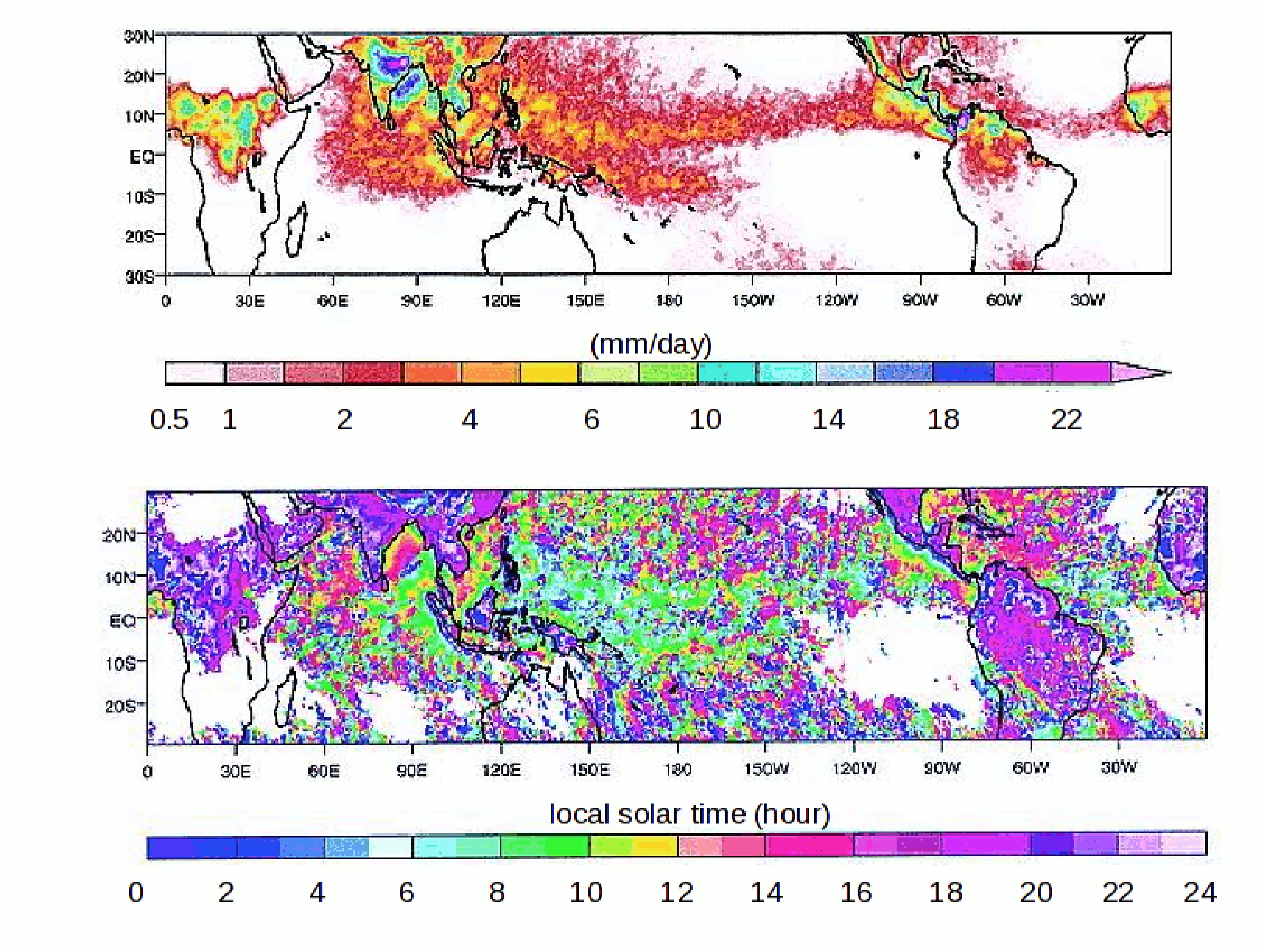

Figure 2-18 : Amplitude (top plot) and phase (bottom plot) of diurnal cycle of estimated precipitation from CLAUS satellite data from Yang and Slingo (2001).

2.2.4 Diurnal cycles over West Africa

Only few studies focused on the diurnal variability over West Africa due to the scarcity of measurements. However, the dynamical diurnal cycle of the WAM has been studied recently by Parker et al. (2005), Peyrillé et al, (2007), Lothon et al. (2008) and Pospichal et al. (2010).

During nighttime, an acceleration of the monsoon flow is observed with a northward propagation of the ITD. The monsoon flow responds to the meridional pressure gradient between the high pressure on the Guinean coast and the Sahara Heat Low as illustrated in Fig.2-19. An advection of cool and moist air is associated with this, which feeds the Sahel with moisture. While during daytime, turbulence in the convective boundary layer slows down the horizontal flow and transports the moisture accumulated during nighttime in altitude. The diurnal cycle of boundary layers was also investigated in few studies as presented in the following sub-sections.

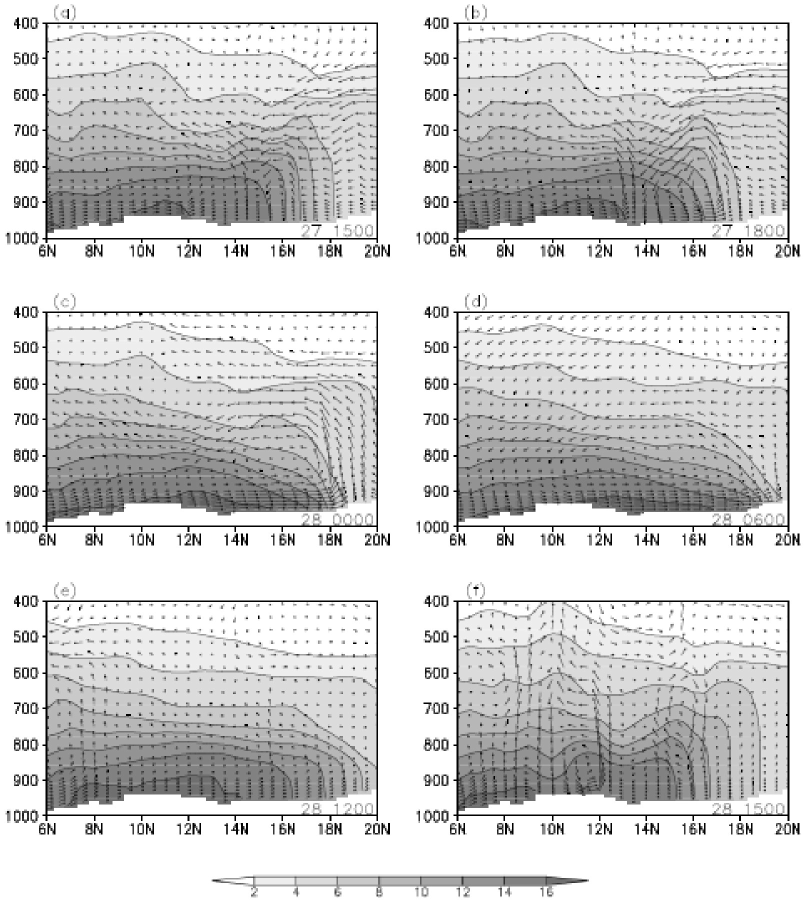

Figure 2-19 : Plots showing the evolution of humidity mixing ratio and winds in a latitude-pressure (in hPa) section from ERA40, averaged over 2.5°W-7.5°E. Fields are taken from ECMWF analyses and forecasts or the period 1500 UTC 27 August to 1500 UTC 28 August 2000. The corresponding dates are indicated at the bottom of each panel. Figure from Parker et al. (2007)

– ***Convective boundary layers***

Over the Sahel, particular vertical structures of the atmosphere such as the monsoon flow, the AEJ and the Harmattan flow, strongly affect the development of atmospheric boundary layers. Some recent studies (Flamant et al., 2007, Cuesta et al., 2008, 2009 and Messager et al. 2010) analysed the structure and dynamics of the Saharan atmospheric boundary layer during the West African monsoon using in-situ and lidar measurements from the AMMA campaign. A remarkable split structure composed of a well mixed convective layer lying beneath a residual layer was identified, as illustrated in Fig 2-14. This residual layer was found to be persistent and advected by laminar flow towards the South.

South of the ITD and during the pre-monsoon period, the convective boundary layers first develop within the monsoon flux, moist and cool air layer. Then, they can reach the SAL which is a dry warm layer loaded with mineral aerosols and characterised by a weakly stratified temperature profile. At the boundary between the monsoon flow and the Harmattan, strong wind shear occurs due to opposing direction of these two flows. This amplifies the entrainment rate as suggested by Culf (1992) and evidenced by Canut et al. (2010) who found entrainment rates up to 0.4. However, during the monsoon period, lower entrainment rates were measured (0.2) due to the fact that the convective boundary layer hardly reached the strong wind shear zone.

During the Hapex-Sahel campaign (Goutorbe et al., 1994), the variability and the relationships between surface energy budgets and atmospheric boundary layers in the Sahel were examined. Wai et al. (1997) and Dolman et al. (1997) studied boundary-layer developments during the wet and drying seasons. They suggested an important role of surface evaporation on CBL development in preventing strong surface heating as well as an important role of horizontal advection and vertical divergence during the wet period. During the drying season (October), they observed a dryer and warmer boundary layers due to less extensive showery weather. This allowed the soil to dry and warm, leading to higher sensible heat fluxes. The seasonal variability of surface energetic diurnal cycles in the Gourma region was studied by Guichard et al. (2009). They found strong differences in the energetic budgets at the surface at the mesoscale, which have a direct impact on the convective boundary layer behaviour.

Convective boundary layers have a direct impact on the WAM, as they partly drive the daytime evolution of CAPE and hence the triggering of deep convection. Moreover, they are important in the vertical moisture transport process via convective mixing. The role of convective boundary-layer development on the position of the ITD was investigated by Pospichal and Crewell (2007) and Cuesta et al. (2008, 2009). They showed that during daytime, the ITD retreats towards the south due to convective mixing, this retreat can reach a hundred kilometres. Boundary layers play also a significant role in determining the meridional gradient of moisture and temperature, which in turns drive the monsoon circulations. It was also suggested the generation of a secondary circulation induced by different boundary-layer developments on the meridional transect that could slow down the retreat process of the monsoon (Wai et al, 1997). Convective boundary layers are also important in determining the low-level properties (temperature, humidity,..) over the meridional transect, which in turns affects the monsoon activity.

– ***Nocturnal boundary layers***

In the Sahel, nocturnal jets have been observed during the AMMA campaign and are considered as important elements of the monsoon system. Indeed, they transport humidity meridionally onto the continent (Parker et al., 2005) but also they play a role in numerous processes ranging from turbulence up to synoptic scale (Lothon et al., 2008). In the low levels, advection of moisture in the Northern part of the Sahel is mainly carried out by the nocturnal jet as during daytime turbulence largely mix momentum that decreases significantly the wind intensity. Nocturnal jet intensity decreases during the wet season and its activity is perturbed which may be linked to convective activity. The percentage of occurrence decreases from 85% in April to 52% in August. At Niamey, the maximal jet was found around 0500UTC and centred at 400m above the ground (Lothon et al., 2008). During the moistening period, the frequency of occurrence is at its maximum as well as its intensity, when the ITD is the closest. Guichard et al. (2009) showed that the atmospheric humidity affects the formation and vertical structure of the low-level jet. In March, as the atmosphere is dry, the jet develops closer to the ground and its intensity is stronger than in May, when the atmosphere is moist (see Fig 2-15 and Lothon et al., 2008). The best signature of the jet can be seen in the Turbulent Kinetic Energy (TKE) and skewness of the air vertical velocity. The nocturnal jet affects the surface layer as it transports momentum downwards, this was observed on TKE by Lothon et al. (2008) in particular when the flow was from the west. Nocturnal boundary layer are important also for daytime as changes in nocturnal boundary layer profiles have an impact on the development of the following daytime convection (De Arellan, 2007).

2.3 Modelling of Diurnal Cycles and Issues

2.3.1 Numerical Models

In 1950, Charney, Fjortoft and von Neumann carried out the first simulation with a computer. Since then, large-scale numerical models have been developed and improved to be able to simulate the atmospheric behaviour and predict the weather as well as the climate. These models are based on sets of equations to transcript the atmospheric behaviour. Nowadays, computational capacities allow increasing spatial and temporal resolutions. There are several types of numerical simulations going from Large Eddy Simulation (LES) (Smagorinsky, 1963 ; Deardorff, 1970, Couvreux et al., 2007) with fine spatial and temporal resolution (50m & few seconds) to General Circulation models (GCM) (Dequé et al., 1994) that can cover the globe, but at coarser spatial and temporal resolutions (a few hundred kilometres and 30min).

The numerical models have become more and more complex with time, including dynamical and thermodynamic, microphysics and radiative processes in the atmosphere. It was only in 1990 that the diurnal cycle of solar radiation was included in simulations (Randall et al., 1985; Randall et al., 1991). It was motivated by the fact that meteorologists started to look at more detailed forecast, down to the diurnal cycle and that they realised that the diurnal processes were important for the longer timescale forecasts.

Boundary layers were first represented using a mixed-layer model based on bulk equations. They include an equation of the boundary layer height, potential temperature, depending on the sensible heat flux and an entrainment of air into the mixed layer fixed to -0.2. In LESs, small scale processes like convection can be resolved directly by the model, whereas in the GCMs 'parameterisation' (representation of the impact of subgrid processes) must be used. The boundary-layer development can be modelled via different order of closure. Models with 1.5 order of closure are based on a Turbulent kinetic Equation (TKE) scheme (Cuxart et al, 2000) that takes into account the encroachment and entrainment processes. There are also more complex closures with exchange coefficients or additional counter gradients.

Recently, there has been an increased effort to accurately simulate thermal activity in the boundary layer. Parametrisations based on mass flux conservation were developed and implemented in mesoscale models as well as GCMs (Rio and Hourdin, 2008; Pergauld et al., 2008). This allowed better representation of the convective boundary-layer growth and the formation of cumulus clouds. An additional parameterisation is included to the representation of small scale turbulence (i.e. TKE scheme) in order to represent the thermals via a mass flux scheme. The microphysics which deal with the states of water, now includes the warm and cold phase of water (Pinty and Jabouille, 1998), it represents the growth of water (and ice) droplets by coalescence and aggregation processes. Differences between water droplets, ice, snow, graupel and hail are made, which is important in particular for the radiative processes. The deep convection schemes are most of the time based on mass flux conservation equation (Kain Frischt, 1990, Betchtold et al., 2001). They are based on three main steps: the convective triggering, the mass flux representation and the closure formulations. The triggering function are often based on LCL of an air parcel at the surface and a condition on the potential cloud depth.

A representation of convective downdrafts is often incorporated, which permits to stabilise the atmospheric low-levels after the passage of a convective system.

The mesoscale atmospheric model Meso-NH used in this PhD work for simulating the atmospheric diurnal cycles over West Africa is presented in section 4.1.

2.3.2 Modelling of boundary layers

The modelling of the convective boundary layers remains complex, as it involves many processes and interaction between these processes. In state of the art numerical model, parameterisations of the boundary layer represent both small scale turbulence as well as the thermal plumes as mentioned in the previous subsection.

In those models, a recurrent drawback is the simulation of a too unstable convective boundary layer. This issue has received much consideration in recent years (Hourdin et al., 2002; Pergaud et al., 2009) and the situation has generally improved. Nevertheless, a number of defaults in the boundary-layer characteristics still persists due in particular to the strong dependency of boundary layer properties on surface turbulent fluxes. The latter depend, as seen previously, on the soil and surface properties as well as the atmosphere above. Other issues remain in particular on the entrainment processes, the cloud feedbacks, transport of humidity in a cloudy boundary layer. The transition phase at dawn between convective and stable boundary layer is also an issue.

Surface-atmosphere energy exchanges decrease considerably during nighttime. However, the modelling of stable boundary layer is also problematic, for other reasons. In particular, parameterisations have difficulties in reproducing the temperature inversion at the surface (Steeneveld, 2007) which is, sometimes, very strong particularly in the Sahel. This has an impact on the modelling of the nocturnal jet, as the intensity and altitude are often hard to simulate correctly. These defaults in the representation of nocturnal boundary layers also impact the model performances for the following days.

2.3.3 Bias in the convection and precipitation diurnal cycles

Large scale models are able to accurately reproduce the large scale dynamics, but have poor skills to capture small scale variability such as convection and precipitation (Dai et al. 1999; Lin et al. 2000; Royer et al. 2000; Yang and Slingo 2001). A timing bias in the triggering of convection has been identified in the models. The models often respond to a radiation forcing at the surface and an increase of CAPE that activates the convective parameterisation scheme. In the Tropics, the convection develops only two hours after sunset in the models, whereas in reality it occurs in the afternoon/late evening (cf Fig. 2-20 which shows example of diurnal cycle of modelled convection compared to the satellite observations). In fact, this error in the timing is linked to the difficulties that models have in representing the transition phase from shallow to deep convection (Betts and Jakob 2002a; Guichard et al., 2004). This behaviour has a strong impact on the diurnal cycle as a whole and on the local and large scale dynamics.

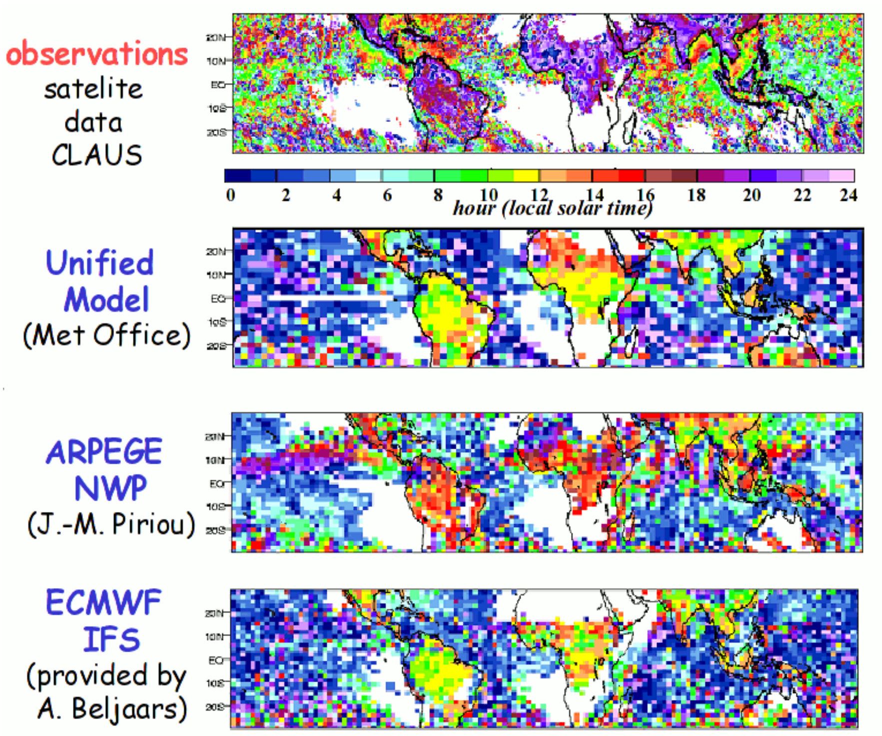

Figure 2-20 : Timing of convective activity observed from satellite (CLAUS data) and simulated by the Unified model (Met office), Arpege NWP and the ECMWF IFS (provided by A. Beljaars).

2.3.4 Modelling of the WAM

Global weather and climate models have systematic difficulties in simulating and predicting the characteristics of the WAM. In particular, the rainfall field is the most problematic characteristic to represent at timescale ranging from seasonal to diurnal. The diurnal timing of convection is badly represented. Usually, the convection starts too early. This has for consequences to modify the surface fluxes and hence the dynamics of the boundary layers. An incorrect representation of boundary layers may affect the dynamic of the monsoon circulation. For example, Thorncroft et al. (2003) showed that AEJ is well captured in both the Met Office Unified model and the ECMWF model in an analysis field, but was badly represented in a 5-day forecast. They suggested that this was due to an inaccurate representation of the diurnal cycle of boundary layers.

2.4 Surface-atmosphere interactions

The West African monsoon is an atmosphere-surface-ocean coupled system. The surface interacts strongly with the atmosphere at different time and space scales. This varies from decadal times-scale (Charney, 1975) through seasonal (Douville and Chauvin, 2000; Douville et al., 2001, Guichard et al., 2009) to diurnal (Taylor and Ellis, 2006; Koehler et al., 2010).

2.4.1 Couplings between surface properties and atmospheric boundary layers

During daytime, strong couplings take place between surface properties and atmospheric boundary layers via radiative transfer and turbulent fluxes of heat and moisture. There are complex interplays of forcings and feedbacks as illustrated in Fig 2-21 (see also Van Heerwaarden et al., 2010, and appendix A). As we have seen in previous section, surface properties modulate the net radiation at the surface via the albedo and longwave emission (for instance, the darker the surface is the lower the albedo is and the greater the net radiation is). The net radiation is then partitioned into latent and sensible heat fluxes depending on the Bowen ratio, which is defined as the ratio between sensible and latent heat fluxes. The Bowen ratio depends on soil properties (soil composition and texture, soil moisture, vegetation cover) and also on the atmospheric demand. Then, this strongly influences the boundary layer dynamics and thermodynamics. In return, the atmosphere modulates the surface radiative fluxes via the cloudiness and the temperature stratification.

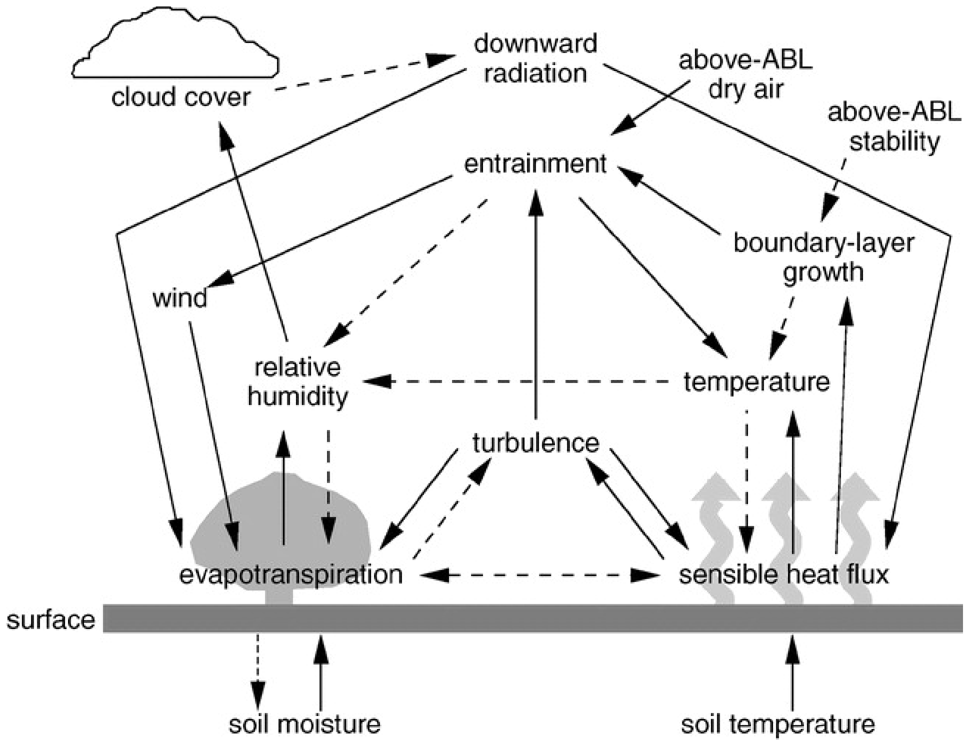

Figure 2-21 : Interactions between surface and atmospheric boundary layer during daytime (Ek and Holtslag, 2004).

Different partitioning of the available energy leads to different boundary-layer growths. A high sensible heat flux will deeply develop the atmospheric boundary layer and warms/dries it whereas, when the latent heat flux dominates, the boundary layer remains shallow and moister. For convection to occur, thermals must reach the LFC. In a stable environment (strong lapse rate) a moist and shallow boundary layer will be more favourable for convection (the decrease of LFC is critical), whereas in less stable conditions a dryer and more developed boundary layer will present more favourable conditions (the growth of boundary layer is critical) (see Fig 2-22). These considerations stress an inherent complexity of convective processes over land, where even mean environmental conditions induce distinct mechanisms of convective initiation.

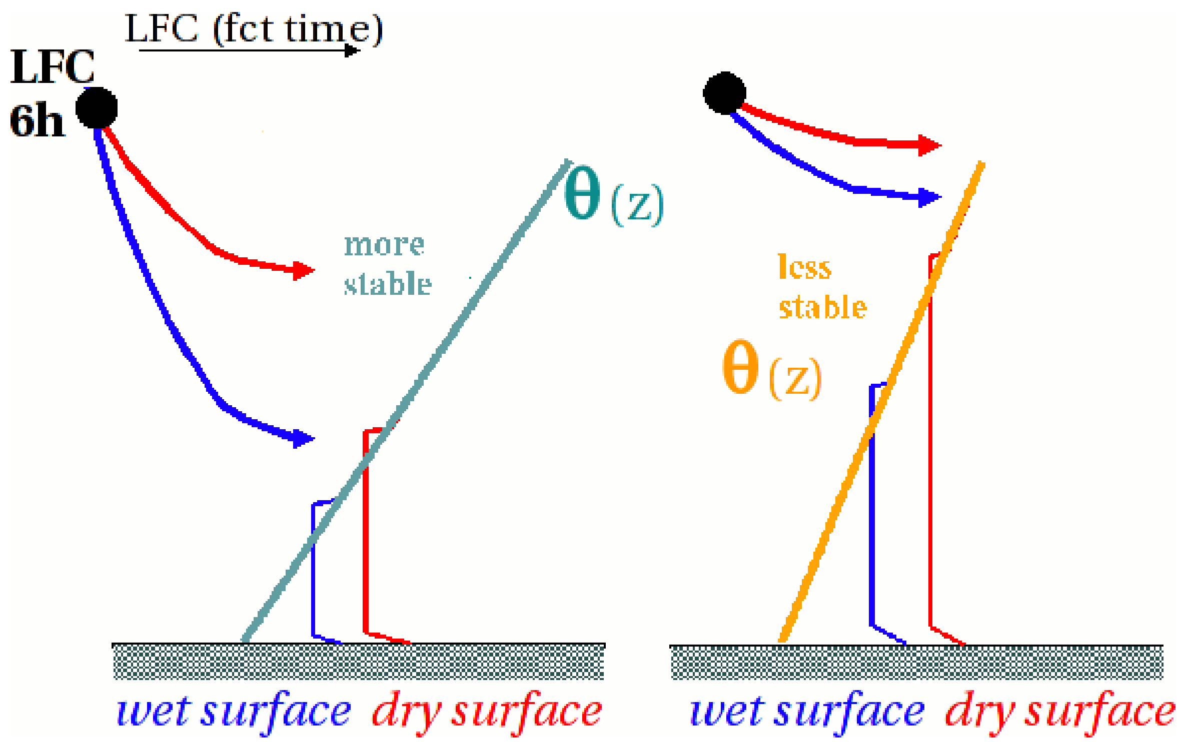

Figure 2-22 : Schematic illustrasting the different mechanism of convection development depending on the atmospheric stability; more stable (left) and less stable (right) over wet (blue) and dry (red) surface conditions.

Related to the discussion above, Findell and Eltahir (2003) developed two indices, the Convective Triggering Potential (CTP) and a low-level humidity index (HI_{low}), for determining atmospheric controls on soil moisture-rainfall feedback. The CTP measures the departure from a moist adiabatic temperature lapse rate in the region between 100 and 300 mb (about 1–3 km) above the ground surface. In case of very low HI or very high HI, convection is atmospherically controlled as well as in the case of negative CTP. For intermediate HI values, they found preferred conditions for convective triggering depending on the soil moisture; Convection is favoured either over moist soils when the atmosphere has HI_{low} between 5 and 10(C) and a CTP between 0 and 300 J/kg or over dry soil when HI_{low} and CTP are higher as illustrated in Fig 2-23.

During night-time, soil moisture conditions can also influence directly the thermodynamic and dynamic properties of the atmospheric low levels. Guichard et al. (2009) showed that the nighttime net radiative budget is influenced by atmospheric moisture content and this has an impact on the dynamical profiles in the atmospheric low levels. During the wet season, the incoming shortwave flux at the surface diminishes due to an increase in cloud cover, however, the net longwave increases due to a reduction of the upwelling flux (lower surface temperature). The net radiative budget at the surface has on strong seasonal dependence in West Africa and this has an impact on the dynamics of the low-level jet (see Fig. 2-15 for difference between profiles in May and March).

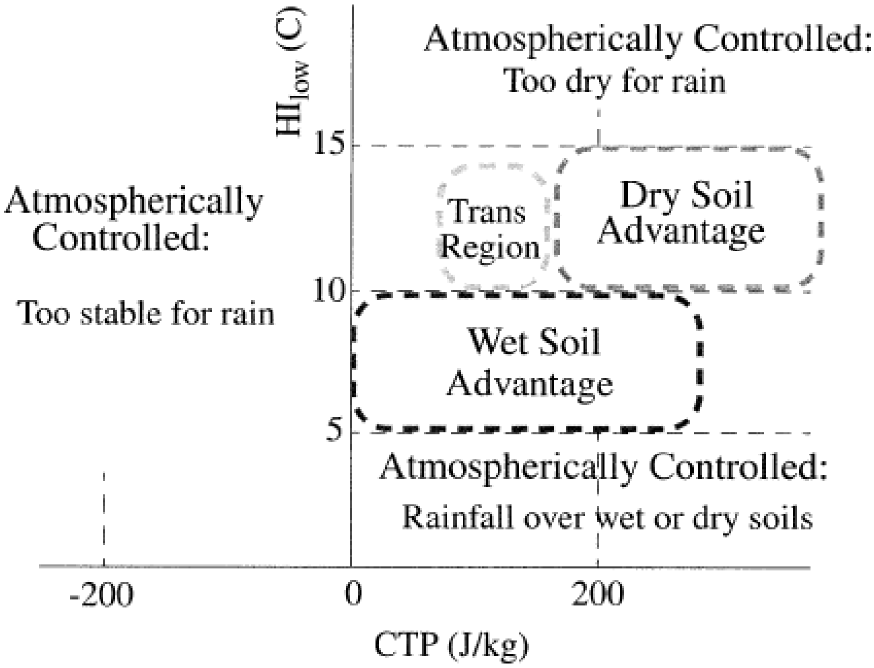

Figure 2-23 : The Convective Triggering Potential (CTP)-HIlow framework for describing atmospheric controls on soil moisture–rainfall feedbacks. Figure from Findell and Eltahir (2003).

2.4.2 Surface heterogeneities and mesoscale circulations

As we have seen in the previous section, surface properties exert a strong control on the net radiation at the surface and then the redistribution of heat and moisture into the atmosphere. The resulting atmospheric-boundary layers can have very different thermodynamic properties (temperature, humidity, turbulence).

In the coastal zones, sea breezes develop when temperature differences increase between land and sea surface. During daytime, usually the land gets warmer than the sea, due to a higher Bowen ratio. A low-level circulation occurs from sea to land and with a return flow above. During night-time, the land cools down faster than the sea, a reversed circulation can develop from the land to the sea if the temperature difference is large enough. These circulations typically favours the formation of convective clouds through an increase of vertical motion that can force convection (Bechtold et al., 1995). This effect has been in particular well observed in Caribbean islands where showering cumulus clouds formed over the island as a result of converging breezes (Malkus, 1963).

Anthes (1984) suggested that the juxtaposition of different vegetation patches in semi-arid regions enhance rainfall (see Fig 2-24). The main mechanisms involved in this were first that an enhancement of vegetation increases the moist static energy at the surface by reducing the albedo and hence increases the net radiation at the surface. This creates more energy available for convection and rainfall. The second mechanism is the formation of a mesoscale circulation that blows from the vegetated zone to the warmer zone that helps the triggering of convection over the second forested patch. This was among the first studies suggesting the impact of mesoscale circulations induced by surface heterogeneities on the development of convective precipitation.

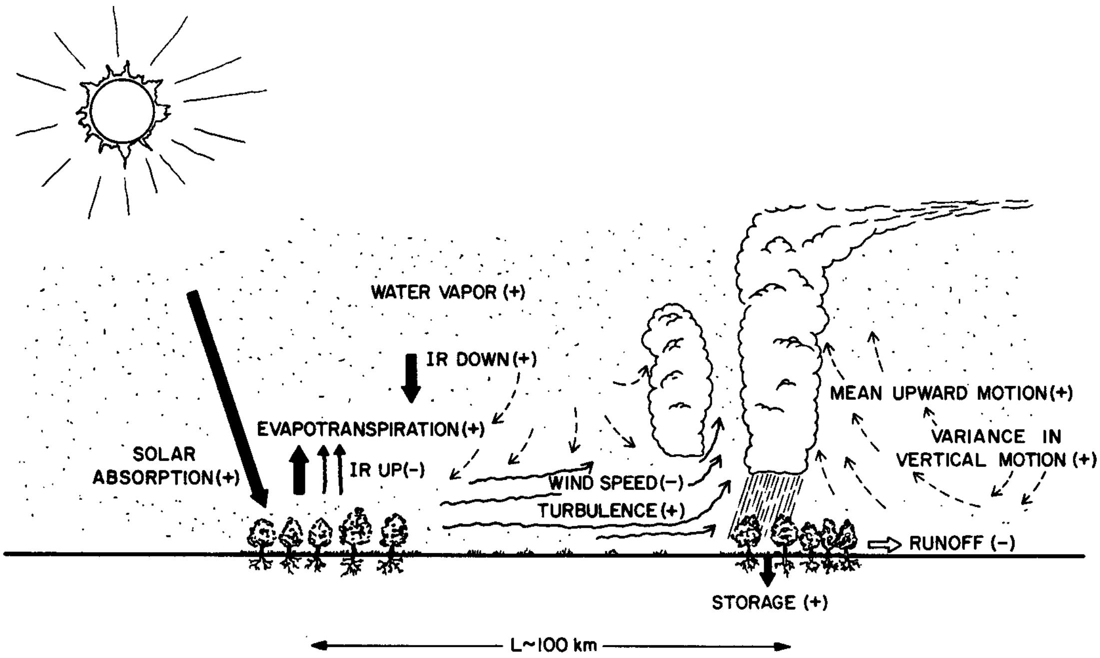

Figure 2-24 : Schematic from Anthes (1984) presenting hypothesised effect of established bands of vegetation in a semi-arid region of previously bare soil. Increases or decreases of an effect are represented by plus or minus symbols, respectively.

A number of modelling studies were carried out in the following decades. For instance, Mahfouf et al. (1987) quantified the circulation induced by surface heterogeneities (soil moisture, soil texture and vegetative cover) on the basis of two-dimensional meso-scale simulations. They showed that horizontal and vertical structures induced by these surface heterogeneities were maximised at the transition zone. A maximum horizontal wind is found on the land side on the sea/land boundary associated with a maximum ascending motion.

The wind blows from sea towards heated land surface during daytime and can have a strong effect on convective cloud formation. This effect has been in particular well observed in Caribbean islands where showering cumulus clouds formed over the island as a result of converging breezes above the island (Malkus, 1963).

A large number of modelling studies have investigated the effect of surface heterogeneities on the dynamics of low-level winds (Mahfouf et al., 1988, Segal et al., 1988, Pielke et al., 2001). The simulations show the setting of breezes between these different zones. The flow goes from the cold to the warm zones. The synoptic conditions generally play a significant role on the characteristics of the circulations. Although several studies indicates that light synoptic conditions favour mesoscale circulations, other studies indicate some evidence of the contrary. Transitions between forests and crops can induce mesoscale circulations (Segal et al., 1988; Rabin et al, 1990; Wang et al., 2009; Garcia-Carreras et al., 2010).

In the Sahel, after a rain event, latent (sensible) heat flux to the atmosphere can increase (decrease) by 100W/m^2 due to an enhancement of soil moisture. This effect can last from few hours up to several days. As the rain is often convective in the Sahel, the pattern is highly non linear. The boundary layer development and atmospheric instability is then perturbed. Boundary layers become shallower and moister. Using satellite data, Taylor and Ellis (2006) found that daytime convection was enhanced over dry zones and suppressed over moister zones. Surface heterogeneities generated by highly variable rainfall on a semi-arid environment creates differences in the boundary layer development. However, the sign of the moisture feedback on the convection seems to be dependent on the timing within the diurnal cycle. It also seems that when a convective system is already well organised with a strong gust front that passage over a moister zone can feed the convection.

Chapter 3
Observations of Diurnal Cycles in West Africa

Contents

3.1 Introduction

As presented in Chapter 2, the diurnal cycle is an important mode of variability in the Tropics (Yang and Slingo, 2001). During the West African Monsoon (WAM) season, strong diurnal cycles are observed, in particular on the monsoon circulation (Parker et al., 2005; Peyrillé et al., 2007, Lothon et al., 2008) and the deep convection (Mathon et al, 2002; Mohr 2004). These key components of the WAM are partly driven by the atmospheric low levels and the meridional gradient in properties of this layer (Gong and Eltahir, 1996). Contrasted diurnal variations in the low levels along the meridional transect significantly affect this gradient and in turn, modulate the monsoon activity.

Due to a lack of observing data, there are only few studies on the diurnal cycles of the West African Monsoon. The Hapex-Sahel campaign, carried out in 1992, provided the first observations on the boundary-layer developments in the Sahel. Radiosoundings launched during the post-onset period and the retreat of the monsoon revealed interesting changes in boundary layer behaviours, but there were limited to a specific site and period of the year. Parker et al. (2005) studied the strong diurnal cycle of the low atmospheric dynamics based on JET2000 observations and ECMWF analysis. They evidenced an acceleration of the monsoon flux in the atmospheric low levels at night in response to the pressure gradient between the Guinean coast and the Saharan heat low (see also p14, 24). This behaviour is inhibited during daytime due to the turbulent mixing in the convective boundary layer. The daytime boundary-layer processes hence favour the conservation of baroclinicity.

The seasonal cycle displays a strong dynamics, which is expected to be accompanied by changes in the diurnal cycle. In short, during the boreal summer, the northward migration of the maximum of insolation generates the inland propagation of a cool and moist flow from the Guinean region towards the Sahel. After a moistening phase, the atmospheric regime changes abruptly due to the northward shift of the Inter Tropical Convergence Zone (ITCZ) from 5°N to 10°N. This transition phase is called the monsoon onset (Janicot et al., 2008). Strong gradients in the thermodynamic and dynamic regimes are observed along the meridional transect going from the Guinean coast up to the limits of the Saharan region. Important couplings are involved between the different processes.

During the AMMA program (Redelsperger et al., 2006) a large observing campaign was carried out to collect observations at different time scales, going from the diurnal to climatologic scale (Parker et al., 2008). It was designed in order to sample the characteristics along the meridional transect, as the monsoon exhibits a remarkable zonal symmetry and a strong meridional climatologic gradient. Another motivation was that by understanding the processes at the diurnal time scale may reap benefits to the larger timescales. On the modelling side, numerical simulations are known to develop drifts within one single 24-hour period (Betts and Jakob, 2002; Guichard et al, 2004). Therefore, getting a better understanding of the diurnal cycles of dynamic and thermodynamic processes appears also as an important step for improving the understanding and predictability of the West African monsoon system.

The first results from the AMMA observations show that nocturnal monsoon flux acceleration is often associated with a nocturnal jet (Lothon et al., 2008; Abdou et al., 2010; and Bain et al., 2010) in the Sahel. A maximum in the nocturnal winds is found at about 0500-0600 UTC at Niamey (Lothon et al., 2008). Associated with this acceleration of the monsoon flow, a strong moistening/cooling of the low levels is observed before the monsoon onset. The moisture is then redistributed vertically during daytime due to turbulent mixing within the boundary layer. A strong diurnal cycle of convective initiation has been observed and documented by Mathon et al. (2002) with satellite data. This study emphasizes the large number of initiations occurring in the end of the afternoon/ beginning of the evening and a strong convective activity during night-time.

In this study, for the first time, the diurnal cycles in the atmospheric low levels are documented and quantified along the meridional transect. The AMMA campaign provided observations to do this at two key stages of the monsoon: in June before the onset and in August during the core of the monsoon. The aim of this study is to get a better understanding of diurnal cycles and the processes controlling them. As a first step towards this goal, in this chapter, the observed diurnal cycles are characterised and extensively discussed.

Dedicated diagnostics have been designed for this purpose. There are further used to evaluate the numerical simulations presented in chapter 4. The data used in this study are described in section 3-2. In section 3-3, the results are presented with, in particular, a characterisation of the diurnal cycles at the surface as well as a description of convective and nocturnal boundary layer behaviours observed along the meridional transect. This chapter ends with conclusions and discussions.

3.2 Data and method

The data were collected during the AMMA campaign in 2006 (Parker et al., 2008). There were two intensive observing periods including one before the monsoon onset (20-29th June 2006) and one during the core of the monsoon (1-15th August 2006). They are hereafter called respectively SOP-1 and SOP-2. These observing periods were devoted to provide the necessary observations at the surface and in the atmospheric low levels to analyse the diurnal cycles along the climatologic transect. In the following, we present the data used in this study to describe and document surface characteristics, atmospheric vertical structures, and cloud covers over the meridional transect.

3.2.1 Vertical structures

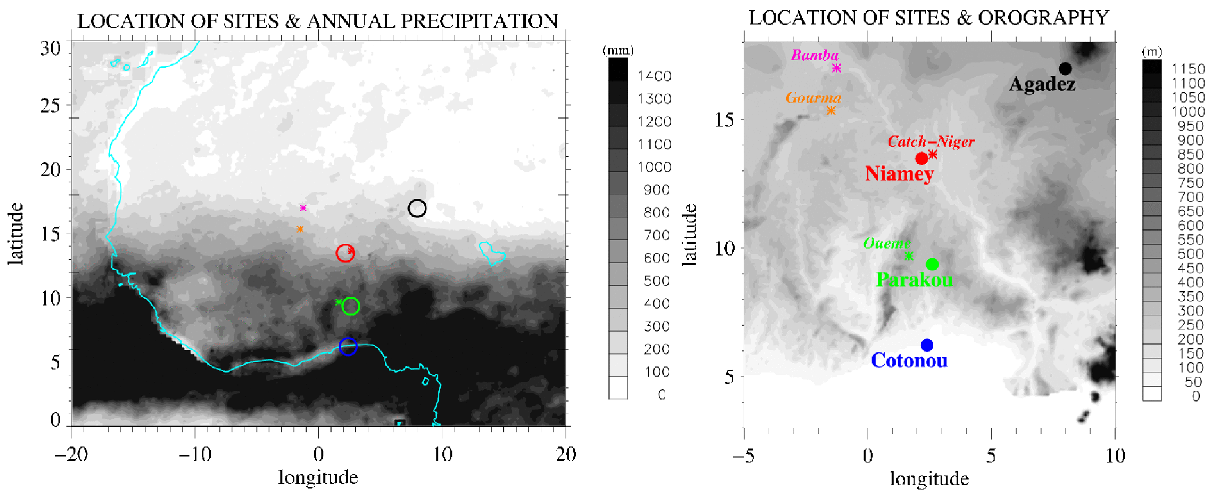

Figure 3-1 : Location of observations sites plotted over mean annual precipitation from GPCP data (left plot); radiosounding stations are indicated using large circles at Cotonou (blue), Parakou (green), Niamey (red) and Agadez (black), the surface flux stations are represented with coloured stars. A zoomed view of the domain is plotted over orography (right plot).

Radiosoundings were launched every three hours during these periods at six different stations (see Fig. 3-1 for localisation). In this study, we focused on the four radiosounding stations (Agadez, Niamey, Parakou and Cotonou) covering the meridional transect (see Tab. 3-1). During the SOP-1 and SOP-2 campaigns, several radiosondes revealed a significant dry bias. This affected half of the soundings in Niamey. In the present study, we use data corrected according to the algorithm developed by Nuret et al. (2008). Data were interpolated on a common grid with a fine resolution of 20m up to 20km.

Several diagnostics on convective boundary-layer heights were tested. Hereafter, convective boundary-layer height estimates were computed based on virtual potential temperature profiles from the radiosoundings. The method consists in comparing the virtual potential temperature (θv) at one level to the mean θv below this level. We get the boundary-layer height when θv of the layer becomes greater than the mean θv+0.25K. The estimates were then checked manually and adjusted when needed.

Similarly, diagnostics on nocturnal boundary layers (height, nocturnal jet, monsoon flow) were tested using different methods. On the nocturnal boundary-layer height, one method consists in calculating a mean temperature lapse rate between 1km and 4km and identify temperature departure from this lapse rate in the low levels. This method works particularly well at Agadez, where the lapse rates within the nocturnal boundary layer and the residual boundary layer are significantly different. The diagnostic of low level jet covers several conditions; the wind speed in the low levels must be greater than the wind in the above free troposphere and must be greater than 5m.s^{-1}. Monsoon flux thickness were estimated using different criteria on the wind profiles, the change in wind direction or the minimum of wind speed. In most cases, the different criteria used to identify the monsoon flow were in good agreement, but the diagnostics were checked manually and adjusted when needed.

3.2.2 Surface data

Surface measurements were collected at different sites. Most of the time collocated with or close to radiosounding launching sites. However, when the measurements were not available, data from relatively close sites or sites which sample the same part of the gradient were used when relevant (see Fig. 3-1 for localisation of the measurement sites).

Radiative measurements at the surface from the IMPETUS network were recorded at Cotonou and Parakou (Fink et al., 2006, http://www.impetus.uni-koeln.de/). It includes upwelling and downwelling shortwave and longwave fluxes. At Niamey, the Atmospheric Radiation Measurement (ARM) station recorded radiative fluxes as well as turbulent fluxes (Miller and Slingo, 2007).

There were no turbulent flux measurements available at Cotonou, Parakou and neither at Agadez. However, turbulent and/or radiative fluxes were recorded at Nalohou, Kelma and Agoufou. Nalohou is situated in the Ouémé basin, 100km away from Parakou (see Fig 3-1). This site is characterised by slightly more vegetation than at Parakou, so it may overestimate the latent heat flux and underestimate the sensible heat fluxes compared to Parakou. Agoufou and Kelma are located in the Gourma region and is representative of Central to Northern Sahel (Mougin et al., 2009) around 15°N and are therefore closer to Agadez in terms of climatology. The surface properties are also slightly different from the ones at Agadez. Kelma is a seasonally flooded open woodland site with 40% tree cover whereas Agoufou is characterised by a grassland that grows over a bright sandy soil (Timouk et al., 2009). Even if the fluxes at these sites may be different from the ones at the radiosounding sites, they are relevant to sample surface energetic along the transect.

In addition, SYNOP data including T, qv, ws, wd at 2 m above the ground were collected at the four radiosounding sites (Agadez, Niamey, Parakou and Cotonou). These surface measurements were recorded over several years and hence allow us to assess the representativity of the intensive observing periods compared to longer timescales.

Site	Country	Latitude	Longitude	Altitude	Sounding	Rad Flux	Tur Flux
Agadez	Niger	16°97 N	7°99 E	501m	**8/day**	No	**No**
Kelma	Mali	15°50 N	7°99 E	330m	No	**Yes**	**Yes**
Agoufou	Mali	15°34 N	1°48W	330m	No	**Yes**	**No**
Niamey	Niger	13°48 N	2°17 E	222m	**8/day**	**Yes**	**Yes**
Parakou	Benin	9°36 N	2°61 E	392m	**8/day**	**Yes**	**No**
Nalohou	Benin	9°74 N	1°60 E	449m	No	No	**Only H**
Cotonou	Benin	6°52 N	2°40 E	5m	**8/day**	**Yes**	**No**

Table 3-1 : ***Geographical characteristics of the measurement sites during the SOP-1 and SOP-2 and the list of measurements carried out at each site.***

3.2.3 Documentation of clouds and convection

Hereafter, information on clouds is used to document the context of the two periods (CLOUDSAT and CALIPSO) as well as to track further synoptic scale fluctuations (ARM data and IRT).

The vertical structure of the cloud cover along the meridional transect comes from Calipso and Cloudsat measurements. They were used to compute monthly mean occurrences of clouds over the meridional transect (Bouniol et al., 2010). Data were available from mid-June 2006. Therefore, not enough data was available for computing a monthly mean for June 2006. However, a comparison between three years (2007-2009) showed that the monthly mean occurrence of clouds do not vary much from one year to the other. Hence, the monthly mean of June 2008 was used in this study for characterising the cloud cover along the transect during this pre-onset period.

At Niamey, observations from the cloud radar and the lidar of the Atmospheric Radiation Measurement Program (ARM) were available during the two SOPs. It provides in particular, information on the cloud cover in the close surrounding of the station. Further information on the cloud cover can also be retrieved from satellite measurements. Brightness temperatures (BT) are thermal emissions of the atmosphere detected by satellite passive instruments. The data used here are measurements at 10.8 micron from Meteosat Second Generation satellite. For our study, we averaged them over a 0.25°x0.25° zone around the site locations. They give an estimation of the cloudiness. The shallow cumulus and stratocumulus clouds are however hard to detect with satellite measurements as they emit longwave radiation at a temperature close to the surface temperature. Minimum, maximum and variability of BT were also computed to give an estimation of sub-scale cloud cover variability. If there is a cloud (and aerosols) free pixel in the selected zone, the maximum temperature can be considered as a good proxy for land surface temperature. The minimum temperature gives information on the highest cloud within the selected zone. The variability of BT reflects whether the cloud field is homogeneous or heterogeneous within the selected zone. A threshold of -40°C was used to flag the development of deep convection.

3.3 Results

The following section presents the analysis of observations made during the two intensive observing periods, SOP-1 and SOP-2. After describing the context of the study periods, this section focuses on the diurnal cycles observed at the surface and in the atmospheric low levels along the meridional transect.

3.3.1 Context of the periods

During the few months preceding the monsoon start, the monsoon flow progresses northwards bringing moisture onto the continent. During the month of June, the position of the Inter-Tropical Discontinuity (ITD), which corresponds to the boundary between the monsoon flow and the Harmattan, oscillates between the North of Niamey and South of Agadez (at around 0°-2E°). Indeed, in Niamey, the atmosphere is already quite moist in June with a precipitable water amount around 40kg.m^{-2} (see Appendix B).

Within the AMMA-MIP project (Hourdin et al. 2010), a large material documents the broad features of the dynamics and thermodynamics of the meridional transect and its changes from month to month as revealed by NWP analyses (see http://www.cnrm.meteo.fr/amma-moana/transect/indexproduct.html). Here, it is illustrated with information on clouds. Figure 3-2 shows the monthly mean occurrence of clouds over the meridional transect. During the month of June, the ITCZ, which is linked to the rainy zone, extends meridionally from 2°N to 8°N (including the Guinean and Soudanian regions). Over the Sahelian region, some shallow cumulus clouds develop quite often, whereas deep convection rarely occurs. High cirrus clouds are often present over the Sahel and Sahara. Mineral aerosol concentration is high in the Sahel, especially in the low troposphere (Slingo et al., 2001; McFarlane et al., 2009).

The onset corresponds to the start of the rainy season over the Sahel. It is associated with the northward shift of the ITCZ from 5°N to 10°N. According to Janicot and Sultan (2007), the average onset period is centred around the 24th of June. In 2006, the onset was slightly delayed compared to this mean value, it occurred between the 25th June to 10th July with the rainy period starting at the end of this period at Niamey (Janicot et al., 2008). The shift of the ITCZ is accompanied by an abrupt change in atmospheric regimes.

During the post-onset period, the ITD has migrated to the North of Agadez. The rainy zone extends from 8°N to 16°N (Soudanian and Sahelian regions) (see Fig. 3-2 bottom plot) with the most intense precipitation located around 10°N. Deep convection is suppressed over the Guinean region and is replaced by a layer of low-level stratiform clouds.

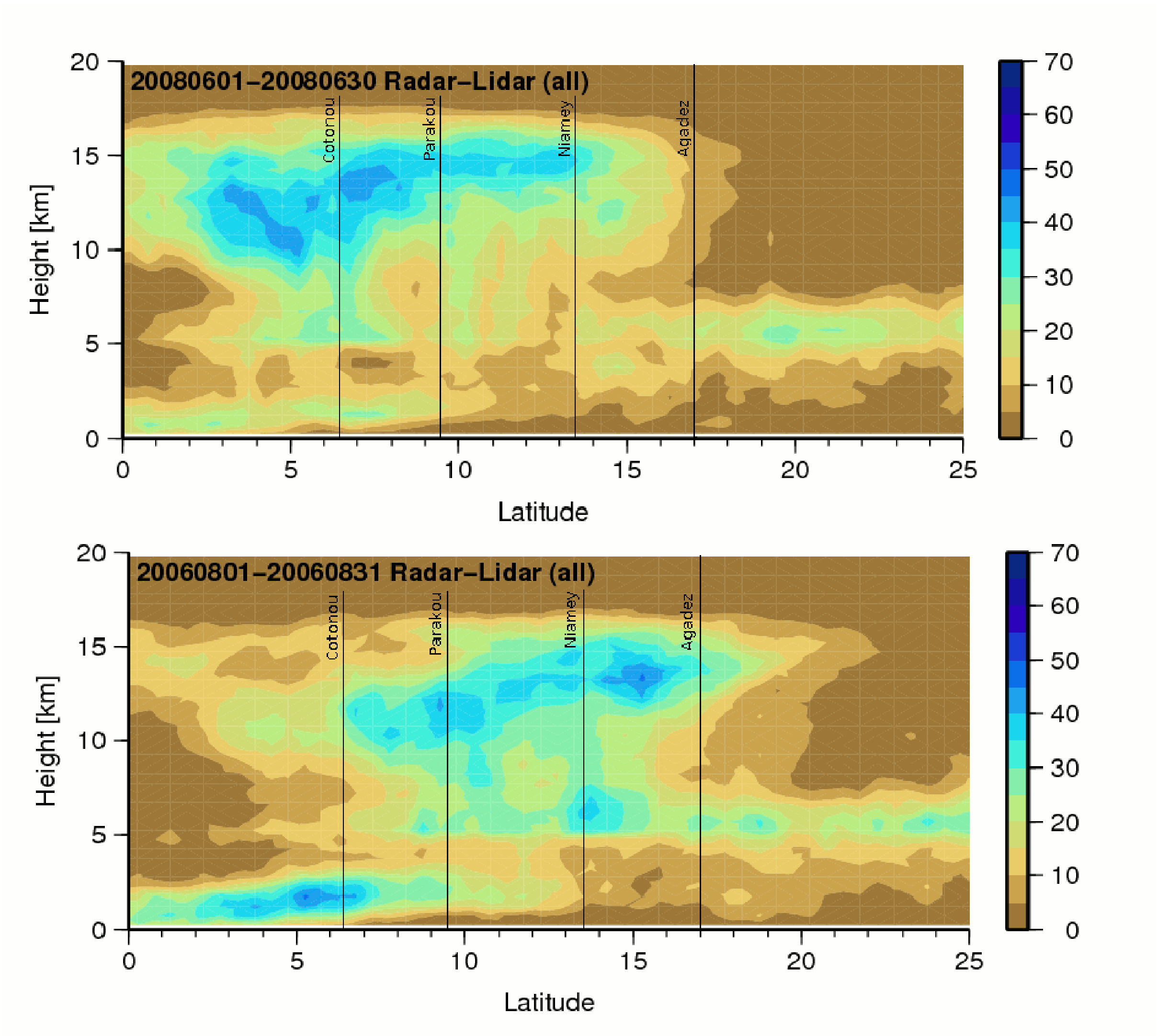

Figure 3-2 : June and August monthly mean cloud occurrence(in %) along the meridional transect averaged between 10°E-10°W derived from CALIPSO and CLOUDSAT data Figure from Bouniol et al., (2010).

The SOP-1 and SOP-2 are centred on key stages of the WAM. The SOP-1 takes place at the end of the moistening phase (pre-onset period) and SOP-2 was carried out a few weeks after the onset of the monsoon (post-onset period). The variability of cloud cover is well and more precisely captured during these two periods at the four radiosounding sites using the evolution of mean BT (in black) as a proxy for cloud cover (see Figs 3-3 & 3-4).

At Agadez, the BT is dominated by the diurnal cycle of surface temperature, meaning that only few sparse and shallow clouds overcast the sky. Indeed, most of the time, the mean BT follows the maximum BT (in red) corresponding to the surface temperature. The minimum BT (in blue dotted line) exhibits some strong negative values related to localised cumulus congestus clouds.

At Niamey, there are slightly more shallow cumulus clouds than at Agadez, as attested by the minimum BT values. There are also some precipitating cloud systems passing over. The weather stations located at Niamey and in the surrounding of recorded four precipitating events which gave between 5 and 10mm of rain in total over the period (21, 25, 27 and 29 June).

In Parakou and Cotonou, the cloud cover is more important, consistent with the monthly mean cloud occurrence. At Parakou, during the SOP-1 deep convection developed almost every day except on the 26th, 27th and 28th of June giving about 23mm of rain in total from REF2 estimates (estimates to take with caution). Shallow cumulus clouds appeared to form easily during daytime. At Cotonou, stratocumulus are frequently observed and regularly, deep convection bring large quantities of rain which agrees with Fig 3-2. The amount of accumulated rain received at Cotonou during SOP-1 was estimated to 78mm based on REF2 satellite measurements.

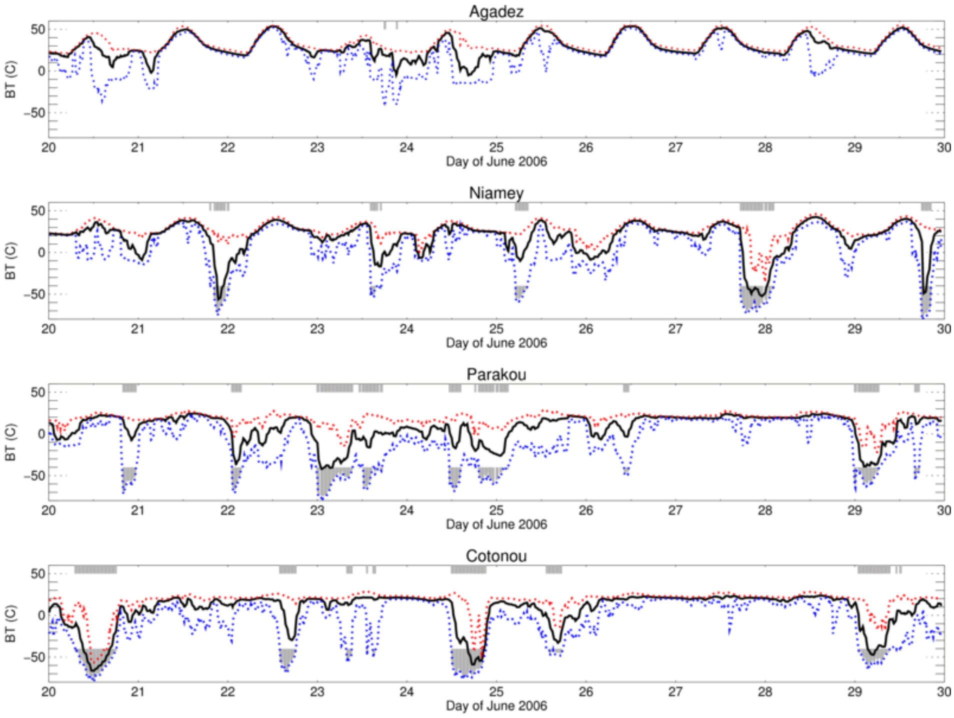

Figure 3-3 : Mean(full black line), minimum(dotted blue line) and maximum (dotted red line) brigthness temperature over a 0.25deg x 0.25deg centered on the 4 sites: Agadez, Niamey, Parakou and Cotonou during the SOP-1. The grey shading represents the development of deep convection.

By contrast, during the SOP-2 (Fig 3-4), deep convection develops frequently in the Sahelian and Soudanian zones, whereas it is suppressed over the Guinean coast. The cloudiness is still important in Cotonou, but deep convection is significantly suppressed, as shown by the absence of strong negative peaks in the BT time series (only 37 mm of rain estimated from REF2 satellite measurements over the 10 first days). This period corresponds to the little dry season taking place along the Guinean coast. More deep convection is observed at Agadez, Niamey and Parakou compared to before the onset. Deep convection reaches higher altitudes at Agadez and Niamey compared to Parakou as can be seen more clearly on Fig 3-2 (see also Zipser et al., 2006). However, the amount of precipitation generated by convective systems is much more important at Parakou (more than 100mm of rain from REF2 measurements).

The characteristics of the two intensive periods are representative of respectively June and August months as attested by the similarities between the composite derived for the two intensive periods and the full month for four consecutive years (2005 to 2008) (not shown) as well as the comparison with the vertical cross section of cloud occurrence.

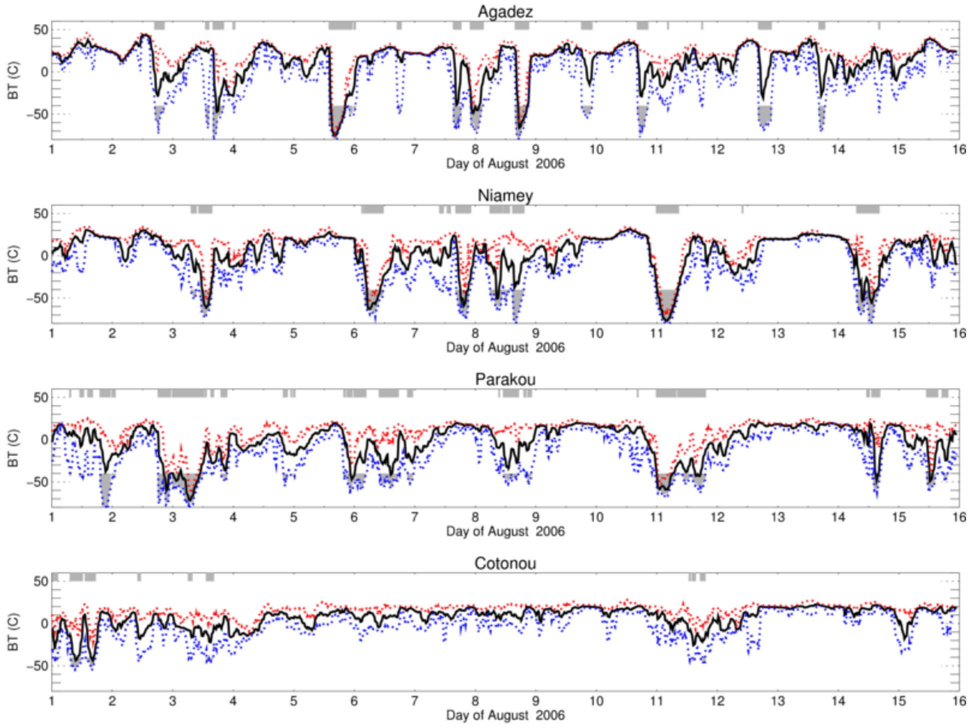

Figure 3-4 : Same as Fig. 3-3 for the SOP-2.

3.3.2 Diurnal cycles at the surface: SYNOP and fluxes

– ***Pre-onset fluxes***

Surface turbulent fluxes are important to determine the atmospheric properties at the surface and in the low levels. Figure 3-5 shows a diurnal composite of the surface net radiation along the transect. The net radiation corresponds to the difference between the incoming radiation (longwave and shortwave) minus the outgoing radiation.

During the SOP-1, no obvious meridional gradient of net radiation is observed along the transect. The two maximum values of Rnet are found at Cotonou (6.5°N) and Kelma (15°N) during the SOP-1 reaching values up to about 550W.m^{-2} at midday. At Niamey and Parakou, Rnet is up to about 450-500W.m^{-2}. After sunset, Rnet becomes negative with the strongest negative values found in the early evening (-80 W.m^{-2}) in the Sahel (Niamey and Kelma). Throughout the night, the intensity of negative Rnet decreases especially in the Guinean and Soudanian regions.

The incoming and upwelling components of the net radiation (SWin, SWup, LWin, LWup) are plotted in Figs. 3-6 and 3-7. During the SOP-1 (left column), the maximum SWin is found at Niamey (max:900W.m^{-2}) corresponding to the zone combining high incoming solar radiation at the top of the atmosphere (TOA) and sparse cloud cover. At the other stations, SWin is lower due in particular to cloud cover (Cotonou, 750 W.m^{-2}; Parakou, 650 W.m^{-2}) or lower SWin at the TOA (Kelma, Agoufou, 850 W.m^{-2}). In the Sahel, mineral aerosols also play a significant role in reflecting/absorbing SWin prior to the monsoon onset. The diurnal cycle of SWin is not symetrical at all stations. Sometimes, the maximum is reached before midday like at Parakou and Cotonou, which is linked to the diurnal cycle of convection.

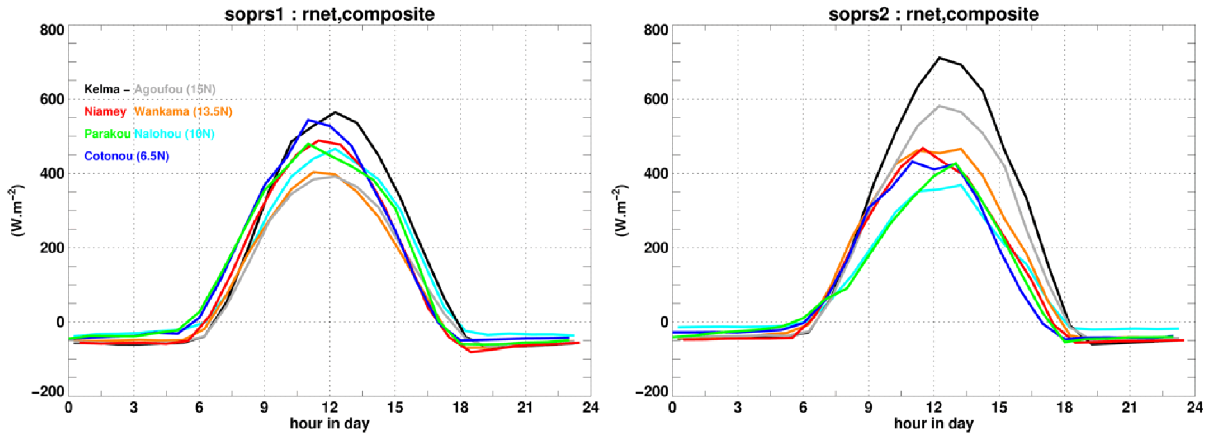

Figure 3-5 : Net radiation fluxes at the surface during the SOP-1 and SOP-2 along the meridional transect: Kelma -Agoufou (15°N , in black and grey), Niamey - Agoufou (13°5N, in red and orange), Parakou - Nalohou (9°5N, in green and light blue) and Cotonou (6°5N, in dark blue).

The SWup is the fraction of incoming solar radiation that is reflected by the surface. At Niamey, Wankama and Agoufou, a high suface albedo (0.27-0.35) is responsible for a strong SWup which contributes to reducing the net radiation. This is partly due to bright surfaces. The albedo at the other stations are lower (0.15-0.18) either due to vegetation cover (Cotonou, Parakou) or darker soil (Kelma).

The LWin depends on the temperature stratification and the constituents (gases, clouds, aerosols) of the atmosphere. Over the transect, the LWin has a mean value between 400 and 440 W.m^{-2} with larger values in the North than in the South. It exhibits a diurnal cycle which is stronger in the Sahel (ΔLWin~60-70W.m^{-2}) compared to the Soudanian and Guinean regions (ΔLWin~20-30W.m^{-2}). Interestingly, the timings of the LWin diurnal cycles are different along the transect. The maxima are reached earlier in the Southern than in the Northern part of the transect. The differences in LWin are smallest in the morning (0600 UTC) and largest in the late of the afternoon (1700 UTC).

The LWup is the radiation emitted by the surface; its intensity depends on the surface temperature to the fourth power and its emissivity. It is higher at Niamey and Kelma (470-630 W.m^{-2}) compared to Cotonou, Parakou and Nalohou (430-500 W.m^{-2}). Niamey and Kelma which have different LWin diurnal cycles, have similar LWup cycles. The net longwave radiation is always negative which corresponds to surface energy loose via longwave emission.

To sum up, during daytime, the net radiation is mainly driven by the incoming shortwave radiation. Large difference in SWin are observed along the transect but, the other components of the radiative budget tend to reduce the differences observed from one site to the other (strong albedo and/or LWup). This leads to a smaller difference in surface net radiation along the transect.

On the other hand, the net radiation is partitioned differently between the ground, the sensible and the latent heat fluxes. This partitioning depends on the Bowen ratio which is mainly controlled by soil properties (moisture content, soil composition, vegetation cover). A gradient is observed in the turbulent flux at the surface as shown in Fig 3-8. Before the onset, as one goes to the North, the maximum of sensible heat flux increases. The sensible heat flux reaches very high values in the Sahel (up to 330W/m² at Niamey and 400 W/m² at Kelma). The differences between Kelma and Niamey are predominantly due to difference in the net radiation as the latent heat flux is very weak before the onset in this region. In the South, the sensible heat flux is weaker associated with higher soil moisture, leading to larger latent heat fluxes.

– ***Post-onset fluxes***

After the monsoon onset, a slight decrease is observed in the net radiation during daytime (-5-10%) as well as during night-time compared to pre-onset period, except at Kelma (and Agoufou), where Rnet reaches up to 700 $W.m^{-2}$. Maximum downwelling shortwave radiation is reduced at all sites (-100-200$W.m^{-2}$) except at Kelma and Agoufou where it does not vary much. The decrease is mostly observed between 1100 UTC and 1600 UTC at Niamey and Cotonou and a bit earlier at Parakou. This is probably due to the increase in cloud cover as seen in Fig 3-2 & 3-3; either cumulus clouds in the Sahel/Soudanian region or stratocumulus clouds over the Guinean coast. Moreover, a change in the asymmetry of SWin at Parakou is observed; the maximum of SWin is found in the afternoon.

The surface albedo slightly decreases in the Sahel which may be linked to the vegetation growth. The maximum LWin and up substantially diminish over the Sahel towards behaviours closer to the ones observed in the South. This is due to lower surface and atmospheric temperatures, as discussed in more details in the following sections.

In the Southern part of the transect, the decrease in Rnet can be mainly attributed to the decrease in SWin. This decrease in Rnet is associated with an increase in cloud cover. This is somewhat damped by a reduction in surface albedo and decrease in Lwup (Niamey). Further North, at Kelma and Agoufou, the SWin does not decrease compared to the SOP-1, the upwelling SW and LW fluxes decreases and the LWin only slightly decreases (few tens of $W.m^{-2}$). Therefore, the decrease in upwelling fluxes explains the increase in Rnet.

A moistening of the soil leads to a drop of the sensible heat flux in the Sahel (-40% at Niamey, -80% at Kelma) as illustrated in Fig 3-8 . The larger reduction of sensible heat flux at Kelma is due to the surface properties. Indeed, during the monsoon season, this area is partly flooded providing more water available for evaporation. At Nalohou (Parakou), the sensible heat flux remains the same as before the onset even with a smaller Rnet. The sensible heat flux warms the atmosphere during daytime and cools it down at night when negative. Meanwhile, the latent heat flux moistens the atmosphere during daytime as Rnet is positive. The properties of the atmosphere at the surface and in the low levels are hence directly linked to these surface fluxes.

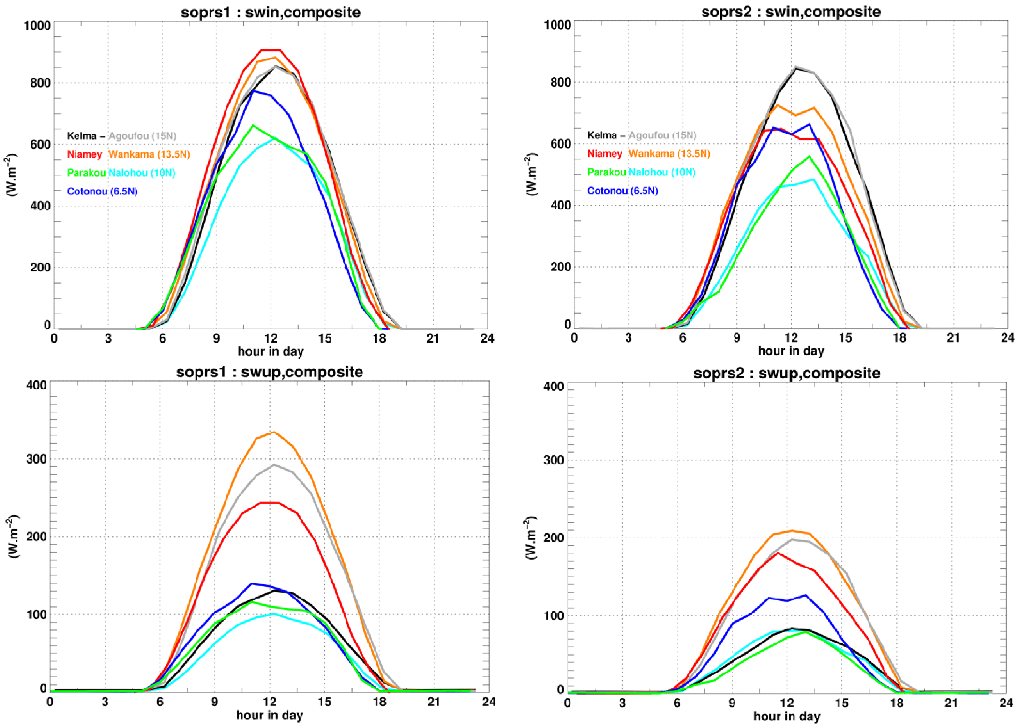

Figure 3-6 : Downwelling and upwelling longwave fluxes at the surface during the SOP-1 (left plot) and SOP-2 (right plot) along the meridional transect: Kelma -Agoufou (15°N , in black and grey), Niamey - Agoufou (13°5N, in red and orange), Parakou - Nalohou (9°5N, in green and light blue) and Cotonou (6°5N, in dark blue).

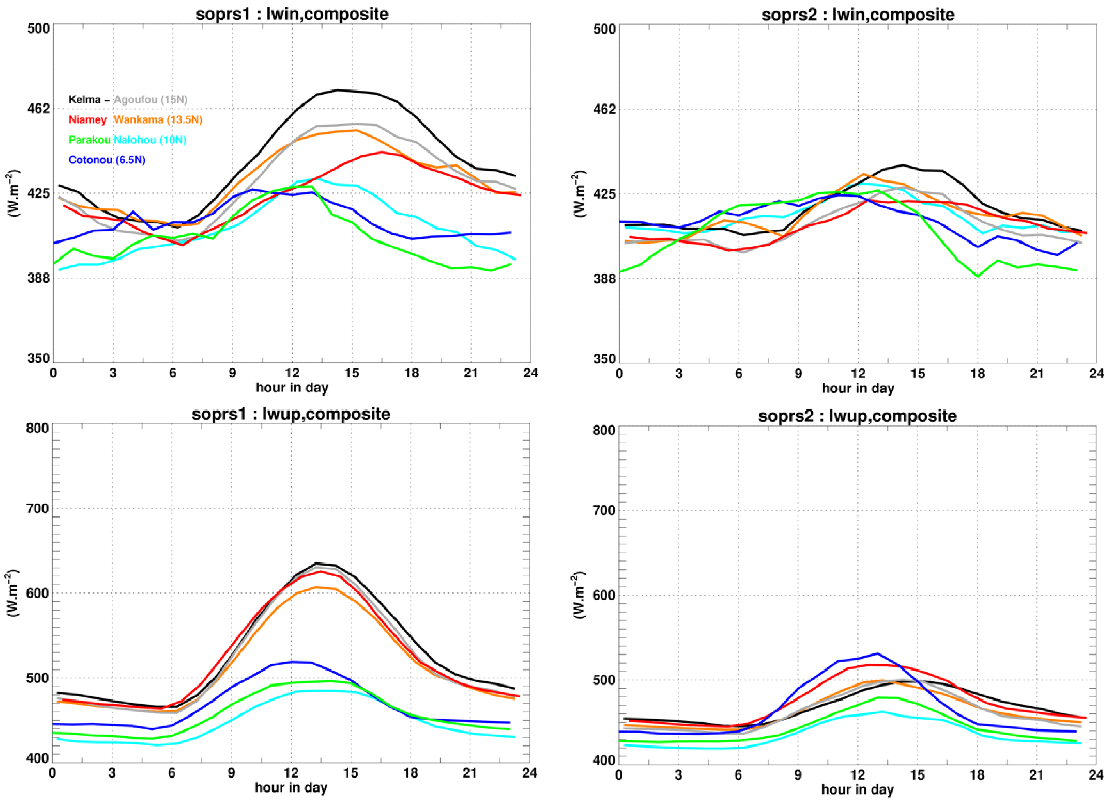

Figure 3-7 : same as Fig. 3-6 for the longwave fluxes.

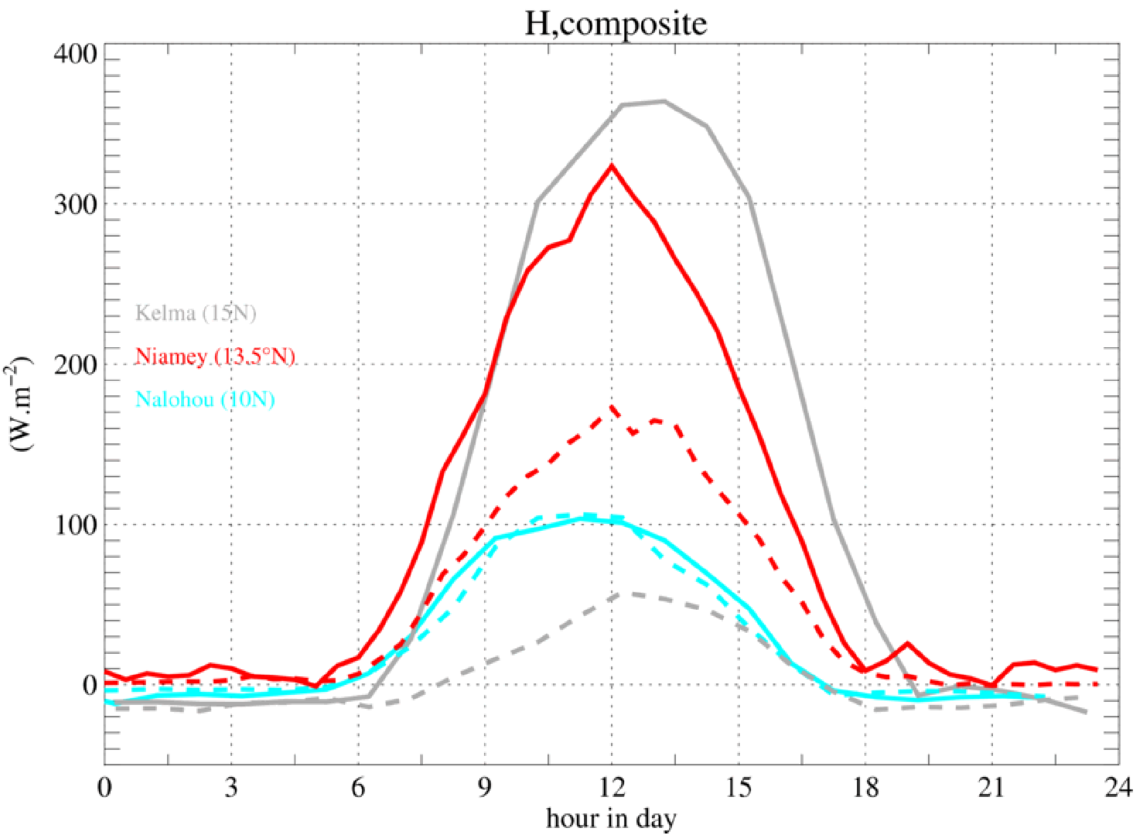

Figure 3-8 : Composite diurnal cycle of sensible heat flux during the SOP-1(full line) and the SOP-2 (dashed line) at four different stations along the meridional transect: Nalohou,10°N (in blue), Niamey,13°N (in red), Kelma, 15°N (in grey).

– ***SYNOPs***

Because high-resolution time series of surface meteorology were not available for all sites, SYNOP data are used instead, in order to provide a comparison among sites. The thermodynamic diurnal cycles at the surface (2m above ground level) computed from the SYNOP data are shown in Fig 3-9.

During the pre-onset period (left column), the amplitude of potential temperature (θ) diurnal cycle increases as one moves northwards, with a Δθ (diurnal potential temperature range) of 4K at Cotonou up to 12.7K at Agadez (cf Tab 3-1). The mean specific humidity decreases when moving northwards (19g.kg^{-1} at Cotonou and 6g.kg^{-1} at Agadez) whereas the amplitude of its diurnal cycle increases with latitude (Δqv=1 g.kg^{-1} at Cotonou and Δqv=3 g.kg^{-1} at Agadez). The diurnal cycles observed along the transect are different; in Parakou and Cotonou, qv becomes larger during daytime, whereas in the Sahel, we observe a daytime drying.

Large contrasts in relative humidity (RH) are found along the transect. Diurnal amplitude increasing with decreasing mean RH values (except at Agadez due to very low humidity content). At Cotonou and Parakou, night-time values are very close to saturation, whereas in the Sahel, values are much lower (10-30%). RH always becomes lower during daytime due to an increase in temperature (and decrease in specific humidity in the Sahel). By contrast, it increases at sunset associated with an

	Δθ (K)		Δqv (g/kg)		ΔRH(%)		ΔθE(K)	
Agadez	12.7	10.1	3.25	2.83	20.0	34.6	11.1	8.9
Niamey	9.3	5.8	2.77	1.43	32.7	26.9	7.2	5.2
Parakou	6.4	4.0	1.50	1.07	24.4	14.7	12.3	8.1
Cotonou	4.0	2.7	0.67	0.36	16.6	12.3	7.0	4.0

Table 3-2 : ***Diurnal Range of potential temperature (Δθ), specific humidity (Δqv), relative humidity (ΔRH), equivalent potential temperature (Δθe) and wind speed (Δws) at the surface during the SOP-1 (blue columns) and during the SOP-2 (white columns). Values calculated from the SYNOP data.***

increase in specific humidity and decrease in temperature. This parameter gives an information on the potential for low-level cloud formation.

The equivalent potential temperature (θe), which results from a combination of potential temperature and water vapour content, is important for deep convection considerations. The meridional gradient in equivalent potential temperature is linked to the monsoon flow penetration onto the continent. θe is much smaller at Agadez (330-340K) compared to the other stations along the transect (350-360K) leading to a large meridional gradient. The maximum of θe is reached around midday and the minimum at 0600 UTC. Even though the maximum Δθ and Δqv are found at Agadez, the maximum of Δθe is reached at Parakou (Δθe=12.3K).

As noted for the surface energy, after the onset (see Fig 3-9 right column), the contrasts in surface meteorology along the meridional transect are also smoothed. There is a global moistening and decrease in temperature over the Sahelian and Soudanian regions. The amplitude of potential temperature and specific humidity diurnal cycles over the Sahel is reduced (e.g. at Niamey: Δθ=5.8K & Δqv=1.4g.kg^{-1}). RH and θe significantly increase at Niamey and Agadez.

The composite of thermodynamic properties in the SYNOP data were also done over the months of June and August 2006. They give similar composite diurnal cycles (not shown) compared to the two SOPs. Composites were also done for four consecutive years, monthly composites were also in agreement with the plots shown here. This gives us confidence on the representativeness of the two SOPs.

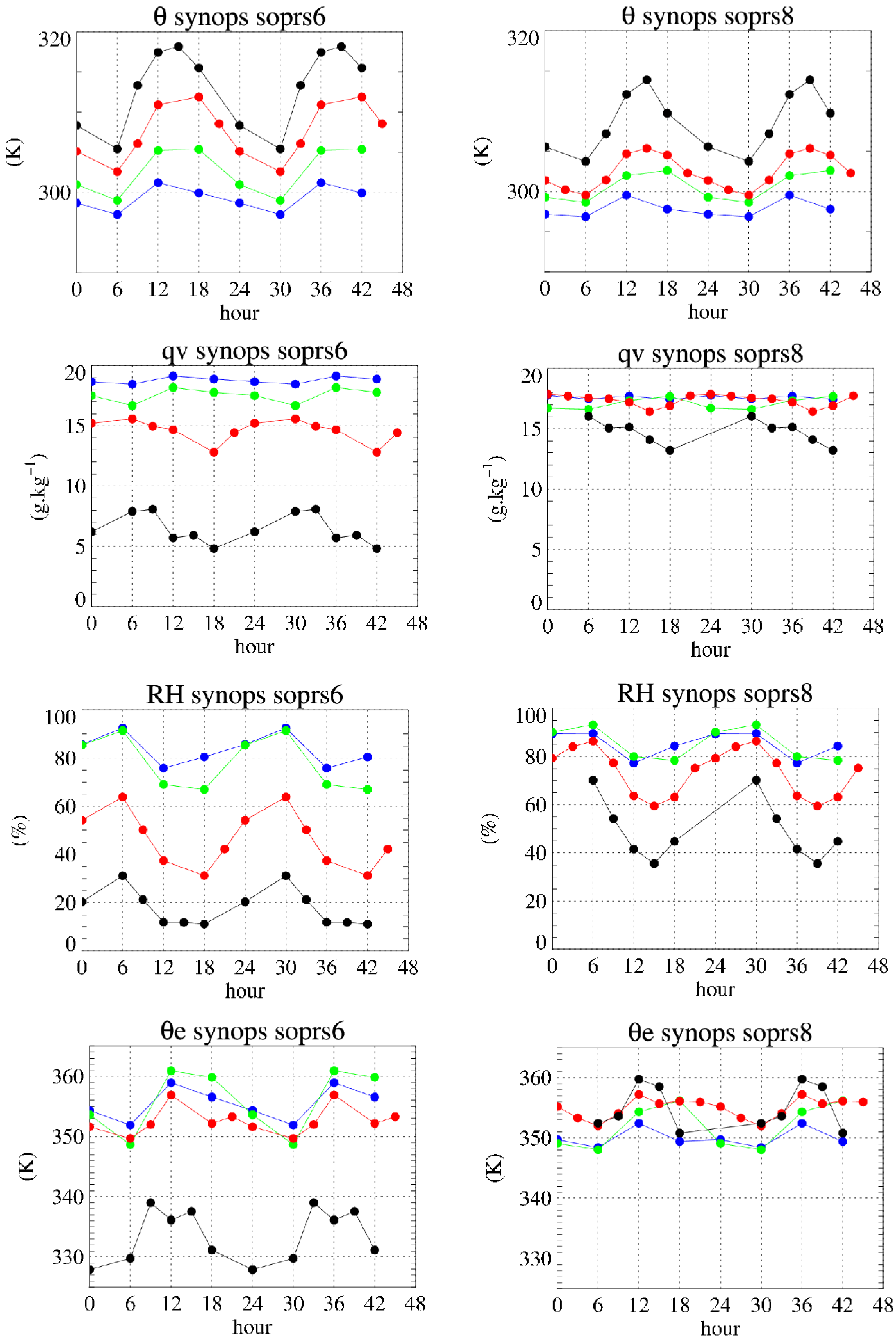

Figure 3-9 : Composite diurnal cycles of thermodynamic and dynamical properties at the surface (2m above the ground) computed from the SYNOP data at Agadez (in black), Niamey (in red), Parakou (in green) and Cotonou (in blue): potential temperature (top plots), specific humidity (top middle plots), relative humidity (bottom middle plot) and equivalent potential temperature (bottom plots) are shown.

3.3.3 Diurnal Cycles in the atmospheric low-levels

Compared to the SYNOP data, the radiosoundings are available over a shorter period (only the two SOPs), but they allow us to study the vertical structures of the atmosphere. They also allow us to assess to what extend the information provided by SYNOP data (close to the surface) inform on the lower atmospheric levels.

Figure 3-10 shows the composite diurnal cycles of the thermodynamic (θ, qv) and dynamic (wind speed) properties of the atmospheric low-levels (0-500m) considering the 'dry properties' of the layer, before and after the onset, whereas Fig. 3-11 presents the 'cloudy properties' of the atmospheric low levels with relative humidity and equivalent potential temperature.

– ***Contrasted diurnal cycles before the monsoon: amplitude and timing***

Before the onset of the monsoon, strong meridional contrasts in thermodynamic and dynamical properties can also be observed in the radiosoundings. There are larger diurnal cycle amplitudes of potential temperature and specific humidity in the North than in the South, as seen at the surface in the SYNOP data. Nevertheless, the contrasts in amplitude are less important when considering the low-levels values (see Tab 3-3). This is particularly striking at Agadez, where the amplitude is 12.7K at 2m above the ground but only 5.9K for low-levels values. The night-time surface temperature almost reach the surface temperatures found at Niamey (see Fig 3-8), whereas when considering the low levels (0-500m), the cooling is much less intense at Agadez. Hence, Agadez exhibits a weaker low-level diurnal cycle of potential temperature than Niamey where Δθ=8.1K. This is directly linked to a distinct nocturnal boundary-layer development, which will be explained in the next sections. Cotonou has also a low-level diurnal cycle much weaker than at the surface (Δθ=1.4K compared to Δθ=4K at the surface) associated with less warming.

The timing of the temperature diurnal cycles is also different along the transect. At Agadez, a rapid increase is observed in the late morning followed by a weak increase. The maximum value is reached around 1500-1600 UTC. This behaviour is also observed in the SYNOP data. In Niamey, a more progressive and long lasting warming occurs; the low-level potential temperature reaches its maximum value at 1800 UTC. The maximum temperatures are reached earlier at Parakou and especially at Cotonou, around midday. The cooling is progressive throughout the night at Agadez, whereas at Niamey, there is a strong cooling in the early evening possibly linked to monsoon flux advection and then, the temperature cools down progressively.

We have quantified the variability among the 10 different days of the period by computing the standard deviation for each time of the diurnal cycle. The maximum of day-to-day variability of θ is found at Niamey and Parakou in the afternoon/early evening, whereas the minimum is observed in the morning, a feature which also distinguishes night-time to daytime regimes

	Δθ (K)		Δ qv (g/kg)		Δ RH (%)		Δ θe (K)		Δ ws (m.s^{-1})	
Agadez	5.9	6.3	3.1	2.6	13.5	24.9	6.8	3.3	3.4	1.9
Niamey	8.1	4.3	4.0	2.2	31.3	19.6	4.5	6.4	4.6	2.1
Parakou	4.8	3.6	2.7	1.1	27.6	19.9	6.2	4.9	3.6	3.4
Cotonou	1.4	0.9	1.9	1.8	14.3	12.2	4.3	4.6	2.6	0.9

Table 3-3 : ***Diurnal Range of potential temperature (Δθ), specific humidity (Δqv), relative humidity (ΔRH), equivalent potential temperature (Δθe) and wind speed (Δws) in the 0-500m atmospheric low levels during the SOP-1 (blue columns) and during the SOP-2 (white columns).***

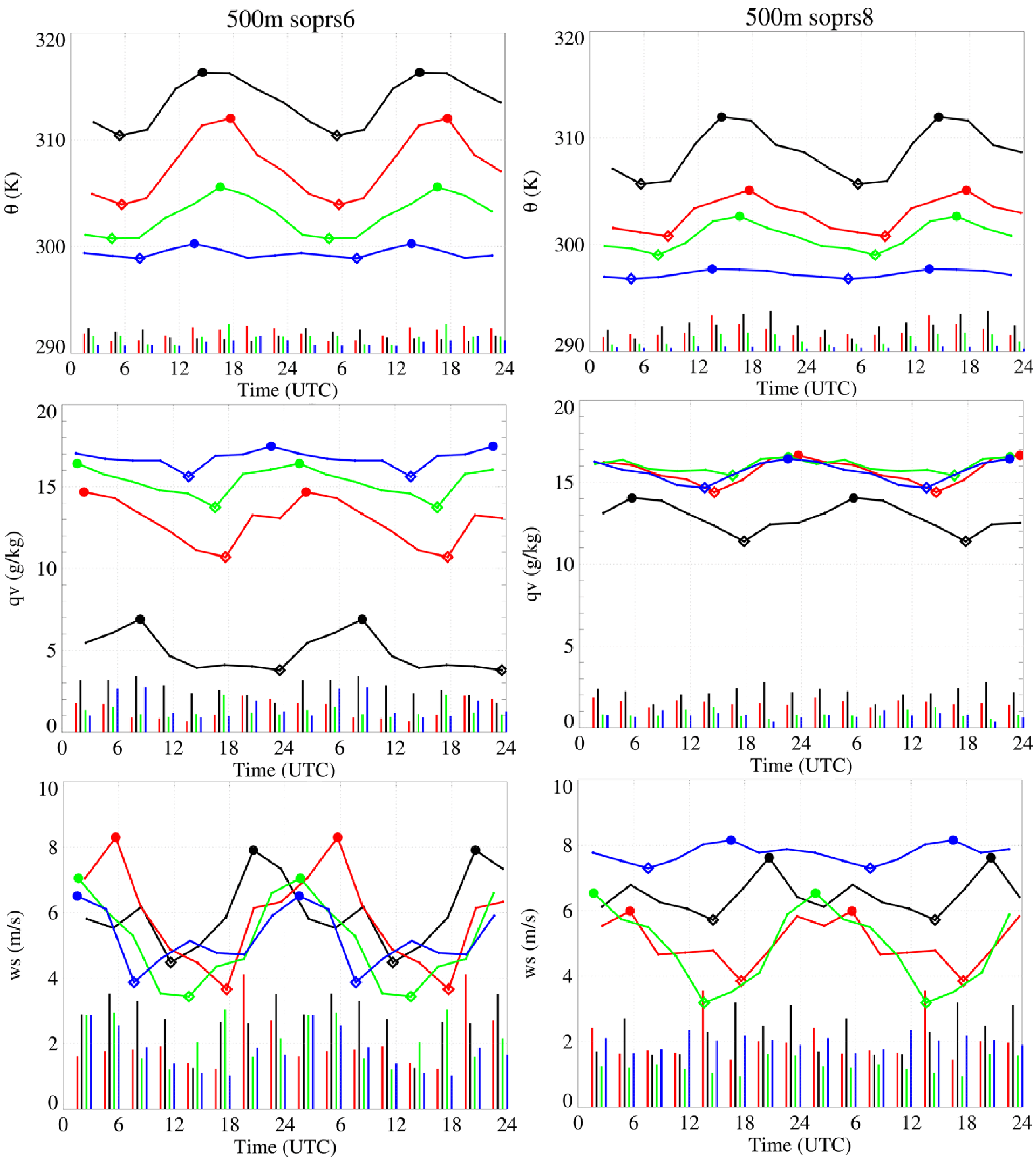

Figure 3-10 : Composite diurnal cycles of thermodynamic and dynamic properties of the atmospheric low levels(0-500m) during SOP-1 (first column) and SOP-2 (second column) at Agadez (in black), Niamey (in red), Parakou (in green) and Cotonou (in blue): potential temperature (top plots), specific humidity (middle plots), wind speed (bottom plots) are shown. The standard deviation associated with each point is represented by a bar at the bottom of each plot. The circle (diamond shape) symbols indicate the maximum (minimum)values.

The diurnal cycles of specific humidity are also contrasted along the meridional transect. The diurnal cycle of specific humidity exhibits a daytime strong drying in the Sahel ($-4g.kg^{-1}$ in Niamey during daytime and $-3g.kg^{-1}$ in Agadez) due to convective boundary-layer processes (described in more details in the next section). This drying is very rapid in Agadez and smoother in Niamey, also consistent with the potential temperature variations.

At Cotonou and Parakou, the low levels record a very weak drying associated with weak convective boundary-layer growth and large latent heat fluxes from moist soil. In the evening, a moistening in the low levels is observed, which may be associated with precipitation (only at Parakou and Cotonou) and monsoon flux advection. This moistening process appears to be shifted in time with latitude, which is consistent with the northward progression of the monsoon flow. The strongest variability from one day to the other associated with the specific humidity is found at Agadez in the early morning (probably due to the variability in ITD position), whereas the smallest value is found at Niamey in the afternoon.

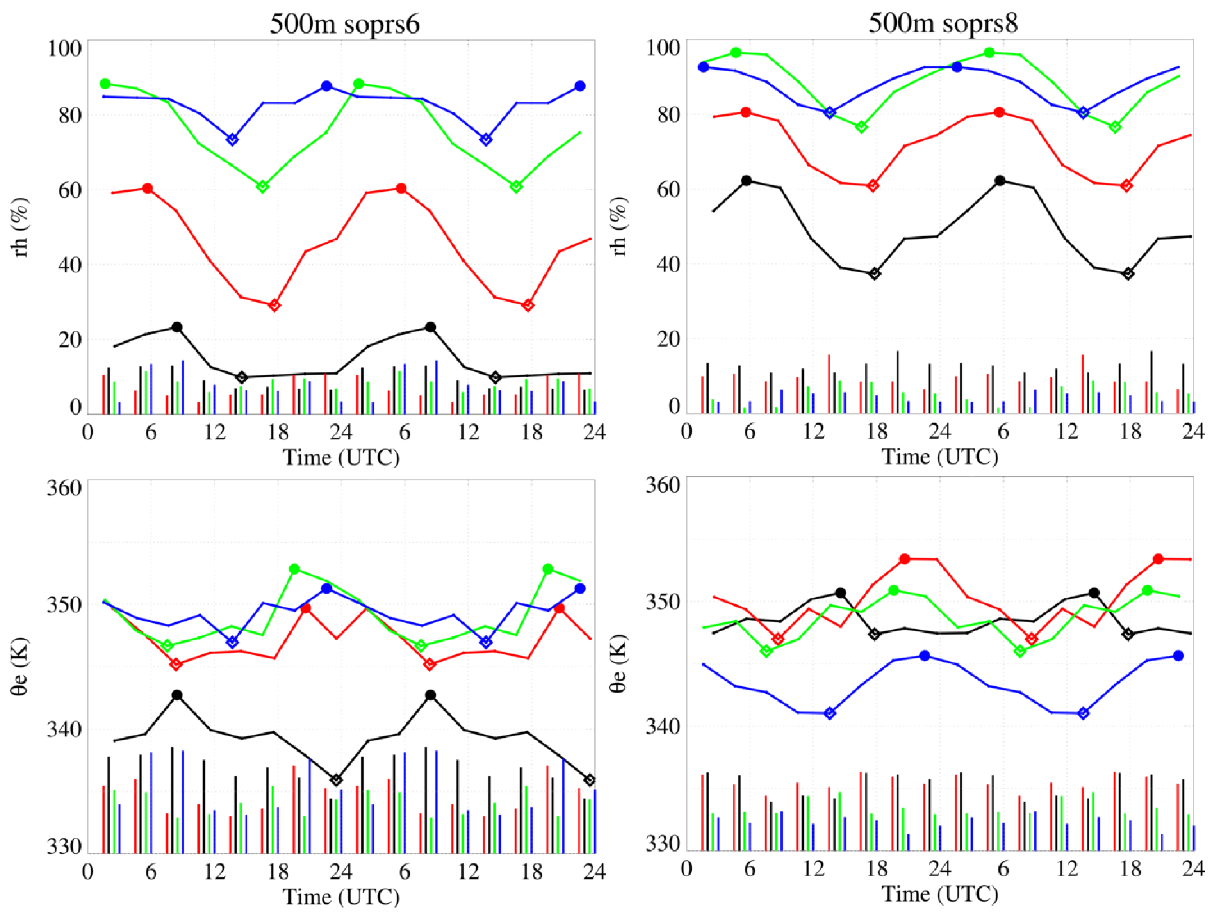

Figure 3-11 : Composite diurnal cycles of relative humidity (top plots) and equivalent potential temperature (bottom plots) of the atmospheric low-levels (0-500m) during SOP-1 (first column) and SOP-2 (second column) at Agadez (in black), Niamey (in red), Parakou (in green) and Cotonou (in blue). The standard deviation associated with each point is represented by a bar at the bottom of each plot. An offset value of +10K was added to θe at Agadez during the SOP-1.

As already shown by Guichard et al. (2009), in this region, the equivalent potential temperature in the atmospheric low levels is a good proxy for convective available potential energy (CAPE). Diurnal compensations between specific humidity and potential temperature occurs, leading to diurnal cycles of much weaker intensity of θe. For example, during daytime, the equivalent potential temperature in the low levels does not increase, can even decrease as shown at Agadez. This is a particular behaviour which may cause problems for models as many deep convection parameterisations are based on CAPE considerations. These low-level behaviour contrasts with surface values, this may be explained by the fact that SYNOP data measures in the surface boundary layer but, care must be taken due to potential remaining biases in the radiosoundings.

The relative humidity in Cotonou is very high and associated with weak DTR. By contrast, at Agadez, the relative humidity is very low, this suggests that the condensation processes will have no control on the diurnal cycle and that the radiative imbalance can be greater. This agrees well with the surface data.

The minimum value of wind speed is found during daytime due to turbulent mixing that slows down horizontal motion. This confirms the findings of Parker et al (2005). The maximum wind speed is always found at night associated with a nocturnal jet, as a response to pressure gradient between the South coast and the Saharian Heat Low (SHL). The timing of this occurrence differs from site to site. At Agadez, this maximum wind speed happens early in the evening (maybe due to orographic effects) whereas at Niamey and Parakou this happens in the early morning (5-6h) which agrees with Lothon et al. (2008).

– ***A collapse of the diurnal cycles during the monsoon***

After the onset of the monsoon, drastic changes of thermodynamic diurnal cycles are observed (see Fig 3-10 & 3-11, right column). First of all, there is a strong mean cooling at all stations especially in the Sahel (at Niamey (-5K), at Agadez (-4K)) The daytime evolution of potential temperature is slowed down especially at Niamey, at 1200 UTC the maximum temperature is almost already reached. However, in Agadez it seems that the diurnal cycle is mainly shifted towards cooler values (-4K) and the amplitude is slightly increased (+0.4K). The cooling process starts earlier consistent with the influence of the monsoon flow. In Cotonou and Parakou, there is a small weakening of the diurnal cycle amplitude, which is proportional to the mean temperature. After the onset, the Inter Tropical Discontinuity (ITD) is located North of Agadez. The atmosphere is moister at all sites except in Cotonou. The diurnal cycles are homogeneous at Cotonou, Parakou and Niamey. There is a daytime drying until 5pm, followed by a moistening until midnight and then again a drying. In Agadez, the diurnal cycle is different from the other stations; the low levels are drier and night-time moistening occurs throughout the night. This post-onset period is characterised by lighter winds at Niamey and Parakou in particular at night and an amplification of south-westerly winds at Cotonou and Agadez especially in the early morning and during daytime. There is also a mean increase in relative humidity over the whole transect (even at Cotonou, where a decrease in specific humidity is observed). A significant augmentation of equivalent potential temperature is found over the Northern Sahel (+15-20K).

– ***Similarities and differences between the atmospheric regimes***

As seen in the previous section, there are large atmospheric regime changes before and after the onset of the monsoon at each station. However, we find similarities between some regimes. Figure 3-12 shows the composite diurnal cycles of specific humidity as a function of potential temperature. A shift towards moister and cooler conditions of the atmospheric regimes is observed after the onset of the monsoon along with the displacement of the ITCZ. Agadez during the SOP-2 presents a diurnal cycle close to Niamey diurnal cycle during the SOP-1. The slight differences can be noticed on the temperatures that are still a bit warmer in Agadez, and the amplitude is weaker. Other similar regimes are observed. Niamey during the SOP-2 closely resembles to Parakou during the pre-onset period. In turn, Parakou during the SOP-2 also exhibits some similarities with the atmospheric regime found at Cotonou during the pre-onset period. Similarities are also found on convective and nocturnal boundary-layer developments, which will be discussed in the next sections.

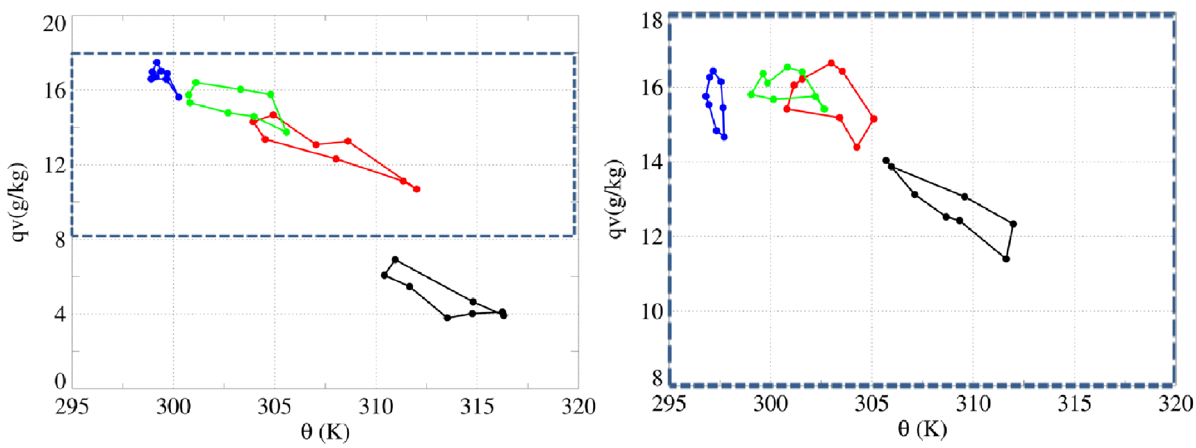

Figure 3-12 : Composite diurnal cycle of specific humidity as a function of potential temperature in the low levels (0-500m) at Agadez (black), Niamey (red), Parakou (green) and Cotonou (blue) before and after the onset of the monsoon) computed from the radiosounding data.

3.3.4 Convective Boundary-Layer Growth and Instability

Figure 3-13 shows the temporal evolution of convective boundary-layer heights. Before the beginning of the monsoon activity over the Sahel, convective boundary-layers developments are very different along the meridional transect. They are particularly thick in the Northern Sahel, in Agadez (up to 5500m) and in Niamey to a lower extend (up to 3000m). They are relatively thin in Cotonou (about 200-400m) and Parakou (about 1000-1500m). They reach a maximum height in between 3 and 5pm. The timing of convective boundary-layer growth is different from one site to another. The growth of the boundary layer depends mainly on the sensible heat flux, the stability of the free atmosphere and the entrainment processes to a lower extent.

In Agadez, after having overcome a strong but very thin nocturnal inversion, convective boundary layers grow very rapidly within a persistent layer characterised by a weak stability called the Saharian Atmospheric Layer. At about 1500 UTC, the convective boundary layer has already almost reached its highest level. Associated with the rapid and large development of boundary layer, a strong drying of the atmosphere (1g.kg^{-1}.hr^{-1}) is observed, as shown in Fig 3-14, due to dry air entrainment. The warming of the CBL is large in the morning but slows down rapidly as the CBL evolves within the SAL (no entrainment of warmer air into the CBL) and dilution of sensible heat flux over a deep layer. This also partly explain the diurnal cycle at the surface and in the low levels.

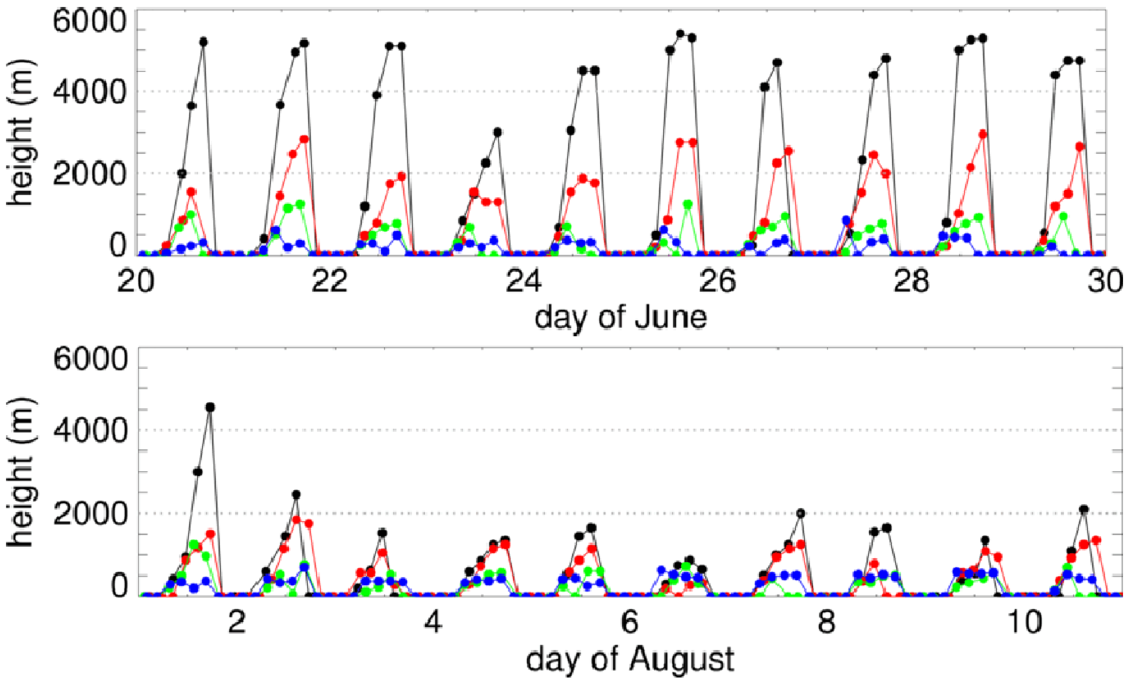

Figure 3-13 : Temporal evolution of boundary-layer height estimated from radiosoundings at Agadez (black lines), Niamey (red lines), Parakou (green lines) and Cotonou (blue lines) during the SOP-1 (top plot) and the ten first days of SOP-2 (bottom plot).

At the other stations, the development is different. CBLs grow within a more stable environment: a deeper residual stable boundary layer and a underlying layer with a stronger lapse rate. In Niamey, the sensible heat flux is almost as large as in Agadez in June (see Fig 3-3) as the soil remains dry. However, the atmosphere is more stable than in Agadez. The boundary layer develops more regularly throughout the day, bringing down drier and warmer air. Hence, the atmosphere dries up and warms all day long. The advection play also a role in the development of the convective boundary layers. In Parakou, cumulus clouds form at the top of the convective boundary layer. This results in stabilising the atmospheric profile and also diminishing the net radiative flux at the surface (by reducing the surface incoming shortwave radiation). This results in a negative feedback; the mixed-layer growth is then stopped in the beginning of the afternoon. In Cotonou, the Bowen ratio (ratio between sensible and latent heat fluxes) is low and the cloud cover is large. Hence, the sensible heat flux remains low. The convective boundary layer is very thin in association with this weak sensible heat flux, a stable atmospheric profile and clouds.

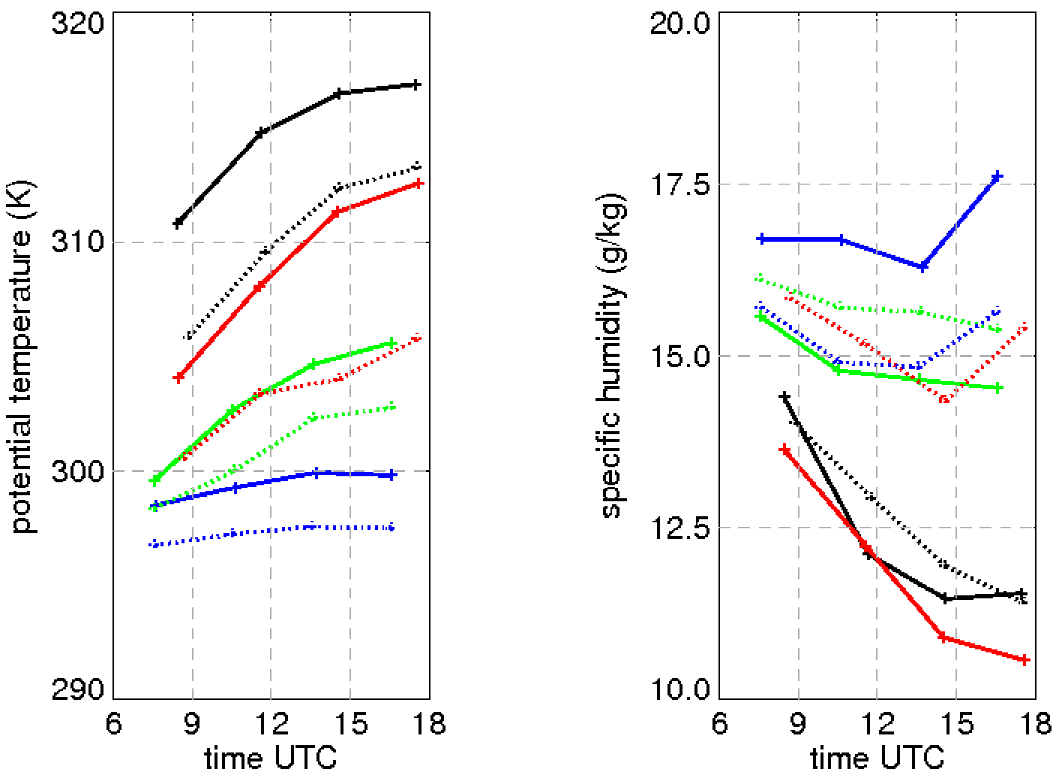

Figure 3-14 : Composite of daytime evolution of convective boundary layers: potential temperature and specific humidity at the different sites along the transect (same colour code as Fig 3-13) during SOP-1 (plain lines) and during the SOP-2 (dashed line).

During the core of the monsoon, the development of convective boundary layers is drastically changed in the Sahel. They expand less, in particular in Agadez (less than 2km instead of 5km in June), they are colder and moister (except in Cotonou where they are drier).

In Agadez, the atmospheric profiles are now influenced by the monsoon flux, this has for consequences to cool down the atmospheric low-levels and therefore, it stabilises the vertical profile. More energy is needed to reach the SAL. Moreover, the sensible heat flux is significantly weaker (see Fig. 3-6). In altitude, the atmosphere is warmer (more stable) than before the onset, which contributes to the decrease in boundary layer growth. Figure 3-15 shows the mean vertical profiles of virtual potential temperature at 1200UTC before and after the onset of the monsoon. Similarities in the profiles are found especially between Parakou-SOPRS1 and Niamey-SOP-2, Cotonou-SOPRS1 and Parakou-SOPRS2.

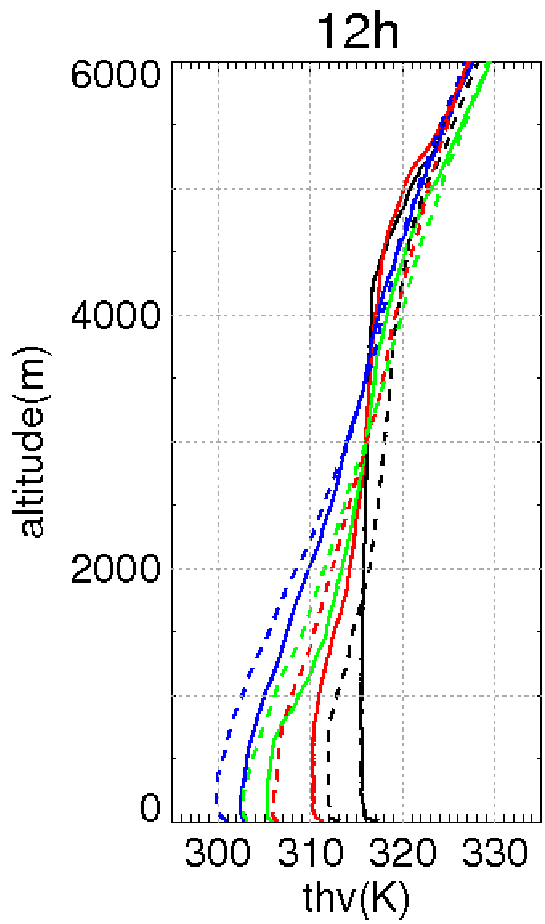

Figure 3-15 : Mean atmospheric profiles of virtual potential temperature from radiosoundings launched around 1200 UTC during SOP-1 (plain lines) and SOP-2 (dashed lines) at the four radiosounding sites (same colour code as Fig3-13).

3.3.5 Nocturnal Boundary layers

Before the onset of the monsoon, there are thin and very stratified nocturnal boundary layers at Agadez associated with large radiative cooling as illustrated in Fig 3-18. At Agadez, the energy budget at the surface at night is largely negative, as seen in Fig 3-2, due in particular to the dryness of the atmosphere. A clear correlation is found between precipitable water and nocturnal cooling at the surface as illustrated in Fig 3-17. The drier the atmosphere is the more negative the net LW radiation at the surface is. The whole atmospheric column is also cooled down by a few degrees. In this stable boundary layer, the wind becomes lighter compared to the free troposphere. A nocturnal jet sometimes forms at the top of this layer, with a frequency occurrence of 40% during the SOP-1.

At Niamey, nocturnal boundary layers are usually much deeper than at Agadez (200-800m) and are associated with more turbulence. The temperature profile is significantly less stable than at Agadez. Sometimes, remarkable cool nocturnal layers with a neutral stability are observed at the surface at Niamey. This thermodynamic structure is linked to the monsoon flow as well as the dynamics of the nocturnal jet which creates turbulence. Indeed, a nocturnal jet forms almost every night at Niamey during the SOP-1. For illustrations, nocturnal profiles of potential temperature for the 26th-27th June are shown for Agadez and Niamey in Fig. 3-16. It illustrates the very thin (less than 100m) and strongly stratified nocturnal boundary layer encountered at Agadez and the relatively cool thick (reaching 700m deep) and neutral nocturnal boundary layer encountered at Niamey. In Parakou, nocturnal boundary layers more stratified than at Niamey.

The vertical profiles do not exhibits clear change in lapse rate which makes difficult to detect the nocturnal boundary-layer height. In Cotonou, the nocturnal boundary layer is weakly stratified are remains shallow (about 100m deep) and there is almost no nocturnal variation in the profiles at the surface. The variability occurs at higher altitudes.

Nocturnal low-level jet are observed along the transect except at Cotonou, where a deep circulation related to the monsoon flow is found. The characteristics of low-level nocturnal jets observed along the transect are listed in Tab. 3-4. The low-level nocturnal jets form at an altitude between 100m and 800m, with a mean altitude of 230m at Agadez, 370m at Niamey and 290m at Parakou. The averaged jet speed is greater at Niamey (11m.s^{-1}) than at Agadez (9.7 m.s^{-1}) and Parakou (9.1 m.s^{-1}), they are also more frequently observed at Niamey than at Parakou and Agadez. At Parakou and Niamey, the nocturnal jet comes from the Southwest, whereas at Agadez it comes from the Northeast. Hence, south of the ITD (Niamey and Parakou), nocturnal low-level jets are associated with the northward transport of moisture which have great impact on the monsoon activity.During the core of the monsoon, mean nocturnal winds weaken at Parakou and Niamey but increase at Agadez, and Cotonou. The occurrence of nocturnal jet diminishes at Niamey due to effect of deep convection as consistent with (Lothon et al, 2008) but are more frequent at Agadez.

Site	**Altitude (m)**		**Speed (m.s^{-1})**	
Agadez	100-450 (230)	130-800 (280)	5.8-15.2 (9.7)	5.2-17.0 (9.5)
Niamey	100-800 (370)	150-700 (350)	5.1-19.0 (11.0)	5.2-15.6 (8.5)
Parakou	200-400m (290)	100-430 (250)	5.2-19.3 (9.1)	6.0-12.0 (7.9)

Table 3-4 : ***Characteristics (Altitude and mean maximum speed) of low level nocturnal jet during the SOP-1 (blue columns) and SOP-2 (white columns). The minimum and maximum values are indicated as well as the mean value (in brackets).***

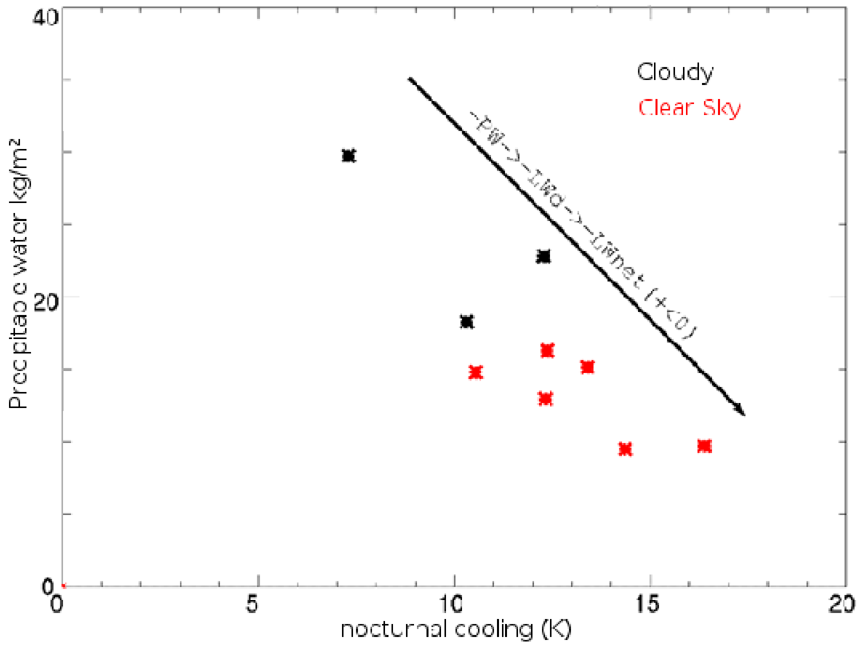

Figure 3-16 : Nocturnal cooling at the surface as a function of precipitable water at Agadez during the SOP-1. The red (black) points are associated with clear sky (cloudy) conditions.

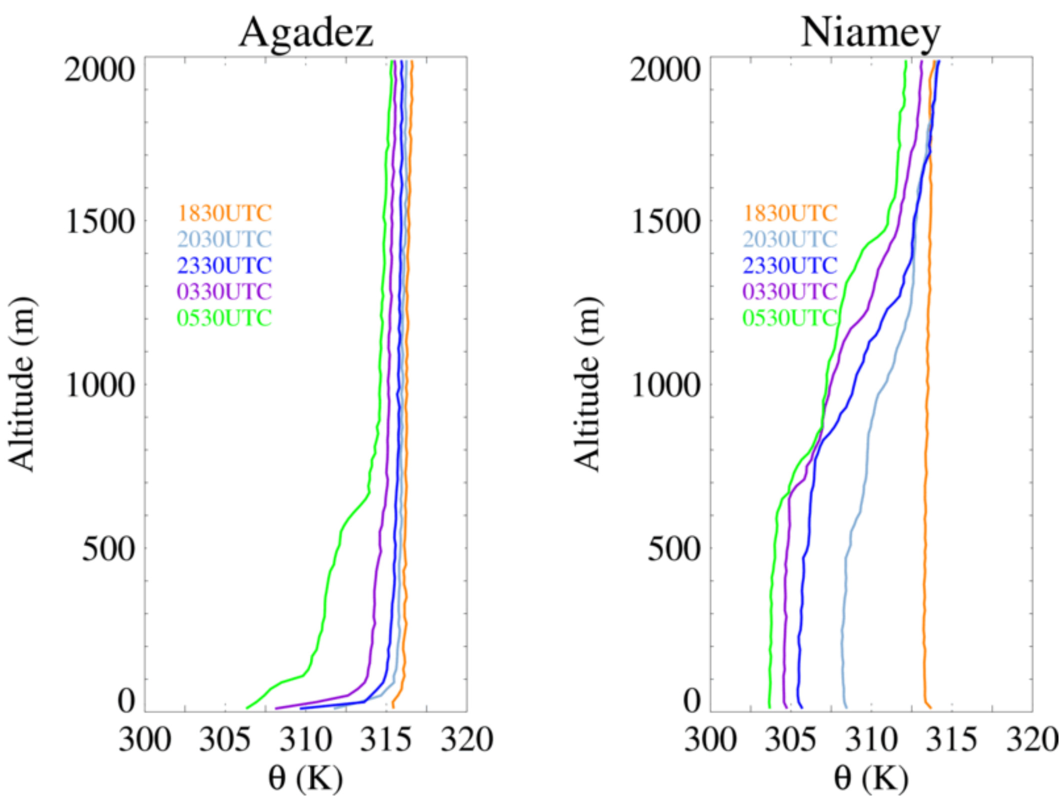

Figure 3-17 : Nocturnal profiles of potential temperature at Agadez (left plot) and Niamey (right plot) between the 26th June 2006 at 1830 UTC and 27th June 2006 at 0530 UTC from radiosounding measurements.

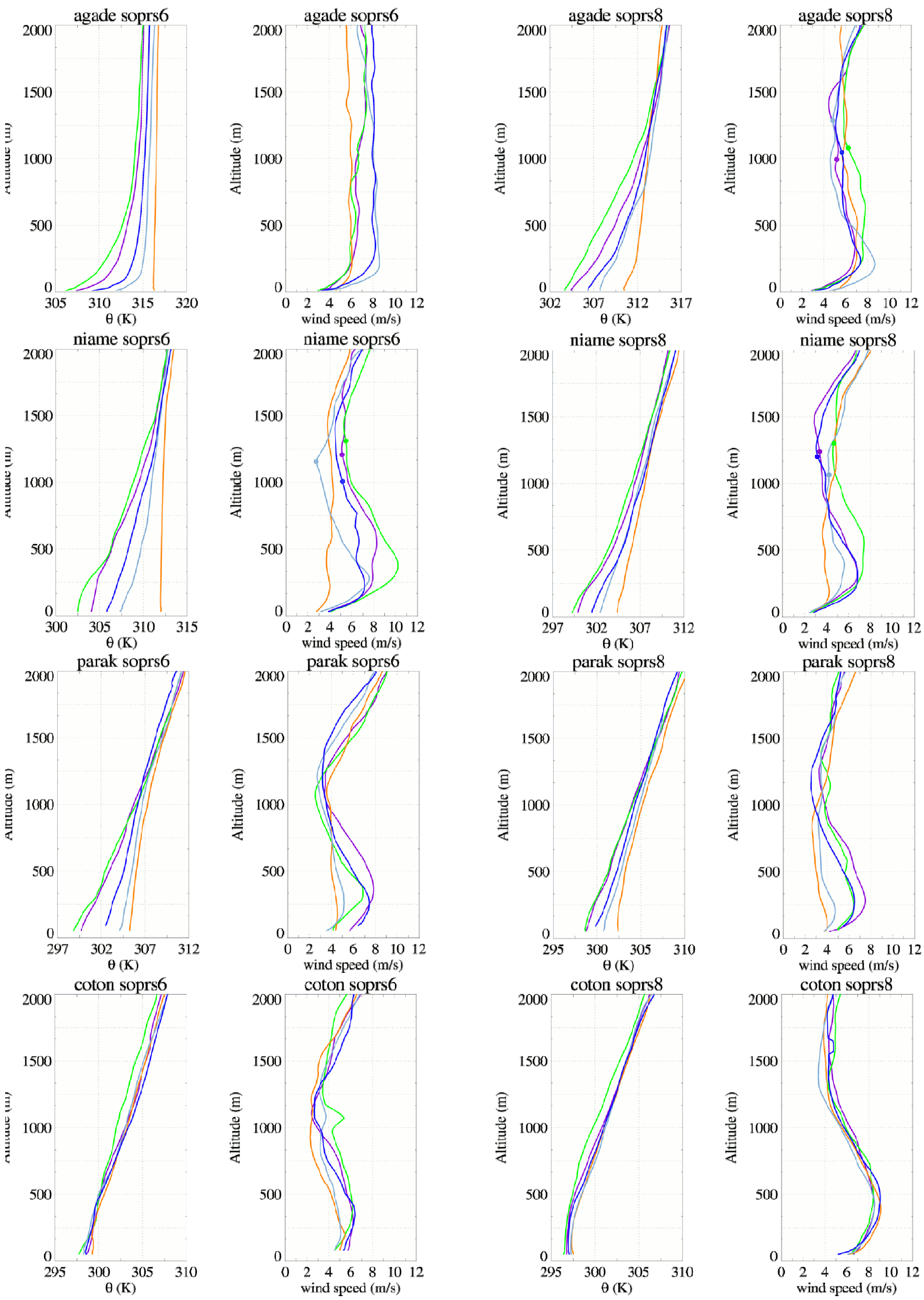

Figure 3-18 : Mean atmospheric profiles of potential temperature and wind speed made from radiosoundings launched at 1800 UTC (orange lines), 2100 UTC (light blue), 2400 UTC (dark blue), 0300 UTC (purple lines) and 0600 UTC (green lines) during SOP-1 (left column) and SOP-2 (right column) extracted from the radiosoundings. The coloured dots indicate the monsoon flux top at Niamey and Agadez.

3.4 Conclusion and Discussion

A unique set of observations was gathered during the AMMA campaign. It was analysed in order to document the diurnal cycles in the atmospheric low levels along a meridional transect extending from the Guinean coast (Cotonou) up to the Northern Sahel (Agadez). This study focused on the moistening phase and the well-established phase of the WAM.

First, the analysis of surface fluxes allowed to characterise and quantify the energetic budget at the surface. Before the onset, even if a strong gradient in incoming shortwave radiation is observed along the transect, there is no distinct meridional gradient in the net radiation. The surface and soil properties play an important role in the meridional variability. The soil moisture strongly modulates the net radiation partitioning between sensible and latent heat fluxes; strong latent (weak sensible) heat flux are found in the Southern part of the transect whereas the opposite is observed in the Sahel. After the onset, the incoming shortwave radiation is significantly reduced over Southern part of the meridional transect due to an increase in cloud cover but not in the Central and Northern Sahel. However, in the Southern part, the surface net radiation is only slightly modified due in particular to a decrease in upwelling shortwave and longwave radiation. The turbulent fluxes are drastically changed over the Sahel, with a large reduction of sensible heat fluxes and an increase in latent heat flux due to a moistening of the soil by precipitation.

Then, the atmospheric diurnal cycles at the surface and in the low-levels were characterised and quantified using SYNOP data and radiosoundings respectively. According to the latitude and season, different timings of temperature and humidity are observed associated with distinct physical and dynamic processes. The amplitude of surface diurnal cycles increases with increasing mean temperature. However, low-level diurnal cycles exhibits slightly different behaviours. For instance at Agadez during the pre-onset period, the amplitude of potential temperature is weaker than at Niamey which is directly linked to atmospheric boundary layer developments.

The radiosounding data allowed us to characterise the vertical structures of convective and nocturnal boundary layers. Diagnostics on convective boundary (ie: height, atmospheric stability, monsoon flow thickness) highlighted the large contrasts in the structures along the transect before the onset of the monsoon. Deep convective boundary layers develop in the Northern Sahel (more than 5km deep) whereas boundary layers remain very shallow on the Guinean coast (less than 500m). After the monsoon start, drastic and coupled changes in the dynamic and thermodynamic diurnal cycles are observed: convective boundary layers in the Northern Sahel collapse (1.5-2km deep), the diurnal cycles become closer together in terms of timing and amplitude. Nocturnal boundary layers were also characterised via diagnostics (height, stability, nocturnal jet, monsoon flow thickness). Different nocturnal behaviours are observed along the transect, with very thin and strongly stratified nocturnal layers at Agadez before the onset, whereas deep and weakly stratified boundary layers are observed in Niamey. Nocturnal jets often occur along the transect except on the Guinean coast. It occurs more often at Niamey during the pre-monsoon period than at Parakou and Agadez. However, during the core of the monsoon, it is often less regularly observed at Niamey and more often at Agadez.

Similarities were found between the different sites/periods when considering surface and atmospheric low level, but also on the convective and nocturnal boundary layers. This characterisation allowed the distinction between four atmospheric regimes encountered during the WAM, ordered below as a function of increasing surface temperature:

- A Guinean monsoon regime characterised in the atmosphere by a stratiform cloud layer in the lower troposphere which gives slight precipitation. The amplitude of thermodynamic and dynamic diurnal cycle is weak ($\Delta\theta$=0.9K, Δqv=1.8g.kg^{-1}), the convective boundary layers do not develop much (less than 500m).
- A Soudanian monsoon regime characterised by intense deep convection that frequently gives important amounts of precipitation. The diurnal cycle of potential temperature is slightly stronger than in the Guinean monsoon regime ($\Delta\theta$=3.6K), but its diurnal amplitude of humidity is weaker (Δqv=1.1g.kg^{-1}). Convective boundary layers are remains shallow with numerous cumulus clouds.
- A Sahelian monsoon regime: wet atmospheric regime where deep convection develop very high into the troposphere, higher than in the Soudanian zone but is less frequent and gives less rain. Convective boundary layers are also regularly topped with shallow cumulus clouds (to a lower extends compared to the Soudanian monsoon regime). ($\Delta\theta$=4.3K, Δqv=2.2g.kg^{-1}),
- A Sahelian pre-monsoon regime: dry atmospheric regime in moistening phase over dry soil. Strong meridional advection bring moisture in the lower troposphere during night-time which is redistributed vertically during daytime into the deep convective boundary layers. ($\Delta\theta$=8.1K, Δqv=4.0g.kg^{-1}),

These distinct low-level diurnal cycles involve an ensemble of interactions among physical and dynamic processes. Numerical modelling of diurnal cycles is still stained by systematic errors such as the diurnal cycle of deep convection. The AMMA observations as well as the characterisation of the diurnal cycle carried out here allowed to further develop a modelling framework in order to identify the strengths and weaknesses of the model to represent the observed diurnal cycles. This is the object of the next chapter.

Chapter 4.
Evaluation of Modelled Diurnal Cycles in the atmospheric low levels

Contents

The previous chapter was devoted to the characterisation of diurnal cycles observed along the meridional transect. It allowed us to identify four main atmospheric regimes. This chapter is dedicated to the numerical modelling of the diurnal cycles observed during the WAM season and in particular, during the four identified atmospheric regimes along the transect. The first section presents the motivations and objectives of this study. The second section describes the modelling framework developed. Then, the experiment carried out are presented. The fourth section is dedicated to the analysis of the simulations performed. Finally, this chapter ends with conclusions and discussions.

4.1 Objectives and Motivation

The diurnal cycle in the atmospheric low levels is a challenging issue for atmospheric models. Most of the models have biases in the timing and location of convective triggering. In the mid-latitudes, convective precipitation usually occurs close to local noon in the model, a few hours before it happens in reality (Betts et al., 1998, Stendel and Arpe, 1997). Over Amazonia, the models also simulate deep convection too early; it happens only few hours after sunrise, whereas in the observations deep convection occurs around midday (Betts and Jakob, 2002a, 2002b). The problem was investigated by the authors using a single column model (SCM) of the ECMWF atmospheric model. They found that the errors on the diurnal cycles were a signature of the model and hence the SCM was a useful (although simplified) version of the full 3-D model to study the behaviour of parameterisation over the diurnal cycle. Their results show that the progressive convective boundary-layer growth is not reproduced in the model. As soon as the model detects instability, deep convection develops and reach the level of neutral buoyancy. This has consequences on the diurnal cycle of other processes, as strong interactions occur between the boundary layer, surface, clouds and radiation. Mean daily precipitation amounts are roughly correct in the simulations, but this is not sufficient as the convective clouds, convective heating and large-scale vertical motions are closely coupled in the Tropics. Moreover, the deep convection directly impacts the shortwave radiation budget and hence, the surface-temperature equilibrium.

Over West Africa, global weather and climate models have systematic difficulties in simulating and predicting the characteristics of the WAM. In particular, the rainfall field is the most problematic characteristic to represent at timescale ranging from seasonal to diurnal. The diurnal timing of convection is badly represented. An incorrect representation of boundary layers may affect the dynamic of the monsoon circulation. For example, it can directly impact the meridional gradient of temperature and humidity, which is recognised as an important factor in the propagation of the monsoon flux. It can also directly affect the local development of mesoscale convective systems.

The objective of this chapter is to investigate the abilities of a model to reproduce the diurnal cycles observed during the AMMA intensive observing periods. For this, a modelling framework was developed based on an interactive surface-atmosphere model. For the first time, enough observations of atmospheric profiles at high temporal resolution have been acquired and enable us to evaluate the model at the diurnal timescale on the meridional transect of West Africa.

The one-dimensional mode is a simplified version of the 3D model but we have good reasons to think that the biases found in the 3D model are also found in the uni-column version (see Betts and Jakob, 2002). The 1D version uses the same parameterisations as the 3D version and a convenient 1D aspect is that the physics can be decoupled from the dynamics. These idealised cases which have some realistic aspects (initial profiles, advective forcings) provide a good framework to analyse the biases and get a better understanding of the reasons why biases develop.

4.2 The Modelling Framework

4.2.1 The surface-atmosphere coupled model

Meso-NH (Meso-échelle Non Hydrostatique) is a non-hydrostatic mesoscale atmospheric model developed jointly by Laboratoire d'Aérologie and CNRM-GAME (Lafore et al, 1998). This is a multi-scale model that enables to handle fine scale simulations (Large Eddy Simulation) as well as large-scale simulations. The non-hydrostatic hypothesis means that the pressure force and gravity equilibrium is not assumed, the vertical velocity is a prognostic variable on the vertical axis. Thus, the vertical velocities associated with convection can be represented. The model is based on the anelastic approximation, which eliminates the acoustic waves by the use of a constant density profile. A leap-frog scheme is used to discretise the system of equations that is presented below. The set of parameterisations chosen for the simulations as well as the interactive surface model are described in the following sub-sections.

In the model, prognostic variables are the turbulent kinetic energy (e), the potential temperature (θ), the mixing ratio of water vapour (rv) and of different species of hydrometeors as well as the three main component of velocity; u (zonal wind), v (meridional wind) and w (vertical wind). The pressure, as said before, is a diagnostic variable, it is determined from an elliptic equation after iteration process.

The equation of Energy Conservation is defined as:

$$\frac{\partial}{\partial \mathrm{t}}(\rho_{\mathrm{d\ ref}}\theta) = \mathrm{Adv} + \mathrm{Turb} + \mathrm{Diff} + \mathrm{Q}* + \mathrm{Qrad}$$

with

- $\frac{\partial}{\partial \mathrm{t}}(\rho_{\mathrm{d\ ref}}\theta)$ the temporal evolution of energy.
- Adv, the advection term.
- Turb, the contribution from the turbulence.
- Diff, the numerical diffusion term
- $\mathrm{Q}*$, heat exchange from microphysics
- Qrad, the term for radiative energy exchanges.

The equation of humidity mixing ratio conservation (rv) is given by:

$$\frac{\partial}{\partial t}\left(\rho_{d\ ref}\ rv\right) = \mathrm{Adv} + \mathrm{Turb} + \mathrm{Diff} + \mathrm{Q}*$$

where $Q*$ represents all the sources and sinks of humidity from microphysics.

In our study, the atmospheric model was operated in an one-dimensional mode (1D hereafter). The grid size is implicitly a few 10s of km. At this scale, parameterisations must be employed to take into account turbulence, dry and moist convection, which all correspond to sub-grid processes.

In Meso-NH, the turbulence is parameterised according to Cuxart et al. (2000). In 1D, the formulation uses a closure by a mixing length (Bougeault et Lacarrere, 1989) which calculates the upward and downward distance that can be reached by a parcel of air according to its kinetic energy. The entrainment at the top of the boundary layer is implicitly represented. In stably stratified conditions ($\frac{d\theta}{dz} \geq 0$), this turbulence scheme is also used. Additionally, vertical rising plumes called thermals, which play an important role in the convective boundary layer growth, have been parameterised (Pergaud et al., 2009). This is a mass flux scheme that allows a better representation of vertical motion and mixing within the convective boundary layer. It also permits to represent the moist thermals and the associated cumulus clouds.

To control moist instabilities arising from saturation, processes of moist convection need also to be parameterised. Several deep convection schemes have been developed over the past years. One such parameterisation is the Kain–Fritsch scheme (Kain and Fritsch, 1990). It was modified and implemented into Meso-NH by Bechtold et al. (2001). It uses the Lagrangian parcel method to estimate whether instability exists, whether any existing instability will become available for cloud growth, and what the properties of any convective clouds might be. The convective scheme can be separated into three parts: the convective triggering function, the mass flux formulation including entrainment and detrainment and the closure assumptions which are based on CAPE considerations. The triggering function is based on LCL of an air parcel at the surface and a conditions on the potential cloud depth (at least 3000m). A representation of the convective downdrafts is incorporated, which permits to stabilise the atmospheric low-levels after the passage of a convective system. Another solution for representing the shallow convection (instead of the mass-flux scheme of Pergaud et al., 2009) is to use an adapted version of the Kain-Fritsch convection scheme.

The radiation scheme allows the representation of solar and infrared emissions as well as the absorption by the surface and the atmospheric column (absorption and emission of atmospheric gases, hydrometeors and aerosols). The shortwave radiation code used in the Meso-NH model is the ECMWF scheme (Morcrette et al., 1991). In the longwave spectrum, emissions and absorptions of radiation are taken into account using the code from Mlawer et al (1997). Each air layer is considered to have absorption and emissivity coefficients. The emission is proportional to the fourth power of the air layer temperature and its emissivity.

Several types of microphysics schemes are implemented into Meso-NH. Processes of nucleation and aggregation, water phase changes are represented. Some include only warm processes and other cold processes as well. The ICE3 scheme includes ice processes. It allows the formation of cloud droplets and different forms of ice particles (ice crystals, snow, hail, graupel).

The aerosol properties (optical properties and vertical structure) can be taken into account. Several parameterisations are available in Meso-NH. One solution is to use a climatology of aerosols like Tegen et al. (1997) or an older climatology from ECMWF based on Tanré et al. (1984). Another solution is to prescribe the aerosol optical depth depending on the soil properties. The vertical profile is then taken from the Tegen et al. (1997) climatology. This is a convenient way to modify the optical depth easily.

In this study, the surface is treated separately by the interactive surface model SURFEX, the surface-atmosphere coupling is an approach newly used in this type of 1D study. The surface model includes, in particular, a model for land surfaces called the Interactions Soil-Biosphere-Atmosphere (ISBA) model (Noilhan et al, 1989). Its main purpose is to determine the lower boundary conditions for the vertical diffusion of temperature, moisture, and momentum, as well as evaluating the evolution of the temperature and moisture in the near-surface soil layer and two deeper soil layers. It computes the hydrological and energy budgets at the surface as well as the way this energy is transmitted to the atmosphere via turbulent fluxes and into the ground. This depends on the soil properties (moisture, texture type, colour, vegetation cover) and the atmosphere above (atmospheric demand). The model first computes the radiative budget and then, the sensible (H) and latent (LE) heat fluxes at the surface as follows:

$$H = \rho_a C_p C_H V_a (T_s - T_a)$$

and

$$L_v E = L_v \rho_a C_p C_H V_a (q_{sat}(T_s) - q_a)$$

where ρ_a, q_a , T_a and V_a represent respectively the density, specific humidity, temperature and wind speed of the air. T_s represents the surface temperature. C_H is the transfer coefficient.

In this study, the model domain extends vertically up to 20 km and has a fine resolution grid including 98 levels with more than 30 levels in the lowest 2km. The parameterisations used in the simulations are listed in Tab. 4-1. It includes the turbulence scheme from Cuxart et al. (2000), a shallow convection scheme (Pergaud et al.,2009), a deep convection parametrisation (Bechtold et al., 2001), a microphysics scheme (ICE3, Pinty and Jabouille (1998)) and a radiation scheme (ECMWF, Morcrette et al., 1991 and Mlawer et al., 1997). The time step of the model is set to 30s. The deep convection and radiation schemes are called every 300s.

Parameterisation	Reference
Turbulence	Mixing length scheme - Cuxart et al. (2000)
Shallow convection	Thermals - Pergault et al. (2008)
Deep convection	Mass flux scheme - Betchold et al (2001)
Shortwave Radiation scheme	ECMWF code - Morcrette et al. (1991)
Longwave Radiation code	RRTM code - Mlawer et al. (1997)
Microphysics scheme	ICE3 - Pinty and Jabouille (1998)
Aerosols	Surf - Adapted from Tegen et al. (1997)
Surface scheme	ISBA - Noilhan and Planton (1989)

Table 4-1 : ***List of the parameterisations used in the reference simulations.***

4.2.2 Data and model products

The AMMA campaign provided extensive datasets including surface measurements, vertical profiles of the atmosphere from radiosoundings and convection data from satellite at a fine temporal resolution at different sites along the meridional transect (see section 2-2 for details on the AMMA campaign and chapter 3 for details on observations). It gave us an excellent opportunity to develop a modelling framework by using these data to initialise, constrain and evaluate the simulations performed.

– ***Data to initialise and constrain the model:***

The ECMWF AMMA reanalysis (Agusti-Paraneda et al., 2010) is an analysis that has integrated all the radiosoundings launched during the 2006 AMMA campaign as well as corrections of biases. In the reanalysis, a correction scheme was implemented to correct the dry bias of Vaisala sounding measurements which led to a better representation of precipitation over the Sahel (Agusti-Panareda et al., 2009). Agusti-Panareda et al. (2010) showed that the extra soundings assimilated in the simulation improve the thermodynamic and dynamic structures of the lower troposphere. Tompkins et al (2005) also highlighted the role of soundings on the structure of the AEJ in the analysis. The AMMA reanalysis are used here to prescribe the initial profiles of potential temperature, specific humidity and wind. The vertical profiles of wind are nudged towards the reanalysis profiles every three hours with a constant damping time of 3hrs. The reanalysis is also used here to compute the large scale advection at each station. It has been carried out on the basis of a 3-hourly dataset provided by M. Koehler, individually for each site, and documenting an area roughly 40 km x 40 km wide. The vertical advection is calculated separately using the vertical gradients of temperature, humidity and the vertical velocity. These reanalysis provide the best estimates of the atmosphere available for 2006 wet season over West Africa at the different sites and periods studied here. It does not mean that is can be considered without caution, as it will be shown later. However, it provides a valuable first guide in the absence of other observationally-based information.

Soil properties and vegetation cover used to initialise the simulations come from the Ecoclimap data base (Masson et al., 2003). Surface properties (humidity and temperature) in the top meters of the ground are extracted from the ISBA simulations performed offline within the ALMIP experiment (Boone et al., 2009).

– ***Data to evaluate the simulations:***

The observations used to evaluate the simulations are listed in Tab 4-2. Radiosoundings launched during the two intensive observing periods SOP-1 and SOP-2 of the campaign are used to evaluate the thermodynamic vertical structures in the simulations. The radiosoundings are interpolated on the model vertical grid to allow a more accurate comparison. Boundary layer diagnostics were calculated from the radiosoundings (see section 3.2 for method). The same diagnostics are performed for the simulated profiles.

Surface measurements were collected at different sites. At Niamey airport (13.5°N) which is located close to the Niamey radiosounding launching site, the Atmospheric Radiation Measurement (ARM) station recorded radiative fluxes as well as turbulent fluxes (Miller and Slingo, 2007). Turbulent fluxes as well as temperature (T), humidity (qv), wind speed (ws), wind direction (wd) and precipitation were measured at Nalohou, a site situated in the Ouémé basin, approximately 100km away from Parakou. This site is characterised with a little more vegetation than at Parakou, so it may overestimate latent heat fluxes and underestimate sensible heat fluxes. However, it is useful for a first order comparison with the simulations. Radiative measurements at the surface from the IMPETUS network were recorded at Parakou and Cotonou. They include downwelling and upwelling shortwave and longwave radiation at the surface. SYNOP data including T, qv, ws, wd at 2 m above the ground were collected at the three sites (see Fig. 3-1 for location of the sites).

Brightness temperatures (BT) are thermal emissions detected by Meteosat Second Generation satellite. The data used here come from the 10.8 micron channel. For our study, we averaged them over a 0.25deg zone around the site locations. They give an information of the cloudiness. The shallow cumulus and stratocumulus clouds are however hard to detect as they emit at temperature close to the surface temperature.

Site	Alt	Lat	Lon	Radiosoundings	Rad. Fluxes	Turb. Fluxes	Synop	BT
Niamey SOP1- 2	222 m	13°48 N	2°17 E	8/day	ARM station	ARM station	Yes	Yes
Parakou	392 m	9°36 N	2°61 E	8/day	Impetus	No	Yes	Yes
Nalohou	449 m	9°75 N	1°61 E	No	No	Only H	No	No
Cotonou	5 m	6°52 N	2°40 N	8/day	Impetus	No	Yes	Yes

Table 4-2 : ***List of measurement site characteristics and the data available at each site.***

4.3 Experiments

4.3.1 The meridional transect

The modelling framework presented above was developed to simulate the different atmospheric regimes observed along the meridional transect during the monsoon season. Four different atmospheric regimes were retained to study the characteristics of the simulated atmospheric diurnal cycles along the transect during the monsoon season. Here is a brief overview of the four regimes that we distinguished (see chapter 3 for more details on the regimes). Figure 4-1 presents the atmospheric regimes observed on the climatic transect along an increasing temperature axis:

- ***Cotonou-SOP2 (1-11th August 2006): Cloudy Regime***. Cotonou is a station located on the Guinean coast. During the full monsoon period, convective activity is almost suppressed over Cotonou. The atmospheric regime is characterised by cooling/drying compared to the pre-onset period. Low-level stratocumulus clouds giving light rain are observed.

- **Parakou-SOP2** ***(1-11th August 2006): Wet Tropics Regime***. Parakou is located in the Soudanian region. During the post-onset period, the atmosphere is moist and convectively very active. Large convective systems develop frequently and give important precipitation.

- **Niamey-SOP2** ***(1-11th August 2006): Convective Sahelian Regime***: Niamey is situated in the Sahel. During the monsoon period, the atmosphere experiences strong modifications of the diurnal cycles compared to the pre-onset phase. Convective storms are active. They develop less often and produce on average less rain than at Parakou but they extend higher and are very strong.

- **Niamey-SOP1** ***(20-30th June 2006): Moist Sahelian Regime***. Before the monsoon onset, the atmosphere is still in moistening phase (Lothon et al., 2008). Thermodynamic diurnal cycles in the atmospheric low-levels are large. Cloud cover is sparse, some cumulus clouds can break through punctually and give some sporadic rain.

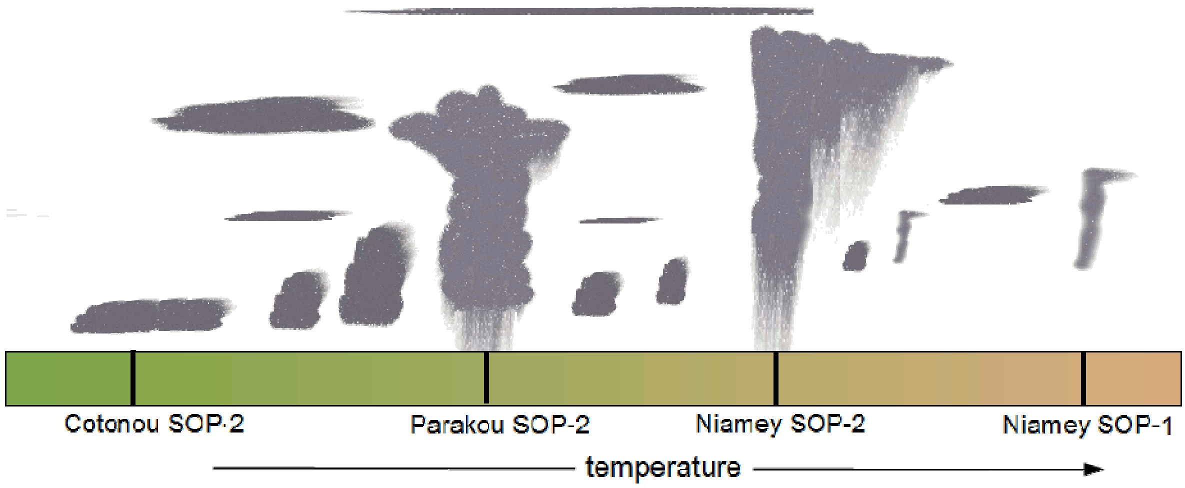

Figure 4-1 : Representation of the atmospheric regimes over the meridional transect as a function of increasing temperature.

4.3.2 Reference simulations

A set of ten 24h simulations were performed over the four regimes presented above (called REF hereafter). The simulations were started at 0600UTC. They were initialised using the dynamic and thermodynamic profiles extracted from the ECMWF reanalysis. Figure 4-2 shows the 0600UTC initial profiles of potential temperature and specific humidity for the SOP1 period at Niamey (full lines) compared to the corresponding radiosoundings (dotted lines). Not surprisingly, the reanalysis is close to the observations, as the radiosoundings were assimilated into the reanalysis. However, there is a small dry bias in the reanalysis possibly associated with the underestimation of moisture advection from the nocturnal jet in the reanalysis. At Cotonou and Parakou, the profiles are sometimes too cold (-1-2K) and too wet (1g/kg) compared to the radiosoundings (not shown). The simulated winds were nudged towards the profiles extracted from the reanalysis.

The advection from the reanalysis were used as synoptic forcings. Figure 4-3 presents the composite diurnal cycles of total advection of potential temperature (left plot) and specific humidity (right plot).

At Niamey during the SOP1, a strong dipole composed with a cooling/moistening (-0.8K.hr^{-1} and 0.7g.kg^{-1}.hr^{-1}) is observed in the atmospheric low levels in the early morning whereas, a slight warming/drying (0.2K.hr^{-1} and -0.1g.kg^{-1}.hr^{-1}) is found in the mid-troposphere (mainly during daytime). This is associated with the monsoon flow, which is accelerated by the nocturnal jet and above, a return flow from the North-East. During daytime, a slight drying is observed on the profiles. These advection are qualitatively in agreement with advections found by Peyrillé et al. (2007).

A different behaviour is observed during the SOP2 at Niamey. The advection of moist and cooler air in the first 2 km are weaker (-0.4K.hr^{-1} and 0.2g.kg^{-1}.hr^{-1}) compared to the pre-onset period. This is due to a weakening of the meridional gradient of temperature and moisture as well as a global weakening of meridional wind. In the free troposphere, some advection of cooler air is found in the mid-afternoon. This is linked to the development of deep convection (vertical advection).

At Parakou during SOP-2, the low-level cooling/moistening is not observed anymore, whereas a stronger cooling/moistening (-0.9K.hr^{-1} and +0.2g.kg^{-1}.hr^{-1}) maximised at 1200-1500UTC is found in the mid-troposphere. Another similar structure is found during night-time (2400UTC-0300UTC). This is associated with moist convection. The horizontal advection are weak (not shown).

At Cotonou during SOP-2, the horizontal advection cools and dries the low levels during the day (-0.4K.hr^{-1} and -0.2g.kg^{-1}.hr^{-1}, consistent with a sea-breeze event) and the vertical advection cools the free troposphere in the morning.

Figure 4-4 shows the mean daily advection of potential temperature and specific humidity for the four regimes. An overall mean cooling is found in the first few kilometres of the atmosphere at Niamey in SOP-1 and SOP-2 as well as in Cotonou. By contrast, no strong advection is detected in the reanalysis at Parakou. Only at Niamey, during the pre-onset period, a strong overall moistening is observed. In the free troposphere, a mean cooling/moistening is observed at Parakou (-5 K.day^{-1} and +1-2 g.kg^{-1}.day^{-1}). At Niamey-SOP2, a mean cooling/moistening is observed above 5km (-1K.day^{-1} and +1g.kg^{-1}day^{-1}) and negative moisture advection dries the profiles below 5km. At Niamey-SOP1 and Cotonou SOP2, advection warms and dries the free troposphere.

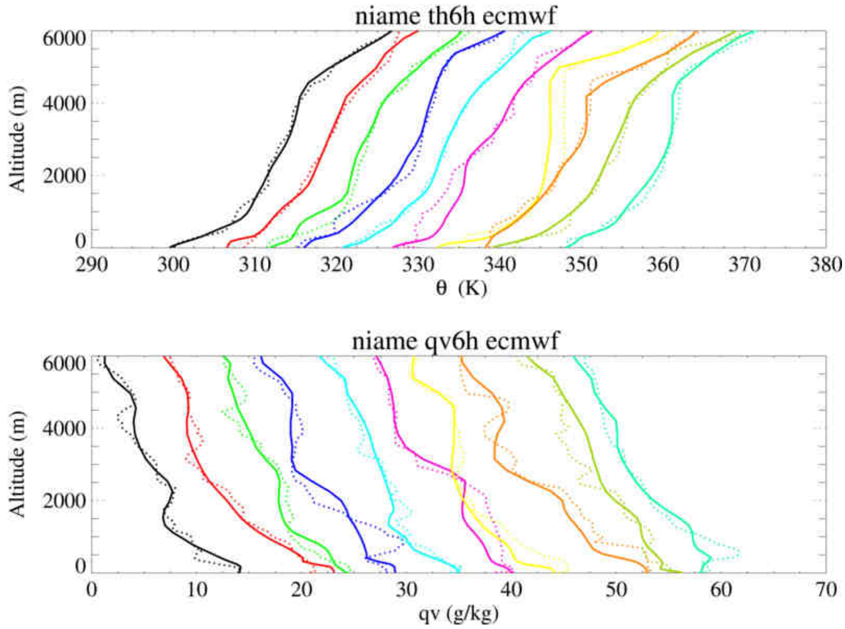

Figure 4-2 : Initial vertical profiles of potential temperature (upper plot) and specific humidity (bottom plot) used to initialise the simulations at 6UTC (full lines) and the radiosounding (dotted lines) launched at Niamey during the SOP-1. The different colours correspond to the different days. An increment of 5K/5g.kg^{-1} respectively was added for each subsequent day for clarity.

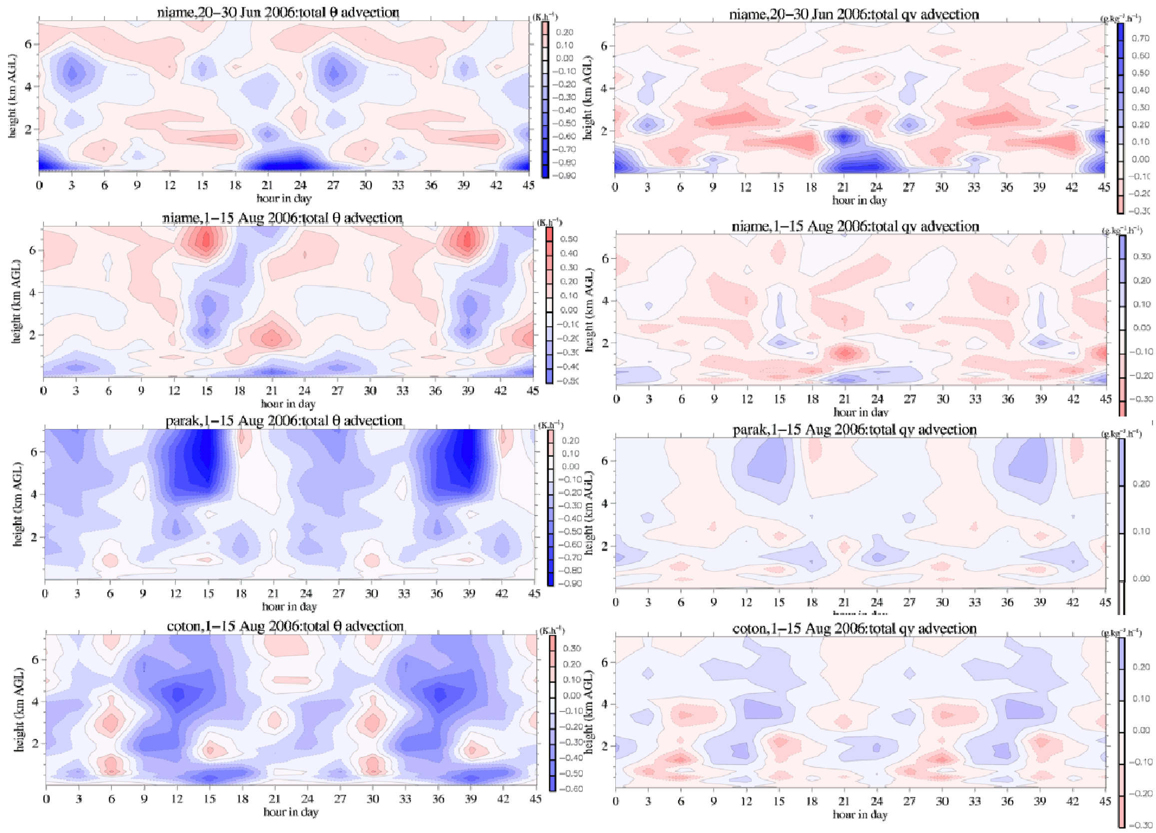

Figure 4-3 : Composite diurnal cycle of total (horizontal and vertical) advection of potential temperature (left column) and specific humidity (right column) at Niamey during the SOP-1 (top plots), Niamey during the SOP-2 (top middle plots), Parakou SOP-2 (bottom middle plots) and Cotonou SOP-2 (bottom plots). Advection extracted from the ECMWF AMMA reanalysis.

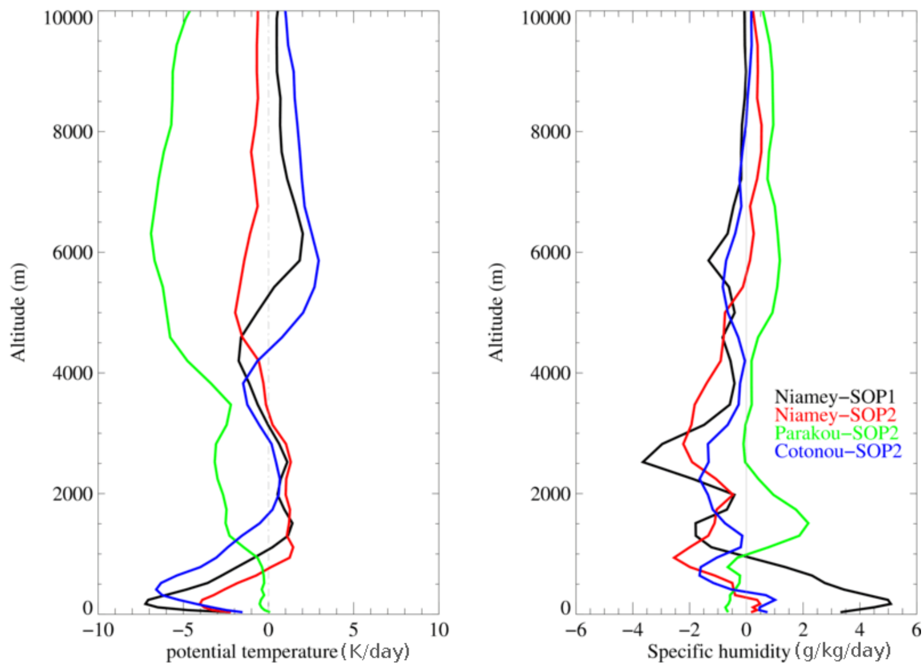

Figure 4-4 : Mean daily advection of potential temperature and specific humidity from the ECMWF reanalysis averaged over the SOP1 or SOP2 periods.

4.3.3 Tests on model setup and configuration

All the different tests performed are listed in Table 4-3. To test the behaviour of the model over a longer period, 10-day simulations were run without reinitialisations (called LONG hereafter). The model settings and parameterisations were the same as for the reference simulations. The advective forcings were also kept identical. Then, we also performed 10-day simulations using a composite of advective forcings to see the impact of synoptic varying advective forcing versus a composite one (called COMPO hereafter) on the mean equilibrium state.

Some sensitivity tests on the model configuration were performed, but are not detailed later on. Nevertheless, the main conclusions are summarised below. The results were not sensitive to the choice of the shallow convection scheme. The time step for the convective and radiation scheme call was tested. Similar results were obtained when using of 30s instead of 300s. Based on computing time considerations, we choose to use a time step of 300s. The advective scheme were also tested showing no significant impact.

For Niamey-SOP1, a simulation was performed with an additional advective term. It appeared that the large scale advection was underestimated especially during monsoon flux pulsation. An additional term was calculated by comparing the simulated profiles after 24hours of simulation to the radiosoundings. The compensation is distributed homogeneously over the whole diurnal cycle. It is explained in more details in section 4.4.5.

For Parakou-SOP-2, simulations were ran to test the influence of vertical advection. One was done with applying only horizontal advection, one with only vertical advection and a later one with no advection at all. This was done in order to investigate the relationship between the diurnal cycle of prescribed vertical advection and deep convection.

Name	type	Advection	Station concerned
REF	10x24hrs	Synoptic varying advection	All
LONG	10 days	Synoptic varying advection	All
COMPO	10 days	Composite advection	All
ADVCOR	10x24hrs	Advection corrected with bias/obs	Niamey-SOP1
NOADV	10x24hrs	No advection	Parakou-SOP2
HORADV	10x24hrs	Only horizontal advection	Parakou-SOP2
VERADV	10x24hrs	Only vertical advection	Parakou-SOP2
ADVHOMO	10x24hrs	Vertical advection distributed homogeneously over the diurnal cycle	Parakou-SOP2

Table 4-3 : ***List of the different simulations performed for this study.***

4.4 Results

4.4.1 General features of the simulations over the transect

– ***Distinct climatological features along the transect***

The temporal evolution of potential temperature simulated by the model (REF, left column) and observed in the radiosoundings (right column) at Niamey-SOP1 and Cotonou-SOP2 is shown in Fig. 4-5. A strong diurnal cycle in the low levels can be observed in the Northern part of the meridional transect, with a nocturnal cooling appearing in green/blue and a daytime warming in orange/red. Much weaker diurnal variations are observed at the Southern sites. The reinitialisation is well marked in the Niamey-SOP1 simulation as the model drifts towards warmer profiles. This is less significant at Cotonou.

Figure 4-6 presents the temporal evolution of water vapour mixing ratio simulated by the model and observed in the radiosoundings. For the same station, qv decreases with altitude; high specific humidity is found in the atmospheric low levels (in blue) and low specific humidity is found in the mid-troposphere (red/black). A strong daytime drying (too strong in the simulations) is seen in the Northern part of the transect, whereas this behaviour is less pronounced in the Southern part.

The evolutions of potential temperature and mixing ratio simulated and observed at Parakou-SOP2 and Niamey-SOP2 can be found in Appendix C. Overall, the model is able to reproduce the distinct climatologic features along the transect (see also Fig. 4-11 detailed later on) but with some systematic defects as discussed below.

The temporal evolution of zonal winds is shown in Fig. 4-7. The wind profiles in the simulation are nudged towards the reanalysis profiles so unsurprisingly, they are in good agreement with the observations. At Niamey SOP-1, the African Easterly Jet (AEJ) can be observed in the mid-troposphere and a south-westerly flow in the atmospheric low levels. One can note that there is no substantial change in mean intensity and structure of the AEJ in Niamey between SOP1 and SOP2. On the other hand, the AEJ is essentially absent over Parakou SOP2 apart from the first days. Further information on the meteorological context is provided in Appendix B.

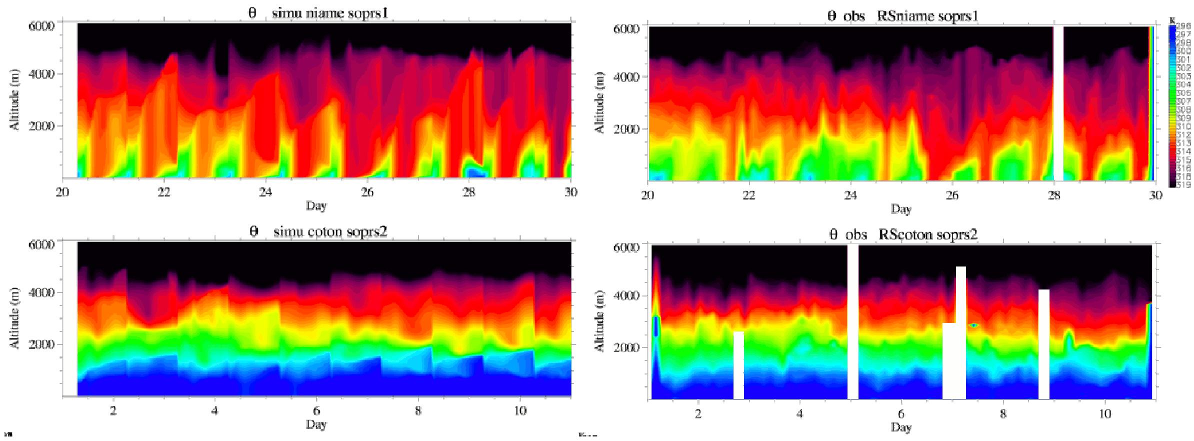

Figure 4-5 : Temporal evolution of potential temperature at Niamey (top plots) and Cotonou (bottom plots) simulated by the model in the daily simulations (REF, left) and observed in the 3 hourly radiosoundings (right) (see Appendices for Parakou and Niamey-SOP2).

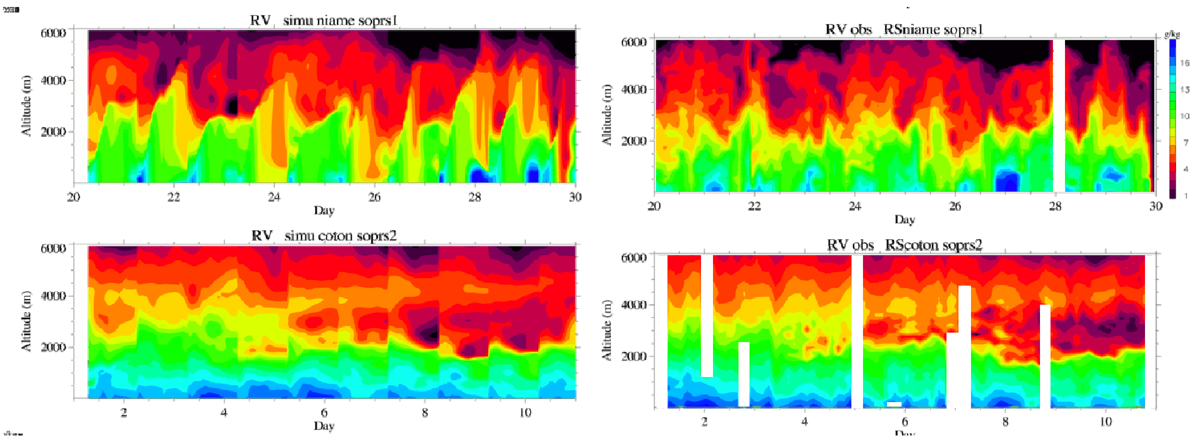

Figure 4-6 : Temporal evolution of water vapour mixing ratio at Niamey (top plots) and Cotonou (bottom plots) simulated by the model in the daily simulations (REF, left) and observed in the 3 hourly radiosoundings (right). (see Appendices for Parakou and NIamey-SOP2).

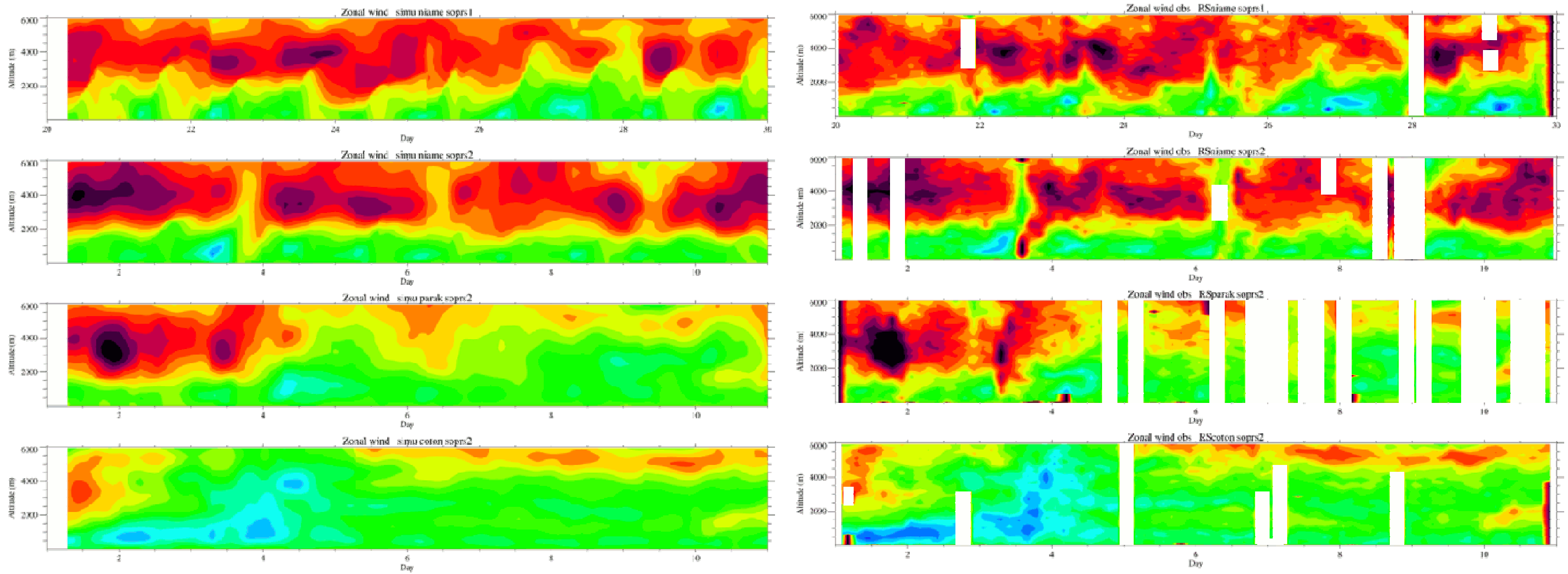

Figure 4-7 : Time series of zonal wind at Niamey-SOP1, Niamey SOP2, Parakou SOP2 and Cotonou SOP2 in the simulations reinitialised every 24hrs (left column) and in the radiosoundings (right column).

– ***Synoptic variability***

As the model is run in one-dimensional mode, the synoptic variability is mostly given by the advective forcings prescribed in the simulations. Figure 4-8 presents a time series of the infrared temperature (IRT) field over Djougou (9°42 N) (upper plot), which represents the deep cloud field, and on the bottom plot, the omega field extracted from the reanalysis at the closest point from Djougou. A good correlation is found between cold IRT (deep convection) and high negative values of omega (ascending motion). The suppressed convection conditions are also consistent (for example from 9 to 10 or 13 to 14 of August). This suggests that the synoptic variability of deep convection is well captured in the reanalysis.

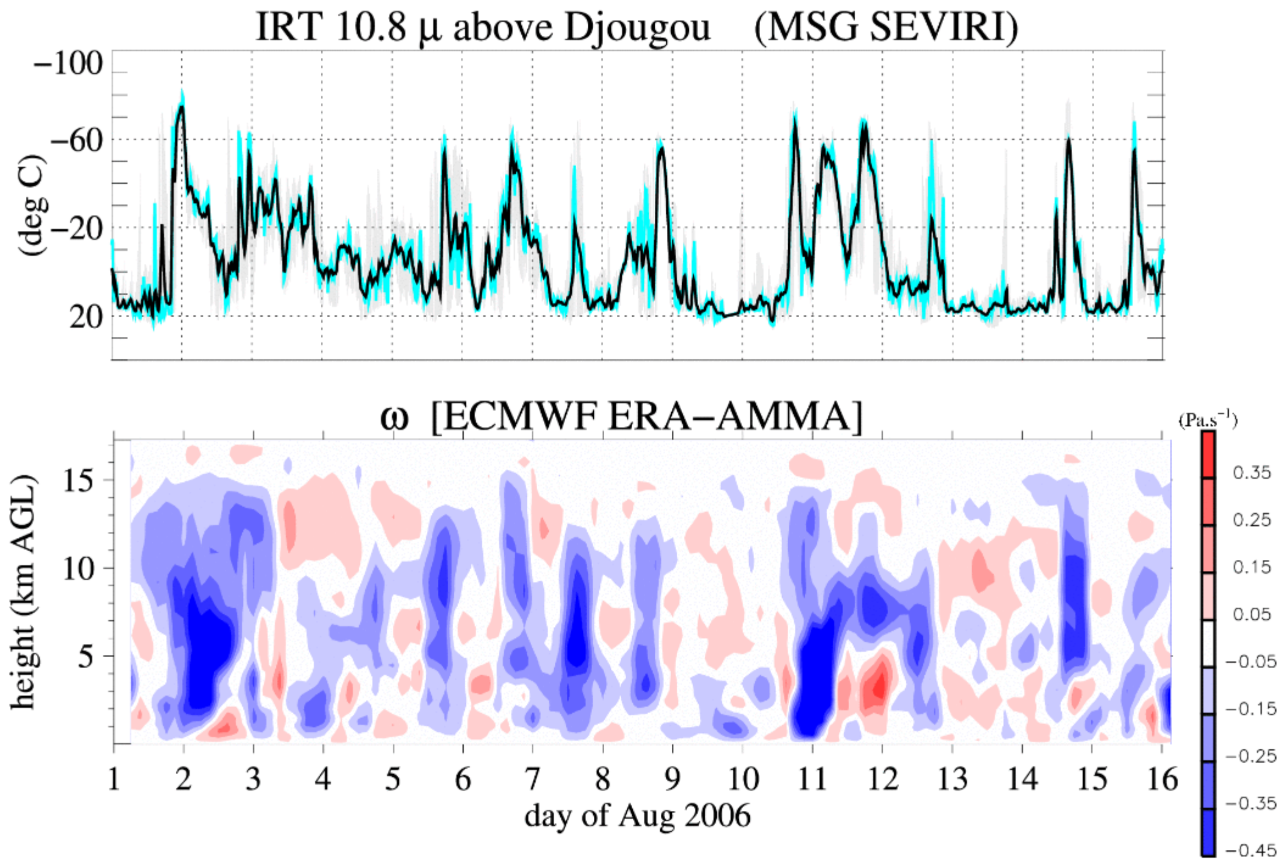

Figure 4-8 : Time series of InfraRed Temperature (IRT) at 10.8µm from MSG-SEVERI over Djougou (top plot) and corresponding time series of vertical motion (ω) extracted from the AMMA reanalysis (bottom plot). Negative ω values (in blue) are associated with ascending motion and positive values (in red) with subsiding motions.

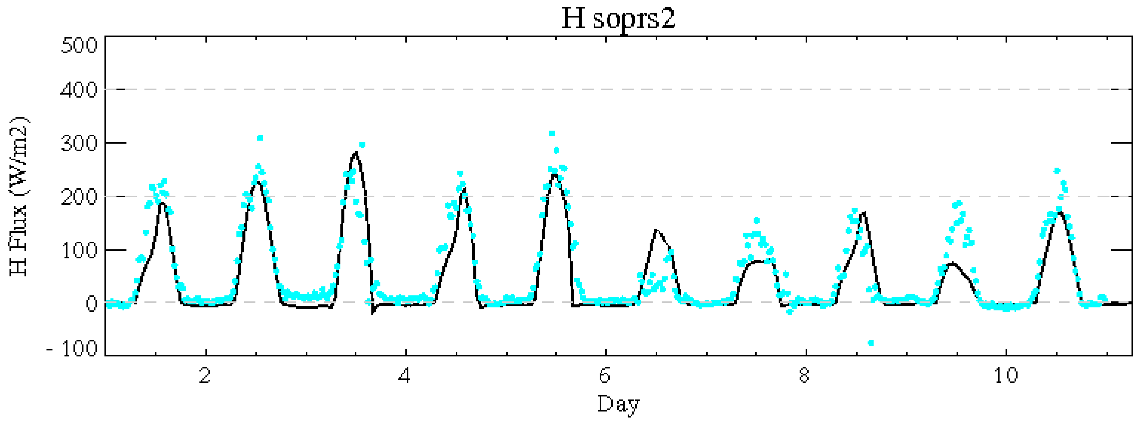

Figure 4-9 : Time series of sensible heat fluxes simulated by the model (REF, black) and measured by the Arm station (blue) at Niamey during the 1-11 August 2006 period.

The time series of sensible heat flux simulated by the model and the observed fluxes at Niamey during the SOP2 are shown in Fig. 4-9. Here also, the synoptic fluctuations of the surface fluxes are quite well captured by the model, with an increase from the 1^{st} to the 3^{rd} of August and then, a decrease on the 6^{th}. For instance, the drastic reduction in sensible heat flux on the 5^{th}, 6^{th} and 7^{th} are related to rainfall. The synoptic variability was also investigated on the precipitation field simulated by the model.

The brightness temperature measured by satellite over each site is plotted in orange in Fig. 4-10. A good correlation is found between the coldest brightness temperatures and the precipitation in the simulations in particular at Niamey-SOP1 and SOP2. This suggests that the synoptic variability of deep convection is also relatively well captured in the advection prescribed.

It is not straightforward to evaluate simulated precipitation at this local scale. Nevertheless, it is still valuable to compare the simulations with some observations. At Niamey, there are observations of rainfall at the ARM stations. Moreover, there are rainfall records at about 30 stations around Niamey (AMMA-catch network). According to these measurements, there were only few rain events that gave between 5 and 10mm of rain during the SOP-1. In the simulations, at Niamey-SOP1, four rain events bring in total 9mm over 10 days. So, this is quite in good agreement with the observations. However, during the SOP-2, the rain gauge network recorded, larger amounts of rain ranging from 40mm at some sites up to 105mm. In both cases, it is much larger than the rainfall amount simulated by the model (12mm). This deficit in precipitation in the model is probably linked at first order to the prescribed advection of humidity and temperature from the ECMWF reanalysis which are underestimated. This hypothesis is consistent with Agusti-Panareda et al. (2010) who found that, even if the AMMA reanalysis was performing slighty better than the operational system over the Sahel, precipitation amounts were still too low. At Parakou and Cotonou, there are no direct observations of precipitation apart from SYNOP data. An estimation of rainfall was obtained from REF2 satellite measurements. These estimates are not expected to be accurate for single rain events, however, they can give an indication over longer periods like here over the SOPs.

At Parakou, the estimate gives a total amount of about 100mm which agrees quite well with the precipitation simulated by the model (111mm). At Cotonou, the REF estimate indicates about 40mm of rain, which is larger than the simulated precipitation (20mm). A large system seems to be missed in the simulation (1st of August), which could partly explain the difference. The estimate, as mentioned above, can also overestimate the amount of rain. Otherwise, the stratiform rain obtained in the simulation seems to correspond to the observed regime.

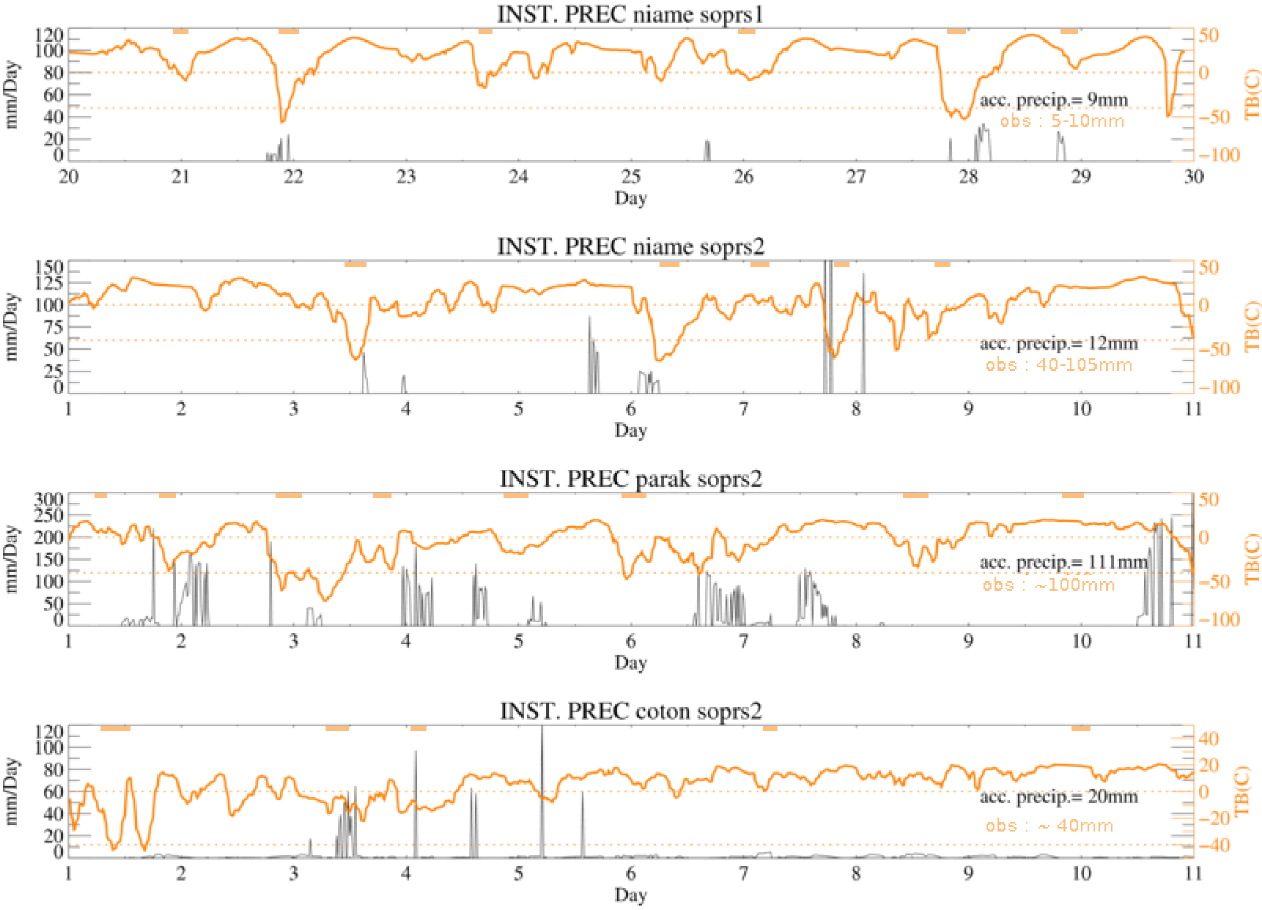

Figure 4-10 : Instantaneous precipitation extracted from the simulations (in black) at Niamey SOP-1 (top plot), Niamey SOP-2 (middle top plot), Parakou SOP-2 (middle bottom plot) and Cotonou SOP-2 (bottom plot). The orange lines correspond to the brightness temperature measured over each site. Cold temperatures(-40°C) can be associated with the presence of deep convective clouds and temperatures in the order of 0° with shallow convection. To mention , the precipitation axis varies with the different sites. Qualitative indications of observed (or satellite estimated) rainfall are represented at the top of each plot in orange.

– ***Diurnal regimes***

Contrasted diurnal cycles are observed along the meridional transect (see Chapter 3). Figure 4-11 shows the composite diurnal of humidity mixing ratio in the atmospheric low levels (0-500m) as a function of potential temperature computed from the simulations (full lines) and from the radiosoundings (dotted lines). As seen in chapter 3, the amplitude of the diurnal cycle increases with increasing mean temperature. The model appears to handle this meridional gradient relatively well. However, there are some noticeable difficulties:

- At Cotonou (in blue), the model simulates a diurnal cycle dominated by variation of potential temperature (294K-297K) with very weak variation of humidity (less than $1g.kg^{-1}$). However in the observations, the mean value of potential temperature is higher and the diurnal cycle is dominated by variation of rv ($2g.kg^{-1}$). The temperature does not fluctuate much.
- Concerning Parakou (in green), the cycle is shifted towards moister and cooler values and the cycle appears different from the one observed. In the simulations, an increase (decrease) of potential temperature is associated with an increase (decrease) of rv, whereas a different correlation is observed in the radiosoundings.
- At Niamey, the diurnal cycle presents an amplitude too important during the SOP-1 and SOP-2 with a drying and warming cycles too strong. However, the mutual behaviour is correct.

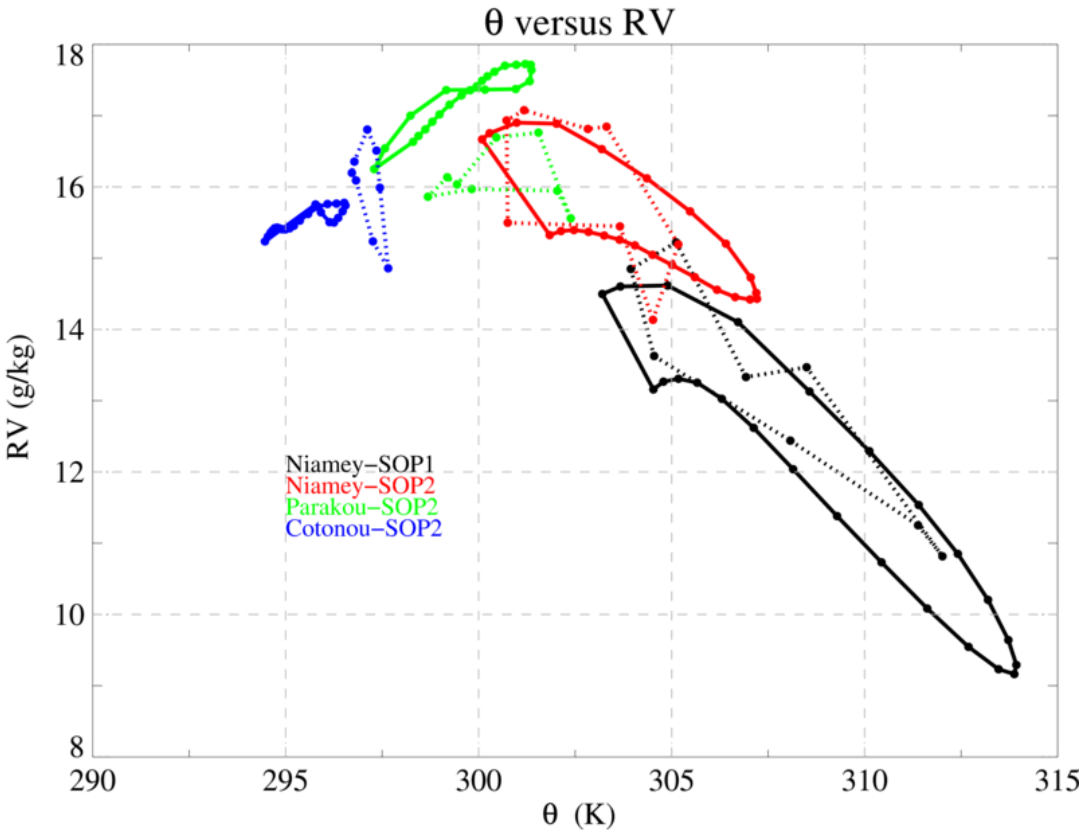

Figure 4-11 : Average diurnal cycle of RV(0-500m) as a function of the average diurnal cycle of θ(0-500) in the reference simulation (full lines) and in the observations (dotted lines).

Daytime Behaviours

After sunrise, the convective boundary layer (CBL) erodes quickly the nocturnal stable boundary layer and grows depending mainly on the sensible heat flux from the surface and secondly on the stability of the atmospheric profile and the entrainment rate in dry conditions. Figure 4-12 shows the average evolution of CBL height in the simulations (full lines) and in the radiosoundings (dotted lines) along the meridional transect. In the observations, the CBLs hardly reach 500-600m at Parakou and Cotonou whereas they develop up to about 1200m at Niamey during the full monsoon period and 2200m during the pre-onset period. In the simulations, the CBL at Cotonou is quite well represented whereas at the three other stations, the boundary-layer height is largely overestimated especially in the late afternoon. The reasons for this are investigated in the next sections.

The daytime evolutions of averaged vertical profiles of potential temperature and humidity mixing ratio are plotted in Figs 4-13 and 4-14. Daytime warming is excessive at Niamey-SOP1 (especially in the morning), during the SOP2 (especially in the early afternoon) and at Parakou-SOP2 (in the morning). At Cotonou-SOP2, the daytime warming is slightly underestimated at the surface and the late afternoon is too cold. At Niamey-SOP1, the excessive daytime warming is associated with an intense drying (slightly overestimated in the simulations). During the SOP2, the model simulates a daytime drying lasting all day, whereas in the radiosoundings a moistening is observed in the late afternoon. At Parakou-SOP2, a strong low-level moistening is simulated by the model, whereas only weak variations are recorded in the observations. At Cotonou-SOP2, the low-level rv variations are very weak in the simulations whereas in the observation a drying is observed in the morning and a moistening in the evening.

Night-time Behaviours

After sunset, the residual convective boundary layer cools down from the surface. A temperature stratification develops through the night. The nocturnal boundary layer deepening and stratification depends on the negative surface fluxes of heat, the advection and the turbulence. The figure 4-14 presents the evolution of averaged nocturnal profiles of potential temperature simulated in the model (left plots) and observed in the radiosoundings (right plots). In the observations, we see that cooling in the low levels is very different from one site to the other. Strong cooling in the lowest few kilometres are observed at Niamey SOP-1 (-5-6K), weaker cooling during the SOP-2 at Niamey (-3K) and Parakou (3K) and very little changes at Cotonou (-1K). Some difficulties can be directly noticed in the simulations. The model stabilised too much the lowest tens meters of the atmosphere whereas in the observations, this cooling is distributed over a deeper layer. This is particularly true at Niamey during the SOP-1 and SOP-2. Additional simulations were performed to assess the sensibility of the results to wind speed. The results were essentially very similar, the sensibility of the turbulence scheme was not enough to substantially modify these results.

During night-time at Niamey-SOP1, a moistening of the low levels is observed in the radiosoundings between 0000 UTC and 0300 UTC (see Fig 4-15). In the simulations, the moistening in the atmospheric low levels is strong, it is found over a deeper layer (0-2000m) and progressive throughout the night. Even if this night-time moistening is strong, it does not allow to recover from the excessive daytime drying. Thus, the daytime drift directly impact the simulation of the following night.

For the three other atmospheric regimes, a slight night-time drying is observed in the low levels. This is not well simulated in the model in the Niamey-SOP2 case which exhibits a moistening in the early evening. The drying is slightly overestimated at Parakou-SOP2 and underestimated at Cotonou-SOP1.

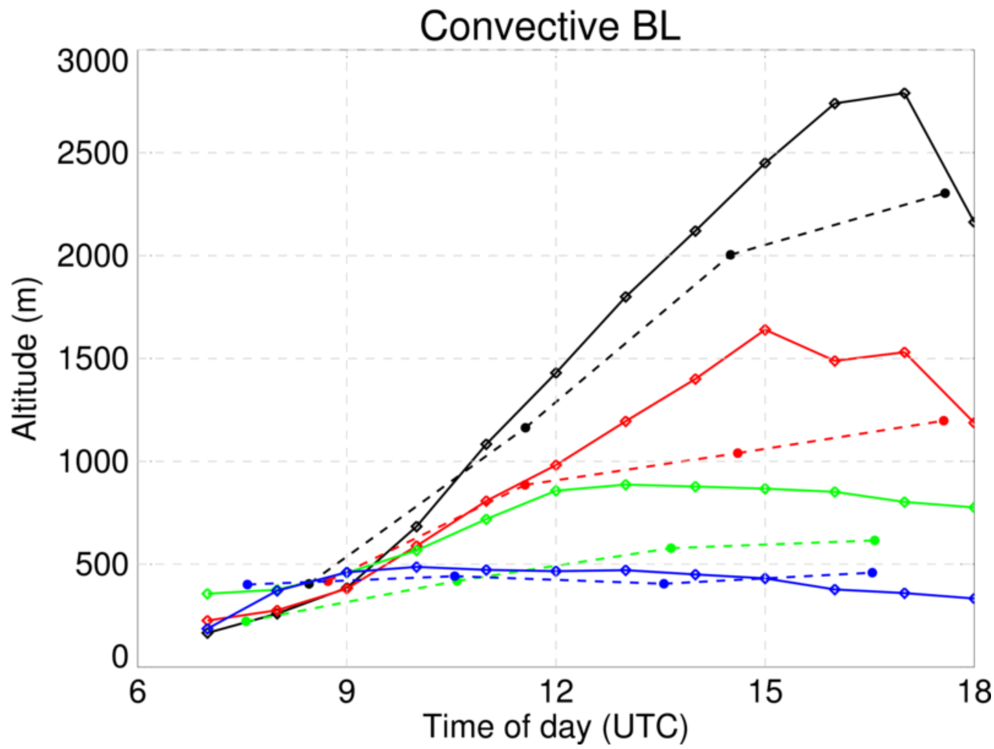

Figure 4-12 : Composite evolution of convective boundary layer height over the transect: Niamey-SOP1 (black), Niamey-SOP1 (red), Parakou-SOP2 (green) and Cotonou-SOP2 (blue) simulated by the model (full lines) and observed in the radiosoundings (dashed lines)

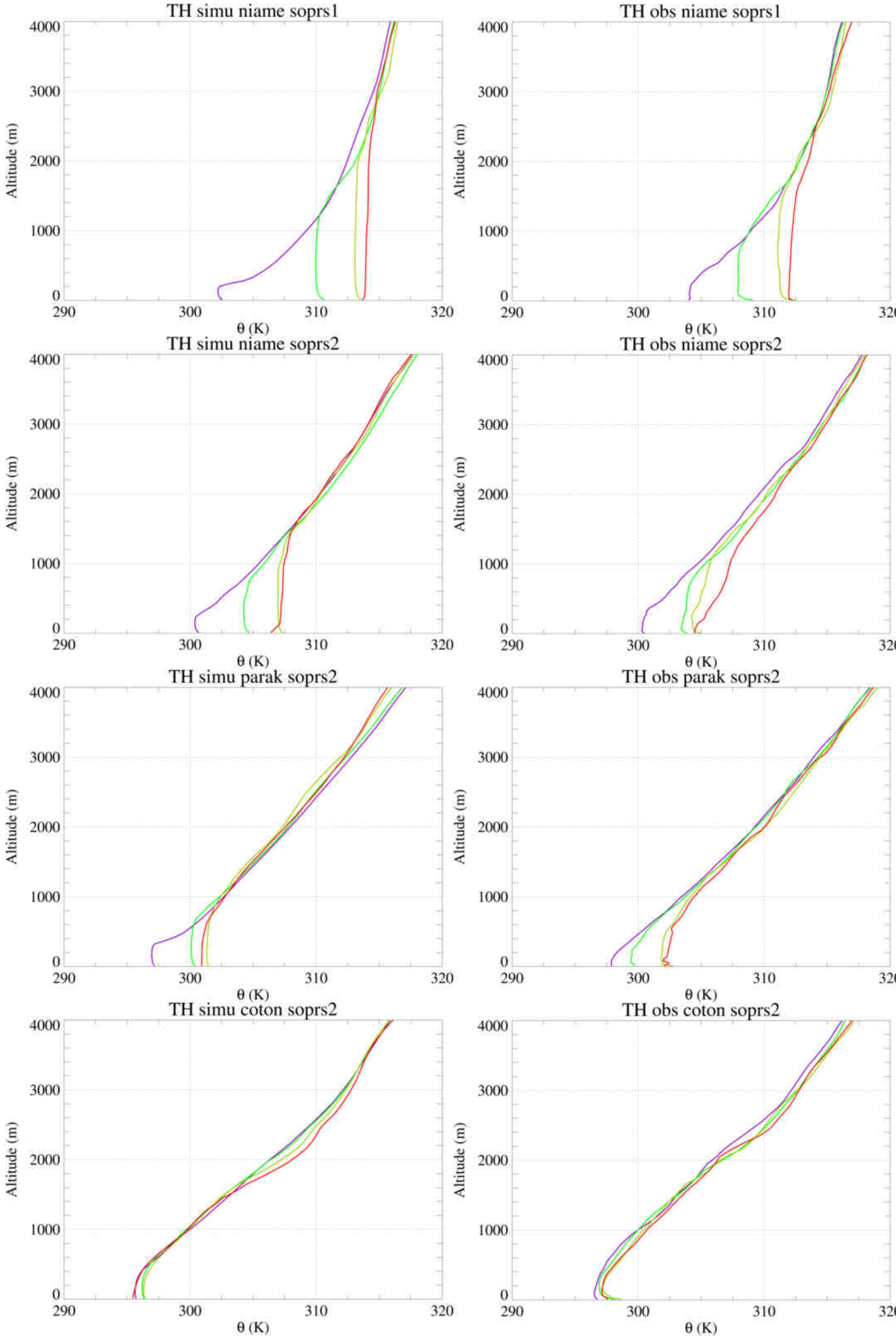

Figure 4-13 : Averaged daytime vertical profiles of potential temperature in the REF simulations (left plots) and in the radiosoundings (right plots) at Niamey-SOP1 (upper plots), Niamey-SOP2 (upper middle plots), Parakou-SOP2 (bottom middle plots) and Cotonu-SOP2 (bottom plots)

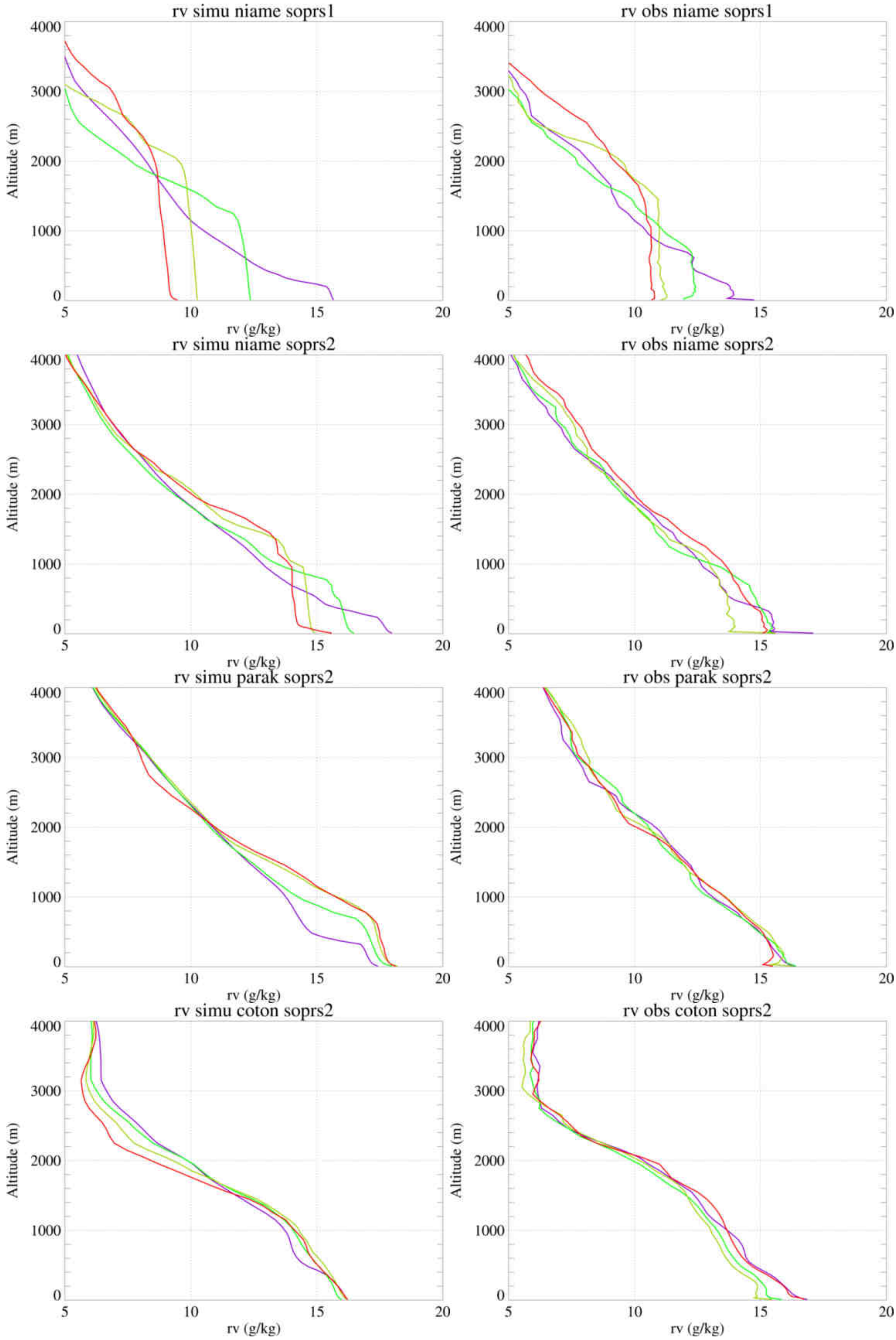

Figure 4-14 : Averaged daytime vertical profiles of water vapour mixing ratio in the REF simulations (left plots) and in the radiosoundings (right plots) at Niamey-SOP1 (top plots), Niamey-SOP2 (top middle plots), Parakou-SOP2 (bottom middle plots) and Cotonou SOP-2 (bottom plots).

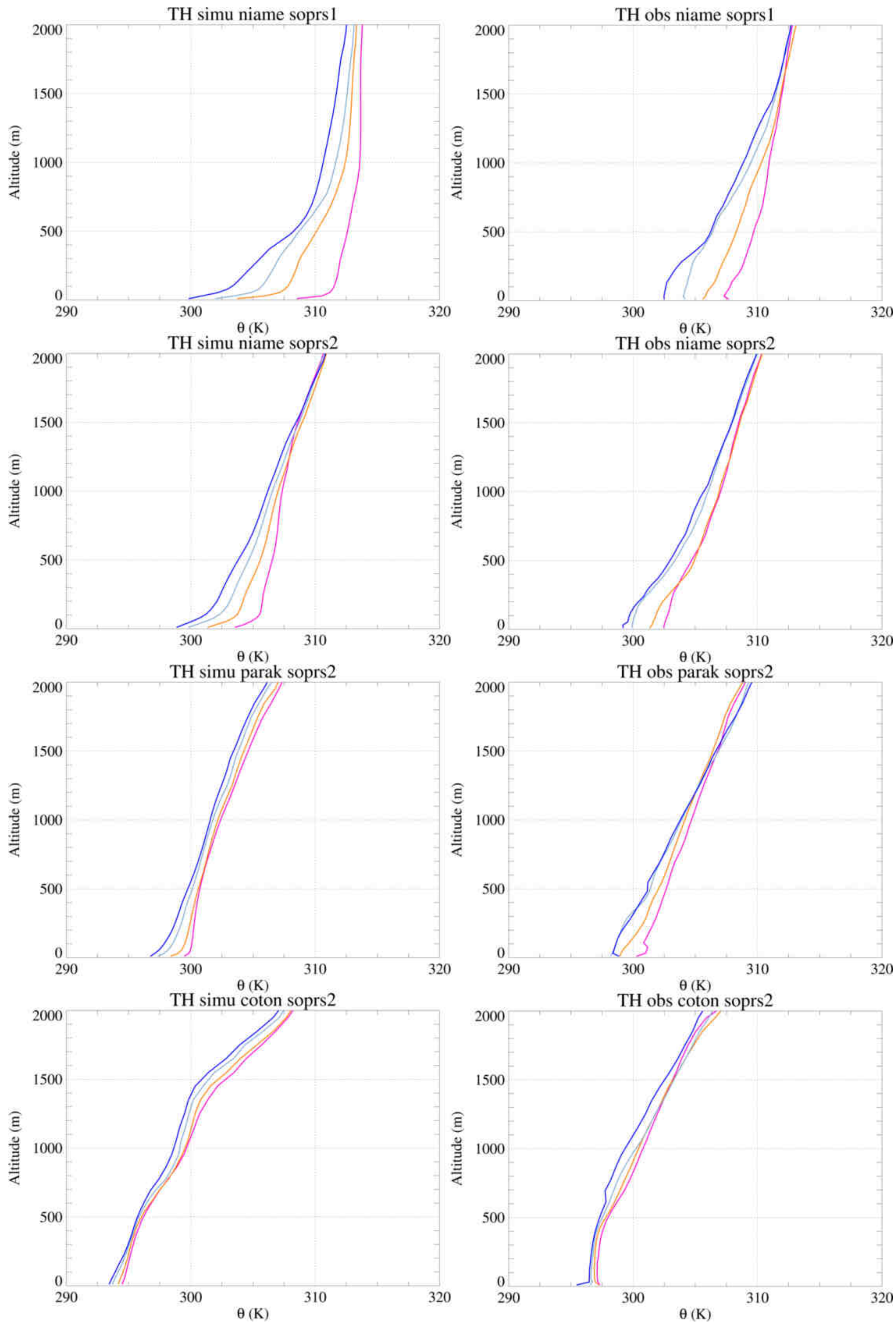

Figure 4-15 : Averaged nocturnal profiles of potential temperature in the daily simulations (left column) and in the radiosoundings (right column) at Niamey-SOP1 (top plots), Niamey-SOP2 (top middle plots), Parakou-SOP2 (bottom middle plots) and Cotonou SOP-2 (bottom plots).

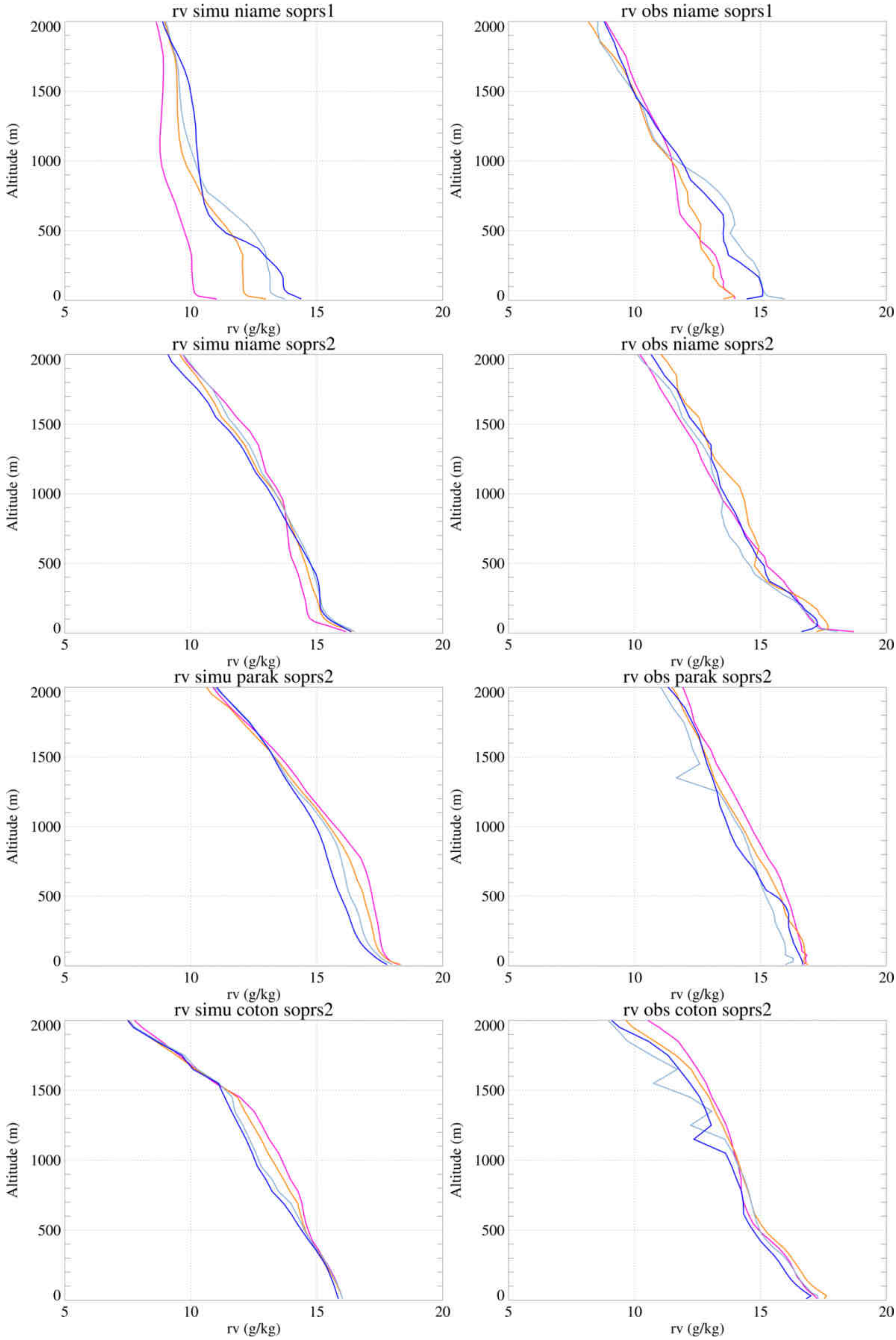

Figure 4-16 : Averaged nocturnal vertical profiles of humidity mixing ratio in the REF simulations (left column) and in the radiosoundings(right plots) at Niamey-SOP1 (top plots), Niamey-SOP2 (top middle plots), Parakou-SOP2 (bottom middle plots) and Cotonou SOP-2 (bottom plots).

– ***Sensitivity to the model setup and configuration***

The model equilibrium states for the four regimes were tested by running the model over ten days without reinitialisation (LONG versus REF). One first set of simulations was performed using the extracted forcings from the reanalysis (LONG) and a second one with a composite diurnal cycle of advection (COMPO). Figure 4-14 presents the evolution of θ and rv in the atmospheric low levels (0-500m) in the REF simulations (reinitialised every 24hrs, black lines), in the LONG simulations (10-days, full grey lines) and the COMPO simulations (10-days with composite forcings; dotted grey lines). The observations are over-plotted in blue. In the reinitialised simulations, the evolution of θ and rv are rather good over the period as well as the diurnal cycle. However, when considering the 10-day simulations, biases develop quickly after a few days. At Cotonou, a cold (-14K) and dry bias (-10g/kg after 10days) affect the simulation. At Parakou, this is also a cold and dry bias but to a lesser extent (-3K, -5g/kg after 10 days). At Niamey-SOP2, the simulations become too warm (5-10K) and too dry (-8g/kg after 10 days). At Niamey-SOP1, also a problem of excessive drying is observed (- 4-8 g/kg). Similar conclusions can be drawn with the COMPO simulations. This suggests that the individual advective forcings are not responsible for the drift of the simulation and, that the biases tend to result from a model equilibrium.

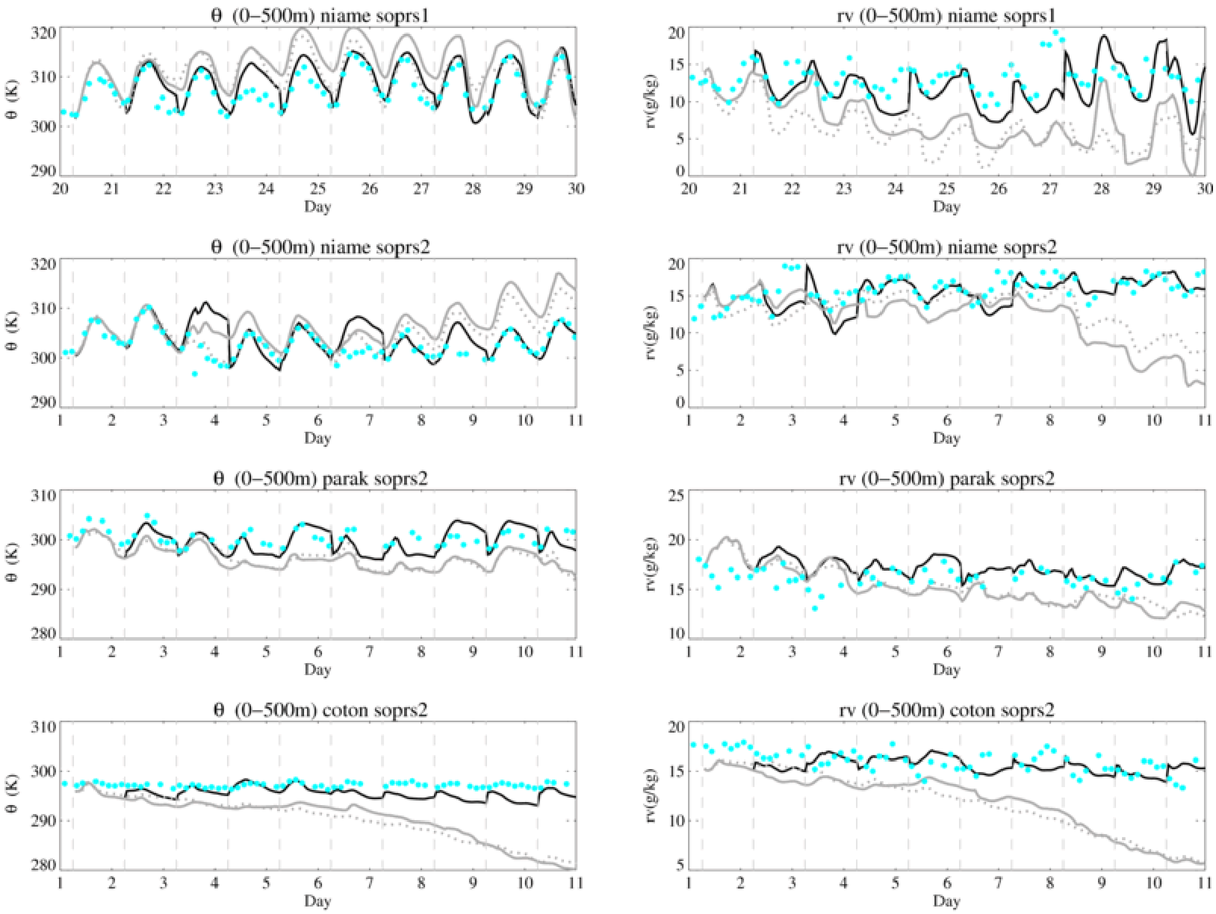

Figure 4-17 : Time series of potential temperature and water vapour mixing ratio in the low-levels (0-500m) in the simulations reinitialised every 24hrs (full black line), the 10-day simulations (grey full lines) and the 10-day simulations with composite forcings (grey dashed lines). The observations are shown in blue dots.

Niamey-SOP1 and Cotonou-SOP2 display particularly consistent drifts. In fact, 10-day simulations emphasize drifts which develop almost every day in the REF simulations. The reasons for each individual problem are investigated in the next sections. Budgets of potential temperature and water vapour mixing ratio have been investigated systematically. The analysis presented below focuses more precisely on surface energy budget components and boundary layers as these appear to be major elements to explain model results.

4.4.2 Cotonou SOP-2: Guinean post-onset regime

During the active monsoon period, deep convection is suppressed over the Guinean coast as the ITCZ moves towards the Sahelian zone (see Fig 3-1). The atmospheric regime at Cotonou is moist and slightly rainy. A stratocumulus layer is often present and reduces the incoming solar radiation.

In the REF simulations, the diurnal cycle of the temperature is too strong and the low levels too cold. Moreover, the atmospheric low levels do not exhibits enough variability in specific humidity (see Fig 4-11). In the LONG simulation, the model drifts towards a cold and dry equilibrium state (see Fig.4-17).

An energy budget strongly affected by clouds

These biases appear to come from close interactions between surface and atmospheric processes. The energy budget at the surface plays an important role in the diurnal cycle as well as on the equilibrium state of the model. The different terms of the radiative budget at the surface are shown on Fig. 4-18. The SWD is reasonably well represented in the first five days of the reference simulation (in black) and then, this flux is well underestimated (200 $W.m^{-2}$) in the simulation compared to the observations (800$W.m^{-2}$). This happens even earlier in the 10 day simulation (in grey). This decrease in incident shortwave radiation is due to the presence of low-level clouds in the simulations (see Fig. 4-19). Indeed, stratiform clouds form between 0 and 2000m above the ground.

The model has difficulties to represent the observed longwave fluxes, especially the mean and the diurnal cycle of the LWU. This flux directly depends on the surface temperature and its emissivity. The underestimation of the LWU (-50 -100 $W.m^{-2}$) is coherent with the underestimation of the 2m temperature and its diurnal cycle (not shown). The LWD fluxes depend on the temperature profile of the atmosphere and its content in water vapour/aerosols. The mean LWD value is relatively correct during the first few days and then, it is overestimated (+25$W.m^{-2}$). The diurnal cycle amplitude is always underestimated in the simulations. The down and upwelling fluxes are in the same order in the simulations (between 400-450$W.m^{-2}$). This results in a small net longwave flux. However, in the observations, the LWU always exceeds the LWD which leads to a cooling (-100 $W.m^{-2}$ during daytime and -50 $W.m^{-2}$ at night).

The net longwave radiation budget is not correctly simulated. However, the bias in the simulated net radiation is dominated by the bias in the net shortwave radiation. The first five days have a correct net radiation at the surface, in the daily simulation but the last days are biased even if the longwave bias slightly compensates for the loss. The soil moisture is high, therefore the net radiation is partitioned mostly into latent heat flux. For this reason, the convective boundary layers remain shallow (500m) as shown in Fig. 4-12. The greatest variability in BL heights is found in the morning in the observation and may be linked to the dynamic structure of the monsoon flow. This is not well captured by the model, which is possibly due to the prescribed advection.

A dry bias due to saturation process and weak latent heat flux

As seen in Fig. 4-11, not enough variability of humidity is represented, whereas too much temperature variability is simulated by the model. During night-time, the low levels cool excessively in the simulation compared to the observation. This accounts for the larger amplitude of theta diurnal cycle. The net radiation flux that drives the cooling, is slightly negative in the simulation, but less than in the surface observations. The advection is also very weak during night-time.

A decrease of qv between 0600UTC and 1200UTC is observed followed by an increase. The decrease in the morning involves boundary layer development, whereas the afternoon increase is possibly related to the input of water vapour by turbulent fluxes within a shallow BL, evaporation of precipitation and advections. However, in the simulations, a slight increase is obtained throughout the day.

The loss in specific humidity appears to be linked to the saturation reached when cooling the atmosphere down. Indeed, as the atmosphere gets cooler, the relative humidity increases and condensation occurs.

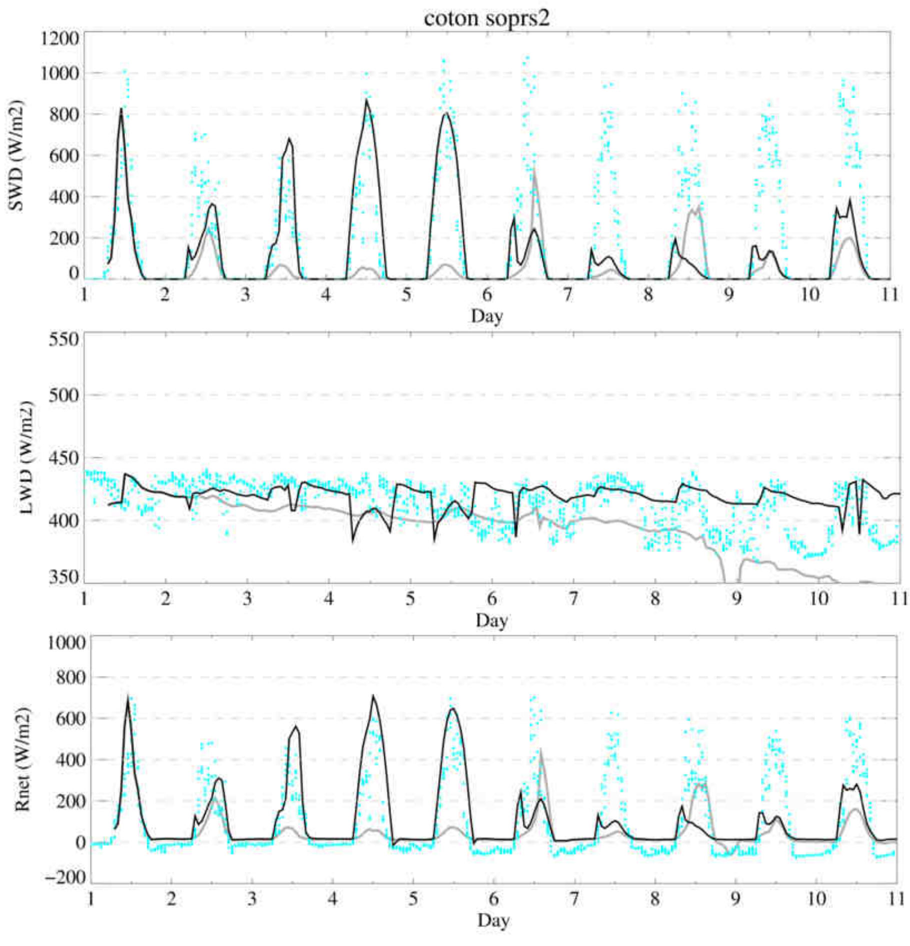

Figure 4-18 : Downwelling shortwave (top plot) and longwave (middle plot) fluxes as well as the net radiation (bottom plot) at the surface in the REF simulations (black lines), in the LONG simulations (grey lines) and measured at Cotonou between 1-11 August 2006 (blue dots). The data come from the IMPETUS measurements.

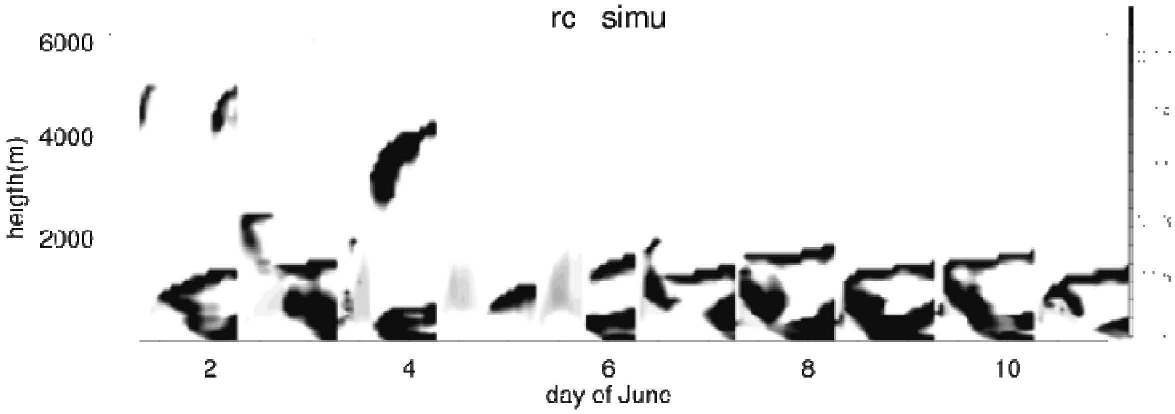

Figure 4-19 : Cloud field at Cotonou-SOP2 simulated by the model in the daily simulations.

4.4.3 Parakou SOP-2: Soudanian regime - convectively very active

Strong and intense convective systems develop and bring important quantities of precipitation at Parakou during the full monsoon period. Most of the time, convective systems form in the Soudanian region in the afternoon. Shallow cumulus clouds are often present in the morning and in the afternoon. The diurnal cycle at Parakou-SOP2 is characterised by a daytime warming/moistening (+8K, +1g/kg) and a night-time cooling/drying (-5K,-1;5g/kg) of the low level atmosphere. The REF simulation exhibits sometimes a cold/wet bias and sometimes a warm/wet bias (cf Fig. 4-17). The convective boundary layers develop too high (cf Fig 4-12). However, a cold/dry bias develops in the LONG simulations.

Figure 4-20 shows the 10 diurnal cycles of θ and qv in the atmospheric low levels (0-500m) simulated by the model (REF, left column) and in the radiosoundings (right column). The spread in the diurnal cycles of the potential temperature starts after 1200UTC in the model and then, it is not recovered (spread of 8K). On the other hand, in the observations, at the end of the nights, the behaviours converge again; i.e.: there is not much variability in theta and rv at the end of the night around 0500UTC. The day-to-day variability is found almost only during daytime (+/-2K during daytime versus +/-0.5K at the end of the night). The mean and the diurnal cycle of specific humidity are often overestimated in the REF simulations. While at 1700UTC, there is a maximum in temperature observed variability, there is a minimum of variability in the specific humidity, which is not simulated.

Figure 4-21 presents the composite diurnal cycle of surface fluxes at Parakou-SOP2 in the REF (black) and LONG (grey) simulations and observed at the IMPETUS station (blue). The SWD is well overestimated in the REF simulations (max=900W.m^{-2}) and to a less extend in the LONG simulation (max=600W.m^{-2}) compared to the observations (max=550W.m^{-2}).

The maxima are reached at different times; in the REF simulation it happens during the morning (1030 UTC), in the LONG simulation later (1130 UTC), whereas in the observations, it is found in the afternoon (1400 UTC). These biases in amplitude and timing of the SWD diurnal cycle are linked to the presence of clouds and their interactions with solar radiation. In the simulations, only resolved clouds interfere with the shortwave radiation scheme. Hence, sub-grid moist convection has no impact on the SWD. This explains the large values of SWD in the morning compared to the observations, when shallow cumulus clouds develop and reduce the incoming solar radiation. During the afternoon, deep convection develop and hence decreases the SWD.

The LWD and LWU are both overestimated in the simulations (except from 0600 to 0900 UTC for LWD). The diurnal cycle of the LWU is relatively good, whereas the amplitude of LWD diurnal cycle is not well captured. The time shifts in LWD & LWU closely follow the shift in SWD. Overall, the bias in the net longwave is not very significant (see Fig. 4-22). Indeed, during daytime, the net radiation bias is very similar to the bias in SWD, the other component of the budget only slightly modulated the intensity. On the other hand, during nighttime, the biais is small due to compensation between LWD and LWU, but in percentage, the difference is large (twice more fluxes in the observations than in the model ($-20 W.m^{-2}$ versus $-10 W.m^{-2}$). The turbulent heat fluxes in the REF and LONG simulations as well as the sensible heat flux from the observations are plotted in Fig. 4-22 (right plot). The latent heat flux dominates over the sensible heat flux with an evaporative fraction of 0.20 in the simulations. Only observations of H are available. The sensible heat flux is low compared to Rnet observed which suggests that the latent heat flux must be quite large (assuming that the ground heat flux is weak) but weaker than what is simulated by the model.

The diurnal cycle of the precipitation is well marked in the model. Figure 4-23 (top plot) shows the average diurnal cycle of instantaneous precipitation in the model in the REF simulations (in black). A distinct peak is observed in the middle of the afternoon and another one less marked during the night. The analysis of brightness temperature (in orange) indicates only a brief peak in the afternoon and an important deep cloud cover during the night.

The role of the advection prescribed in the simulation on this diurnal cycle was investigated through some sensitivity tests. The figure 4-24 shows the composite diurnal cycle of instantaneous precipitation obtained for the HOADV simulation (in red), the VERADV (in green), the ADVHOMO (in blue) and the REF simulation (in black). In all the daily simulations, there is no deep convection between 0600 UTC and 0000 UTC, there are two periods of precipitation, one in the afternoon (from 0600 to 1200 UTC) and one during the night (from 2100 to 0600 UTC). This afternoon peak occurs earlier in the sensitivity tests especially in the ADVHOMO simulation (1300 UTC). The evening weakening (from 1800 to 2100) is also observed in the different simulations. It is however less pronounced in the ADVHOMO simulation. The nocturnal precipitation appears in the four simulations but are weak in the HOADV. The similar behaviour obtained in the four simulations suggest that this precipitation diurnal cycle is due to the model physics and not to a lesser extend to the advection prescribed.

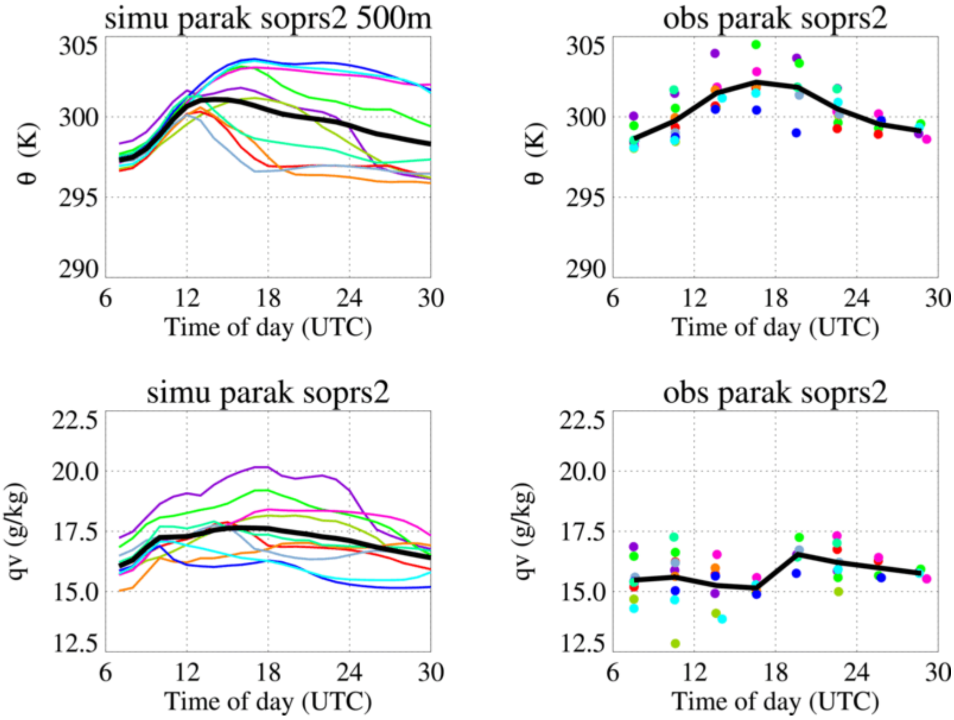

Figure 4-20 : Diurnal cycles of potential temperature (top plots) and specific humidity (bottom plots) in the atmospheric low levels (0-500m) in the REF simulations (left plots) and in the observations (right plots) over Parakou-SOP2. The black lines represents the composites over the period.

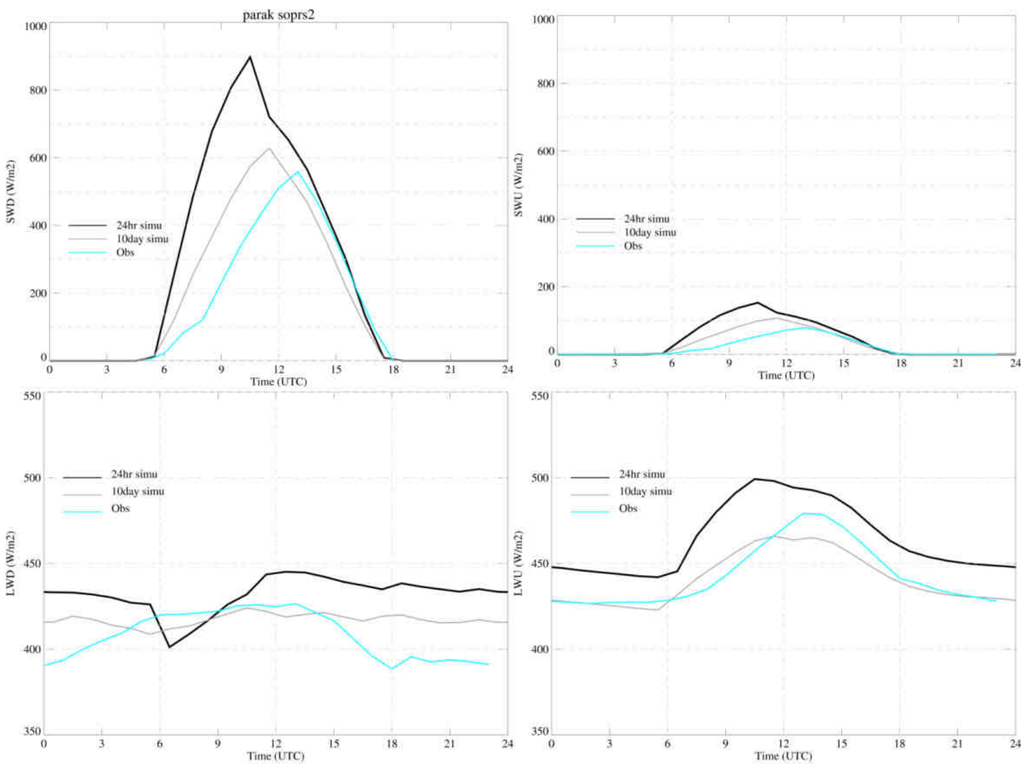

Figure 4-21 : Composite diurnal cycle of surface radiative fluxes at Parakou during the SOP-2: Downwelling and upwelling shortwave (top plots) and longwave (bottom plots) fluxes in the REF simulations (black full line), in the LONG simulations (grey) and from the IMPETUS fluxes measurements.

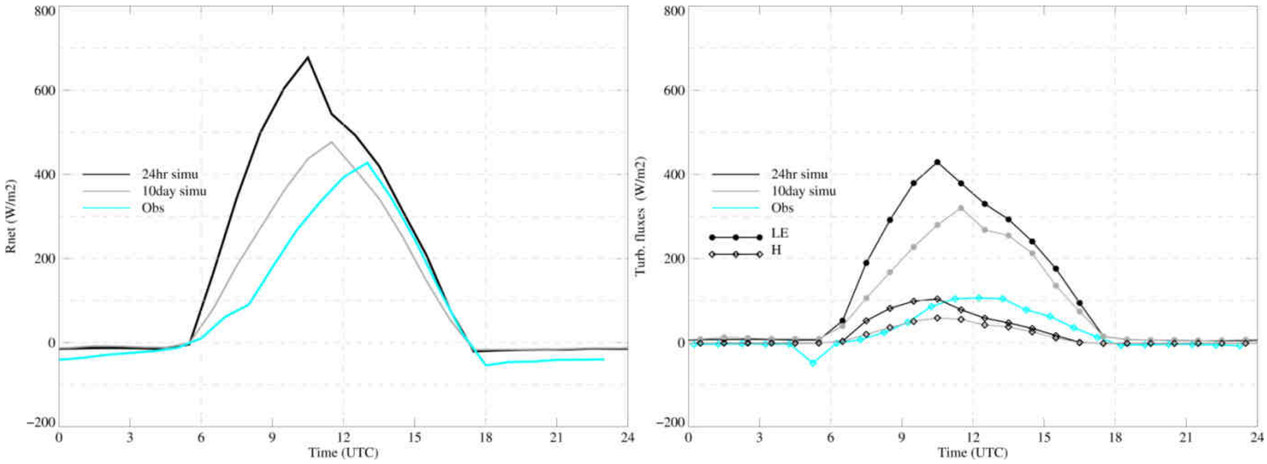

Figure 4-22 : Averaged surface net radiation (left plot) and turbulent fluxes (right plot) at Parakou-SOP2 in the REF simulations (black curves), in the LONG simulations (grey curves) and in the observations (blue curves).Only the net radiation and the sensible heat fluxes are available at Parakou.

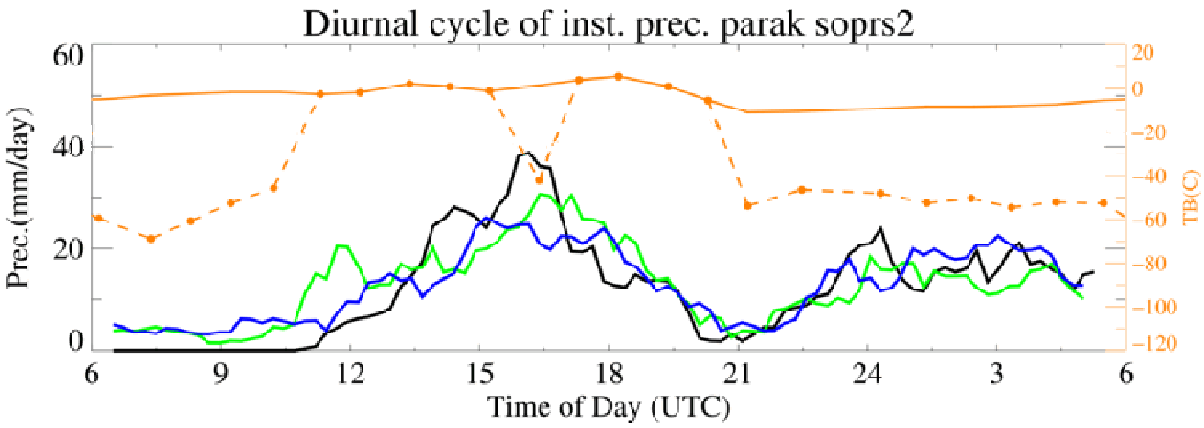

Figure 4-23 : Diurnal composite of instantaneous precipitation in the REF simulations (in black), in the LONG simulations (in green) and in the COMPO simulation (in blue). The full orange lines represent the composite diurnal cycle of brightness temperature, the orange dashed lines when a -40°C threshold is applied.

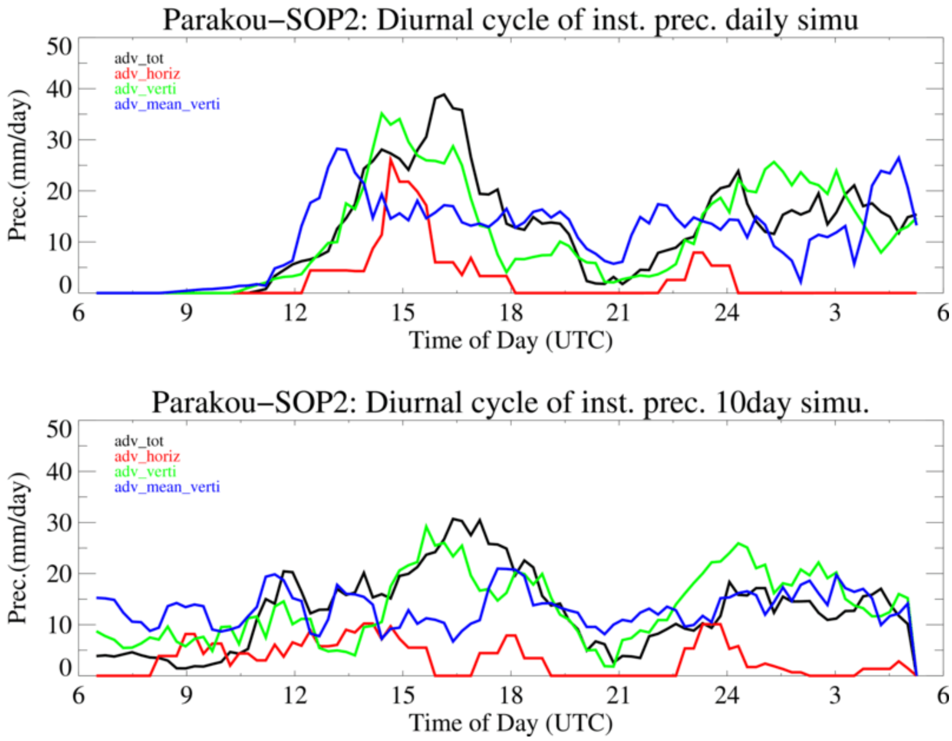

Figure 4-24 : Sensitivity of the diurnal cycle of precipitation to the advection field prescribed: Top plot: diurnal composite of instantaneous precipitation in the REF simulations (in black), in the HORADV simulation (in red), in the VERADV simulation (in green) and in the ADVHOMO simulation (in blue). Bottom plot: same as top plot for the 10-day simulations.

4.4.4 Niamey SOP-2: Sahelian post-onset regime: moist and convective

At Niamey-SOP2, the atmosphere is moist, large meso-scale convective systems develop very high into the troposphere and reach altitude higher than above the Soudanian region. However, they are less frequent than at Parakou and the cumulated rainfall is less. The soil is moist and hence, water is available for evaporation. The atmosphere is partly cloudy, but the net radiative forcing at the surface remains quite large (up to 450W.m^{-2}). The convective boundary layers have large equivalent potential temperature. As also noticed for Parakou-SOP2, the convective boundary layers also extend too high into the troposphere over Niamey (see Fig 4-12). In the Sahel, deep convection is often triggered in the afternoon. However, over Niamey, deep convection is for the most part associated with mesoscale convective systems initiated several hundred of km to the West and these are observed to sometimes last until the morning (e.g. the 6th and 11th of August, see also Rickenbach et al., 2009).

Figure 4-25 presents the composite diurnal cycle of surface radiative fluxes (SWD, SWU, LWD, LWU) in the REF (black), LONG (grey) simulations and in the observations (blue) at Niamey-SOP2. The SWD is larger in the simulations (max:900 W.m^{-2}) than in the observations (max: 780 W.m^{-2}.). The sub-grid clouds interact too weakly with the shortwave radiation. Hence, they do not reduce the incoming shortwave radiation. The SWU is overestimated only due to the larger SWD, the albedo in the simulation (0.26) is close to the observed one (0.22-0.28). The LWD is also overestimated in the simulations compared to the observations, especially during daytime. This is linked to the daytime warming of the atmosphere particularly strong in the simulations.

The simulated nighttime LWU are in good agreement with the observations, whereas the daytime values are too strong (max: 150 $W.m^{-2}$ higher than the observed maximum). In the morning, the resulting net radiation is excessive in the simulations compared to the observations as shown in Fig.4-26. However, in the afternoon and during nighttime, the simulations are quite close to the observations.

The average sensible and latent heat fluxes in the simulations and in the observations are shown in Fig. 4-27. The latent heat flux is over estimated in the REF simulations (230 $W.m^{-2}$) and in the LONG simulations (150 $W.m^{-2}$) compared to the observed flux (120 $W.m^{-2}$). In the REF, this can be due to the initialisation of surface properties that are too moist. The sensible heat flux is overestimated in the LONG simulation whereas it appears underestimated in the REF simulations.

The REF simulation is slightly too moist compared to the observation. The overestimation of latent heat flux plays a role in this bias for the non-precipitating days. This is partly compensated by the development too important of the convective boundary layers. However, the 10-day simulations drifted towards too warm and dry states, which can be explained mainly by the convective drying due to a excessive development of CBL. The partitioning of net radiation goes towards sensible heat flux and gives boundary layers too warm and too developed. Errors in precipitation bias cannot account for the observed trend.

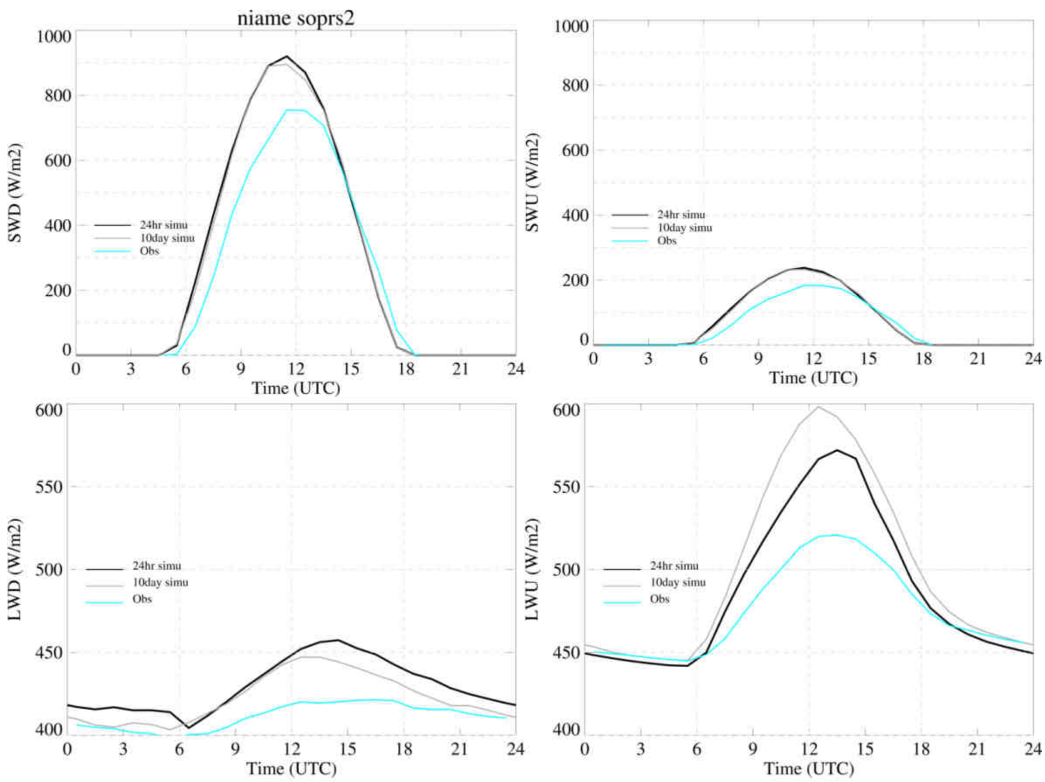

Figure 4-25 : Composite diurnal cycle of radiative fluxes at the surface at Niamey during the SOP-2: Downwelling and upwelling shortwave (top plots) and longwave (bottom plots) fluxes simulated by the model in the daily simulations(black full line), in the 10day simulations (grey) and from the impetus fluxes measurements.

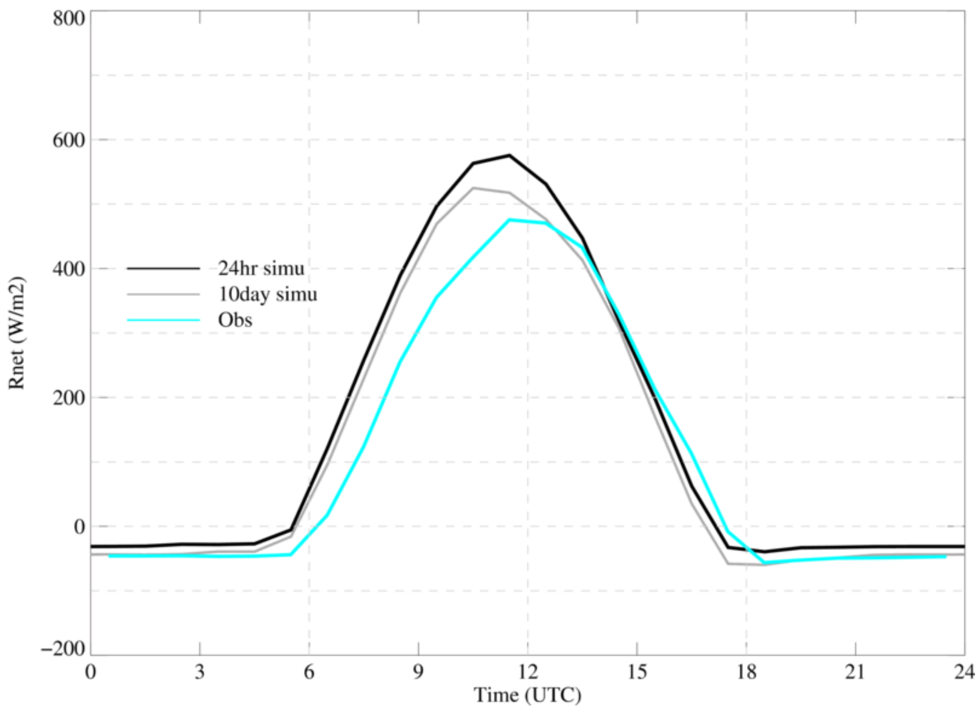

Figure 4-26 : Net radiation at the surface at Niamey-SOP2 in the REF (black) and LONG (grey) simulations and in the ARM observations (in blue).

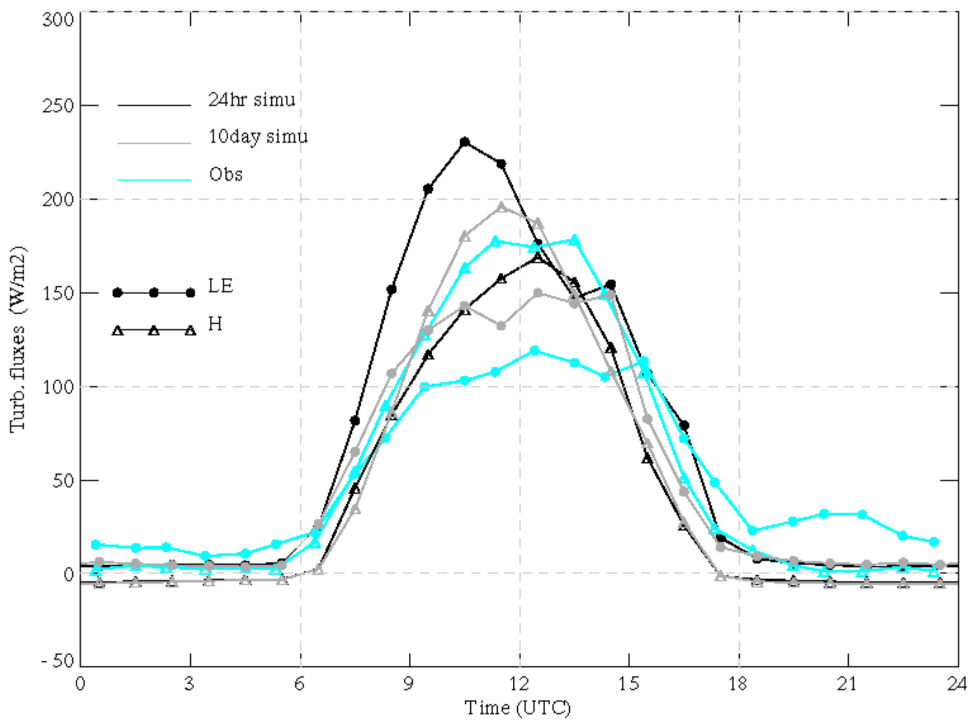

Figure 4-27 : Averaged turbulent fluxes at the surface at Niamey-SOP2 in the daily simulations (black curves), in the 10 day simulation (grey curves) and in the observations (blue curves).The sensible is represented with dots and the latent heat flux with triangles.

4.4.5 Niamey SOP-1: Sahelian pre-onset regime:

During the pre-onset period at Niamey, moisture is brought during night-time by the nocturnal jet in the atmospheric low levels. The moisture is then redistributed in altitude via turbulence of convective boundary layers. They reach high altitude (up to 2500m) and vertically stretch the monsoon flow. The entrainment of dry and warm air into the boundary layer is large in these conditions (Canut et al., 2010). Few cumulus clouds form at the top of the boundary layer. The net radiation budget is high (500 $W.m^{-2}$). Aerosols can though reduce the incoming shortwave radiation (optical depth up to 0.2) (McFarlane et al., 2009; Kocha, 2010). The soil is dry so the latent heat flux is usually weak (up to ~50W/m^2) and the sensible heat flux is very high (up to 400$W.m^{-2}$).

During daytime, the potential temperature increases too rapidly in the simulations compared to the observations. The simulated fluxes are in good agreement with the observed fluxes, as shown in Fig.4-28. Therefore, the surface fluxes cannot be responsible for this trend. The initial humidity is somewhat too high, but then decreases too rapidly. This behaviour can be associated with a excessive entrainment at the top of the convective boundary layer. Another reason has been identified. Three pulsations of monsoon flux are observed over Niamey. Pulsations are identified on the 21th, 23nd and 26th of June. In the simulations, these days are the most problematic ones. The simulations exhibits very high biases in temperature and humidity as can be seen in Fig. 4-5. The difference between the profiles simulated after 24hrs of run and the observed profiles are plotted in Fig. 4-29. We can see that on most days, the low levels are between 2 and 5K warmer than the observations and 1K cooler in the layer between 3km and 5km. The underestimation of the pulsations, that bring cool and moist air in the low-level atmosphere, could leads to a too quick warming of the boundary layer. The heating of the boundary layer not being slowed down by the large-scale advection can develop faster and warm faster.

Correction terms were calculated according to the bias obtained after 24hrs of simulations. They were then redistributed in an homogeneous manner over the 24hrs to correct the bias. As expected, they lead to reduce most of the biases. Thus, in that case, it appears that the prescribed advection is playing a major role in driving the model towards a dry and warm state, in an environment where the daytime boundary layer growth can be quite fast, within the Saharan air layer characterized by a relatively weak stability (small vertical gradient of potential temperature). The underestimation of the monsoon cool and moist advection tends to erode and even remove the delicate frontier separating these otherwise distinct layers. This leads to a mean state which is too warm and too dry in the low levels, and less cloudy.

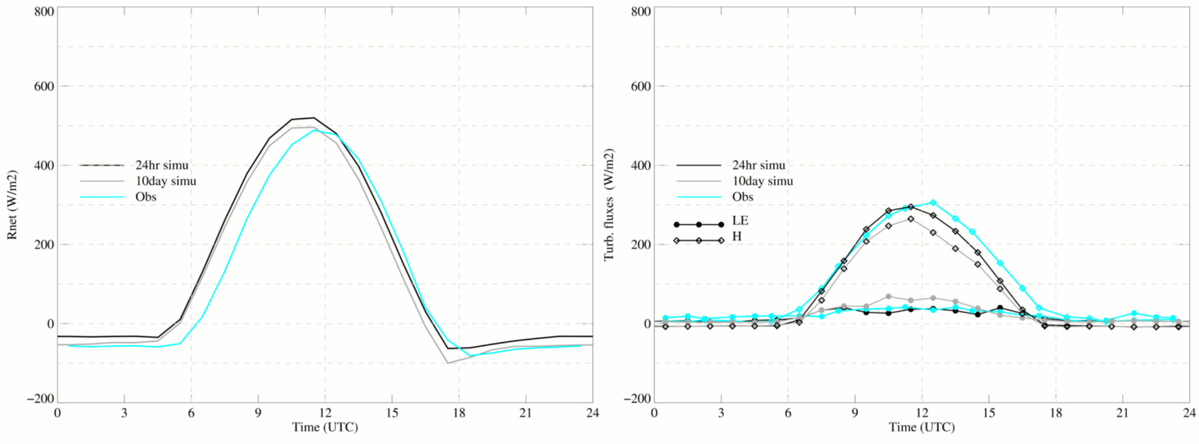

Figure 4-28 : Averaged net radiation (left plot) and turbulent fluxes (right plot) at the surface at Niamey-SOP1 in the daily simulations (black curves), in the 10 day simulation (grey curves) and in the observations (blue curves).

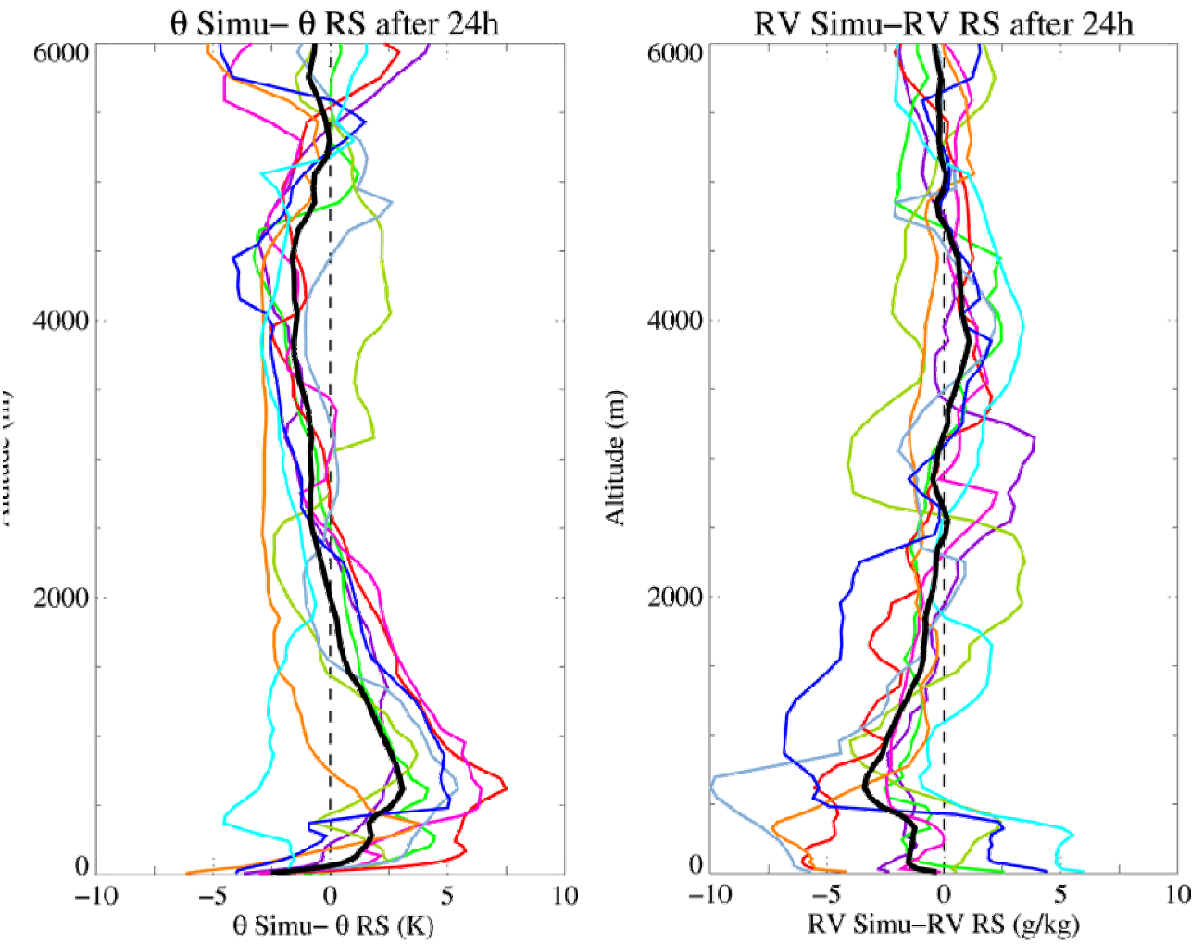

Figure 4-29 : Difference between the simulated profiles of potential temperature (left plot) and water vapour mixing ratio (right plot) after 24hrs of run and the radiosoundings.

4.4.6 Comparison with 2D simulation outputs

2D simulations of monsoon regime were performed by Peyrillé et al (2007) which represented a perpetual July month over a domain extending from 10°S to 40°N and averaged in the zonal dimension from 10°E to 10°W. The mean thermodynamic profiles closest to the radiosounding sites were extracted from the simulations and compared to the radiosoundings launched during the SOP2 at Niamey, Parakou and Cotonou. The results are presented in Fig 4-30. The simulated profiles are too dry in the Guinean regime and also in the Soudanian regime compared to the radiosounding profiles. The Soudanian regime presents also a cold bias. At Niamey, the simulation is excessively warm in the atmospheric low levels and dry compared to the radiosoundings. Thus, the 2D simulations present biases similar to the ones found in the 1D simulations. This suggests that the 1D modelling framework we developed here is a valuable idealisation of the simulations and can provide a useful test bed to test sensitivities. A further investigation could be on surface energy budgets to check whether the biases are associated with excessive incident fluxes.

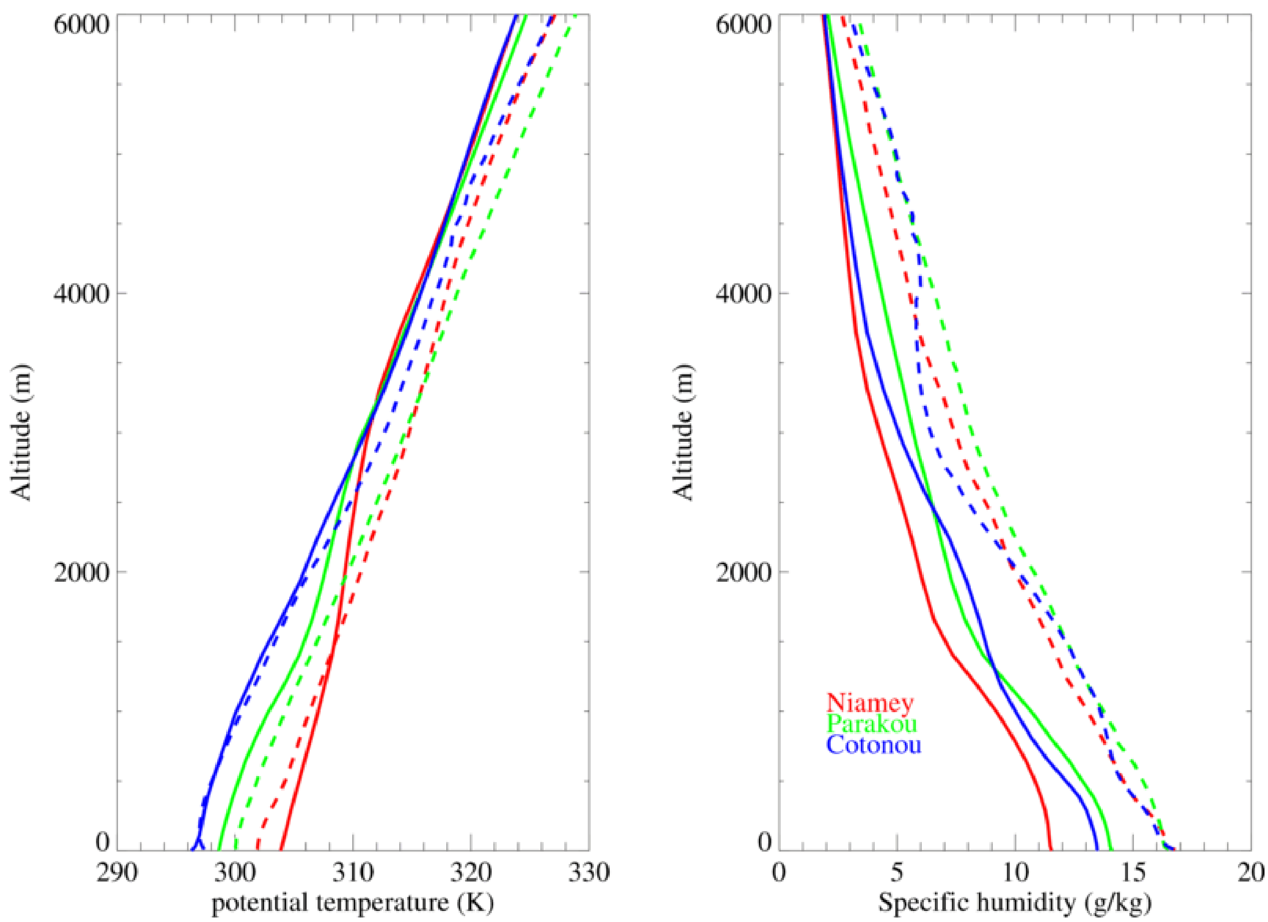

Figure 4-30 : Comparison of averaged θ and qv vertical profiles extracted from the 2D simulations (from Peyrillé et al, 2007) with the radiosoundings at Cotonou, Parakou and Niamey during the SOP2. The 2D simulation corresponds to a perpetual July month

4.5 Discussions and Conclusion

This study developed a new framework to study the modelling of the diurnal cycle under different regimes, based on AMMA observations and other products. This framework was used to investigate the ability of a coupled surface-atmosphere model to reproduce the diurnal cycles of four atmospheric regimes observed during the West African monsoon. The daily simulations capture relatively well the diurnal cycles and the synoptic variability. However, there are some biases in the diurnal cycles which, in the longer simulations, make the simulations drift. The model exhibits distinct biases for the different regimes revealing some complex and distinct interactions between processes.

The Guinean post-onset regime drifts towards an excessively cool and dry equilibrium state. The main causes for this is the formation of **excessive low-level stratiform cloudines**s that reduces considerably the incident shortwave radiation at the surface. The resulting sensible and latent heat fluxes at the surface are too weak to sufficiently warm and moisten the atmospheric low levels. The cooling induces a saturation reached more easily and hence condensation accentuates the drying process.

The Soudanian convectively active regime at Parakou during the SOP2 simulated by the model also presents some defaults. Indeed, in the daily simulations, convective boundary layers are too developed and too warm. This is largely due to **an underestimation of the shallow cumulus** cloud impact in the morning/early afternoon. The long simulations however drift towards a cooler and drier state.

The Sahelian monsoon regime, is relatively well simulated in the daily simulations. However, it exhibits some warm biases in cloudy and rainy conditions. In the longer term simulations, the equilibrium state drifts towards too warm and dry conditions, associated with excessive incident solar fluxes. The convective boundary layers develop too high and hence contribute to the warming and drying of the atmospheric low levels.

In pre-monsoon Sahelian regime, the model also presents some warm and dry biases. The radiative and turbulent fluxes are well represented in the model. The drift partly comes from the underestimation of monsoon pulsations which bring some cooler and moister air in the atmospheric low levels. The convective boundary layer warms too quickly and hence develops too high. The convective boundary layer grows within the Sahelian Air Layer which is a weakly stable layer, the model presents maybe also some difficulties to handle this kind of sensitive features.

Interestingly, the same simulated features are found using a simpler configuration (composite diurnal cycle of advection). This suggests that a simpler configuration could be used to test the model, its parameterization and sensitivities. The comparison with 2D simulations (including the same physics) show similar bias along the transect. This implies that this 1D framework provides an appropriate way to test the model behaviours. Some biases are linked to the prescribed advection and it would be valuable to conduct further tests to this forcing (e.g. advection from ARPEGE) and to investigate more systematically temperature and water vapour budgets.

Finally, this study stressed the importance of clouds over land. Over West Africa, they are either overestimated along the Guinean Coast or underestimated in the Soudanian and Sahelian regions. This turns out to have strong consequences at short timescales (diurnal) and is likely to affect longer timescales. When considering the meridional transect, the simulations present a cool bias in the South and warm biases in the Northern part of the transect. This corresponds to an increase in meridional temperature gradient. This favours the propagation of monsoon flow towards the Sahel and could lead to an overestimation of the low level meridional circulation and the monsoon flow. However, there is a dry bias at almost all stations that would disfavour the propagation of moisture towards the North.

Chapter 5
Links between Storm Initiations and Surface Properties

Contents

In this chapter, the couplings between surface properties and daytime initiation of deep convection are investigated with satellite observations. The section 5-1 presents the motivations and objectives of the study. The satellite data and the meteorological analyses used in the study are described in section 5.2. The methodology and the results of a mesoscale statistical study (at 1deg x 1deg scale) of the links between surface properties and storm initiations is presented in section 5.3. Finally, section 5.4 is dedicated to a study at finer scale (a few tens of km) on the links between gradient of surface temperature and storm initiations.

5.1 Motivation and Objectives

A number of previous modelling studies have stressed the significance of surface variability down to the mesoscale for clouds and convective precipitation (Anthes 1984, Chen and Avissar 1994; Pielke, 2001; Cheng and Cotton, 2004). On the other hand, observational studies are rare due to the scarcity of in-situ measurements (Taylor et al., 2006; Taylor et al., 2010), but critical to better evaluate and constrain numerical models.

Soil moisture plays an important role in the surface energy budget; it controls the partitioning of turbulent fluxes between latent and sensible heat fluxes (Betts et al., 1996) and it directly impacts the development of convective boundary layers at diurnal timescales (e.g.: Couvreux et al., 2009; Koelher et al, 2010).

Here, we specifically focus on the Sahel, a sub-tropical region characterised by a sparse vegetation cover. When a convective cloud brings rainfall there, the response of the soil to precipitation is strong, as it is only slightly damped by vegetation. Rain events induce a strong surface cooling and wetting, and, when and where the vegetation is sparse, it produces a decrease in albedo (Samain et al., 2008). Following a rain event, there is a significant enhancement of the surface evaporative fraction, which typically lasts a couple of days, especially in late Spring and early Summer, when the surface is hot and dry. According to past studies, the Sahel is a region where interactions between soil moisture and convection may be particularly significant to the regional climate and therefore, where studying interactions between soil moisture and convection is particularly relevant. Modelling studies have suggested that important interactions take place between surface moisture and precipitation in particular in the Sahel (Koster et al., 2004).

Mesoscale Convective Systems explain 70-80% of the precipitation in the Sahel (Mathon and Laurent, 2001). Most of them form in the afternoon or early evening and can last until the following morning (Mohr, 2004; Yang and Slingo, 2001). Convection is a complex phenomenon that involves large-scale atmospheric conditions like synoptic-scale African Easterly Waves (Burpee, 1972; Thorncroft et al., 2003). However, these large-scale phenomena cannot explain convective initiation which occurs at the mesoscale and is tightly linked to the properties of the atmospheric low levels. The (in)stability of the atmosphere in the Sahel, as elsewhere in the Tropics, is primary driven by the atmospheric low levels (Williams and Reno 1993; Guichard et al., 2008 ; Koelher, 2010). Indeed, CAPE is mostly controlled by the evolution of temperature and moisture in the lowest few kilometres of the troposphere and exhibits a strong diurnal cycle as well the CIN.

Wang et al.(2009) studied the development of convection over the Amazonian basin using in-situ and satellite data. They found that shallow convection was most often triggered over dry deforested region, but moist and more intense convective clouds were favoured over forested areas. They explained the more pronounced occurrence of clouds over the deforested areas by more convergence due to mesoscale circulations, from the forested regions to the deforested regions. The mesoscale circulations help overcoming the convective inhibition. However, over forested area the energy available for convection is larger due to more available moisture, which explains the occurrence of more intense storms.

Over West Africa, Taylor and Ellis (2006) studied over 100 individual storms occurring close to a wet patch with TRMM data. They found that deep convection tended to be suppressed over wet soils, whereas it was enhanced over dry soils. They suggested that low-level thermodynamics and dynamics could play a role in this result, but could not confidently state this conclusion because off the relatively coarse resolution of the TRMM dataset (around 30-40km) and the lack of observation of atmospheric low-level properties.

Several mechanisms are possible for the triggering of moist convection. Related to findings discussed above, it is interesting to note that Findell and Eltahir (2003) proposed the existence of distinct mechanisms of surface-atmosphere interactions depending on both surface and atmospheric conditions. They suggest that if the temperature profile between 900 and 700 hPa is close to the dry adiabatic, then the triggering of moist convection is more likely when soils are dry, otherwise convection should be more favoured over moist soil conditions.

This chapter presents a satellite based study on the links between surface properties and **initiation of convection**. In this study, we investigate whether or not deep convection is preferentially triggered over specific surface properties and whether the behaviour observed over Amazonia by Wang et al (2009) also valid in the Sahel. We will also investigate further the work of Taylor and Ellis (2006) who found that well-developed convection is suppress or weakens when passing over moist surface patches in the Sahel by looking whether the initiation of convection is also influenced by surface properties. And if so, is it in the same way?

This work originates from a close collaboration with my supervisors Françoise Guichard and Fleur Couvreux, and researchers from CEH-Wallingford; Chris Taylor, Phil Harris and Richard Ellis. This chapter is organised in the following way; First, the data used in this study are presented and discussed. This includes surface property estimates and location of convective initiations. Then, the second section focuses on a statistical analysis of the links between soil moisture and initiation of convection at a length scale of 1*1deg², the method and the results are presented and discussed. The third section presents a finer scale study and focuses on the links between soil moisture and convection at smaller scale on the order of few tens of kilometres. Finally, this section ends with discussions and conclusions.

5.2 Satellite Datasets

5.2.1 Surface properties

Satellite measurements, unlike to in-situ measurements, can cover a large spatial scale. To monitor surface properties (soil moisture, land surface temperature, LAI, etc..), satellite measurements are very useful, as they allow us to get information at a length scale which is likely to affect convection. Several estimates of surface properties based on microwave and infrared measurements are used in this study. First the AMSR-E soil moisture estimates and then, the Land Surface Temperature (LST) from MSG are presented.

– ***AMSR-E soil moisture estimates***

The Advanced Microwave Scanning Radiometer on Earth Observing System (AMSR-E) is a multi passive microwave instrument onboard the AQUA satellite. It was launched in 2002 in order to measure the brightness temperature at five different frequencies. The satellite passes twice a day over West Africa (1.30am and 1.30pm), as it operates in polar sun-synchronous orbit. The AMSR-E passive microwave radiometer measures at six different frequencies including 6.925, 10.65, 18.7, 23.8, 36.5, and 89.0 GHz.

Soil moisture products are derived from brightness measurements of microwave radiometers using a Land Parameter Retrieval Model (LPRM; Owe et al.,2008), which is linked to the dielectric constant of the soil. The spatial resolution is 0.25deg x 0.25deg. This product was evaluated against in-situ measurements in West Africa, more precisely on the AMMA-Mali site which is located in the semi-arid Sahelian area by Gruhier et al. (2008, 2010). These results suggests that AMSR-E soil moisture products provide reliable information on the seasonal soil moisture variations as well as after rainy events. It must be noted that soil emission is damped by densely vegetated areas and this reduces the sensitivity of the signal (Owe et al., 2008). Therefore, in our study, the southern part of West Africa (south of 10°N), which is densely vegetated, is not considered.

Figure 5-1 presents a comparison between the different soil moisture estimates carried out by Gruhier et al. (2010) for the Sahelian region. The black curve corresponds to the in-situ measurements and the coloured ones to the satellites based estimates. There are two different estimates based on the AMSR-E measurements; the difference comes from the retrieval methods. The AMSR-E/NSIDC (orange curve on Fig. 5-1) is obtained from an iterative inversion algorithm using 10.7 GHz and 18.7 GHz data. The second estimate is the AMSR-E/VUA product (purple curve) which was developed by the VU University Amsterdam in collaboration with NASA. It uses the dual polarised 6.9GHz channels to retrieve soil moisture and vegetation cover simultaneously. Therefore, it does not need additional information on vegetation for the retrieval. Additionally, two different estimates based on the European Remote Sensing (ERS) satellite measurements (ERS-CETP, ERS-TUW) are also compared. These dataset have significantly less data available.

A wide range is found among the different estimates revealing that there are still some difficulties to estimate precisely the soil moisture from satellite. In view of the comparison results, the AMSR-E estimates from the University of Amsterdam (AMSR-E - VUA) is the best product for the Sahelian region. In this study, we chose to use these estimates and we mainly worked with anomalies of soil moisture estimates (method presented in the next section), which are less dependent on the retrieval method.

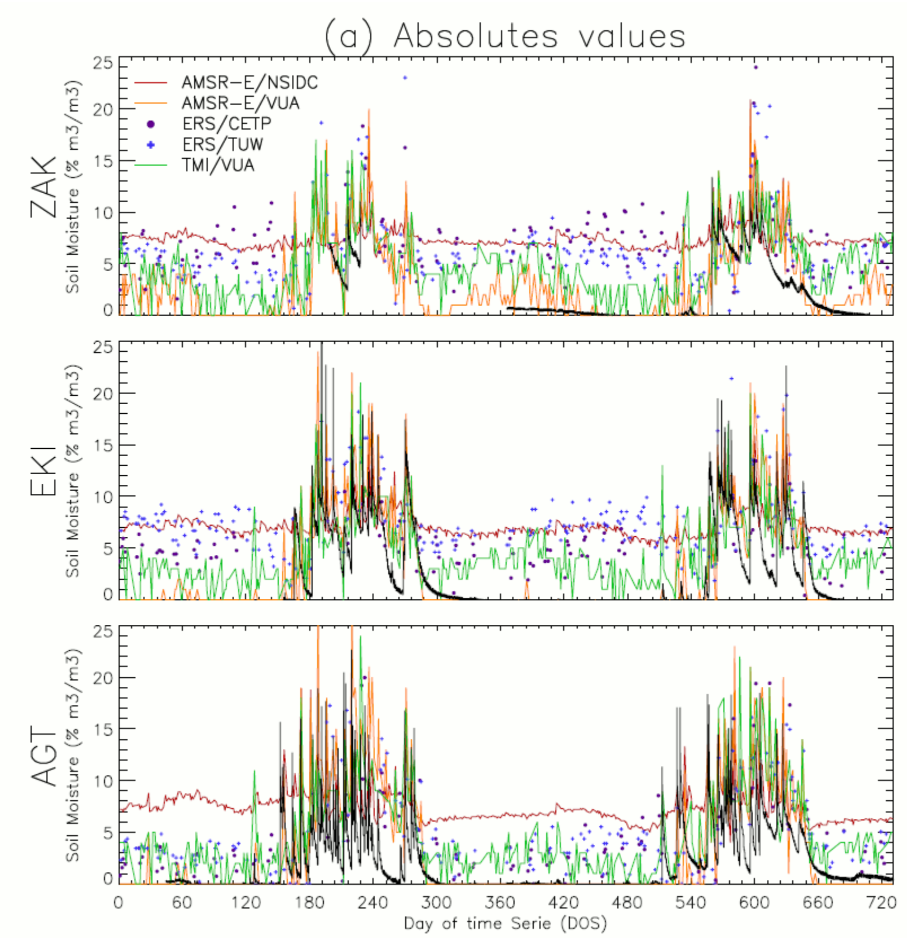

Figure 5-1 : Soil moisture values for all soil moisture products over three ground stations(ZAK: In Zaket (16.5°N, 1.8°W), EKI: Ekia (15°9, 1.2°W) and AGT: Agoufou (15.3°N, 1.4°W)). The ground measurements are presented in black and the different colour lines represents the different products: AMSR-E/NSIDC (purple), AMSR-E/VUA (orange), TMI/VUA (green) and colour dots the ERS estimates: ERS/CETP (purple), ERS/TUW (blue).(figure from Gruhier et al., 2010).

The AMSR-E soil moisture products are estimates of soil moisture in the top few centimetres of the soil. This is appropriate for our study in the sense that we are interested in the interactions between the surface and the atmosphere occurring on short time scales (hours to diurnal time scale) . The properties of this layer control the partitioning of energy flux between latent and sensible heat fluxes at the sub-diurnal scale.

Figure 5-2 presents a map of AMSR-E soil moisture field over the Sahel (left panel) after the passage of a MCS, whose sequence is documented on the right panel with MSG IR data. A clear mesoscale moisture pattern which appears in red on the figure is depicted by the satellite estimate. This soil moisture feature was consistent with in-situ soil-moisture data (not shown). This illustrates that the AMSR-E estimates provide valuable information on the impact of MCS at the surface and that they are also well suited for mapping recent rainfall patterns. These strong wet anomalies observed in the aftermath of rainfall are rapidly attenuated and disappear after a few days due to sparse vegetation and strong solar heating. The AMSR-E measurements see through cloud and aerosol covers and hence, can sample soil moisture in almost all atmospheric conditions. This is not the case for the second surface property estimate that we present in the next section.

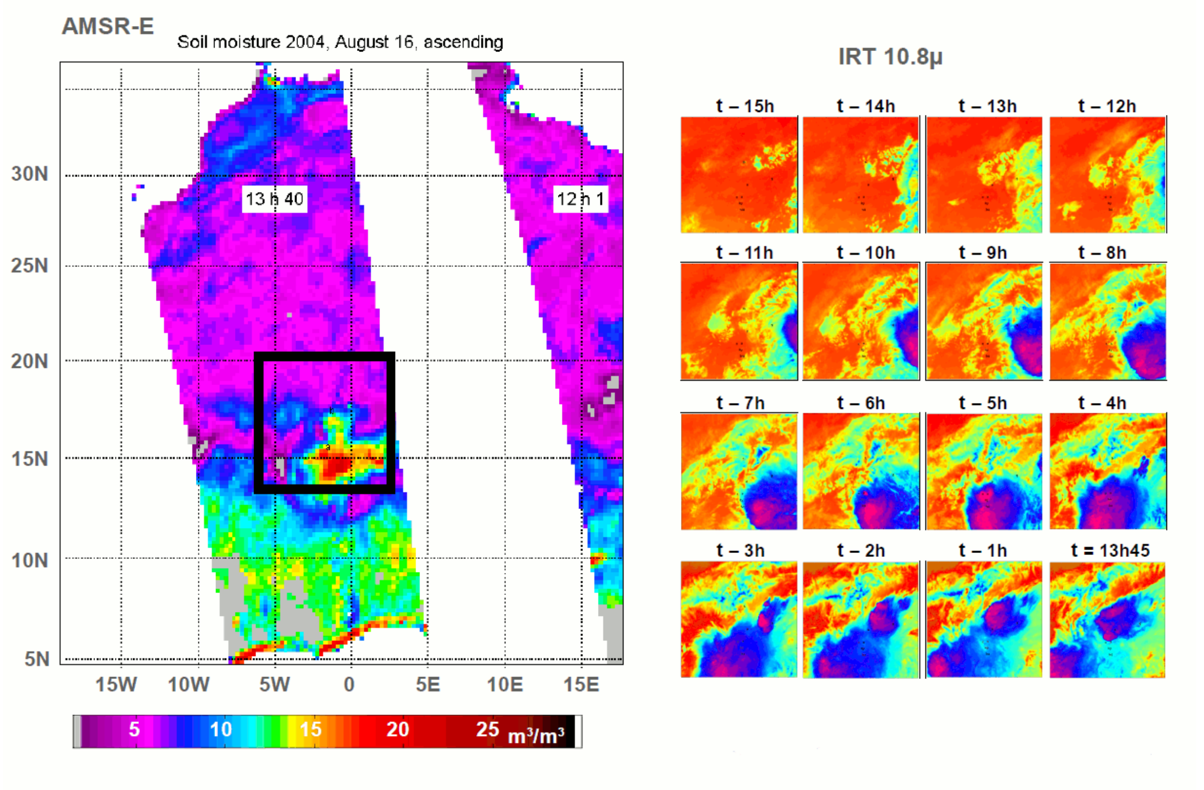

Figure 5-2 : Mapping of soil moisture field from AMSR-E estimates during its ascending swath (left plot). This illustrates the strong heterogeneities induced by a mesoscale convective system activity which crossed this area a few hours before. On the right panel, the trajectory of this system as tracked by MSG infrared temperature at 10.8 microns is shown, the black rectangle in the left panel indicates the area documented by the IRT maps. (figures from Gruhier, Kergoat and De Rosnay)

– ***Land Surface Temperature***

The Land Surface Temperature (LST) is defined as the skin temperature of land surface measured in the direction of the sensor. It is estimated from derived satellite measurements of infrared emissions of the Earth. Retrieval methods based on radiative transfer are used to approximate the value of the skin temperature taking into account the atmospheric influence and the land surface emissivity, which must be adequately known. The accuracy of the atmospheric corrections depends on the quality of radiative transfer models, uncertainties in atmospheric molecular absorption coefficients, aerosol absorption/scattering coefficients and errors in the atmospheric profiles.

In this study, we use LST derived from SEVIRI (Spinning Enhanced Visible and InfraRed Imager) instrument onboard Meteosat Second Generation (MSG). The retrieval of LST is done by the LandSAF group (http://landsaf.meteo.pt). It is based on clear sky measurements in the thermal infrared window at 10.8 and 12.0 microns. The identification of cloudy pixels is obtained via a cloud mask generated by the Nowcasting and Very Short Range Forecasting Satellite Application Facility (NWC SAF) software. The Generalised Split-Window (GSW) algorithm (Wan and Dozier, 1996) was used to retrieve LST. The spatial resolution of this product is 3x3km² and it has an image-repeat cycle of 15 minutes.

Additional cloud/aerosols screening techniques were applied to remove contaminated LST data over West Africa. The principle of this technique consists in looking at the temporal variability of each individual pixel and keeping only the ones with slowly changing LST as expected in clear sky conditions. The dust detection is based on an algorithm developed by Chaboureau et al. (2007). This consists in comparing two channel emissions (10.8 and 12 microns). An example of LST map is presented in Fig. 5-4. This situation is characterised by well defined structures at the mesoscale; hot spots indicated in yellow and cool ones in green. The analysis of turbulent fluxes and in-situ soil moisture measurements at different sites (Niamey, Wankama and Banizoumbou) let us think that these patches are associated with the passage of antecedent rainfall. This indicates that LST fields are also shaped/controlled by antecedent rainfall. LST patterns were also found to be effective in locating recent soil moisture pattern associated with MCS during the Jet2000 Experiment(Taylor et al., 2003).

However, there are uncertainties in the absolute value of LST. Relatively strong differences in LST are found when comparing different LST satellite estimates. A comparison of LST from MSG and LST from MODIS TERRA was done for one special day (10th July 2006) over Niamey and showed that the two estimates can differ by several degrees during daytime. However, they were strongly correlated suggesting that the variability is reliable. These results were very similar to those obtained by Trigo et al. (2008) over Spain. In this case study, MSG LST provided the best estimates according to an evaluation with in-situ data (not shown).

In this study, we do not directly use LST but mostly rely on LST anomalies computed via the method presented below. It can be expected that this anomaly field is more accurately depicted by satellite estimates than absolute LST values, as it relies less on the retrieval method.

LST anomalies (LSTA) were computed relatively to longer-term mean (21 days) for each pixel in order to locate cool patches associated with rainfall events. The mean is calculated between 0645UTC and 1730UTC. It is expressed as follows:

$$LSTA(j) = LST_{0645-1730}(j) - \langle LST_{0645-1730} \rangle_{21j}$$

With estimates of LSTA, only the transient part of the signal is retained. More permanent features like the effect of vegetation on the soil moisture are partly removed in the LSTA compared to the LST estimates. The patterns due to antecedent rainfall are hence emphasised.

5.2.2 Identification of Convective Initiation from satellite data

– ***ISIS storm tracking system***

Initiations of convection were located using a cloud tracking algorithm called ISIS (Instrument de Suivi dans l'Imagerie Satellitale) or RDT (Rapid Detection Tracking) in English, which was initially developed by Morel and Senesis (2002). This algorithm is an automated cloud tracking system that consists in identifying sets of connected pixels corresponding to clouds and having an infrared temperature lower than a threshold. The thermal infrared temperature images come from a Meteosat channel at 10.8 microns. They are acquired every 15 minutes at a resolution of 3x3km².

The ISIS algorithm uses a variable threshold going from -10°C to -65°C that enables the detection of early convection, contrary to most existing codes that usually used a fixed temperature threshold (e.g. Mathon et al., 2002). The code was initially adapted for the West African region by C. Piriou and further refined by Tomasini et al. (2006). This mainly consisted in changes on some parameters, as ISIS was specifically developed for the mid-latitudes where convection is less strong (warmer cloud tops). A convective system is detected and retained only if its size reaches a minimum area of 5000 km² corresponding to an equivalent radius of 40 km. This means that only large and lasting storms are sampled.

Apart from information on convective initiation, a large range of morphological and dynamical properties are retrieved for each system including its size, expansion rate, the centre of gravity, the propagation speed. Figure 5-3 shows an illustration of the ISIS algorithm over West Africa showing the westward propagation of the MCSs over the continent. Many systems are detected in the operational systems but only the ones covering the requirements mentioned above are retained in the dataset we used (area detected greater than 5000 km²).

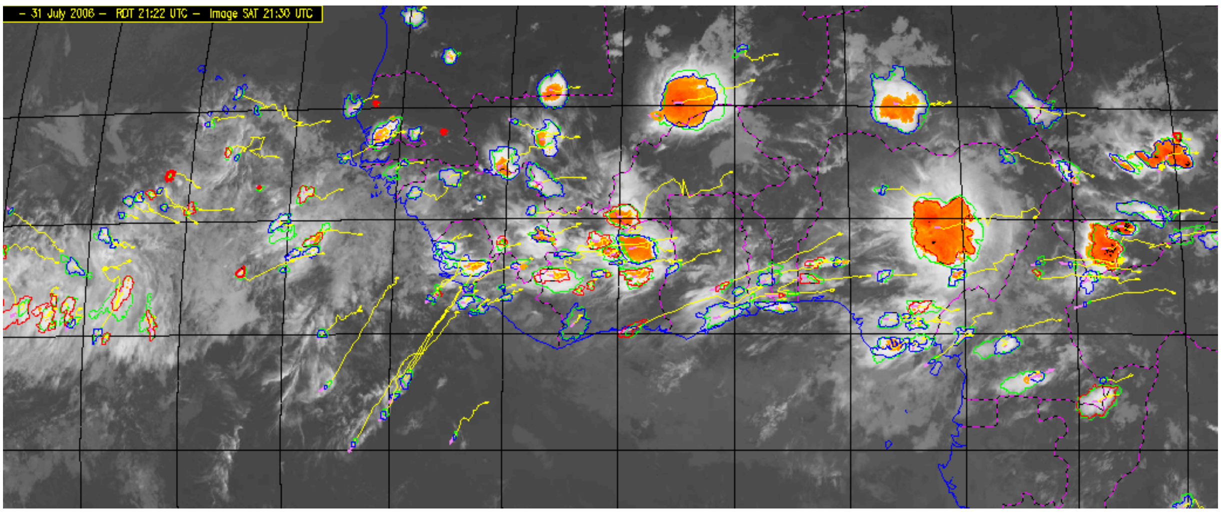

Figure 5-3 : Example of ISIS automated MCS tracking system over West Africa. The orange zones corresponds to the convective clouds detected by the algorithm, the yellow lines show theirs trajectories. Red contours around the convective cells mean that the convective system is in a developing phase whereas the blue contours indicate decaying storms.

– ***Refinement of ISIS initiation detection***

The daytime storms of 2006 wet season triggered between 1000UTC and 1900UTC and situated within a geographical domain extending from 10°W to 10°E and 10°N to 20°N were extracted for this study. This contains an ensemble of 586 storm initiations. Although this tracking method gives earlier detection of convective systems than most algorithms (Machado et al., 1998, Mathon and Laurent, 2001), there is a delay in the detection time and position. Figure 5-4 shows the initiation and trajectory of a system that developed in the surrounding of Niamey on the 10th of July 2006. The system was tracked by ISIS and it was also detected from the ARM radar data. The later allowed an earlier detection of the storm initiation (at 1540 UTC) than the ISIS tracking system (at 1700 UTC). A difference in timing and location of about 1hr 20 min after it was really initiated and about 0.30deg to the West . This example is quite typical of the delay generally observed from the comparison with series of IRT maps.

Thus, an additional backtracking method was applied to locate more precisely storm initiations. The initial location given by ISIS was used as a first guess. Then, the method consisted in detecting, within a defined zone around this initial point, the earliest location of low IRT temperatures. Contours of -40°C temperatures of infrared images obtained every 15 minutes were used back in time to define a progressively more precise location of initiation. This is illustrated in Fig. 5-5 where an initiation was found at 1700 UTC and 3.0°E, 11.8°N by ISIS (marked by X). The green contours indicate the different location of cold cloud cover back in time. The new initiation point is defined as the centre of the earliest/smallest cold cloud contours found at 1530 UTC some 20 km to the east (marked by O).

After applying the backtracking method, refined initiation locations were typically between 10 and 50 km to the east with a weak meridional component (the meridional component is given by the difference between the black and the green curves) as illustrated in the Fig. 5-6. The time delay was found to be between 60 to 120 min earlier than detected by ISIS. The new initiation dataset exhibits a better defined peak centred around 1400 and 1500UTC. The grey histograms in Fig 5-7 shows the latitudinal distribution of storm initiations over the domain of study. A peak in the population is found between 11° and 12°N. The initiations are distributed homogeneously across longitudes except in the easternmost part of the domain, where some mountain range like the Air Mountains are found. Initiations associated with significant topography were removed from the dataset or specific mountainous zones were not considered in the studies.

These new initiation points can be considered closer to the actual location where deep convection was triggered and can be thought to be more closely linked to surface properties influence. The timing of initiation, consistent with previous studies on diurnal cycle of convection over the Sahel (Mohr , 2004) corresponds roughly to the time of maximum low-level temperatures and few hours after that surface fluxes reach their maximum.

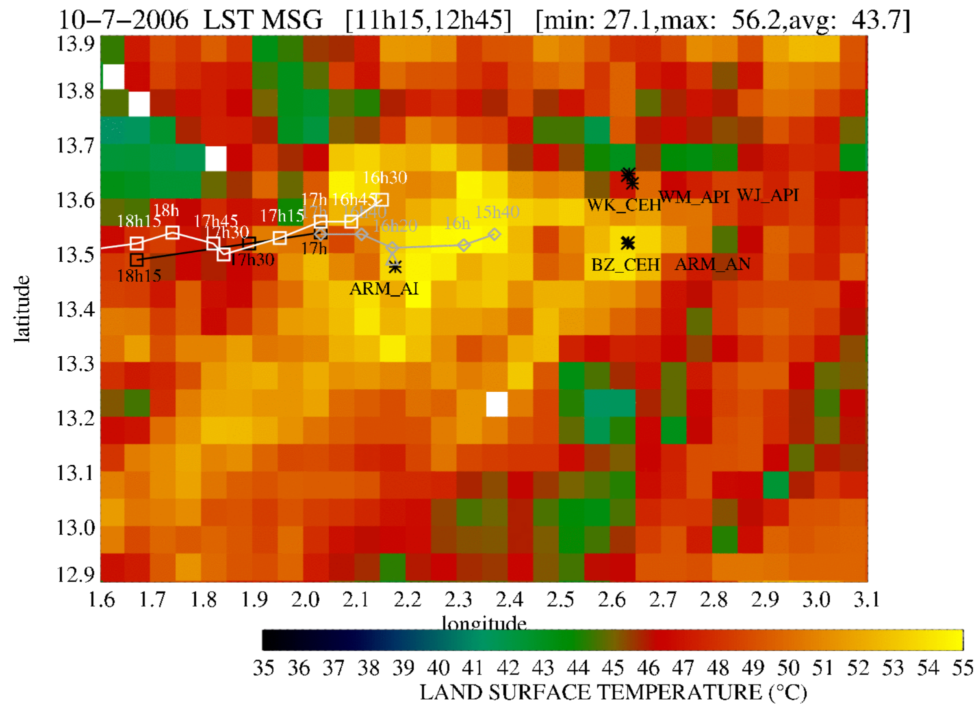

Figure 5-4 : Storm Initiation over Niamey (Niger) on the 10th of July 2006 located by ISIS (black rectangles), another tracking method (white rectangle) and from the radar images (grey diamond).This illustrates the delay in the detection of storm initiation obtained with the ISIS tracking algorithm. Land surface temperatures from MSG are plotted in the background. The ground-based measurement sites are indicated with black stars.

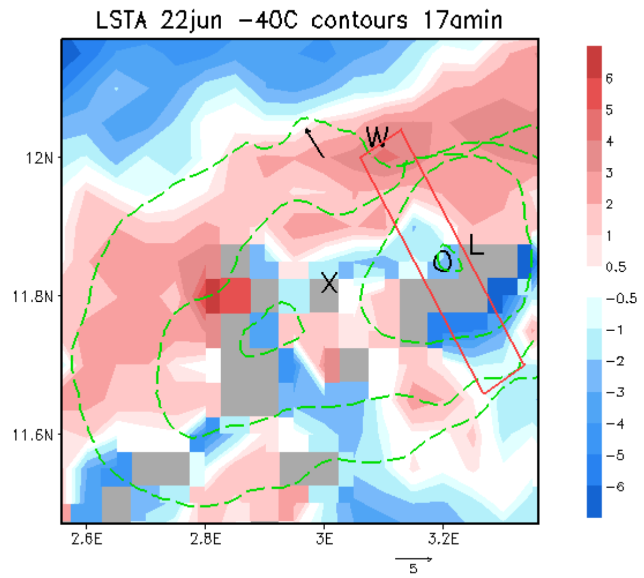

Figure 5-5 : Illustration of the backtracking method developed to locate more accurately the location of storm initiations. The cross indicates the location of initiation detected by ISIS, the isolines represent series of MSG IRT -40°C contours earlier in time and the black circle indicates the location of the initiation after backtracking. Land surface temperature anomalies are plotted in the background. The arrows indicates the low-level wind direction.

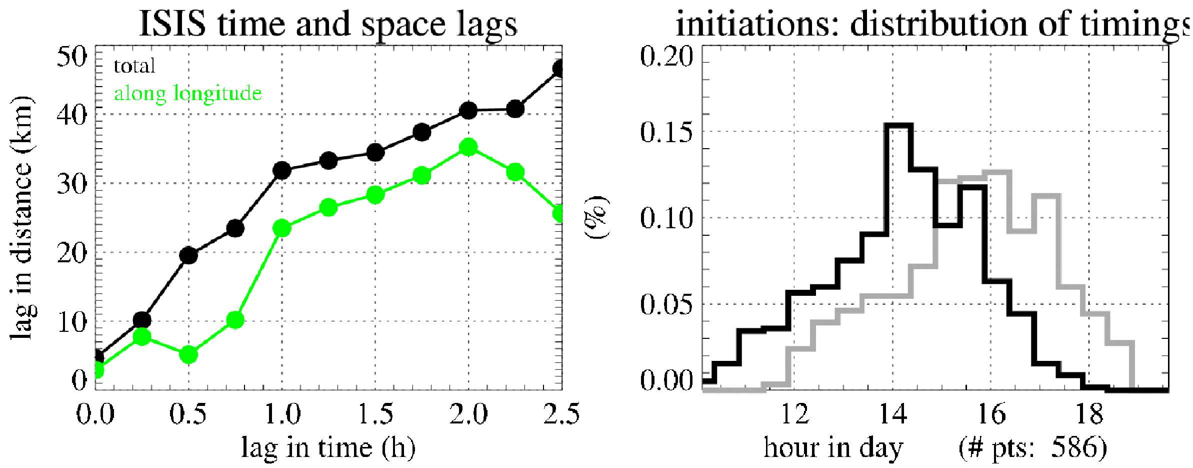

Figure 5-6 : Statistical comparison of the main differences between the initiations obtained from ISIS and after backtracking: On the left: ISIS space lags (total in black and longitude in green) compared to the refined location plotted as a function of the time lags. On the right: Distribution of storms initiation time detected by ISIS and after backtracking (grey and black respectively).

– ***Alternative detection algorithm***

In a second stage of this study, the analysis was extended to four years. This enabled to enhance the size of the sample and test how consistent the results for 2006 were with a larger set of data. It was necessary to use an alternative detection algorithm because the ISIS products presented above were available only for 2006.

This algorithm was developed by C. Taylor to analyse the cloud field and locate the storm initiations. The cloud field was mapped using infrared measurements from the Meteosat series of geostationary satellites. A threshold for cold clouds was defined at -40°C. Initiations were detected by the appearance of cold clouds when no cold cloud existed in the previous image within a radius of 40 km (Taylor et al, 2010). This algorithm allowed to retrieve storm initiation that occurred during the four monsoon seasons between 2006 and 2009. This represents a large set of data including almost 3000 storm initiations (2944 exactly).

Figure 5-7 presents the distributions of initiations as a function of time of the day and latitude. First, the initiations detected by this new algorithm were compared to the initiations obtained with ISIS for 2006 and the backtracking method (upper panels). Overall, the agreement was very good. The new algorithm always detects the same number of initiations as ISIS and the repartition of systems over the domain is identical as well as the timing of the initiations. The slightly larger number of points with this new method as indicated in Fig. 5-7 is due to the choice of a slightly wider time window, which extends more in the evening hours. The distributions were also very similar from one year to the other. We can notice a slightly smaller number of MCS in 2008 (673 storms) and a larger number in 2007 (789 storms) which may reflect the fact that 2007 monsoon season was relatively more active.

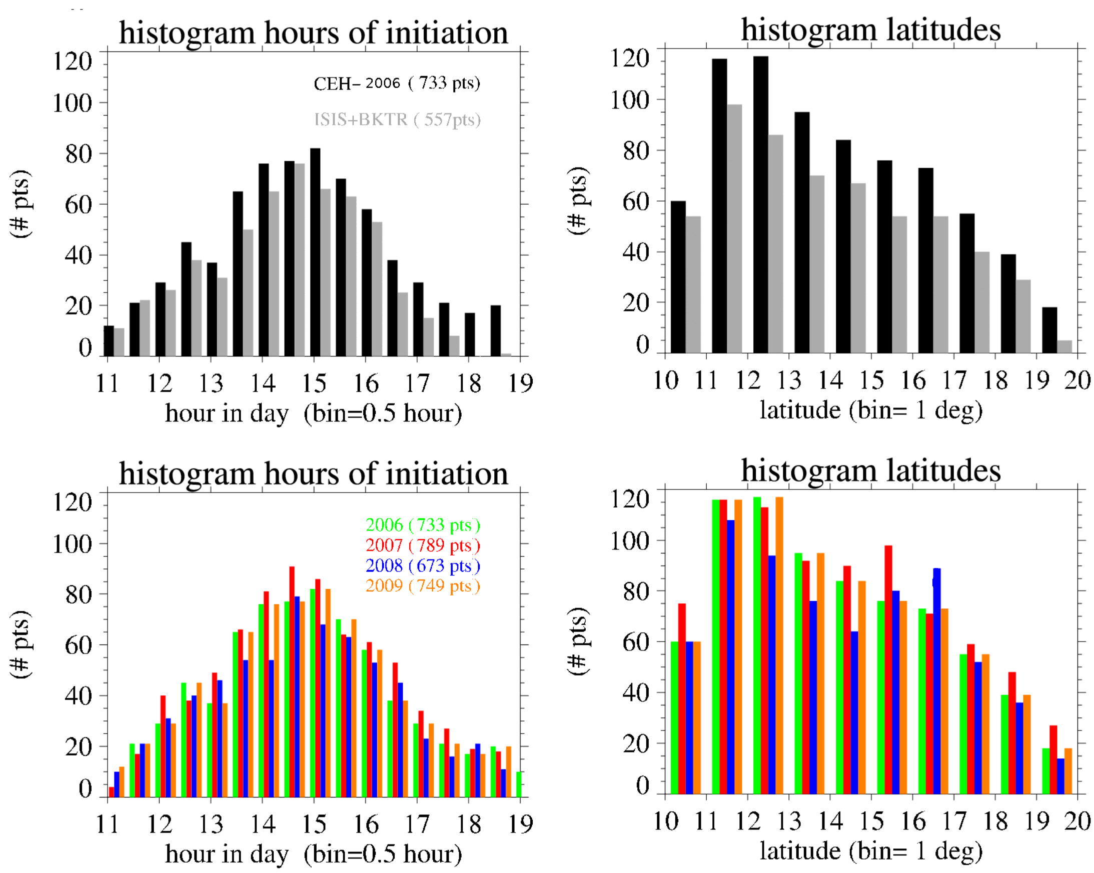

Figure 5-7 : Distributions in time (left panels) and along latitudes (right panels) of the initiation points. Top plots: Comparison of the histograms over the Sahel for the 2006 monsoon season located using either ISIS+backtracking (grey) and the alternative detection algorithm (black). Bottom plots: Comparison of the histograms of initiation times and latitudes for the years 2006 to 2009 using only the alternative detection algorithm.

5.2.3 Atmospheric conditions

Atmospheric conditions were extracted from the ECMWF IFS analysis. This is an analysis available every 6hours. It took into account a number of measurements from the AMMA campaign and in particular, the intensive radiosounding measurements (see chapter 3 for details). The horizontal resolution of the analysis is 0.3 degree and its vertical grid is composed of 91 levels with 20 levels in the lowest 3000 m.

The atmospheric profiles closest to the different initiation cases were extracted from the IFS analysis on the model levels. This includes profiles of temperature, specific humidity and winds for the four synoptic hours (0000UTC, 0600UTC, 1200UTC, 1800UTC). The high vertical resolution of the profiles enabled us to estimate boundary layers and convective indexes for each of these profiles including boundary-layer height and mean thermodynamic and dynamic properties, LCL, LFC, CAPE and CIN.

This analysis is the best representation of the atmosphere over the Sahel in 2006 we had at this time, this information is valuable, but one must keep in mind that the analysis also rely on the model parameterisation. A comparison of the analysis profiles was carried out with the radiosoundings launched during the AMMA campaign to document this issue. Figure 5-8 presents a comparison of thermodynamic and dynamics profiles during the pre-onset (May) and post-onset (August) periods at Niamey. These results are quite representative of the findings obtained when considering all the Sahelian sounding sites.

This shows that the nocturnal temperature profiles are close to the observations and that cooling/moistening is only a bit too strong during the pre-onset period. However, a warm bias typically develops during daytime (about 1-2K) which is linked to a too strong convective boundary-layer growth. Overall, early morning temperature profiles appear as more reliable than midday ones. This is also reflected in the fact that differences among different analyses are much weaker in the early morning than at midday, where a much larger spread between them is observed (not shown).

During the pre-onset season prior to rainfall, the overestimation of specific humidity in the low levels is related to some shortcomings in the model. In short, it seems that there is an overall underestimation of the horizontal advection of specific humidity, which is partly compensated by an increment in the soil moisture. This, in turn artificially enhances the latent heat flux at the surface and hence leads to too much water vapour in the atmospheric low-levels (see Meynadier et al. 2010 and Dursch and Viterbo 2007). The opposite is found, during the wet season (August), with a dry bias in the humidity profiles. This is likely to play a role in the fact that there is not enough development of convection in the ECMWF-IFS forecast (Agusti-Panareda et al., 2009).

In general, the wind is underestimated in the analysis. This is particularly true in the morning and early afternoon. The model smoothes the nocturnal jet especially during the pre-onset season when the wind speed is strongest.

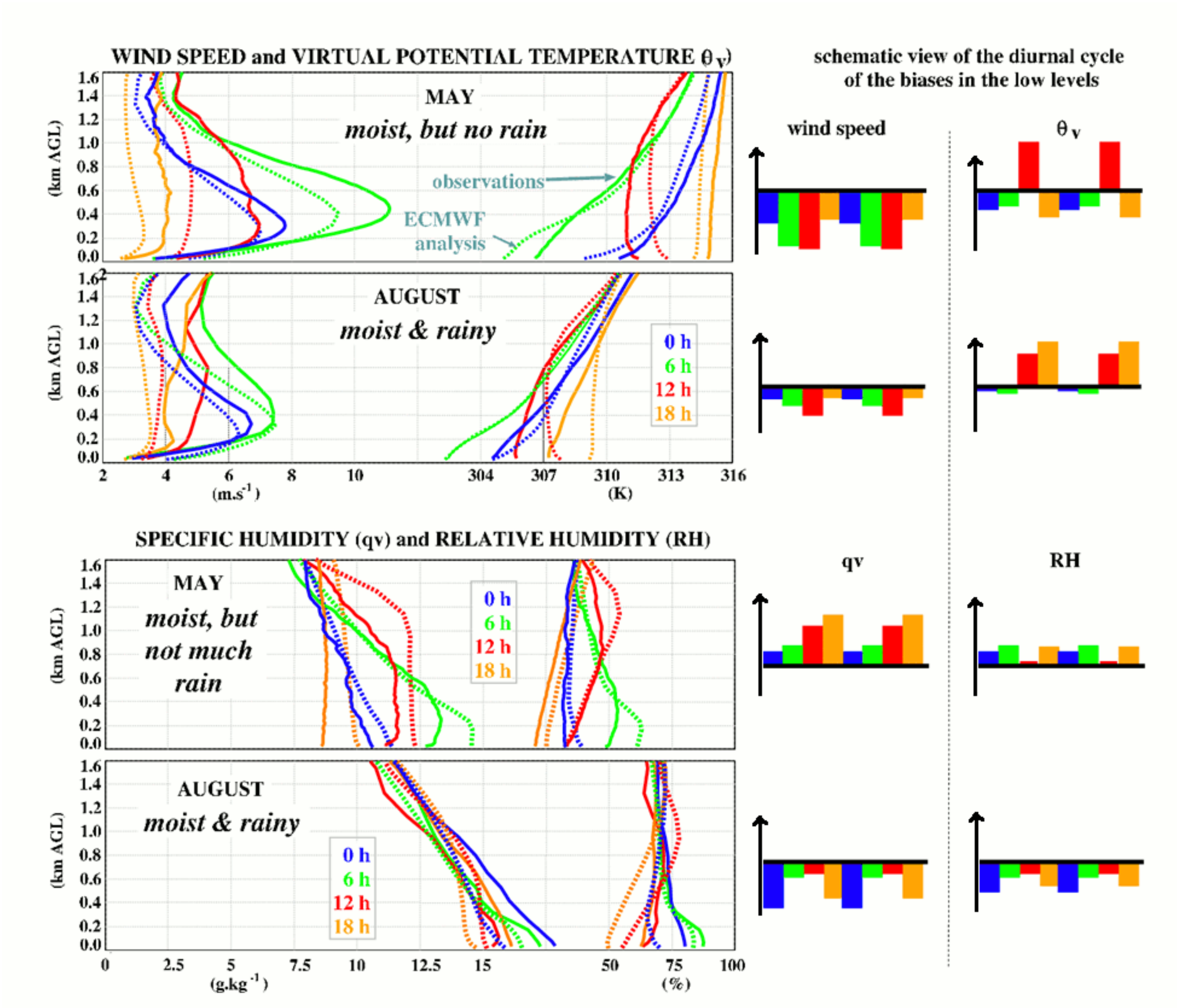

Figure 5-8 : Comparison between monthly mean atmospheric profiles of wind and potential temperature (upper panels), specific humidity, relative humidity (lower panels) extracted from the ECMWF IFS analysis (dotted lines) and the radiosoundings (full lines) in May and in August 2006 at Niamey at the four synoptic hours (0000 UTC, 6000 UTC, 1200 UTC, 1800 UTC). On the right, a schematic view of the diurnal cycle of the biases in the low levels compared to the radiosoundings is presented.

5.3 Statistical Analysis at 1degx1deg scale

As previously explained in section 5-1, the aim of this study is to investigate the relationship between initiation of convection and the underlying surface properties at the mesoscale. More precisely, the objective is to determine if there is a preference for systems to initiate over drier or wetter zones or neither. For this, a methodology was developed and is presented in section 5-3-1. The results of the analyses obtained with the different surface properties estimates (AMSR-E soil moisture and LSTA from MSG) as well as the different storm initiation datasets (refined ISIS and CMT tracking) is shown and discussed in the following sections.

5.3.1 Method

– ***Domain of Study***

The method consists in combining storm initiation datasets with satellite based estimates of surface properties. For this, a geographical domain was defined, as illustrated in Fig. 5-9. It extends from 10°N to 20°N and 8°E to 10°W and avoids areas of significant topography (e.g. the Aïr mountains).

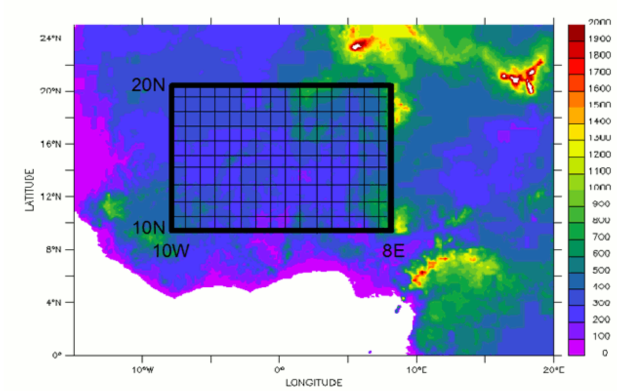

Figure 5-9 : Illustration of the domain of study extending from 10°N to 20°N and from 10W to 8°E. This domain was divided into bands of latitudes and pixels of 1deg sideways. In the background, the topography is plotted.

The domain covers a large area including the Sahelian zone. This design was chosen to be able to work on a large data set that enables to obtain good statistics. The atmospheric regimes are not simultaneously comparable; however, as the monsoon season progresses, the different zones overcome similar regimes (as shown in Chapter 3). For instance, the Sahelian post-onset regime is close to the Soudanian regime before the onset of the monsoon.

This domain was then divided into latitudinal bands 1deg wide and then into pixels of 1deg sideways. This corresponds to surface pixels of mesoscale length which are likely to affect initiation of convection and have a sufficient size to incorporate enough surface data.

For each latitudinal band, a mean soil moisture was computed by averaging soil moisture in every pixel within the latitudinal band over a whole month. A mean standard deviation for each latitude and month was computed in the same way. As illustrated in Fig. 5-10, the soil moisture strongly decreases between 10° to 17°N and weakly varies between 17°N and 20°N. A strong seasonal evolution associated with the monsoon activity is observed, in particular in the southern part of the domain. The soil moisture increases between 4 % (in m^3/m^3) and 6 % from June to September depending on the latitude. The maximum increase happens at 13-14°N.

The mesoscale variability of soil properties is estimated by calculating the standard deviation of soil moisture within each pixel of 1deg square. This is indicated by the horizontal bars in Fig. 5-10. The plot on the right shows the variability depicted by the LSTA estimates, whereas on the left, the variability of soil moisture is presented. During the pre-monsoon phase, the variability is larger in the southern part of the domain. This variability decreases as the monsoon becomes well established whereas, in the Northern part of the domain, the variability increases. This is linked to the northward propagation of the monsoon and of the convective activity through the season. A large difference is observed between the two products. More variability and seasonal evolution of this variability is observed in the LSTA field compared to the soil moisture field. This can be explained by the different characteristics of surface property estimates. First, the LSTA data have a finer resolution compared to AMSR-E products and this could primary explain the difference in standard deviation. Then, these two products measure distinct surface properties. Indeed, AMSR-E estimates quantify soil moisture in the top few centimetres, and this upper soil layer dries up quickly after a rain event. The surface temperature measured by MSG, however, can be affected on slightly longer timescale and hence reveals more variability. Moreover, LST anomalies highlight the variability by removing the longer term signal (intraseasonal signal). This can also explain the stronger variability.

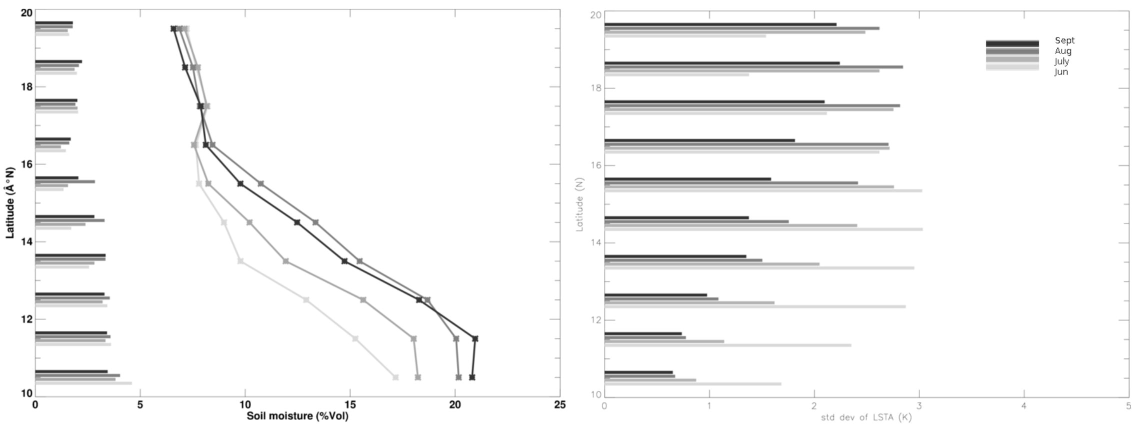

Figure 5-10 : ***Latitudinal monthly mean soil moisture (lines) and its associated moisture variability as expressed in standard deviation (horizontal bars) within a pixel as a function of latitude for June (light grey), July (medium grey), August (dark grey) and September (black) using AMSR-E estimates. The plot on the right presents the variability of LSTA within a pixel as a function of latitude.***

As seen in section 5-2, there is a higher density of mesoscale convective systems triggered over the Southern part of the domain. Thus, at large scale, there is a positive relationship between the number of triggered systems and the soil moisture, which also involves the large scale circulation (Inter Tropical Convergence Zone).

The distributions of soil moisture by latitudinal band exhibit a double peak in the northern latitudes (see fig 5-12 a). It could be tempting to interpret this feature as an indicator of soil moisture convection feedbacks (D'odoricco et al., 2004). However, this bimodality can also arise from the fact that the AMSR-E soil moisture estimates reveal the moisture in the top few centimetres, which is strongly affected by rainfall at a short timescale. Indeed, rain from MCS falling over very dry surfaces can generate strong wet anomalies and lead to the second peak in the soil moisture distribution.

– ***Normalisation of surface properties***

Soil moisture/ LSTA normalisation

The focus of this study is the relationship between surface properties and initiation of convection at mesoscale. Therefore, a method for removing the large-scale signal was applied. A spatial and temporal normalisation was carried out with commonly-used methods (Wilks, 1997). For the LSTA analysis, a normalisation was also applied because the variability of LSTA varies with latitude and month (see Fig 5-11). Therefore, to be able to get a whole set of data composed with similar distributions, we apply a normalisation using spatial monthly latitudinal average of mean and standard deviation of LSTA as follows:

$$SM_{norm} = \frac{SM-\overline{SM}}{\overline{\sigma SM}} \quad \text{and} \quad LSTA_{norm} = \frac{LSTA-\overline{LSTA}}{\overline{\sigma LSTA}}$$

This spatial and temporal normalisation allows us to obtain an anomaly compared to the monthly mean latitudinal band. Moreover, this kind of transformation can also be useful when one is interested in working simultaneously with batches of data that are related, but not strictly comparable. One instance of this situation occurs when the data are subject to seasonal variations. Direct comparison of raw monthly temperature will usually show little more than the dominating influence of the seasonal cycle. For example, a record of warm January will still be much colder than a record cool July. In situations of this sort, presenting the data in terms of standardized anomalies can be very helpful (Wilks, 1997).

Figure 5-11 (a-b) shows the distributions of AMSR-E soil moisture respectively before and after normalisation. As seen previously, the mean and the variability of soil moisture varies with latitude. The distributions are centred on values between 5 and 20 m^3/m^3. After normalisation, all the distributions are centred around 0 and the standard deviations are similar. This data processing enables us to get a whole set of data composed with different distributions that can be considered similar after normalisation. This was confirmed by applying a statistical test, namely the Wilcoxon Mann-Whitney (WMW hereafter) Test (Mann and Whitney (1947)).

This statistical test allows comparing two populations which are not assumed to be normally distributed. This test consists in assessing whether two independent samples of observations have equally large values. If the p-value resulting from this test is greater than 0.05, the two samples can be considered to be equally distributed.

For the LSTA analysis, a normalisation was also applied because the variability of LSTA varies with latitude and month (see Fig 5-10).

Soil moisture/LSTA variability

In order to study the variability of soil moisture, each latitudinal distribution was also normalised. The logarithm function is well suited for applying a transformation in the case of highly variable and skewed distributions, as it allows a distribution closer to normal to be obtained. In the case of soil moisture variability field, distributions are highly skewed, as illustrated in Fig. 5-11(c).

The normalisation for the soil moisture variability was performed as follows:

$$Y_{SM} = \ln\big(\sigma(SM)\big) \quad \text{and then} \quad \sigma(SM)_{norm} = \frac{Y_{SM} - \overline{Y_{SM}}}{\sigma(Y_{SM})}$$

and for the variability of LSTA :

$$Y_{LSTA} = \ln\big(\sigma(LSTA)\big) \quad \text{and then} \quad \sigma(LSTA)_{norm} = Y_{LSTA} - \overline{Y_{LSTA}}$$

Figure 5-11 (c-d) shows the different steps of the normalisation of soil moisture variability. The distributions of the initial field are centred on values going from 1 to 2 m^3/m^3 and varying width as shown by the top plot. After normalisation, the distributions are all centred on 0 and have similar standard deviations (plot d). The results of the WMW tests show that the different distributions after normalisation can be considered similarly distributed.

The normalisation of LSTA variability is shown in Fig. 5-12. Before normalisation, the distribution of variability of LSTA within a pixel are centred between 1 and 2K. They have different spreads and are all positively skewed. After changing the variable using the logarithm function, the distributions are closer to normal and have similar width, however, they are still not centred on the same value. The last step, consisting in removing the mean value of each distribution, allows us to get all the distributions centred on 0. Therefore, we obtain similar distributions of variability over the whole domain. This methodology thus provides a dataset from which the strong seasonal and latitudinal imprints have been largely removed.

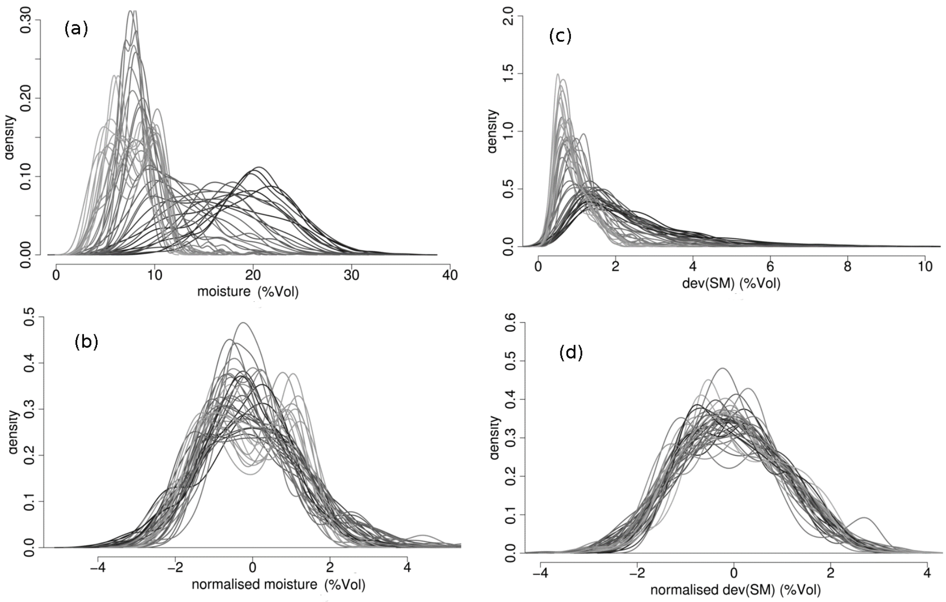

Figure 5-11 : (a) Distributions of soil moisture by latitude bands and months. The darker the line is the further to the south the latitude band is located. (b) distributions of soil moisture after normalisation (c) distributions of standard deviation of soil moisture (d) same distributions as (c) but after normalisation.

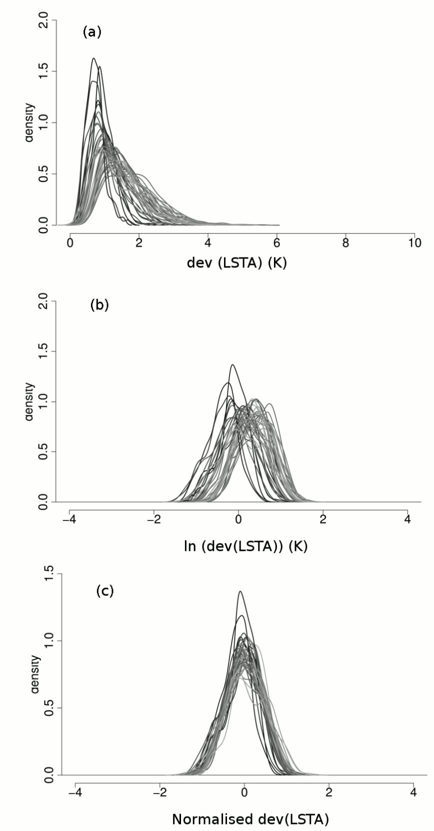

Figure 5-12 : ***Normalisation of the variability of LSTA data by latitudinal bands (a) distributions of mean variability of LSTA within a pixel (b) distributions after changing to logarithm values and (c) corresponds to the distributions after the complete normalisation process (see above).***

– ***Combining Method***

The pixels were sorted according to a criteria on the convective initiation dataset. If one system or more occurred over the pixel, this pixel is sent to the "initiation group" otherwise to the "non-initiation group". The number of pixels associated with storm initiations are different in the two analysis, as they depend on the surface properties available. This reduces particularly the number of initiation pixel in the soil moisture analysis. Indeed, the Aqua satellite passes only twice a day over a limited area, whereas MSG covers the whole domain (with only a few data points removed due to contamination by clouds or aerosols). The number of pixels included in each group is listed in Tab. 5-1. For the soil moisture analysis, convection was initiated over 272 pixels, whereas in the LSTA analysis, there were 354 cases (which corresponds to clear sky conditions, as pixels contaminated by cloud are removed). The 'no-initiation' sample is considered as the reference sample hereafter

.

	SMA - JJAS 2006	LSTA - JJAS 2006	LSTA - 4years
Initiation pixels	272 (557)	354(557)	1947(2944)
No-initiation pixels	12551	14156	59061

Table 5-1 : ***Number of pixels in the initiation group and non initiation group taken into account in the soil moisture analysis(SMA) and in the LSTA analysis for the study carried out with the refined ISIS initiations(LSTA JJAS 2006) and the storm initiations for the four years(LSTA 4years).The number in brackets correspond to the initial number of storm initiations.***

5.3.2 Results based on AMSR-E data

– ***Summary results for 2006 monsoon season***

Figure 5-13 presents the distributions of normalised soil moisture of the 'initiation group' in blue and 'no initiation group' in black for the whole 2006 monsoon season. The distribution of normalised soil moisture of the initiation group presents a larger (smaller) number of negative (positive) values than in reference sample.

A quantification of the differences observed between these two distributions is obtained via the statistical diagnostics recapitulated in Tab. 5-2. The WMW test between the initiation and no-initiation distribution indicates a p-value of 7.0e-07, which is significantly less than 0.05 and hence confirms that the two distributions are not similar. The distribution of the initiation group has a mean value shifted by 0.38 towards the negative values compared to the no initiation group. The median is slightly less shifted (-0.37 m^3/m^3) and the standard deviation of the distribution is slightly smaller (-0.14 m^3/m^3).

By comparing the first quartile values of the distribution, we find that there is a larger number of negative values in the 'initiation' sample compared to the 'non-initiation' sample, which corresponds to drier pixels. The first quartile, in the no-initiation sample, is obtained at -0.91 corresponding to 25% of the values whereas in the initiation sample 31% of the soil moisture pixel values are smaller than this quartile value. This corresponds to 6% more chances for initiation to occur over a soil presenting a strong dry anomaly. On the other side, there are 9% less chance for initiation to occur over a soil displaying a strong wet anomaly.

These results suggest that, in the Sahel and at the mesoscale, initiations of convection tend to occur preferentially over soils presenting a spatial dry anomaly. A dryness index was calculated associated with each initiation pixel from the ECMWF analysis, it was plotted as a function of convective triggering potential in Fig. 5-14. This shows that, according to the Findell and Eltahir indexes, most of the initiation of convection would be favoured over dry soil but some of our initiation cases should also be favoured over wet soils. By analysing the results, we found that storm initiation is favoured over dry soil presenting a dry anomaly and wet soils associated with a soil moisture anomaly (not shown).

The right column in Fig 5-13 presents the distributions of normalised soil moisture variability associated with storm initiation cases in brown and the one associated with pixels where no initiation occurred, in black. The initiation distribution appears slightly shifted towards positive values compared to the 'no initiation' sample. The similarity of the two distributions was tested using statistical parameters (see Tab. 5-2). By running a WMW test, a p-value of 1.1e-02 was obtained which means that the distributions are different. The initiation group distribution has a mean value 0.19 greater than the reference distribution. This corresponds to a larger number of pixels presenting more variability in the initiation sample than in the reference sample. By looking at the last quartile of the distributions, we see that 32% of values are found instead of 25% expected. This corresponds to 7% more than in the reference sample. According to this result, at the mesoscale, convective initiation seems to occur preferentially over region presenting slightly more soil moisture variability than its surrounding.

– ***Contrasts between pre-onset and post-onset periods***

A partitioning of the dataset was carried out to investigate the sensitivity of our results to the season. Two groups were formed according to the onset of the monsoon. The onset of the monsoon corresponds to the northward shift from 5°N to 10°N of the ITCZ. In 2006, on average, the onset period extends from 25th June to 10th July (Janicot et al., 2008). We chose the 15th July to divide the dataset into 2 and keep a relative balance.

The distributions of soil moisture pixels values for the pre-monsoon period (noted JJ) and for the full monsoon period (noted AS) are presented in Fig. 5-13. A seasonal sensitivity is found between these two periods. A stronger positive signal appears in the dataset corresponding to the pre-onset period, 12% (37-25) more storm initiations over drier soil compared to the reference distribution (see Tab. 5-2). An opposite signal appears in August, where only 23% of the storms occur over dry soils compared to 25% in the reference distribution. This suggests that conditions favouring the initiation of convection over dry soil are more frequent during the pre-onset period.

Concerning the variability of soil moisture, a slight difference was found between the two periods with less soil moisture variability associated with storm initiation during the pre-onset period (26%> last ref quartile) and more variability after the onset (34% > last ref quartile).

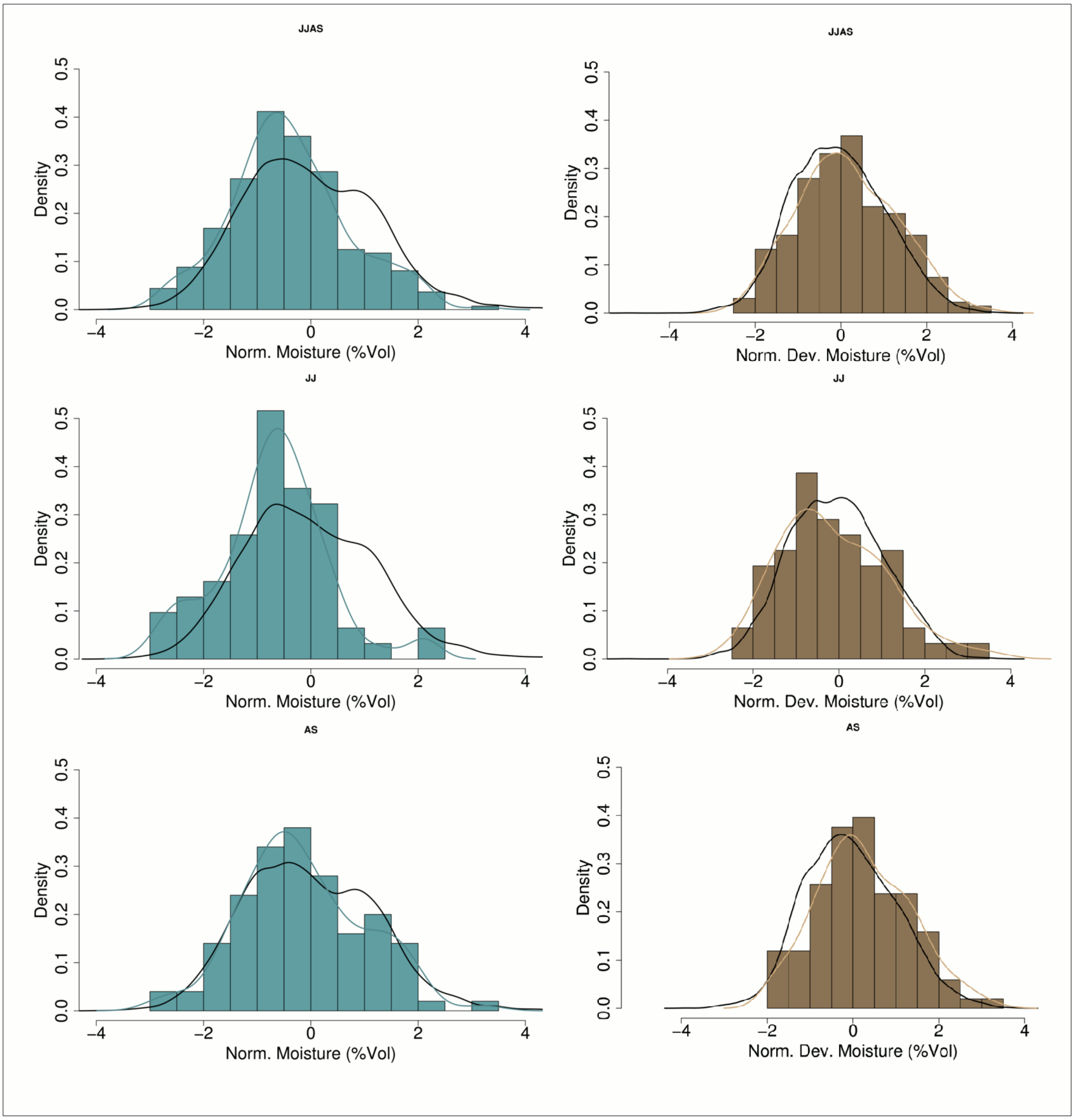

Figure 5-13 : Results from the combined analysis of AMSR-E soil moisture estimates with the refined ISIS storm initiations. The left figures show the distributions of normalised soil moisture of the 'initiation group' (blue) and the distribution of the 'no initiation group' (black) for the 2006 monsoon season (top figure), the pre-onset period (middle) and the post-onset period (bottom). On the right, the figures presents the results of the analysis on the variability of soil moisture with the same organisation as the left figures.

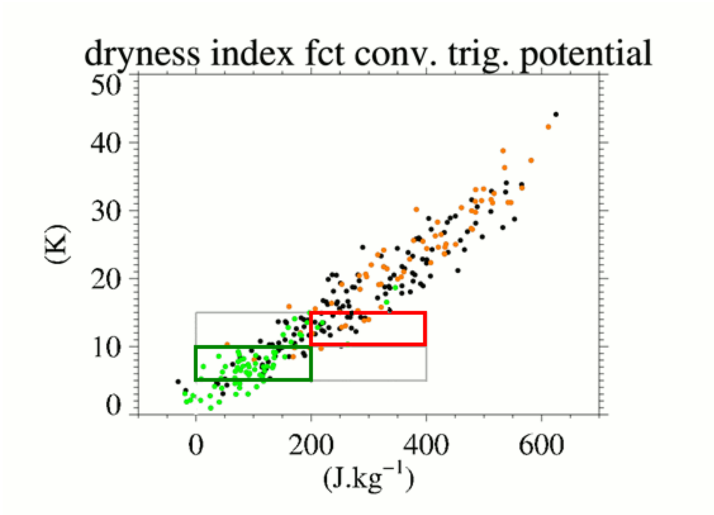

Figure 5-14 : The dryness index of the initiation pixels, calculated according to Findell and Eltahir (2001) method (see chapter 2), is plotted as function of convective triggering potential. The boxes are the different zones for describing atmospheric control on soil moisture rainfall feedback. The red (green) box corresponds to atmospheric conditions where convection is favoured over dry (wet) soils. The data points correspond to atmospheric conditions associated with observed convective initiations and the colours indicate the underlying soil moisture conditions(green=moist anomaly, orange=dry anomaly and black=neutral).

		Difference between the initiation distribution and the reference				
	p-value	Mean	Median	Sigma	% < 1st q	% >4th q
Soil Moisture - Mean						
JJAS	7.0e-07	-0.38	-0.37	-0.14	31%	14%
JJ	1.2e-04	-0.57	-0.47	-0.13	37%	5%
AS	6.1e-01	-0.07	-0.16	-0.08	23%	22%
Soil Moisture -Variability						
JJAS	1.1e-02	0.19	0.18	0.07	20%	32%
JJ	3.5e-01	-0.09	-0.34	0.14	31%	26%
AS	1.0e-02	0.29	0.21	0.01	17%	34%

Table 5-2 : ***Statistical results of the differences between the distribution of normalised soil moisture (NSM) pixel values associated with storm initiation and the reference distribution corresponding to the pixel values where no convective initiation occurred. The first three lines correspond to the NSM analysis when considering all the 2006 storm initiations, then only storms initiated before and after the onset of the monsoon. The same is done for the variability of soil moisture within pixels. The p-value corresponds to the results of the MWM test between the two distributions. The two last columns represent respectively the percentage of values encountered in the initiation distribution that are inferior to the 1st quartile of the reference distribution and superior of the 4th quartile of the reference distribution.***

5.3.3 Results based on LSTA data

– ***Summary results for 2006 monsoon season***

The results of the statistical analysis using the LSTA anomalies are presented in Fig. 5-15. The same colour codes as in the result section on AMSR-E soil moisture are used (mean LSTA anomaly in blue and variability of LSTA in brown).

The distributions of normalised LSTA for the initiation group is shifted towards positive values compared to the 'no initiation' distribution. There is a statistical significant difference between the distributions, as confirmed by the WMW test, which gives a p-value of 0.11e-07 (see Tab. 5-3). The mean of the initiation group distribution is shifted towards positive values by 0.5K compared to the 'no initiation' sample. This suggests that initiations tend to occur preferentially over soil presenting a larger normalised LSTA. As discussed previously, LSTA can be considered to be a proxy for soil moisture anomalies. A positive LSTA anomaly corresponds to a dry/warm soil anomaly. Therefore, this result also suggests that initiation of convection would tend to occur over soils presenting a dry anomaly. 34% of the values associated with storm initiations are greater than the last quartile value of the reference distribution. This corresponds to 9% more chances to develop over warm anomalies that what we would expect.

The variability of LSTA has also been studied. These results are presented in Fig. 5-15, right column. A small difference between the initiation distribution and the reference is obtained. The WMW test indicates that the distributions are different (p-value=0.78e-02). The initiation distribution is centred on more positive values of LSTA compared to the no-initiation distribution, the difference in mean is equal to 0.05. 29% of the values in the initiation distribution are larger than the last quartile value of the reference distribution. This shows a tendency of convective systems to develop over region with a higher variability in the LSTA/ soil moisture field.

– ***Contrasts between pre-onset and post-onset season***

The pre-onset phase exhibits a stronger signal than the post-onset period on the LSTA distributions. During the pre-onset period, 39% of the systems occur on strong positive anomaly of LSTA (greater than the last quartile of the reference) whereas during the post-onset phase there is 34%.

When considering the variability of LSTA, a more positive signal is found after the onset of the monsoon. This corresponds to more surface variability underneath storm initiations in the post-onset period. This partly agrees with the soil moisture analysis, as more variability was also found for the post-onset period. However, the results for the pre-onset period are less coherent as the distribution was shifted towards negative values in the previous study (less variability). As discussed before, we tend to assume a greater confidence of the LSTA variability analysis as the resolution is higher and better suited for what we are looking at.

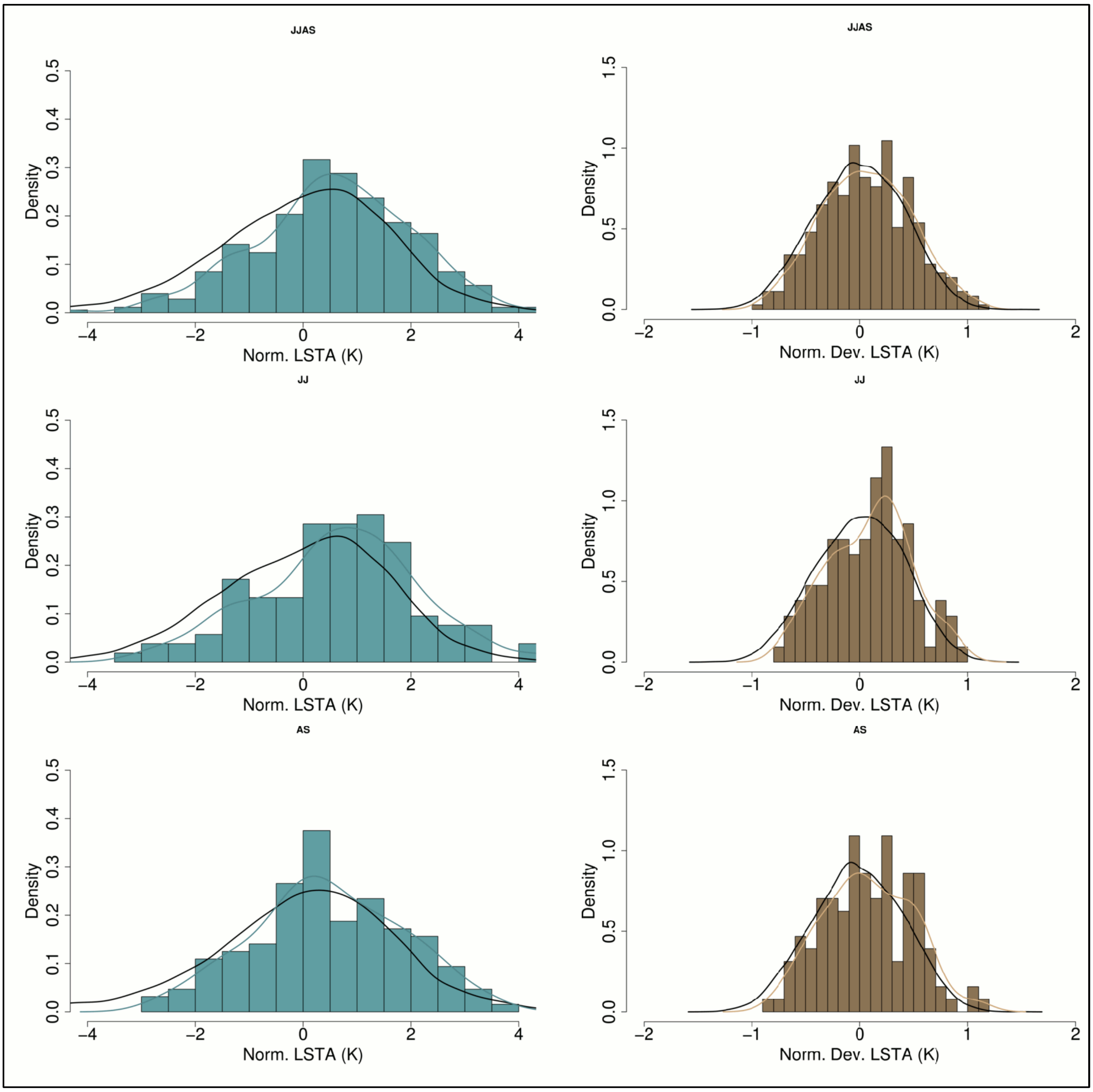

Figure 5-15 : Results from the combined analysis of LSTA estimates with the refined ISIS storm initiations. The left figures show the distributions of normalised LSTA of the 'initiation group' (blue) and the distribution of the 'no initiation group' (black) for the 2006 monsoon season (top figure), the pre-onset period (middle) and the post-onset period (bottom). On the right, the figures presents the results of the analysis on the variability of LSTA with the same organisation as the left figures.

		p-value	Mean	Median	Deviation	1st quart.	4th quart.
Mean LSTA							
	JJAS 2006	0.11e-07	0.50	0.46	-0.20	16%	34%
	Pre-onset	0.21e-03	0.60	0.54	-0.09	16%	39%
	Post-onset	0.89e-02	0.43	0.19	-0.36	17%	34%
Variability of LSTA							
	JJAS 2006	0.78e-02	0.07	0.05	-0.67e-03	21%	29%
	Pre-onset	0.33e-01	0.09	0.15	-0.03	20%	26%
	Post-onset	0.22e-01	0.09	0.06	-0.67e-02	20%	35%

Table 5-3 : ***Statistical results of the differences between the initiation and reference distributions of LSTA pixels when considering all the 2006 storm initiations (JJAS), only the pre-onset period and the post-onset period. The same is done for the variability of LSTA. The p-value corresponds to the results of the MWM test between the two distributions. The two last columns represent respectively the percentage of values encountered in the initiation distribution that are inferior to the 1st quartile of the reference distribution and superior of the 4th quartile of the reference distribution.***

In summary, the AMSR-E and the LSTA statistical analyses at the mesoscale both showed that initiations of convection are triggered preferentially over drier soils compared to its surrounding in the Sahel. It is especially significant during the pre-onset phase of the monsoon (+14% chances to develop over dry/warm surfaces). Significant links also emerged between variability of surface properties during the post-onset period (+10% chances for systems to be triggered over soil presenting a strong positive anomaly in variability) at 1°x1° spatial scale. The results were obtained from two independent datasets, which gives more confidence in the reliability and robustness of conclusions. However, these results were obtained only for one year of data (354 (272) storm initiations in LSTA (AMSR-E) analysis). The robustness of these results is tested using a 4year dataset and is presented in section 5-3-5. Before this, an analysis of the atmospheric conditions associated with the storm initiations of 2006 monsoon season is presented in the following section.

5.3.4 Atmospheric Environment associated with observed storm initiation

The atmospheric profiles associated with the initiations of convection (for 2006 monsoon season) were extracted from the ECMWF analysis. Basic boundary layer and convective diagnostics have been calculated from these profiles, including boundary-layer heights and mean properties, lifting condensation level (LCL), level of free convection (LFC), convective available potential energy (CAPE) and convective inhibition (CIN). The analysis of these profiles shows several important features.

Figure 5-16 shows the series of convective boundary layer heights, LCL and LFC sorted according to different criteria. First, when ordered by increasing day of year (top plot); at the beginning of the season, boundary layers (black) reach altitude higher than 1km (900mb) (as shown in Chapter 3) and LCL and LFC are generally much higher (800mb-700mb). These conditions do not favour the initiation of convection as the layer between the boundary layer height and the LCL and LFC is large. This suggest that the atmospheric conditions alone cannot be responsible for the initiation of convection. After the onset of the monsoon (around mid-July), convective boundary layers are shallower and more various. The LFC and LCL are also more various with sometimes cases of very high LFC/LCL (hard to trigger convection) and sometimes LFC/LCL almost at the boundary layer height level (easy conditions for convective triggering).

Then, when ordering the diagnostics by decreasing LFC, one can note that the LCL becomes closer to the LFC for large values of LFC. This suggests that shallow convection remains sparse and if the LCL is reached it can then quickly turn into deep convection. Therefore, this suggests that the surface can have a more direct impact on the atmosphere in these conditions. Storm initiations appear to be triggered also over a large range of CAPE and CIN values (not shown).

These analyses suggest that deep convection is triggered in various atmospheric conditions that appear sometimes relatively difficult especially during the pre-onset period, with high LCL and LFC but also deep convective layer. A number of difficult cases are also found during the post-monsoon period

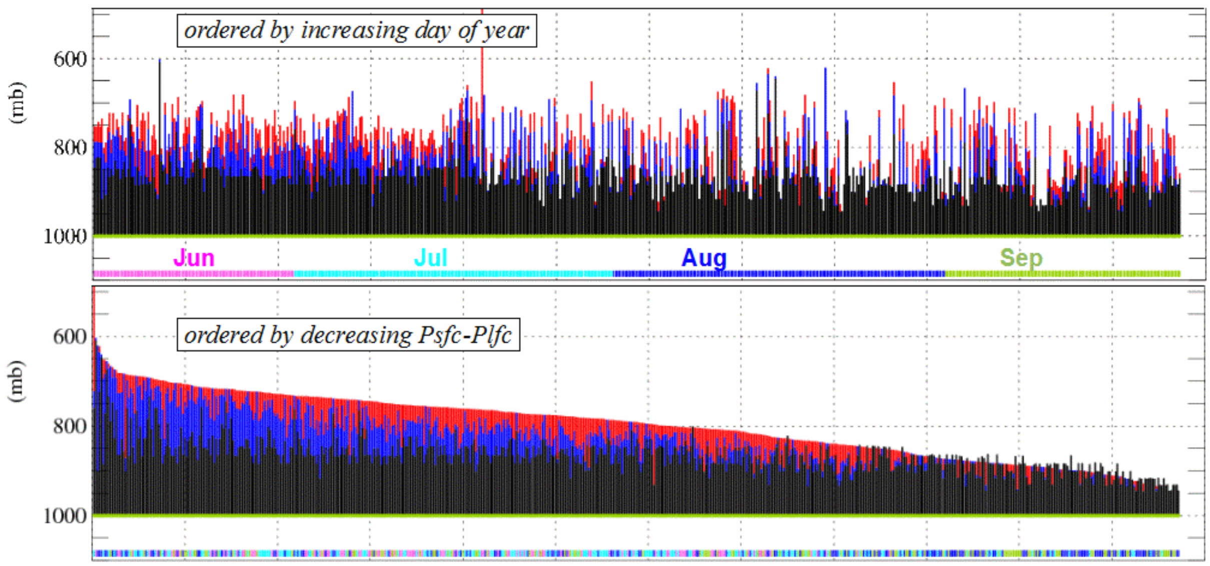

Figure 5-16 : Time series characterizing the atmospheric boundary layer thickness (black segment), the height of the LCL above the CBL (blue segment) and of the LFC above the LCL (red segment) of the initiation cases (estimated from 1200 UTC profiles). They are ordered by function of day of year (top plot) and height of the LFC (bottom plot). All are expressed as departures from the surface pressure, which has been set to 1000 mb

– ***Soil moisture-atmospheric fields correlations***

The couplings between the atmospheric profiles extracted at the initiation points with corresponding the soil moisture pixel from the previous analysis was investigated in this section.

Strong couplings are indeed found between soil moisture and the atmospheric convective fields extracted from the AMMA analysis. The correlation coefficients of different atmospheric fields with soil moisture are listed in Tab. 5-4. Correlation coefficients of 0.87 and 0.85 are obtained between soil moisture and LCL and LFC respectively at 0600 UTC. This correlation increases during daytime, between 0600 UTC and 1200 UTC, with an R coefficient increasing up to 0.95. This is linked to the influence of surface fluxes and boundary layer growth on the LCL and LFC. Another strong coupling is found with the potential temperature (R^2=0.92) and also with specific humidity (R^2=0.77).

Couplings usually increase during the day except for CAPE and the equivalent potential temperature which is also related to CAPE. It is controlled by the evolution of specific humidity and potential temperature in the atmospheric low-levels. They evolve in different directions: qv decreases whereas theta increases during daytime. This can explain why CAPE and thetae do not show any significant correlation with soil moisture during daytime. CIN, however, is found to be closely correlated to soil moisture, which is linked to boundary layer properties and growth.

	R^2 at 6UTC	R^2 at 12UTC
LCL	0.87	0.95
LFC	0.85	0.94
CAPE	0.36	0.04
CIN	0.92	0.92
theta	0.92	0.96
Theta e	0.36	0.04
Qv	0.77	0.79

Table 5-4 : ***Correlation coefficients between initiation soil moisture values and the corresponding atmospheric fields; Lifting condensation level (LCL), Level of Free Convection (LFC), Convective Available Potential Energy (CAPE), Convective INhibition (CIN), potential temperature (theta), equivalent potential temperature (theta e) and specific humidity(qv).Values in blue correspond to negatively correlated values, in red positively correlated and black no high correlation.***

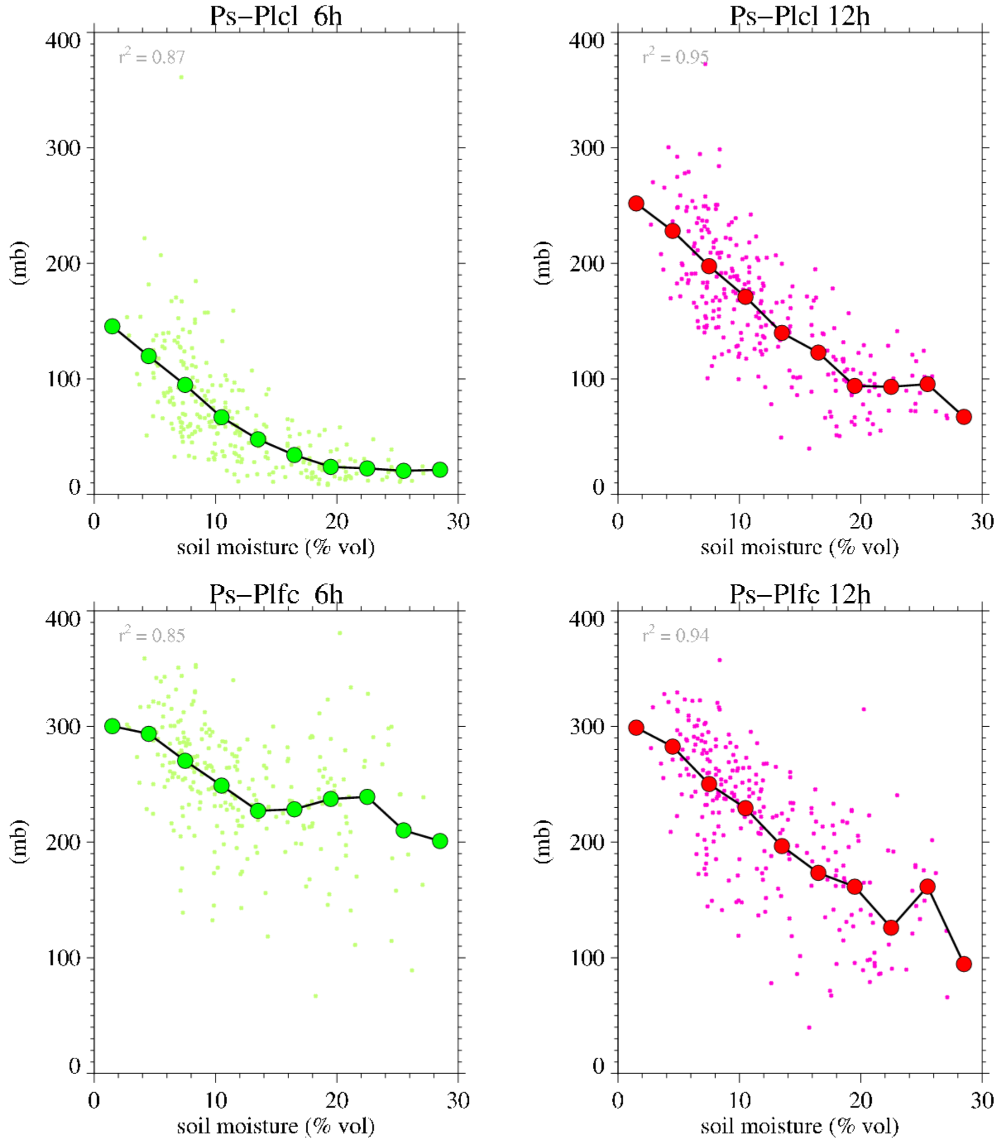

Figure 5-17 : The thickness(in mbar) between the surface and the Lifting Condensation Level (LCL, upper plots) and the Level of Free Convection(LFC, bottom plots) are plotted as a function of soil moisture for two different time in the day; 6UTC (left column) and 12 UTC (right column). The initiation soil moisture values are extracted from the 1degx1deg analysis. The atmospheric parameters (LFC and LCL) come from the IFS analysis.

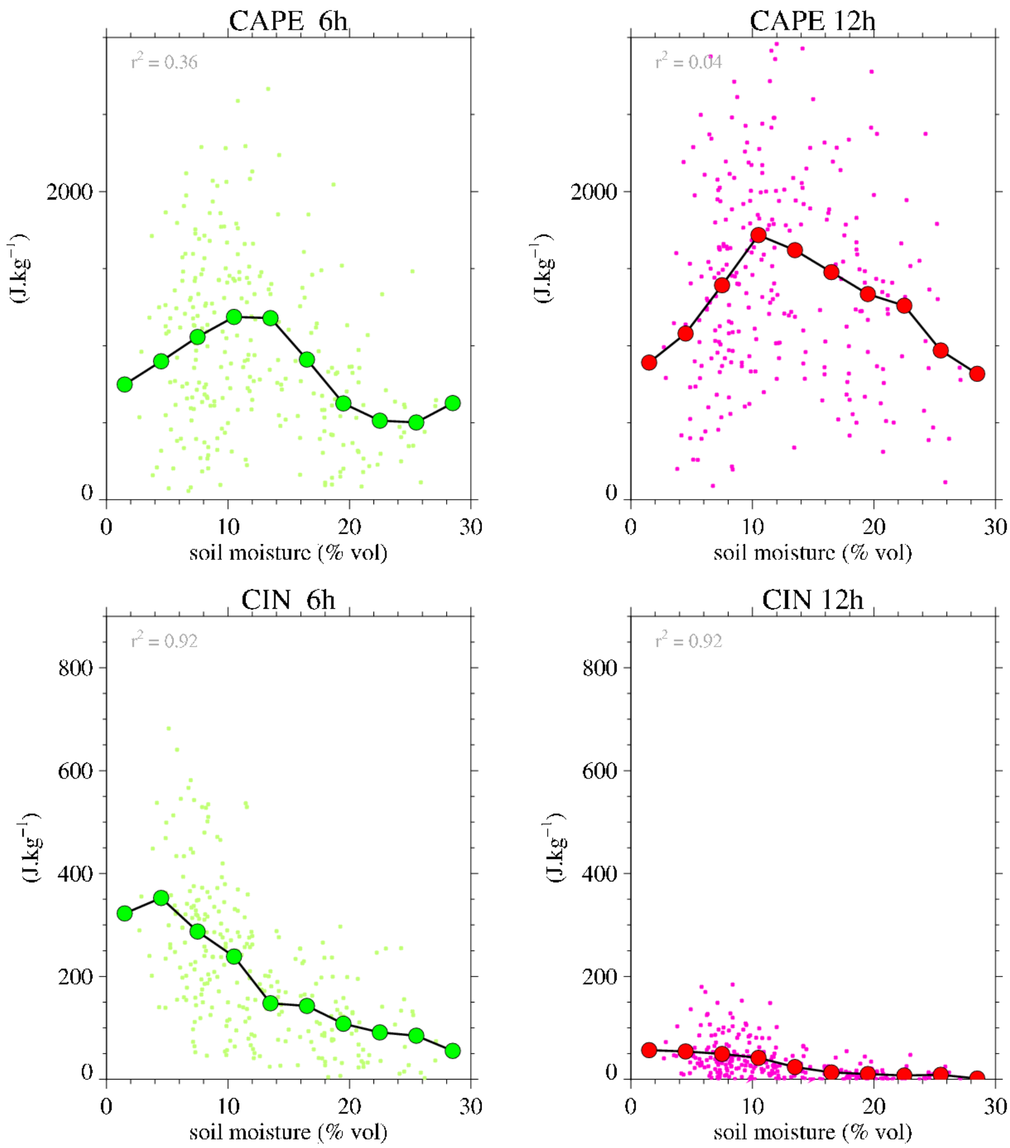

Figure 5-18 : The CAPE (upper plots) and the CIN (bottom plots) values are plotted as a function of soil moisture. The soil moisture values are values extracted from the 1degx1deg analysis associated with storm initiations. The atmospheric parameters (CAPE and CIN) come from the ECWMF analysis.

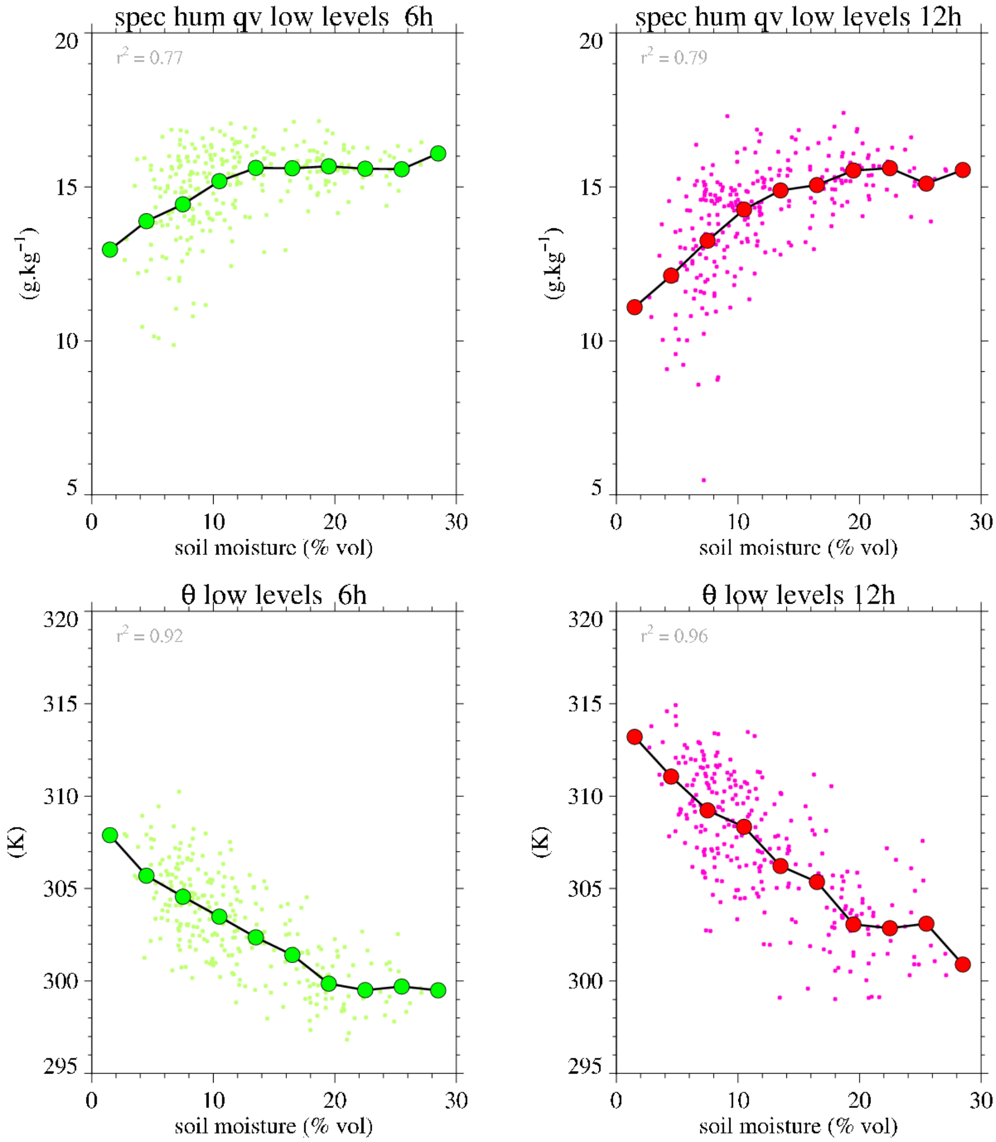

Figure 5-19 : Specific humidity qv (upper plots) and potential temperature(bottom plots) plotted as a function of soil moisture. The soil moisture values are value extracted from the 1degx1deg analysis and associated with the storm initiations. The atmospheric parameters (qv and theta) come from the IFS analysis.

A strong coupling exists also between the soil moisture and the lifting condensation level (LCL), as shown in Fig. 5-17. Over dry soils, the LCL is higher than above moist soil, the LCL decreases with increasing soil moisture. However, above a soil moisture threshold, the relationship vanishes and the mean value remains low. This may be explained by controlling factors, like the available energy for evaporation or the atmospheric demand of moisture. The coupling strength is slightly stronger at midday than in the morning due to surface fluxes and convective boundary layer development (R^2=0.87 at 6UTC R^2=0.95 at 12UTC). Larger differences in LCL between wet and dry soils are found at noon. The LCL rises as the low-levels become drier and warmer. This increase is the most important over dry soils.

The level of free convection (LFC) is also highly correlated with soil moisture (R^2=0.85): the drier soil is, the higher the LFC is. The LFC goes down during daytime, but it is only over moist soils that this lowering becomes significant. Indeed, the LFC are still very high at noon. This means that the triggering of storms requires low-level air parcels to reach this level if convection is actually driven by the dynamics of the atmospheric low levels.

The analysis of CAPE shows that there are large values of energy available for convection especially above soils with intermediate values of moisture (see Fig 5-18). The amount of available energy gets larger during the afternoon, especially over the wetter surfaces. In the morning, the convective inhibition is quite large. It becomes much smaller in the afternoon, although substantial amounts of CIN can still be found over drier surfaces at noon.

From the AMMA analysis, we see conditions of relatively weak wind associated with the storm initiations (see Fig 5-20). The low-level winds are stronger in the morning than in the afternoon. This is associated with the nocturnal jet which vanishes during daytime as the convective boundary layer grows and the turbulent friction becomes more important. The comparison of the AMMA analysis with the radiosoundings shows (see section 5-2-3) that the wind is usually underestimated. However, even if this is taken into account, the wind conditions can still be considered relatively weak after midday, which is when we consider storms initiation.

The observed cases of convective initiation identified above are found to occur over a variety of environments. This is not unexpected given the predominant diurnal mode of convective initiation over a region displaying large fluctuations in the low levels. In other words, a variety of atmospheric conditions appear to support the initiation of daytime convection.

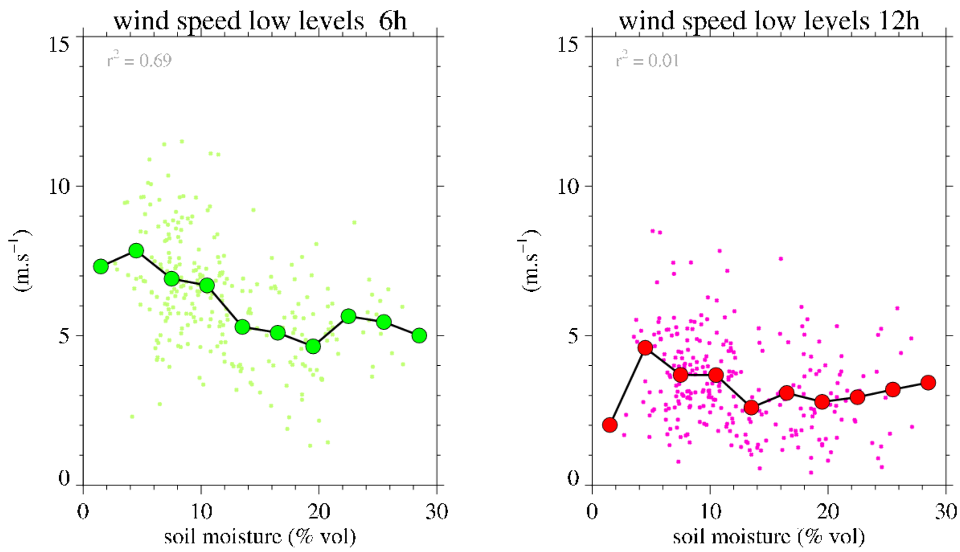

Figure 5-20 : Wind speed in the atmospheric low levels plotted as a function of soil moisture. The soil moisture values are values extracted from the 1degx1deg analysis and associated with the storm initiations. The wind speed comes from the IFS analysis.

5.3.5 Generalisation to a 4year dataset

More recently, and in order to test the robustness of the results obtained with the refined ISIS initiation dataset, the statistical analysis was extended to four wet seasons using the storm initiations detected using the alternative algorithm (see section 5-2-2). They were combined with LSTA datasets using the same method as for the previous analysis. 1947 pixels were associated with storm initiations over the four monsoon seasons.

The normalised LSTA distribution of these pixels and the reference distribution are shown in Fig 5-21. A distinct positive signal appears in the distribution of normalised LSTA compared to the reference. The initiation distribution is shifted by 0.44 towards positive values. The 'quartile study' reveals that 35% of the values in the initiation distribution are larger than the value of the last quartile of the reference distribution, meaning that there is 10% more chance for convective initiation to occur over soil presenting a strong positive anomaly. In the 2006 ISIS storm initiation dataset, percentage of 9% and 6% were found in the LSTA and AMSR-E soil moisture analysis respectively.

The same seasonal sensitivity is also found in this analysis. A much larger sensitivity to mean LSTA is found during the pre-onset phase (41.3% of initiation values found in the last quartile of reference distribution) compared to the post-onset period (31.7%). This time, we benefit from a large sub-set of data with good statistics that can be analysed with more confidence. This seasonal sensitivity could be linked to a role of the vegetation, which is much more developed after the onset of the monsoon and could potentially damp the response of the surface to rainfall events during the pre-onset phase. Indeed, atmospheric moisture is brought by advection and this is especially the case before the onset of the monsoon in the Sahel. The higher the convective boundary layer brings the advected moisture the greater the chance for convection to be triggered.

When looking at the variability of LSTA, which is shown in the top right plot of Fig. 5-21, we see also a slight difference between the initiation distribution and the reference. More variability is found in the initiation sample than in the reference. In June, no significant differences are found between the distributions, whereas after the onset of the monsoon, we see more variability in the dataset associated with initiation compared to the reference. These new results are entirely consistent with the results found using the 2006 refined ISIS initiation dataset and can be considered as statistical very robust.

Difference between initiation distribution and reference distribution							
		p-value	Mean	Median	Deviation	1st quart.	4th quart.
Mean LSTA							
	4 JJAS	8.98e-46	0.44	0.51	-0.06	15.3%	35.4%
	Pre-onset	2.92e-22	0.66	0.71	-0.18	11.9%	41.3%
	Post-onset	1.90e-11	0.30	0.40	0.02	17.9%	31.7%
Variability of LSTA							
	4 JJAS	2.50e-11	0.063	0.058	-0.0078	20.2%	29.7%
	June	5.98e-01	0.012	0.005	-0.0088	25.0%	25.5%
	Pre-onset	3.57e-01	0.020	0.015	-0.0150	22.9%	25.1%
	Post-onset	1.34e-11	0.096	0.090	-0.0190	17.0%	32.7%

Table 5-5 : ***Statistical results of the differences between the initiation and reference distributions of LSTA pixels when considering all the 2006-2009 storm initiations (4 JJAS), only the pre-onset period and the post-onset period. The same is done for the variability of LSTA. The p-value corresponds to the results of the MWM test between the two distributions. The two last columns represent respectively the percentage of values encountered in the initiation distribution that are inferior to the 1st quartile of the reference distribution and superior of the 4th quartile of the reference distribution.***

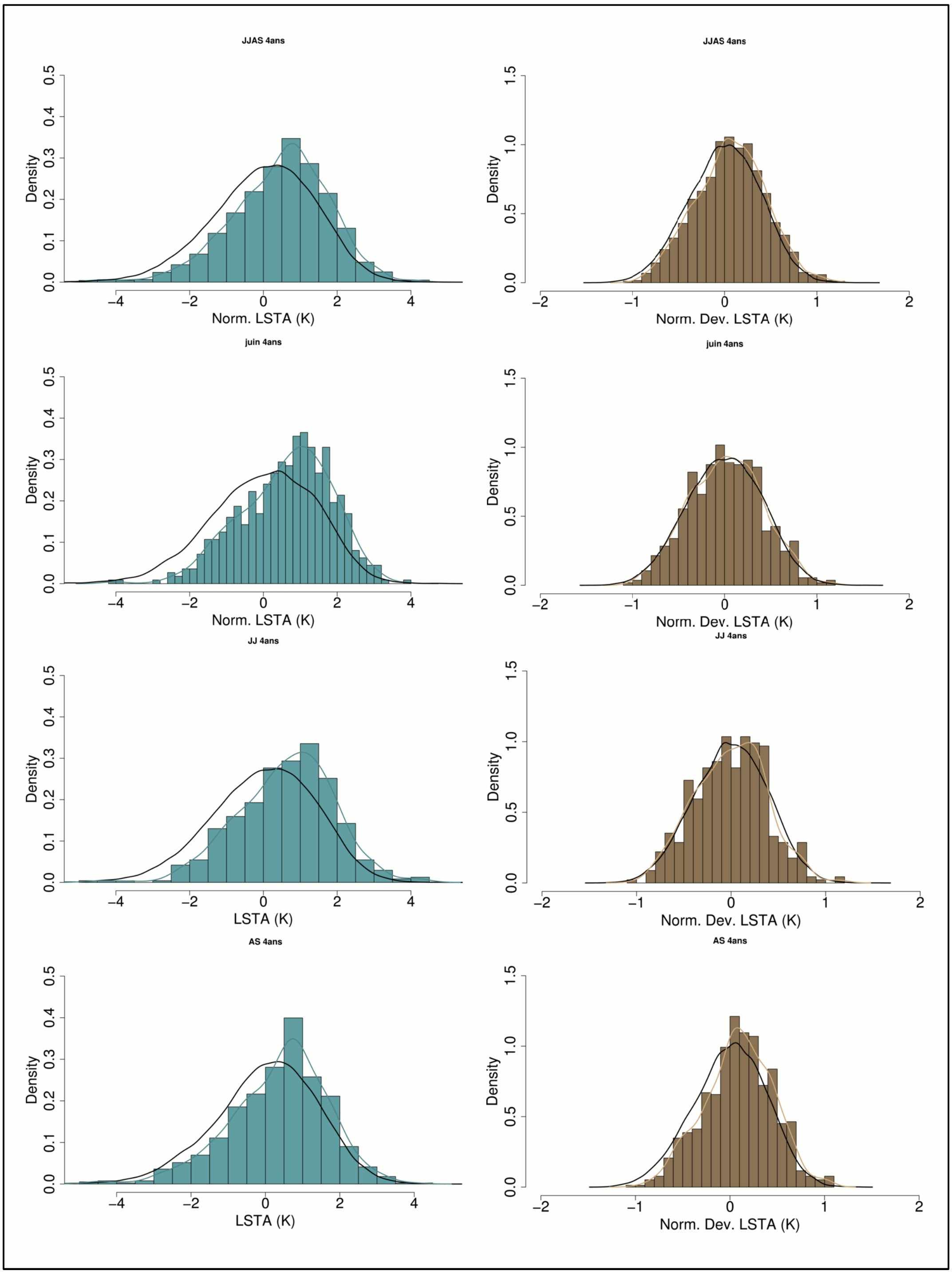

Figure 5-21 : Distributions of normalised LSTA (left column) and variability of LSTA (right column) of the 'initiation group' (blue histograms & curve) and 'no initiation group' (black curves) for the 4 monsoon seasons (top figure), the 4 Junes (middle up) , the pre-onset periods (middle down) and the post-onset periods(bottom). On the right, the figures presents the results of the analysis on the variability of LSTA with the same organisation as the left figures.

5.3.6 Sensitivity Tests to Length Scales and latitude

Several sensitivity tests were performed. First, some sensitivity tests were carried out using slightly different LSTA estimates. Theses temperature anomalies were computed compared to a seasonal mean (21day mean in the study). Similar results were found with seasonal LSTA compared to the 21day mean anomalies.

Then, the importance of the length scale on the results was investigated. For the mean LSTA study, the maximum amplitude of the signal is always obtained at a length scale of 1-1.5deg, it decreases for smaller and larger values. It is also noticeable that the pre-onset period always exhibits the strongest signal. The results for the variability of LSTA shows that the signal is robust for the post-onset period and exhibits much more sensitivity at the smaller scale during the pre-onset period. LSTA variability associated with initiation increase for smaller length scale. The sensitivity of the results to geographical/climatologic zones was investigated. The initial domain was divided into two sub-domains according to the latitude, one extending from 10°N to 13°N and the other one from 14°N to 20°N. No sensitivity of the results to the latitude was observed.

Another methodology was developed to evaluate the links between theses storm initiations and the underlying surface properties consisting in comparing the directly a small zone centred on the initiations compared to a larger domain. The results obtained using this methodology are entirely consistent with the results presented in this chapter (Taylor et al., 2010).

5.3.7 Conclusion

In this section, first, the precise locations of more than 500 initiations of daytime deep convection were determined for the 2006 West African monsoon season over the Sahel. They were combined with two different satellite based surface property datasets to study their relationship at the mesoscale. First, we combined the refined ISIS initiation data with the AMSR-E soil moisture estimates. They are estimates of the moisture in the top few centimetres of the soil, available in any weather conditions, but their spatial resolution is relatively low (40kmx40km). Then, the storm initiations were combined with land surface temperature anomalies, which are well suited for detecting the moisture patterns associated with recent rainfall events. These data have a higher spatial resolution than the AMSR-E data, but samples only clear-sky conditions.

The combination of daytime storm initiations with AMSR-E estimates showed that at the mesoscale (1°x1°), initiations of convection tends to occur preferentially over drier soils (+6%) compared to the surrounding with a stronger signal during the pre-onset period (+12%). Moreover, the storms appeared to be favoured over soils presenting more variability during the post-onset period (+9%). A relationship between LSTA and initiation of deep convection was also evidenced, showing that initiations are more frequent over surface associated with larger positive LSTA values (9% in JJAS 2006 and 14% for the pre-onset period). A signal was also found on the heterogeneity of LSTA, indicating that storm initiations tend to be triggered over surfaces that exhibits more LSTA variability especially during the post-onset period (+10%).

The study was then extended to four monsoon seasons (2006-2009) including more than 2000 daytime storm initiations. The results were entirely consistent with the ones obtained for the single 2006 monsoon season. Deep convection was found to be triggered 10% more often over surfaces having a strong positive LSTA. When considering only the pre-onset period, this result reach 16%. Considering the variability, 5% more convective systems are triggered over surface presenting a high variability and 8% when considering only the post-onset period. The mesoscale variability seems to be less important during the pre-onset period.

The soil property datasets are independent datasets. The fact that the results agree gives us confidence on the robustness and reliability of the results. Moreover, the extension of the study to 4 years giving a good statistics, reinforce our conclusions.

The mechanisms involved in convective initiation are complex and occur in very contrasted environments as shown by the analysis of ECMWF analysis profiles. In some cases, the atmosphere appears to be characterised by difficult conditions for deep convection with high large CIN especially during the pre-onset period. The couplings between initiation soil moisture and atmospheric properties have been investigated. The LCL as well the LFC are higher as the soil moisture decreases. During daytime, the difference between LFC and LCL decreases more over moist soils (that can be drier than their surrounding). There is large range of CAPE values associated with the storm initiations. There are various processes associated with distinct environments. This study however shows that the tendency for convective systems to be favoured over drier soils is found over the whole domain (no difference in latitude) but favoured in a pre-onset regime.

There has been only a few observationally-based studies to address the issue presented above. Taylor and Ellis (2006) had identified a preference for developed convection over dryer soil which is consistent with this study. Both our dataset and our methodology are different from this prior study which focused on JJAS 2000. This study provides an observational evidence based on more than 2000 cases that deep convection over the Sahel is preferentially triggered over drier soil presenting more surface heterogeneities. In particular, the present study provides a more direct link between surface properties and the process of convective initiation, which had not been so firmly established before.

5.4 Gradients of temperature and convective initiation

In the first part of this work, we evidenced a preference for initiation to develop over warm/dry zones compared to its surrounding at the mesoscale. There was also some signal on the variability of soil moisture; initiation of convection tends to be favoured over surfaces associated with more surface heterogeneities, especially at fine spatial scales. To further investigate this results, we decided to develop a method to identify and quantify gradients of surface properties at the scale of few tens of kilometres.

Our hypothesis is that mesoscale circulations induced by soil moisture gradients at the local scale can help the triggering of convective systems. So, first we quantify the surface LSTA gradients found over the zone where convection initiated and then to see whether these gradients are stronger than the ones in the surrounding area.

5.4.1 Method for calculating gradients

LSTA data has a resolution fine enough to be able to study fine structures like gradients over few tens of kilometres. The method used here to calculate the temperature gradient is illustrated in Fig. 5-22. First, a rectangle zone centred on the initiation point is selected. This rectangle is chosen aligned with the wind direction. The information on the wind comes from the ECMWF analysis (see section 5-2-3 for details). This is important, as in our hypothesis, wind direction is an important parameter. Gradients are obtained by computing a slope (linear regression) using LSTA data within the selected rectangle. The different parameters of the area as the length(L), the width(W), the angle with wind(θ) as well as the distance from the initiation point (dx) can be varied. The settings of the reference computation of LSTA gradient are:

- L=0.3deg
- W=0.08deg
- θ=0deg
- dx=0deg

These settings are always used in the following results except if the contrary is mentioned. On average, about 30 data points were used to compute a gradient. When less than 70% of the data points were available, the storm initiation case was excluded.

To assess whether or not larger LSTA gradients are found in the initiation zone compared to its surrounding, we sample homogeneously the LSTA gradients in the environment, in the same way as for the initiation, on a regular grid as shown in Fig. 5-23. The method was designed in order to have a large populations of gradients in the surrounding of the initiation location(44samplings) in the same latitudinal band. A simple metric consisting of comparing the medians of the distributions was used to evaluate the difference between the initiation and environment samples as illustrated in Fig. 5-24.

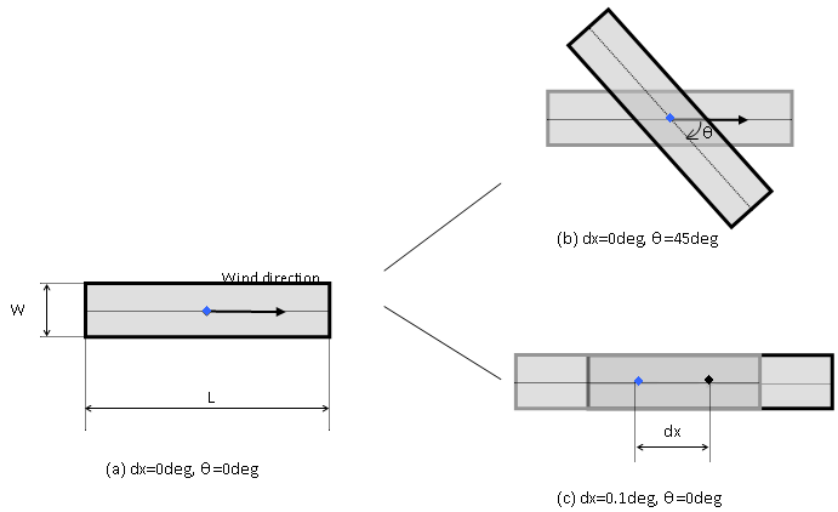

Figure 5-22 : ***Schematic illustrating the geometrical properties of LSTA gradients computed at the convection initiation point: a zone of length L and width W is selected centred on the convection initiation point and aligned with the wind direction(wd). This zone can be slid sideways by a distance (dx) and rotated around the initiation point by an angle (θ).***

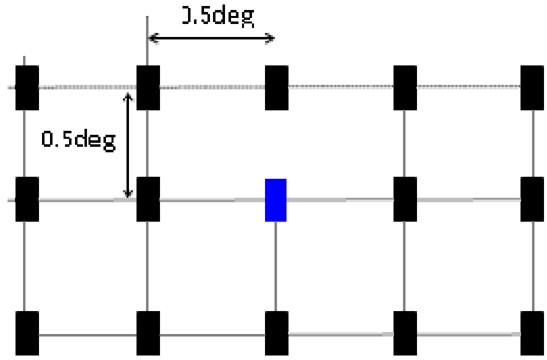

Figure 5-23 : Method for sampling the "background gradient": the LSTA gradients are calculated from data within 44 black rectangles (only 14 are represented on the schematic), spaced every 0.5deg (the 44 points are all in the 1°wide zonal band), with the same geometrical properties as for the initiation (blue) rectangle.

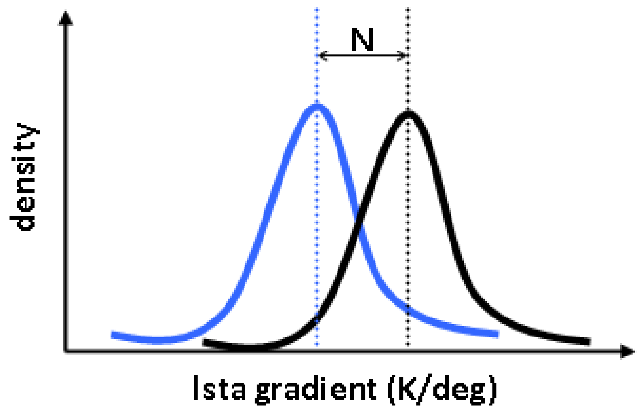

Figure 5-24 : Schematic illustrating the definition of 'N' (K.deg^{-1}): difference between the medians of two distributions: initiation sample (in blue) and the environment sample (in black).

A correlation coefficient gives an estimation of the quality of the gradients. A high coefficient gives good confidence on the gradient calculation. From the estimations, we have got large gradients that are associated with high correlation coefficients. This give us confidence in the robustness of the strong gradients values. The surface gradient analysis was initially carried out with the refined ISIS storm initiations for 2006 monsoon season and then with the storm initiation dataset for the 4 monsoon seasons. As the results with the four years were completely consistent with the former gradient analysis, we chose to show only the last results corresponding to the large dataset that offers a good statistics (more than 2000 storm initiations).

5.4.2 Results of the N parameter analysis

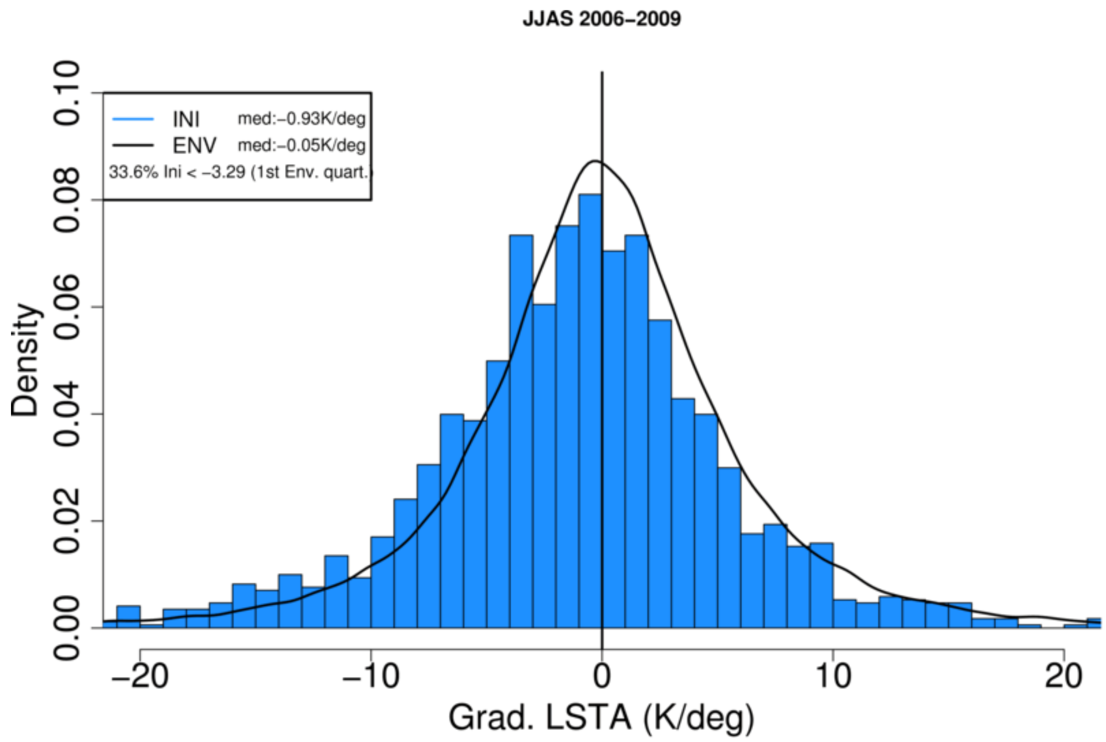

Figure 5-25 : Distributions of LSTA gradients computed at the CMT storm initiation points(blue) and in the background with the default choices; L=0.3deg, W=0.04deg.

Surface temperature gradients were computed at every initiation points as well as in the environment following the method described above. This was done using the default choices of geometrical properties of the gradient boxes. This was designed in order to sample the surrounding gradients in a same latitude band. The distributions of LSTA gradients at the initiation points and in their surroundings are plotted in Fig. 5-25. The black curve represents the density distribution of gradients in the environment of convective initiations. Table 5-6 recapitulates the difference found between the initiation and background distributions. By comparing the distributions, we find a population of initiation gradients that is systematically shifted towards strong negative values by -0.93K/deg. This difference was tested statically using the WMW test, which gave a p-value of $5.1e^{-14}$ corresponding to significant difference between the initiation distribution and the background distribution. In the initiation sample, there are 8% of the gradient values that are more negative than the value of the first quartile of the background distribution. The dataset were split into months, a sensitivity was found with a larger signal during the pre-monsoon (June-July) period compared to the post-onset period (August-September).According to this result, it would mean that initiations tend to occur more often over zones that exhibit stronger temperature gradients than their surroundings. The sign of the tendency is negative. A negative gradient corresponds to a transition zone characterised by a warm zone upwind and a cooler zone downwind. As theoretical study showed, this configuration would tend to create a mesoscale circulation going from the warm zone to the cooler one, so in the opposite direction compared to the synoptic flow.

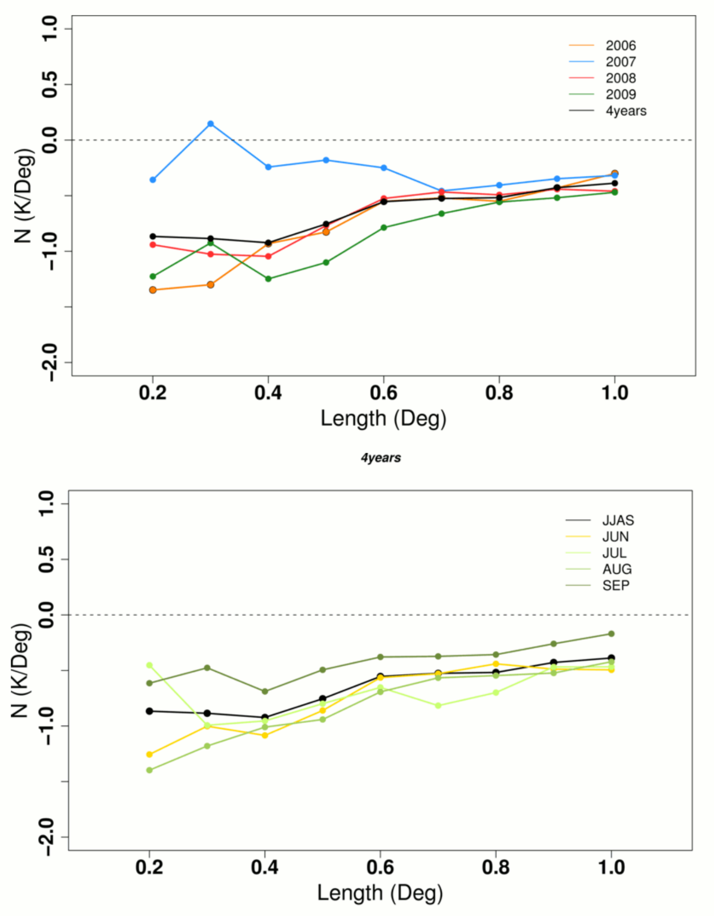

Figure 5-26 : Sensitivity of N parameter (in K/deg) as a function of gradient length (in deg). The black curve in the two plots corresponds to the values when the whole four year dataset is considered. The top plot shows the results when the data is split into years(2006, 2007, 2008 and 2009). The bottom plot presents the results when split into months (June, July, August and September).

– ***Sensitivity of the gradient features to length scale***

A sensitivity study was carried out to investigate the dependence of gradient values to the geometrical properties of the box that we use in the calculations. This also allows to better characterise the gradient features in a spatial way. First, the length of the gradient was varied from 0.2 to 1deg. The smaller scale could not be investigated as the resolution of the LSTA does not allow it. The N parameter value, which compares the initiation and the background gradient distributions was calculated for each length. The results obtained are shown in Fig. 5-26. As the length increases, the magnitude of N decreases. The value of L for which we obtained the maximum N varies between 0.2deg and 0.4deg. This indicates that strong surface gradients are found at the storm initiation points at the small scales. In fact, soil moisture estimates such as provided by AMSR-E or TRMM, whose spatial resolution is on the order of a few tens of kilometres, cannot allow detecting the fine scale structures highlighted here. A good agreement among the different months with a slightly larger signal found in the pre-onset month. There is also a good agreement among the different years except for 2007 which appears to present much less sensitivity. This may be due to the monsoon activity that was especially strong during this year. Larger precipitation were recorded compared to the other years. The growth of vegetation started earlier in the Sahel which could have lead to a reduction of the LSTA sensitivity to precipitation.

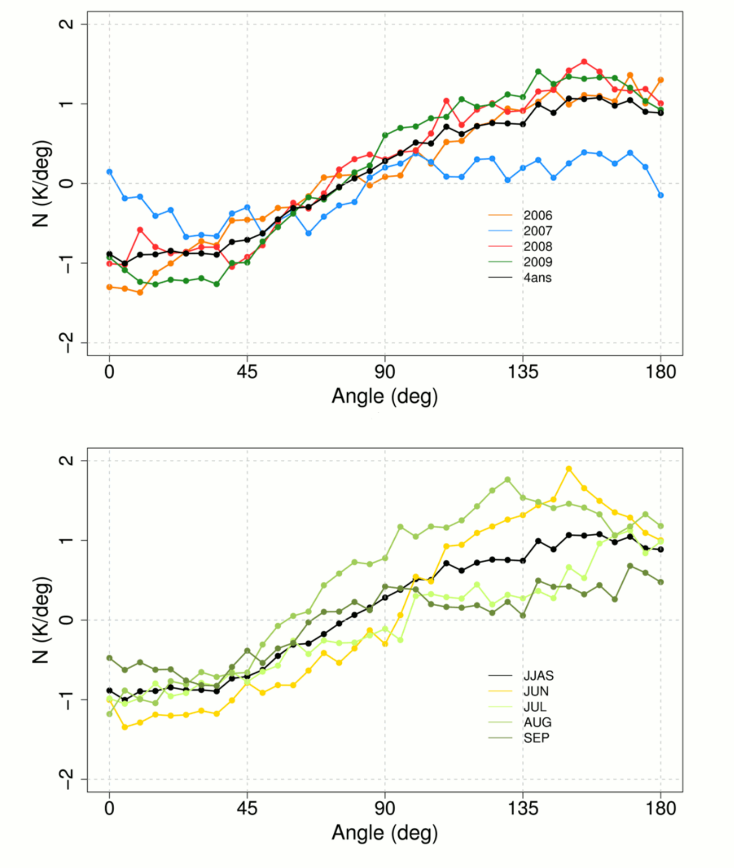

Figure 5-27 : Sensitivity of N parameter (in K/deg) as a function of angle with wind (in deg). The black curve in the two plots corresponds to the values when the whole four year dataset is considered. The top plot shows the results when the data is split into years(2006, 2007, 2008 and 2009). The bottom plot presents the results when split into months(June, July, August and September).

– ***Sensitivity to angle with wind***

The wind direction in the ECMWF analysis is generally well captured and enables us to do a sensitivity test on the wind direction. Figure 5-27 presents the sensitivity of N to the angle with wind direction. As the angle with wind increases, the N parameter becomes less and less negative. It becomes close to 0 at about 80-90 degrees and increases to reach a value of 1K/deg. As found in the previous section, a stronger signal is observed in June compared to the other months. 2007 appears again to be weaker than the other years. The N parameter follows very well the rotation of the box around the point of initiation. This lets us think that the feature has an egg-shape with symmetrical properties on each side, which could explain the "flat gradient" perpendicular to the wind direction at this scale.

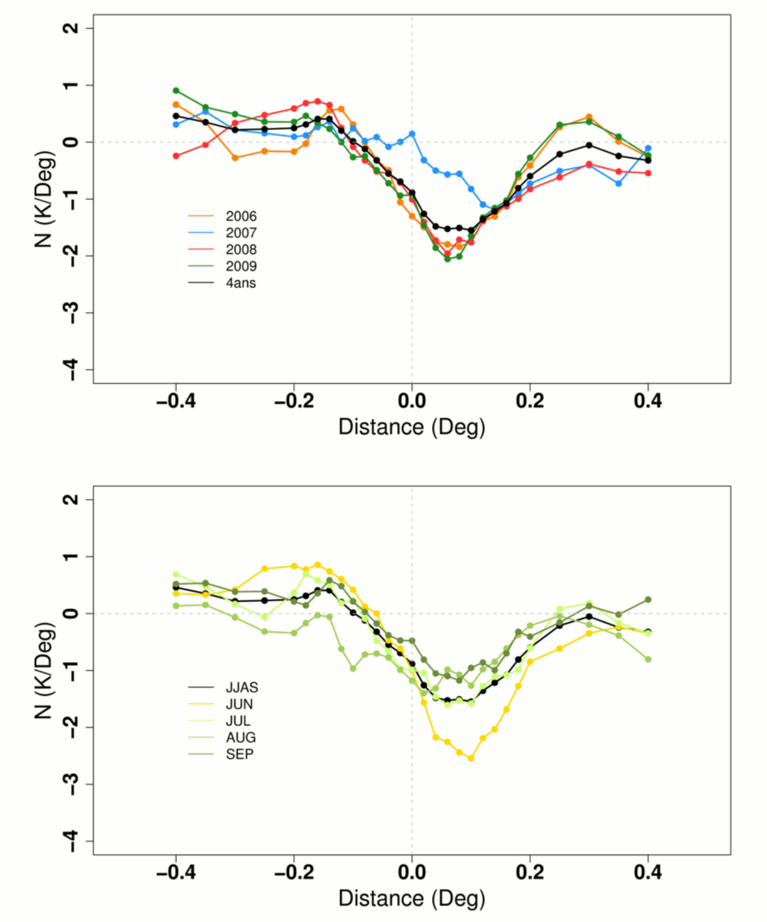

Figure 5-28 : Sensitivity of N parameter (in K/deg) as a function of distance(in deg) from the storm initiation. The black curve in the two plots corresponds to the values when the whole four year dataset is considered. The top plot shows the results when the data is split into years (2006, 2007, 2008 and 2009). The bottom plot presents the results when split into months (June, July, August and September).

– ***Sensitivity to distance from the initiation of convection***

The position of the box compared to the location of the storm initiation point was varied to investigate the characteristics of the surface gradients along the wind direction. The distance was varied from -0.4 deg (in the opposite direction of the wind) to +0.4 deg. The results are presented in Fig 5-28, where the N parameter is plotted as a function of the distance from the initiation point. The results are plotted for the different years (Fig 5-28a) as well as for the different months (Fig 5-28). The black curve indicates the results found with all the data together. A striking feature appears in the different resulting curves. A maximum negative value of N is obtained for a distance close to 0.1deg downwind from the storm initiation that decreases in both directions until it reaches a maximum positive value for dx=-0.2deg. A seasonal sensitivity is observed with the strongest signal appearing in June. In August and September, the features are less well defined. From year to year, the same pattern is observed, except in 2007 where the maximum is weaker and is obtained a bit further down from the location of storm initiation. These features, when put in the spatial context, would mean that the storm initiations tend to occur preferentially around 0.1deg upwind of the warm to cold transition.

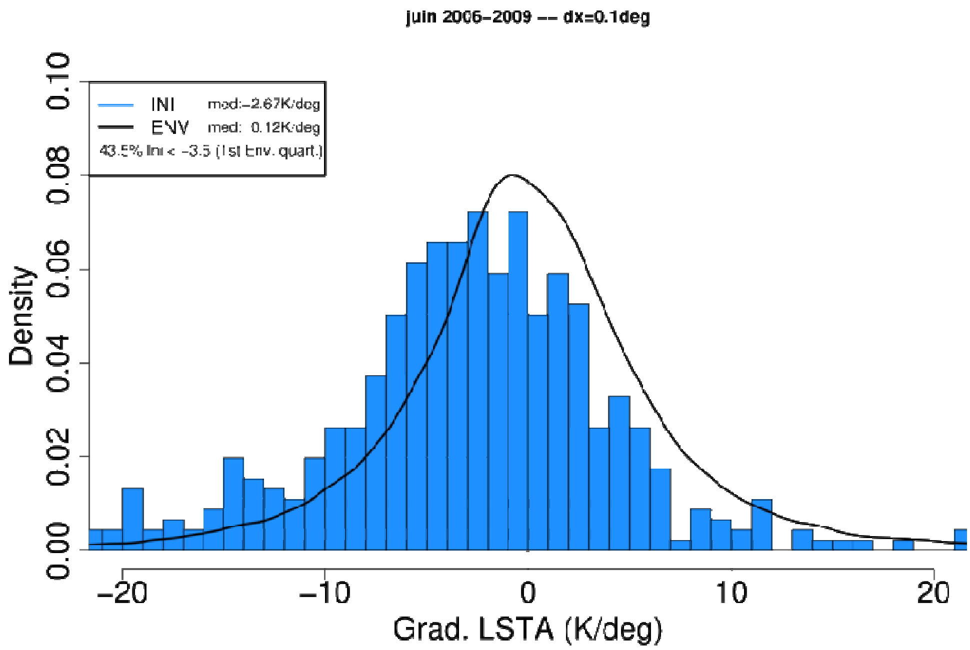

Figure 5-29 : The distribution of gradients calculated 0.1 deg downwind from the storm initiations in blue and the smoothed density distribution corresponding to the background environment sample in black.

– ***Optimised calculations***

Based on the different sensitivity tests carried out, we defined a set of parameters to optimise the computations; θ=0°deg, Length=0.3° (not 0.2° because of resolution limits and to insure the robustness of the results), and dx=0.1° for the months of June. The resulting distributions of gradients are plotted on Fig 5-29. The distribution of initiation gradients is significantly shifted towards negative values compared to the background sample. The difference between the initiation and the background gradient distributions are summarised in Tab. 5-6. A p-value of 5.3e-31 (5.1e-14 for dx=0°) is obtained meaning that there are significantly different. Differences of -2.85 K/deg (-2.55 K/deg) between the means (medians) the initiation and ref distributions were found, which corresponds to much larger negative gradient values in the initiation distribution compared to the background distribution. 43% of the initiation values are smaller than 25% (first quarter) of the background distribution. This suggests that there are 18% more chance for initiation to be triggered over a strong negative gradient that expected from the background distribution. This is quite a significant percentage, that is on the same order of magnitude than orography triggering mechanism.

	p-value	Mean	Median	1st quart.	3rd quart.
JJAS Ref	5.1e-14	-1.27 K/deg	-0.88 K/deg	33.6 %	21.1 %
June dx= 0.1deg	5.3e-31	-2.85 K/deg	-2.55 K/deg	43.5 %	14.9 %

Table 5-6 : ***Statistical results of the differences between the "initiation" distribution of gradients and the "background" distribution. The 1st(3rd) quarter values corresponds to the percentage of initiation values smaller (larger) than the 1st(3rd) quarter value of the reference distribution.***

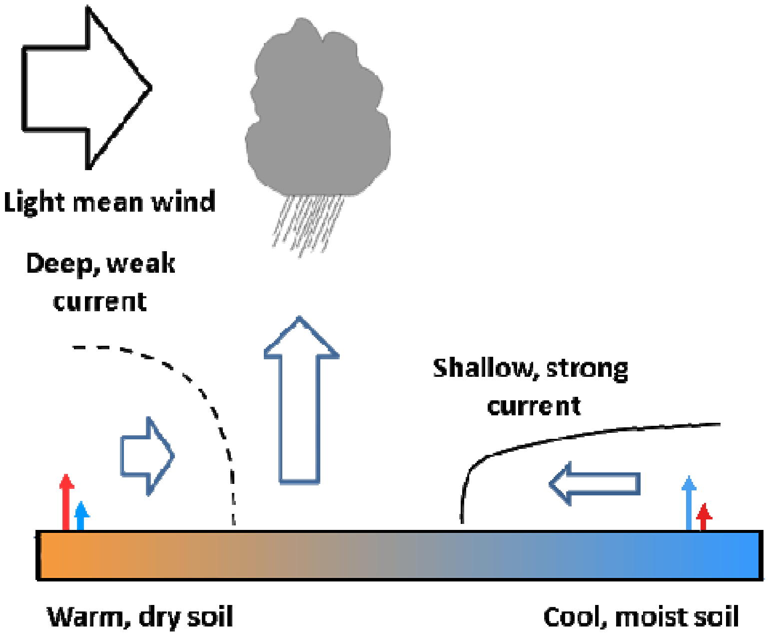

Figure 5-30 : Schematic illustrating the low-level mechanisms involved in the triggering of deep convection over large LSTA gradients.

The schematic on Fig 5-30 illustrates the possible mechanisms involved in the triggering of convective storms over large temperature gradients. From our results, the initiation of deep convection happens on the dry (warm) side of a dry to wet (cool) transition. On the dry side, the sensible heat flux is large and the latent flux is weak. This results in a deep warm convective boundary layer. By contrast, on the moist side, the boundary layer remains shallower and moister as the sensible heat flux is weak and the latent heat flux large. The synoptic wind flows from the warm patch to the cold patch, whereas the expected mesoscale circulation should flow from the cold to the warm patch, in the opposite direction of the synoptic flow. This suggests a convergence between these two flows which may help overcome the convective inhibition. Further investigation on the atmospheric stability associated with this initiation points suggests that higher LFC (corresponding to less favourable conditions for initiations) are associated with strong gradients (not shown).It also appears that is some cases, initiation occurs over a warm anomaly of LSTA corresponding to two transitions on both sides. The initiation occurs more precisely on the 2nd edge of the wet to dry to wet anomaly suggesting either that the first transition does not allow enough convergence (as it is in the same direction as the synoptic wind) or that in some cases it may help the triggering of convection on the second transition.

5.4.3 Conclusions and Discussions

This study has investigated whether or not there is a preference for storms to initiate over regions presenting stronger surface property gradients than theirs surroundings at the mesoscale and with respect to the direction of the atmospheric flow. For this, a method was develop to calculated gradient at the initiation points using a high-resolution satellite dataset of LSTA (3km) combined to precise satellite detection of storm initiations. The computation was done for more than 2000 storm initiations over the Sahel. A larger population of negative gradients was found compared to the background gradients. Some sensitivity tests on the geometrical properties of the zone used to calculate the gradients gave us further information and quantification on the patterns associated with storm initiations.

To summarise, the results show that storm initiations tend to occur 13% (up to 18% in June) more often over zones presenting a strong LSTA gradient. This is of the same importance compared to orographic triggering. The sign of the gradients is negative corresponding to storm initiations occurring on a warm to cool transition with the synoptic wind blowing from the warm zone to the cool zone. The wind direction seems to be important in the calculations; when the gradients are calculated perpendicular to the wind direction a weak signal is obtained. The maximum gradient is found 0.1deg downwind of the initiation point which corresponds to initiations occurring on the warm side of the warm to cool transition.

Our results on the sensitivity to gradient length suggest that LSTA gradients affects storm initiations at small scale (on the order of few tens of kilometres). Synoptic wind conditions are likely to affect the formation of mesoscale circulations. The ECMWF analysis and sounding data both suggest that daytime winds associated with initiations are relatively weak and this possibly favours the development of such surface induced mesoscale circulations. Here, more initiations over negative gradients are observed which suggests that mesoscale circulation opposite to the mean wind direction could be generated and create convergence on the warm side of the transition. Larger CIN are associated with large negative gradients with is also consistent with a mesoscale circulation that allow to overcome the atmospheric stability.

The mechanisms of convective triggering evidenced by this observational study occur at fine scale (few tens of kilometres) are currently not considered in large scale models. This is likely to play a role in model difficulties in triggering convection in place where deep convection does not occur in the model (e.g. ECMWF over the Sahel, see Chap2&4).

Chapter 6
Conclusions and Perspectives

This thesis work was devoted to the study of diurnal variations over West Africa during the monsoon season. First, chapter 2 presented the context of this study including a brief description of the West African monsoon (WAM) system, the main characteristics of diurnal cycles over land, a discussion on modelling issues as well as a review on surface-atmosphere interactions taking place at diurnal timescales. Then, chapter 3 focused on the characterisation of diurnal cycles observed before and after the monsoon onset and established their climatology along the latitudinal transect. The simulation of these diurnal cycles, presented in chapter 4, revealed some strengths and weaknesses of the model in the representation of their characteristics. Finally, chapter 5 was dedicated to the study of the links between storm initiations and surface properties at a diurnal timescale.

6.1 Conclusions

Characterisation of the WAM diurnal cycles

In this work, we took advantage of a unique set of observations gathered during the AMMA field campaign, in particular during two multi-day periods prior and after the monsoon onset, when soundings were launched every three hours at a few sites. It was analysed in order to document the diurnal cycles in the atmospheric low levels along a meridional transect extending from the Guinean coast (Cotonou) up to the Northern Sahel (Agadez). This study focused on the pre-monsoon and the well-established phase of the WAM. The results of this analysis allowed to characterise:

The dynamic and thermodynamic diurnal cycles at the surface and in the atmospheric low levels: No distinct meridional gradient in surface net radiation is observed along the transect prior to the monsoon onset. However, the strong meridional gradient in soil moisture determine the partitioning of net radiation between sensible and latent heat fluxes along the transect which has a large impact on the atmospheric low-levels. The amplitude of the diurnal cycles is found to increase with increasing daily-mean temperature. According to the latitude and season, different timings of temperature and humidity diurnal cycle variations are also observed, as a result of different balances of processes.

The vertical structures of convective and nocturnal boundary layer: This was carried out via an ensemble of diagnostics, including boundary layer and monsoon flow properties, convective indexes. Large contrasts in the structures along the transect were evidenced and quantified. Deep dry convective boundary layers develop in the northern Sahel (up to 5 km deep), whereas boundary layers remain very shallow on the Guinean coast (less than 500 m). It is noticeable that no daytime increase in CAPE nor in low level equivalent potential temperature was observed in the Sahel prior to the onset. This specific feature is explained by a large daytime boundary-layer growth, which efficiently dilute the water vapour with drier air in the absence of any significant water vapour flux from the surface, nor from the monsoon flow after the morning hours. Peculiar features were also observed during night-time in this region, with often strong low-level winds and a fairly weak stabilization in the first hundred metres, under moist conditions.

After the monsoon onset, drastic changes in the dynamic and thermodynamic diurnal cycles are observed: sensible heat fluxes are largely reduced, convective boundary layers in the Northern Sahel collapse (1.5-2km deep) and the diurnal cycles along the transect become closer together in terms of timing and amplitude and more strongly affected by the occurrence of boundary layer clouds.

This diurnal cycle characterisation along the transect allowed the distinction between four atmospheric regimes encountered during the WAM, which can be order as a function of increasing surface temperature as follows:

- A Guinean monsoon regime characterised by a stratiform cloud layer in the lower troposphere, which is accompanied by some precipitation. The amplitude of thermodynamic and dynamic diurnal cycle is quite weak, the convective boundary layers do not develop much (less than 500m) and remains close to saturation.
- A Soudanian monsoon regime characterised by intense deep convection that frequently gives important amounts of precipitation. Boundary layers do not develop very high and are topped with cumulus clouds.
- A Sahelian monsoon regime where deep convection develop very high into the troposphere, even higher than in the Soudanian zone but is less frequent and gives less rain with more day-to-day variability.
- A Sahelian pre-monsoon regime where the atmosphere is moist but does not give rise to much cloudiness nor rainfall. Strong meridional advection bring water vapour in the lower troposphere during night-time, and this water vapour is redistributed vertically during daytime as a result of strong convective boundary-layer growth in the dry SAL.

These distinct low-level diurnal cycles involve an ensemble of interactions of physical and thermodynamic processes which vary according to the considered regime. Numerical modelling of diurnal cycles is still stained by systematic errors such as the diurnal cycle of deep convection (e.g. Yang and Slingo, 2001; Betts and Jakob, 2002; Guichard et al. 2004). The analysis of the diurnal cycle carried out here allowed to develop a common modelling framework. Its aim is to identify the strengths and weaknesses of the model to represent the observed diurnal cycles for these distinct regimes and to help testing its sensitivity and parameterisations.

Simulations of observed diurnal cycles

The modelling framework has been designed for single column models or LES type models. Here, the 1D version of the Meso-NH model has been used, in a fully coupled mode with the surface scheme (SURFEX). Initial and boundary conditions have been designed from the AMMA reanalysis and ALMIP offline ISBA runs. This is a rather simple modelling framework, which is however realistic enough to be able to capture the observed synoptic variability.

The set of simulations is able to reproduce the meridional gradient observed in the diurnal cycle amplitudes. The simulations reinitialised every 24 hours capture somehow the diurnal cycle. However, systematic biases are observed in the simulations and this leads to significant biases for simulations carried out over longer durations. These biases arise from errors in the simulation of the processes and of their interactions at diurnal timescale.

- In the heavily cloudy and weakly precipitating Guinean monsoon regime, the model has difficulties to handle the stratiform cloud layer. The cloud cover excessively reduces the incoming shortwave radiation at the surface. This leads to a drift towards a too cold and dry mean state.

- In Soudanian monsoon regime, characterised by intense and frequent convective events, the model manages to correctly simulate the precipitation. However, the model has difficulties in representing the strong morning variability and the weak nocturnal variability. The simulations again drift towards a too cold and too dry mean state.

- In a Sahelian monsoon regime, the simulations exhibit a too large convective boundary layer growth. Daytime low-level cumulus clouds are underestimated, they do not interact with the radiation scheme and this leads to an overestimation of the surface heat fluxes. This has for consequence a drift towards a too dry but now also too warm mean state. Thus, even if the cloud cover is less important than under moister conditions, they still have a major impact on the daytime evolution of the low levels.

- In a Sahelian pre-monsoon onset, the atmospheric stability is relatively weak. Daytime convective boundary layers again develop too much compared to the observations. It is also noticeable that monsoon pulses are underestimated in the reanalyses used to constrain the model and this is partly responsible for the excessive warming in the low troposphere. Another issue is the difficulty of the model to handle fine structures such as the delicate separation between the convective boundary layer and the Saharian air layer above.

From there, additional simulations were performed in order to explore whether these features were still obtained in a more idealized context, by using a diurnal composite for boundary conditions instead of the multi-day time sequence involving synoptic variability. Interestingly, they reveal a similar behaviour.

Considering now the meridional dimension, these distinct biases lead to a strengthening of the meridional gradients of temperature, from too cold in the Guinean regions to too warm in the Sahel. Interestingly, these temperature and moisture biases appears as relatively close to those displayed by the more complex two-dimensional simulations of Peyrillé and Lafore (2007) performed with the same model. This suggests that the fairly simple framework presented here could provide a complementary tool for further testing of the model.

Links between daytime storm initiations and surface properties

Couplings between daytime initiation of deep convection and surface properties have been investigated based on combined satellite datasets. Two different sets of satellite based estimates of surfaces properties were used: surface temperature (LST-MSG) and soil moisture (AMRS-E/AQUA). First estimates of the daytime storm initiations were obtained from the convective tracking system ISIS (Morel and Senesi 2002, Tomasini et al. 2006). They were further refined via the use of a back-tracking method in order to determine more precisely the location of initiation (work carried out by C. Taylor, CEH). These satellite estimates cover a large spatial and temporal domain, which is necessary to statistically study the links between deep convection and surface properties. In addition, thermodynamic and dynamic profiles associated with each storm initiations were extracted from the ECMWF analysis in order to characterize the local atmospheric environment. The dataset initially covered the 2006 monsoon season but was further extended to four monsoon seasons.

In a first step, the couplings were investigated at mesoscale (1 deg x 1 deg) over a Sahelian domain. A methodology was developed in order to get rid of the latitudinal gradient of moisture, which develops at large scale. The analysis of surface properties associated with the storm initiations at this scale shows that storm initiations are favoured over dry soils (+13% more chances) especially prior to the WAM. It also suggests that storm initiations are favoured over surfaces presenting more spatial variability. The analysis was carried out with the two independent surface property datasets (land surface temperature and soil moisture) and gave very consistent results; in summary, storm initiations are favoured over the warmer and drier surfaces. The analysis of local atmospheric profiles showed that storm initiations are triggered in very disparate mean atmospheric and surface conditions (in terms of CAPE,CIN, mean humidity), but involves strong couplings between the surface and the atmospheric mean properties.

In a second step, the links between surface properties and storm initiations were investigated at finer scale (on order of few tens of km) with LSTA estimates. Gradients of temperature were computed at each initiation point as well as in the environment of storm initiation. The results indicate that storm initiations are more frequent over zones presenting a strong negative gradient along the wind direction (compared to the environment). This corresponds to a warm to cold transition along the wind direction with the initiation located on the warm side of the transition. This study was further extended to a 4-year data set including more than 2000 storm initiations and the results were essentially similar. This provides observationally based evidence of an influence of mesoscale circulations induced by surface heterogeneities on the triggering of deep convection over the Sahel.

6.2 Outlook

Low level diurnal cycles: processes and modelling

Characterising is the first step before identifying the role of different processes involved in the climatology of diurnal cycles. Numerical modelling, when the model correctly simulate the diurnal cycle, can appear as an appropriate tool for analysing the role of the physical and dynamical process via the energy budgets. The analysis of daily simulation budgets when weakly biased could quantify the role of each processes involved in the observed diurnal cycles.

On the other hand, the diagnostics, which have been developed here, provide solid ground for testing and improving parameterisations. They should be helpful for the evaluation of large-scale models as well, e.g. in the context of the CMIP project involving the climate models of the IPCC AR5.

The modelling framework together with the diagnostics derived from observations should be useful for further studies, either focussing on basic process understanding or parameterisation issues. Indeed, one could perform similar simulations with a fine scale model instead of a 1D parameterised model. As a first step though, it appears necessary to assess more fully the initial and boundary conditions employed. Horizontal advection were shown to be underestimated prior to the monsoon onset in the Sahel. Such analyses should be carried out at the other sites as well in order to lead to more accurate estimations of advection.

In this PhD work, I concentrated mostly on daytime hours, and the model usually drifted too much after 12h of simulation for an in-depth exploration of the nocturnal phase. However, It would be useful to assess more precisely the ability of the model to simulate the night-time hours. This could be simply carried out by starting simulations in the evening at 18h instead of in the early morning at 6h.

Finally, as mentioned above, preliminary comparisons of the 1D simulations performed here with the more complex 2D parameterised simulations of Peyrillé and Lafore (2007) suggest some similarities in the biases of the model with respect to the diurnal cycle. It would be useful to more fully explore this issue. In particular, it would be valuable to assess whether changes in the features of the simulated diurnal cycle are associated with changes in the large-scale features of the WAM, for instance, the position of the ITD, the strength of the monsoon flow, the amount and location of the ITCZ.

Triggering mechanism of deep convection

Numerous mechanisms can lead to the triggering of deep convection such as topography or surface heterogeneities induced circulations, tropospheric gravity waves or density current generated by convective systems. My thesis work suggests the importance of mesoscale circulations induced by surface temperature heterogeneities on the storm triggering over the Sahel. However, these hypotheses are mainly based on surface property considerations. Hence, an interesting outlook aspect would be to study the spatial variability of precipitable water associated with convective triggering over strong temperature gradients and analyse whether or not there is coherences with the surface structures. Several estimates of precipitable water are available (e.g. MODIS, IASI). In the literature, some studies stress the interesting potential of this products (ie Li et al., 2003, Couvreux et al., 2009) However, there is a need to first evaluate these products against local measurements for example against GPS measurements of precipitable water which have a good accuracy. The soil moisture estimate ASAR could be evaluated against LST-MSG estimates in order to precise the relationship between soil moisture, surface temperature and surface temperature gradients. Therefore, the spatial variability of precipitable water and its correlation with surface structures could be studied using a methodology close to the one used in my thesis work. One can expect opposite fluctuations of these fields (warm and dry versus cool and humid). Nevertheless, they should be affected by the low-level advection of moisture. Moreover, a similar study on triggering mechanism would be interesting to use ASAR fine scale soil moisture estimates with the convective initiations where there is no LST data due to the presence of cloud.

Another interesting aspect could be to explore the links between small convective systems triggered over the Sahel and surface properties. Indeed, these smaller convective systems are not retained in the tracking algorithm but they are likely to play a role in the vertical redistribution of water between the low levels and the troposphere above, and therefore to affect the water cycle associated with the WAM system.

Modelling of convection initiation

The large number of initiation cases provides a unique dataset to evaluate the capacity of models to trigger convection in different atmospheric conditions. The approach developed above allow a systematic evaluation the convective initiation simulated in the models. It would be possible to use the modelling framework developed during my thesis to simulate individually the different observed cases of initiation as documented with all the surface and atmospheric datasets. It could consist in analysing the capacity of the model to simulate the initiation of convection, and see whether it is synchronous with the observations. The atmospheric initial conditions and the advection could be extracted from the AMMA reanalyses from ECMWF. The surface properties could be taken from ALMIP (Boone et al., 2009) as was done during my thesis work. On this basis, model performances could be analysed according to:

- atmospheric regimes (stable versus instable and dry versus humid)
- surface mesoscale variability

This would allow in particular to see whether the model has noticeable difficulties to trigger convection in specific conditions, like when surface heterogeneities are strong.

References

Abdou et al. (2010): The diurnal cycle of lower boundary layer wind in the West African monsoon, *Quart. J. Roy. Meteor. Soc.,* 136, 66–76.

Agusti-Panareda, A. A.Beljaars, M. Ahlgrimm, G. Balsamo, O. Bock, R. Forbes, A. Ghelli, F. Guichard, M. Kohler, R. Meynadier and J.-J. Morcrette (2010): The ECMWF re-analysis for the AMMA observational campaign. *Quart. J. Roy. Meteor. Soc*., 136, 1457 – 1472

Agusti-Panareda et al (2009): Radiosounde humidity bias correction over the West African region for the special AMMA reanalysis at ECMWF, *Quart. J. Roy. Meteor. Soc,*. 135, 595-617

Ali and Lebel (2009): The Sahelian standardized rainfall index revisited, *Int. J. Climatol.,* 29, 1705–1714.

Anthes (1984): Enhancement of convective precipitation by mesoscale variations in vegetative covering in semiarid regions. *J. Climate Appl. Meteor.,* 54, 541–555.

Avissar and Liu (1996): 3-dimensional numerical study of shallow convective clouds and precipitation induced by land-surface forcing, *J. Geophys. Res. - Atmosphere*, 101, 7499-7518.

Bain, C. L., D. J. Parker, C. M. Taylor, L. Kergoat, and F. Guichard, 2010: Observations of the nocturnal boundary layer associated with the West African Monsoon*, Mon. Wea. Rev.*, 138,3142-3156

Bechtold et al. (1995) : Modeling of trade wind cumuli with a low-order turbulence model : toward a unified description of Cu and Sc clouds in meteorological models *, J. Atmos. Sci.*, vol. 52, no4, pp. 455-463

Bechtold, P., E. Bazile, F. Guichard, P. Mascart and E. Richard (2001): A Mass flux convection scheme for regional and global models, *Quart. J. Roy. Meteor. Soc.*, 127, 869-886.

Bechtold, P., J.-P. Chaboureau, A.Beljaars, A.K. Betts, M.Kolhler, M.Miller, and J.-L. Redelsperger (2004): The simulation of the diurnal cycle of convective precipitation over land in a global model, *Quart. J. Roy. Meteor. Soc.,* 130, 3319–3137.

Bergman, J.W. and M.L. Salby (1996): Diurnal variations of cloud cover and their relationship to climatological conditions., *J. Climate*, 9, 2802–2820.

Bergman, J. W. and M. L. Salby (1997): The role of cloud diurnal variations in the time-mean energy budget., *J. Climatol.,* 10, 1114–1124.

Betts AK, Ball JH, Beljaars ACM, et al. (1996): The land surface-atmosphere interaction: A review based on observational and global modeling perspectives, *J. Geophys. Res. - Atmosphere*, 101(D3) ,7209-7225.

Betts, A. K. and C. Jakob (2002a): Evaluation of the diurnal cycle of precipitation, surface thermodynamics, and surface fluxes in the ECMWF model using LBA data, *J. Geophys. Res. - Atmosphere*., 107D, 8045.

Betts, A.K. and C. Jakob (2002b): Study of the diurnal cycle of convective precipitation over Amazonia using a single column model., *J. Geophys. Res.,* 107

Betts, A. K., and J. H. Ball (1998): FIFE surface climate and site-average dataset 1987-89, *J. Atmos. Sci.*, 55, 1091-1108.

Bindlish, R., T. J. Jackson, E. Wood, H. L. Gao, P. Starks, D. Bosch, and V. Lakshmi (2003): Soil moisture estimates from TRMM Microwave Imager observations over the Southern United States, *Remote Sens. Environ.*, 85, 507-515.

Blackadar, A. K. (1962): The Vertical Distribution of Wind and Turbulent Exchange in a Neutral Atmosphere*, J. Geophys. Res*., 67(8), 3095–3102, doi:10.1029/JZ067i008p03095.

Blanca, E., P. Quiriona, and E. Strobl (2008): The climatic determinants of cotton yields: Evidence from a plot in west africa, *Agricultural and Forest Meteorology,* 148, 1093–1100.

Bock, O., M.N. Bouin, E. Doerflinger, P. Collard, F. Masson, R. Meynadier, S. Nahmani, M. Koité, K. Gaptia Lawan Balawan, F. Didé, D. Ouedraogo, S. Pokperlaar, J.-B. Ngamini, J.P. Lafore, S. Janicot, F. Guichard, and M. Nuret, (2008): The West African Monsoon observed with ground-based GPS receivers during AMMA*, J. Geophys. Res*., 113, D21105

Boone, A., J.-C. Calvet and J. Noilhan (1999)**:** The inclusion of a third soil layer in a Land Surface Scheme using the Force-Restore method., *J. of Appl. Meteor.*, 38, 1611-1630.

Boone, A. and de Rosnay, P. (2007): AMMA forcing data for a better understanding of the West African monsoon surface-atmosphere interactions. Quantification and Reduction of Predictive Uncertainty for Sustainable Water Resource Management, *IAHS Publ.,* 313, 231-241.

Boone, A. and P. de Rosnay (2007): Towards the improved understanding of land-surface processes and coupling with the atmosphere over West Africa, *iLEAPS Newletter*, 3, 33-34.

Boone, A., P. de Rosnay, G. Basalmo, A. Beljaars, F. Chopin, B. Decharme, C. Delire, A. Ducharne, S. Gascoin, M. Grippa, F. Guichard, Y. Gusev, P. Harris, L. Jarlan, L. Kergoat, E. Mougin, O. Nasonova, A. Norgaard, T. Orgeval, C. Ottlé, I. Poccard-Leclercq, J. Polcher, I. Sandholt, S. Saux-Picart, C. Taylor, and Y. Xue, (2009): The AMMA Land Surface Model Intercomparison Project, *Bull. Amer. Meteor. Soc.*, 90(12), 1865-1880, doi:10.1175/2009BAMS2786.1

Bougeault and Laccarrere (1989): Parameterization of orography-induced turbulence in a mesobeta-scale model, Monthly weather review 117, pp1872-1890.

Braganza, K., D. J. Karoly, and J. M. Arblaster (2004): Diurnal temperature range as an index of global climate change during the twentieth century, *Geophys. Res. Lett.*, 31, L13217, Doi: 10.1029/2004GL019998.

Burpee, R.W. (1974): Characteristics of North African Easterly Waves During the Summers of 1968 and 1969, *Journal of Atmospheric Sciences*, 31, Issue 6, pp.1556-1570

Burpee, R. W. (1972): The origin and structure of easterly waves in the lower troposphere of North Africa, *J. Atmos. Sci,* 29, 77–90.

Caminade, C. and L. Terray (2006): Influence of increased greenhouse gases and sulphate aerosols concentration upon diurnal temperature range over africa at the end of the 20th century, *Geophys. Res. Lett,* 33.

Caniaux, G., J.-L. Redelsperger and J.-P. Lafore (1994): A numerical study of the stratiform region of a fast-moving squall line. Part I. General description, and water and heat budgets, *J. Atmos. Sci,* 51, 2046-2074.

Caniaux et al., (2010): Link between the onset of the Atlantic cold tongue and the West African monsoon, Geophysical Research abstracts Vol. 12, EGU2010-1789.

Canut, G., M. Lothon, F. Saïd, and F. Lohou (2010): Observation of entrainment at the interface between monsoon flow and the saharan air layer, *Quart. J. Roy. Meteor. Soc.* , 136, 34–46.

Carleton, A. M., J. Adegoke, J. Allard, D. L. Arnold, and D. J. Travis (2001): Summer season land cover - convective cloud associations for the Midwest US "Corn Belt", *Geophys. Res. Lett.*, 28, 1679-1682.

Caselles V., E. Valor, C. Coll and E. Rubio (1997): Thermal band selection for the PRISM instrument 1.Analysis of emissivity-temperature separation algorithms, J. Geophs. Res., 102, D10, 11145-11164.

Chaboureau, J.-P., P. Tulet, and C. Mari, 2007: Diurnal cycle of dust and cirrus over West Africa as seen from Meteosat Second Generation satellite and a regional forecast model. *Geophys. Res. Lett*., 34, L02822, doi:10.1029/2006GL027771.

Charney, J. G. (1975): Dynamics of deserts and drought in the Sahel. *Quart. J. Roy. Meteor. Soc.,* 101, 193–202.

Chen, F., R. Avissar (1994): Impact of Land-Surface Moisture Variability on Local Shallow Convective Cumulus and Precipitation in Large-Scale Models. *J. Appl. Meteor.*, 33, 1382–1401.

Cheng, W. Y. Y., W. R. Cotton, (2004): Sensitivity of a Cloud-Resolving Simulation of the Genesis of a Mesoscale Convective System to Horizontal Heterogeneities in Soil Moisture Initialization. *J. Hydrometeor*, 5, 934–958.

Comer, R., A. Slingo, and R. Allan (2007): Observations of the diurnal cycle of outgoing longwave radiation from the geostationary earth radiation budget instrument, *Geophys. Res. Lett, 34,* L02823, doi:10.1029/2006GL028229.

Cook K.H. and K. Vizy (2006): Coupled Model Simulations of the West African Monsoon System: Twentieth- and Twenty-First-Century Simulations, Journal of Climate, 19, 3681-3704.

Couvreux, F., F. Guichard, J.-L. Redelsperger, and V. Masson, 2007: Negative water vapour skewness and dry tongues in the convective boundary layer: observations and LES budget analysis. Boundary-Layer Meteorol., 23, 269–294.

Couvreux, F., F. Guichard, P. H. Austin, F. Chen (2009): Nature of the Mesoscale Boundary Layer Height and Water Vapor Variability Observed 14 June 2002 during the IHOP_2002 Campaign. Mon. Wea. Rev., 137, 414–432, doi: 10.1175/2008MWR2367.1

Couvreux, F., F. Guichard, O. Bock, B. Campistron, J.-P. Lafore, and J.-L. Redelsperger (2010): Synoptic variability of the monsoon flux over West Africa prior to the onset. *Quart. J. Roy. Metor, 136*, 159–173.

Culf, A. D., (1992): An application of simple models to Sahelian convective boundary-layer growth. Bound.-Layer Meteor., 58:1–18.

Cuesta, J., et al. (2008), Multiplatform observations of the seasonal evolution of the Saharan atmospheric boundary layer in Tamanrasset, Algeria, in the framework of the African Monsoon Multidisciplinary Analysis field campaign conducted in 2006, J. Geophys. Res., 113, D00C07, doi:10.1029/2007JD009417.

Cuesta, J., Marsham, JH, Parker, DJ, Flamant, C (2009): Dynamical mechanisms controlling the vertical redistribution of dust and the thermodynamic structure of the West Saharan atmospheric boundary layer during summer *, Atmos. Sci. Lett*., 10, 34-42. doi:10.1002/asl.207

Cuxart, J., Bougeault, Ph. and Redelsperger, J.L., (2000): A turbulence scheme allowing for mesoscale and large-eddy simulations, *Quart. J. Roy. Meteor. Soc.,* 126, 1-30.

Dai, A. (2001): Global precipitation and thunderstorm frequencies. Part II: diurnal variations, *J. Climate,* 14, 1112–1128.

Dai, A., F. Giorgi, and K. E. Trenberth (1999): Observed and model simulated precipitation diurnal cycle over the contiguous United States, *J. Geophys. Res.*, 104, 6377–6402.

Dai, A. and K. E. Trenberth (2004): The diurnal cycle and its depiction in the community climate system model, *J. Climate,* 17, 930–951.

Deardorff, J. (1970). A numerical study of three-dimensional turbulent channel flow at large Reynolds numbers, *Journal of Fluid Mechanics*, 41(2), 453-480

De Arellan, J. V.-G. (2007): Role of nocturnal turbulence and advection in the formation of shallow cumulus over land, *Quart. J. Roy. Meteor. Soc.*, 133, 1615–1627.

Déqué M., C Dreveton, A Braun and D Cariolle (1994): The ARPEGE/IFS atmosphere model: a contribution to the French community climate modelling, *Climate Dynamics*, 10, 4-5, 249-266, DOI: 10.1007/BF00208992

D'Odorico and Porporato (2004): Preferential states in soil moisture and climate dynamics, *PNAS*, 101, 24, 8848–8851.

Dolman, A. J., A. D. Culfb, and P. Bessemoulin (1997): Observations of boundary layer development during the hapex-sahel intensive observation period, *Journal of Hydrology,* 188-189, 998–1016.

Douville, H. and F. Chauvin, 2000: Relevance of soil moisture for seasonal climate predictions: a preliminary study. Climate Dyn, 16:719–736.

Douville, H., F. Chauvin, and H. Broqua (2001): Influence of soil moisture on the Asian and African monsoons. Part I: Mean monsoon and daily precipitation, *J. Climate,* 14, 2381–2403.

Drobinski, P., B. Sultan, and S. Janicot (2005): Role of the Hoggar massif in the West African monsoon onset, *Geophys. Res. Let.,* 32*,* L01705, doi:10.1029/2004GL020710 .

Durand, P., J. Frangi, and A. Druilhet (1988): Energy budget for the sahel surface layer during the eclats experiment, *Boundary-Layer Meteorol.,* 42, 27–42.

Drusch, M., and P. Viterbo, 2007: Assimilation of Screen-Level Variables in ECMWF's Integrated Forecast System: A Study on the Impact on the Forecast Quality and Analyzed Soil Moisture. Mon. Wea. Rev., 135, 300–314

Duvel, J.-P. (1989): Convection over tropical Africa and the Atlantic Ocean during northern summer. Part I: Interannual and diurnal variations, *Mon. Weather Rev.*, 117**,** 2782–2799

Ek, M., and L. Mahrt (1994): Daytime evolution of relative humidity at the boundary layer top, *Mon. Weather Rev.*, 122, 2709-2721.

Eltahir, E. A. B. and C. Gong (1996): Dynamics of wet and dry years in West Africa, *J. Climate* , 9, 1030–1042.

Easterling D. R. et al. (1997): Maximum and Minimum Temperature Trends for the Globe, *Science,* 18 , 277, 5324, 364- 367, doi: 10.1126/science.277.5324.364

Ferraro, R. R., E. A. Smith, W. Berg, and G. J. Huffman (1998): A screening methodology for passive microwave precipitation retrieval algorithms, *J. Atmos. Sci.*, 55, 1583-1600.

Findell, K. L., and E. A. B. Eltahir (2003): Atmospheric controls on soil moisture-boundary layer interactions. Part I: Framework development, *J. Hydromet.*, 4, 552-569.

Fink, A. H., D. G. Vincent, V. Ermert (2006): Rainfall Types in the West African Sudanian Zone during the Summer Monsoon 2002, *Mon. Wea. Rev.*, 134, 2143–2164.

Fisch, G., J. Tota, L. A. T. Machado, M. A. F. S. Dias, R. F. da F. Lyra, C. A. Nobre, A. J. Dolman, and J. H. C. Gash (2004): The convective boundary layer over pasture and forest in amazonia, *Theor. Appl. Climatol.,* 78, 4759.

Flamant C., J.-P. Chaboureau, D. J. Parker, C. M. Taylor, J.-P. Cammas, O. Bock, F. Timouk, J. Pelon (2007): Airborne observations of the impact of a convective system on the planetary boundary layer thermodynamics and aerosol distribution in the inter-tropical discontinuity region of the West African Monsoon, . *Quart. J. Roy. Meteor. Soc.*, 133, 626, 1175–1189.

Flaounas, E., S. Bastin, and S. Janicot (2010): Regional climate modelling of the 2006 west african monsoon: sensitivity to physics schemes using, wrf. *Clim. Dyn.,* in press.

Frappart, F., P. Hiernaux, F. Guichard, E. Mougin, L. Kergoat, A. M., F. Lavenu, M. Koité, P. J.E., and T. Lebel (2009): Rainfall regimes across the sahel band in the gourma region, mali, *Journal of Hydrology* , *375*, 128–142.

Garcia-Carreras, Parker, Taylor, Reeves, Murphy (2010): Impact of mesoscale vegetation heterogeneities on the dynamical and thermodynic properties of the planetary boundary layer, Journal of Geophysical Research, VOL 15.

Garrat, J.R, 1992: The Atmospheric Boundary Layer, *Cambridge University Press*, Cambridge, UK, 316.

Garratt, J.R, 1994: THE ATMOSPHERIC BOUNDARY-LAYER – REVIEW. EARTH-SCIENCE REVIEWS. 37, 89-134.

Gash, J. H. C., P. Kabat, B. A. Monteny, M. Amadou, P. Bessemoulin, H. Billing, E. M. Blyth, H. A. R. de Bruin, J. A. Elbers, T. Friborg, G. Harrison, C. J. Holwill, C. R. Lloyd, J. P. Lhomme, J. B. Moncrieff, D. Giannini, A., M. Biasutti, and V. M. (2008): A climate model-based review of drought in the sahel: Desertificatio, the re-greening and climate change, *Global and Planetary Change,* .

Giannini A., R.Saravanan R, and P. Chang P, 2003: Oceanic forcing of Sahel rainfall on interannual to interdecadal time scales . *Science,* 302 , 1027-1030

Gong, C.L., and E. A. ELtahir, 1996: Sources of moisture for rainfall in west Africa. Water Resour. Res., 32, 3115-3121.

Goutorbe, J.-P., T. Lebel, A. Tinga, P. Bessemoulin, J. Brouwer, A. Dolman, E. Engman, J. Gash, M. Hoepffner, P. Kabat, Y. Kerr, B. Monteny, S. Prince, F. Said, P. Sellers, and J. Wallace (1994): Hapex-sahel: a large-scale study of land-atmosphere interactions in the semi-arid tropics, *Annales Geophysicae,* 12, 53–64.

Grodsky, S. A. and J. A. Carton (2001): Coupled land/atmosphere interactions in the West African monsoon, *Geophys. Res. Lett.,* 28, 1503–1506.

Gruhier et al. (2008): Evaluation of AMSR-E soil moisture product based on ground measurements over temperate and semi-arid regions, *Geophys. Res. Lett.,* 35, L10405.

Gruhier et al. (2010): Soil moisture active and passive microwave products: Intercomparison and evaluation over a Sahelian site, *Hydrol. and Earth Syst. Sci.*, 14, 141-156.

Guichard, F. et al. (2004): Modeling the diurnal cycle of deep precipitating convection over land with cloud-resolving models and single-column models, *Quart. J. Roy. Meteor. Soc.*, 130, 3139–3172.

Guichard, F.; Couvreux, F.; Nuret, M.; Agusti-Panareda, A. (2008): Roles of low-level thermodynamics on surface-convection interactions over West-Africa, *EGU abstract*.

Guichard, F., L. Kergoat, E. Mougin, F. Timouk, F. Baup, P. Hiernaux, and F. Lavenu (2009): Surface thermodynamics and radiative budget in the sahelian gourma: Seasonal and diurnal cycles, *Journal of Hydrology*, 375, 161–177.

Hall, N. M. J., G. N. Kiladis, and C. D. Thorncroft (2006): Three-dimensional structure and dynamics of African easterly waves. Part II: Dynamical modes. *J. Atmos. Sci.*, 63,2231–2245.

Hastenrath, S., Climate dynamics of the tropics, 488 pp., Kluwer Eds, New York, 1995.

van Heerwaarden, C.C., J. Vila-Guerau de Arellano, A. Gounou, F. Guichard, and F. Couvreux, 2010: Understanding the daily cycle of surface evapotranspiration: a new method to quantify the influence of forcings and feedbacks. J Hydromet., doi:10.1175/2010JHM1272.1

Hourdin F., Couvreux F and L. Menut (2002): Parameterization of the Dry Convective Boundary Layer Based on a Mass Flux Representation of Thermals, *J. Atmos. Sci.*, 59, 1105-1124.

Hourdin, F., I. Musat, F. Guichard, P. M. Ruti, F. Favot, M.-A. Filiberti, M. Pham, J.-Y. Grandpeix, J. Polcher, P. Marquet, A. Boone, J.-P. Lafore, J.-L. Redelsperger, A. Dell'Aquila, T. L. Doval, A. K. Traore, and H. Gallée (2010): AMMA-Model Intercomparison Project, *Bull. Amer. Meteor. Soc.*, 91(1), 95–104.

Houze R. A. (2004): Mesoscale convective systems. Rev. Geophys., 42, RG4003

Huang Yan, Robert E. Dickinson, and William L. Chameides (2006): Impact of aerosol indirect effect on surface temperature over East Asia, *PNAS*, 103, 12, 4371–4376.

Hulme, M., 1992: Rainfall changes in Africa: 1931-1960 to 1961-1990. Int. J. Climatol., 12, 685–699.

IPCC Fourth Assessment Report of the Intergovernmental Panel on Climate Change. Climate Change 2007: The Physical Science Basis, Solomon, S., D. Qin, M. Manning, Z. Chen, M. Marquis, K.B. Averyt, M. Tignor and H.L. Miller (eds.). Cambridge University Press, Cambridge, United Kingdom and New York, NY, USA, 996 pp.

Jackson, T. J. (1993): Measuring Surface Soil-Moisture Using Passive Microwave Remote-Sensing .3, *Hydrol. Proc.*, 7, 139-152.

Janicot, S. (1992). Spatiotemporal variability of West African rainfall. Part I: Regionalizations and typings. *J. Climate 5*, 489–497.

Janicot et al.(2008): Large-scale overview of the summer monsoon over WEst Africa during the AMMA field experiment in 2006. Ann. Geophys., 26, 2569-2595.

Kain, J. S., and J. M. Fritsch. 1990: A one-dimensional entraining/detraining plume model and its application in convective parameterization. J. Atmos. Sci., 47, 2784–2802

Kalapureddy, M. C. R., M. Lothon, Campistron, F. Lohou, and F. SaÂ¨Ä±d (2010): Wind profiler analysis of the african easterly jet in relation with the boundary layer and the saharan heat-low. *Quart. J. Roy. Meteor. Soc.*, 136, 77-91.

Karl, T. R., K. G., and G. J. (1984): Decreasing diurnal temperature range in the united states and canada from 1941 through 1980. *J. Climate Appl. Meteor.,* 23, 1489–1504.

Karoly D.J. and K. Braganza (2005): Attribution of Recent Temperature Changes in the Australian Region, Journal of Climate, 18, 347-355.

Kohler, M., N. Kalthoff, and C. Kottmeier (2010): The impact of soil moisture modifications on cbl characteristics in west africa: A case-study from the amma campaign. *Quart. J. Roy. Meteor.,* 442 – 455.

Koster, R. D., P. A. Dirmeyer, Z. C. Guo, G. Bonan, E. Chan, P. Cox, C. T. Gordon, S. Kanae, E. Kowalczyk, D. Lawrence, P. Liu, C. H. Lu, S. Malyshev, B. McAvaney, K. Mitchell, D. Mocko, T. Oki, K. Oleson, A. Pitman, Y. C. Sud, C. M. Taylor, D. Verseghy, R. Vasic, Y. K. Xue, and T. Yamada (2004): Regions of strong coupling between soil moisture and precipitation, *Science*, 305, 1138-1140.

Kummerow, C., W. Barnes, T. Kozu, J. Shiue, and J. Simpson (1998): The Tropical Rainfall Measuring Mission (TRMM) sensor package, *J. Atmos. Oceanic Technol.*, 15, 809-817.

Lafore, J. P., J. Stein, N. Asencio, P. Bougeault, V. Ducrocq, J. Duron, C. Fischer, P. Hereil, P. Mascart, J. P. Pinty, J. L. Redelsperger, E. Richard, and J. Vila-Guerau de Arellano (1998): The Meso-NH Atmospheric Simulation System. Part I: Adiabatic formulation and control simulations, *Annales Geophysicae*, 16, 90-109.

Lafore, J.-P. and M. W. Moncrieff (1989): A numerical investigation of the organization and interaction of the convective and stratiform regions of tropical squall lines, *J. Atmos. Sci.*, 46, 521–544.

Laing, A. G. and J. M. Fritsch (1993): Mesoscale convective complex in Africa, *Mon. Wea. Rev.,* 121, 2254–2263.

Lin, X., Randall, D. A. and Fowler, L. D. (2000): Diurnal variability of the hydrologic cycle and radiative fluxes: Comparisons between observations and a GCM, *J. Climate*, 13**,** 4159–4179

Le Barbé, L., T. Lebel, and D. Tapsoba (2002): Rainfall variability in West Africa during the years 1950–90. *J. Climate*, 15, 187–202.

Lebel (1995): Hydrologie et météorologie de méso-échelle dans Hapex-Sahel, ORSTOM éditions

Lebel, T., D. J. Parker, C. Flamant, B. BourlÃ¨s, B. Marticorena, E. Mougin, C. Peugeot, A. Diedhiou, J. M. Haywood, J. B. Ngamini, J. Polcher, J.-L. Redelsperger, and C. D. Thorncroft (2010): The amma field campaigns: multiscale and multidisciplinary observations in the west african region, *Quart. J. Roy. Meteor.,*136, 8–33.

Leroux, S., N. M. J. Hall (2009): On the Relationship between African Easterly Waves and the African Easterly Jet, *J. Atmos. Sci.*, 66, 2303–2316.

Li , Z. H., J. P. Muller, and P. Cross (2003): Comparison of precipitable water vapor derived from radiosonde, GPS, and Moderate-Resolution Imaging Spectroradiometer measurements. J. Geophys. REs., 108D, 4651.

Lothon, M., F. Said, F. Lohou, and B. Campistron (2008): Observation of the diurnal cycle in the low troposphere of West Africa, *Mon. Wea. Rev.,* 136, 3477–3500.

Machado, L.A.T., Rossow, W.B., Guedes, R.L. and Walker, A.W. (1998): Life cycle variations of mesoscale convective systems over the Americas, *Mon. Weath. Rev.,* 126, 1630-54

Mahfouf, J.-F., R. E., and M. P. (1987): The influence of soil and vegetation of mesoscale circulations, *J. Climate Appl. Meteor.*, 26, 1483–1496.

Malkus, J. S., 1963: Tropical rain induced by a small heat source. J. Appl. Meteor., 2:547–556.

Mann, H. B. and D. R. Whitney. 1947. On a test of whether one of 2 random variables is stochastically larger than the other. Ann. Math. Stat. 18:50–60.

Masson V., J.-L. Champeaux, F. Chauvin, C. Meriguet and R. Lacaze, (2003): A global database of land surface parameters at 1km resolution in meteorological and climate models, *J. Climate*, 16, 1261-1282.

Mathon, V., H. Laurent, and T. Lebel (2002): Mesoscale convective system rainfall in the Sahel, *J. Appl. Meteorol.*, 41, 1081-1092.

Mathon, V. and H. Laurent (2001): Life cycle of sahelian mesoscale convective cloud systems. *Quart. J. Roy. Meteor. Soc. 127*, 377–406.

Matthews, A. J. (2004): Intraseasonal variability over tropical Africa during northern summer. *J. Climate*, 17, 2427–2440.

McFarlane SA, EI Kassianov, JC Barnard, CJ Flynn, and TP Ackerman (2009): Surface shortwave aerosol radiative forcing during the Atmospheric Radiation Measurement Mobile Facility deployment in Niamey, Niger, *Journal of Geophysical Research. D. (Atmospheres)*, 114, D00E06, doi:10.1029/2008JD010491

Messager, C., D. J. Parker, O. Reitebuch, A. Agusti-Panareda, C. M. Taylor, and J. Cuesta (2010): Structure and dynamics of the Saharan atmospheric boundary layer during the West African monsoon onset: observations and analyses from research flights of 14 and 17 July 2006. *Quart. J. Roy. Meteor. Soc,* 136(s1), 107–124.

Meynadier, R., O. Bock, S. Gervois, F. Guichard, J.-L. Redelsperger, A. Agusti-Panareda, and A. Beljaars, 2010b: The West African Monsoon water cycle. Part II: assessment of NWP water budgets. J. Geophys. Res., 115, D,19107.

Miller and Slingo, (2007): The ARM mobile facility and its first international deployment, *BAMS*,1229-1244.

Mlawer, E.J., S.J. Taubman, P.D. Brown, M.J. Iacono, and S.A. CLough, (1997): Radiative transfer for inhomogeneous atmospheres: RRTM, a validated correlated-k model for the longwave, *J. Geophys. Res.*, 102D, 16663-16682.

Mohr, K. I., (2004): Interannual, Monthly, and Regional Variability in the Wet Season Diurnal Cycle of Precipitation in Sub-Saharan Africa, *J. Climate*, 17, 2441–2453.

Morel, C., and S. Senesi, 2002: A climatology of mesoscale convective systems over Europe using satellite infrared imagery. I: Methodology. Quart. J. Roy. Meteor. Soc., 128, 1953-1971.

Mougin, E., and coauthors, (2009): The AMMA-CATCH Gourma observatory site in Mali: Relating climatic variations to changes in vegetation, surface hydrology, fluxes and natural resources, *J. Hydrol.*, 375, 14-33.

Morcrette, J.-J., (1991): Radiation and cloud radiative properties in the European center for medium range weather forecasts forecasting system, *J. Geophys. Res*., 96, 9121-9132.

Negri, A. J., R. F. Adler, L. M. Xu, and J. Surratt (2004): The impact of Amazonian deforestation on dry season rainfall, *J. Climate,* 17, 1306-1319.

Nesbitt, S. W. and E. J. Zipser (2003): The diurnal cycle of rainfall and convective intensity according to three years of TRMM measurements. *J. Climate 16*, 1456–1475.

Nicholson, S. (1980): The nature of rainfall fluctuations in subtropical West Africa, *Mon. Wea. Rev.*, 108, 473–487.

Nicholson, S. E., A. I. Barcilon, M. Challa, and J. Baum (2007): Wave activity on the tropical easterly jet. *J. Atmos. Sci.*, 64, 2756–2763.

Noilhan, J., and S. Planton, (1989): A simple parameterization of land surface processes for meteorological models, *Mon. Wea. Rev*., 117, 536-549.

Noilhan, J. and J.-F. Mahfouf (1996): The ISBA land surface parameterization scheme, *Global and Planetary Change*, 13, 145-159.

Nuret et al. (2008): Correction of humidity bias for Vaïsala RS80 sondes during AMMA 2006 Observing Period, J. Atmos. Ocean. Tech., 25, 2152-2158.

Owe, M., R. De Jeu and T. Holmes, 2008: Multi-sensor historical climatology of satellite derived global land surface soil moisture, J. Geophys. Res., 113.

Parker, D. J., R. R. Burton, A. Diongue-Niang, R. J. Ellis, M. Felton, C. M. Taylor, C. D. Thorncroft, P. Bessemoulin, and A. M. Tompkins (2005): The diurnal cycle of the West African monsoon circulation, *Quart. J. Roy. Meteor. Soc,* 131, 2839–2860.

Parker, D. J., C. D. Thorncroft, R. R. Burton, and A. Diongue-Niang (2005): Analysis of the African easterly jet, using aircraft observations from the JET2000 experiment, *Quart. J. Roy. Meteor. Soc*, 131, 1461-1482.

Parker, D. J., A. Fink, S. Janicot, S., J.-B. Ngamini, M. Douglas, E. Afiesimama, A. Agusti-Panareda, A. Beljaars, F. Dide, A. Diedhiou, T. Lebel, J. Polcher, J.-L. Redelsperger, C. Thorncroft, and G. A. Wilson, 2008: The AMMA radiosonde program and its implications for the future of atmospheric monitoring over Africa. Bull. Amer. Meteor. Soc., 89, 1015-1027.

Peath H., Born K., Podzun R. and Jacob D. (2005): Regional dynamical downscaling over West Africa: model evaluation and comparison of wet and dry years, *Meteorologische Zeeitschrift*, 14, 3, 349-367.

Peath H. (2004): Key factors in African climate change evaluated by a regional climate model, *Erdkund*, 58, 290-315.

Pereira, L. and R. S.A. (2006): Diurnal cycle of shallow and deep convection for tropical land and an ocean environment and its relationship to synoptic wind regimes, *Mon. Wea.,* 134, 2688–2702.

Pergaud, J., V. Masson, S. Malardel, and F. Couvreux (2009): A parameterization of dry thermals and shallow cumuli for mesoscale numerical weather prediction, *Boundary- Layer Meteorol*., 132(1), 83-106.

Peyrillé P. 2005: Etude idéalisée de la mousson ouest-africaine à partir d'un modèle numérique bi-dimensionnel. PhD thesis, Université Toulouse III, France.

Peyrillé, P., J.-P. Lafore, and J.-L. Redelsperger (2007): A idealized two-dimensional framework to study the West African monsoon. Part I: Validation and key controlling factors, *J. Atmos. Sci.*, 64, 2765–2782.

Peyrillé P, Lafore J-P.(2007). An idealized two-dimensional framework to study the West African Monsoon. Part II: Large-scale advection and the diurnal cycle*. J. Atmos. Sci.* 64: 2783–2803.

Pielke RA, (2001): Influence of the spatial distribution of vegetation and soils on the prediction of cumulus convective rainfall, *reviews of geophysics*, 39, 151-177

Pino, D., J. Vilà-Guerau de Arellano, P. G. Duynkerke, 2003: The Contribution of Shear to the Evolution of a Convective Boundary Layer. J. Atmos. Sci., 60, 1913–1926.

Pinty, J.-P. and P. Jabouille, (1998): A mixed-phase cloud parameterization for use in mesoscale non-hydrostatic model: simulations of a squall line and of orographic precipitations, *Proc. Conf. of Cloud Physics, Everett, WA, USA, Amer. Meteor. soc.*, 217 - 220.

Pospichal, B. and S. Crewell (2007): Boundary layer observations in West Africa using a novel microwave radiometer, *Meteorologische Zeitung*.

Pospichal, Karam, Crewell, Flamant, Hunerbein, Bock and Said (2010): Diurnal cycle of the intertropical discountinuity over West Africa analysed by remote sensing and mesoscale modelling, Quart. J. Roy. Meteor. Soc., 136, 92-106.

Puech, H. Soegaard, J. D. Taupin, A. Tuzet, and A. Verhoef (1997): The variability of evaporation during the HAPEX-Sahel intensive observation period, *J. Hydrol.*, 189, 385-399.

Rabin, R. M., S. Stadler, P. J. Wetzel, D. J. Stensrud, and M. Gregory (1990): Observed effects of landscape variability on convective clouds, *Bull. Am. Meteorol. Soc.*, 71, 272-280.

Ramage, C. S. (1971): *Monsoon Meteorology*. New York and London: Academic Press.

Raman, M., J. Rao, V. Ratnam, M. Rajeevan, and al. (2009) : Characteristics of the tropical easterly jet: Long-term trends and theirs features during active and break monsoon phases, *J. Geophys. Res., 114.*

Ramel, R., H. Gallée, and C. Messager (2006): On the northward shift of the West African monsoon, *Clim. Dyn.*, 26(4), 429–440.

Randall, D., A. J., and C. T. (1985): Seasonal simulations of the planetary boundary layer and boundary layer stratocumulus clouds with a general circulation model, *J. Atmos. Sci.,* 42, 641–676.

Randall, D. A., Harshvardan, and D. A. Dazlich (1991): Diurnal variability of the hydrologic cycle in a general circulation model. *J. Atmos. Sci*., 48, 40–62.

Redelsperger, J.-L., C. D. Thorncroft, A. Diedhiou, T. Lebel, D. J. Parker, and J. Polcher (2006): African Monsoon Multidisciplinary Analysis: an international research project and field campaign. *Bull. Amer. Meteor. Soc*., 87, 1739–1746.

Rio, C. and F. Hourdin (2008): A thermal plume model for convective boundary layer: representation of cumulus clouds. *J. Atmos. Sci.*, 65, 407–425.

Royer, J.-F., Belamari, M.,Ceron, J.-P., Chaumat, L.,Gueremy, J.-F., Piriou, C., Redelsperger, J.-L., and Tyteca, S. (2000): Cloud Archive User Service (CLAUS), CNRM-*ENM final report (ENV4-CT96-0356)*, European Commission, Brussels, Belgium.

Samain, O., L. Kergoat, P. Hiernaux, F. Guichard, E. Mougin, F. Timouk and F. Lavenu, 2008: Analysis of the in-situ and MODIS albedo variability at the multiple time scales in the Sahel, J., Geophys. Res., 113, D14119.

Segal, M., R. Avissar, M. C. McCumber, and R. A. Pielke, 1988: Evaluation of vegetation effects on the generation and modification of mesoscale circulations. J. Atmos. Sci., 45:2268–2292.

Slingo, A., et al. (2006), Observations of the impact of a major Saharan dust storm on the atmospheric radiation balance, Geophys. Res. Lett., 33, L24817, doi:10.1029/2006GL027869.

Smagorinsky, J. (1963): General Circulation Experiments with the Primitive Equations, *Monthly Weather Review*, 91 (3), 99-164.

Steeneveld, G. J., B. J. H. V. de Wiel, and A. A. M. Holtslag (2007): Diagnostic equations for the stable boundary layer height: evaluation and dimensional analysis. *J. Appl. Meteor. Climatol.,* 46, 212–225.

Steeneveld, (2007): Understanding and Prediction of Stable Atmospheric Boundary Layers over Land. PhD thesis.

Stendel and Arpe, (1997): ECMWF Re-analysis project report series: Evaluation of the Hydrological cycle in reanalysis and observations.

Stone, D. and A. Weaver (2003): Factors contributing to diurnal temperature range trends in twentieth and twenty-first century simulations of the ccma coupled model, *Clim. Dyn.*, 20, 435–445.

Stone, D. A., and A. J. Weaver (2002), Daily maximum and minimum temperature trends in a climate model, Geophys. Res. Lett., 29(9), 1356, doi:10.1029/2001GL014556.

Strong, C., J. D. Fuentes, G. M., and A. K. Betts (2005): Daytime cycle of low-level clouds and the tropical convective boundary layer in southwestern amazonia, *J. Appl. Meteorol.*, 44, 1607–1619.

Stull, R. B. (1988): An introduction to boundary layer meteorology, *Springer*, 670., ISBN: 978-90-277-2769-5

Sultan, B., C. Baron, M. Dingkuhn, B. Sarr, and S. Janicot (2005): Agricultural impacts of large-scale variability of the west african monsoon. *Agricultural and Forest Meteorology*, 128, 93–110.

Sultan, B. and S. Janicot (2000): Abrupt shift of the ITCZ over West Africa and intra-seasonal variability. *Geophys. Res. Lett.,* 27, 3353–3356.

Sultan, B. and S. Janicot (2003): The West African monsoon dynamics. Part II: The “preonset” and “onset” of the summer monsoon, *J. Climate*, 16, 3407–3427.

Tanre, D., Geleyn, J.-F. and Slingo, J. M., (1984): First results of the introduction of an advanced aerosol-radiation interaction in the ECMWF low resolution global model, *Aerosols and Their Climatic Effects*, H.E. Gerber and A. Deepak, Eds., A. Deepak Publ., Hampton, Va., 133-177.

Taylor, C. M., and T. Lebel (1998): Observational evidence of persistent convective-scale rainfall patterns, *Mon. Weather Rev.*, 126*,* 1597-1607.

Taylor et al. (2003): Linking boundary-layer variability with convection: A case-study from JET2000, Quarterly Journal of the Royal Meteorological Society, 129, 2233-2253.

Taylor, C. M., and R. J. Ellis, (2006): Satellite detection of soil moisture impacts on convection at the mesoscale. Geophys. Res. Lett., 33, L03404

Taylor, C. M., Harris, P. P. and Parker, D. J. (2010), Impact of soil moisture on the development of a Sahelian mesoscale convective system: a case-study from the AMMA Special Observing Period. Quarterly Journal of the Royal Meteorological Society, 136: 456–470. doi: 10.1002/qj.465

Tegen, I., P. Hollrig, M. Chin, I. Fung, D. Jacob, and J. Penner, 1997: Contribution of different aerosol species to the global aerosol extinction optical thickness: Estimates from model results. J. Goephys. REs., 102, 2389523915.

Timouk et al. (2009): Response of surface energy balance to water regime and vegetation development in a Sahelian landscape, *Journal of Hydrology*, 375, 1-2, 30, 178-189

Tomasini, M., J-P. Lafore, C. Piriou, R. Roca, K. Ramage, H. Laurent, C. Morel et S. Senesi, 2006: Atlas on a climatology of West African mesoscale convective systems, AMMA-EU report Du2.1.3.a.

Tompkins et al. (2005): The African easterly jet in the ECMWF Integrated Forecast System: 4D-Var analysis, *Quart. J. Roy. Meteor. Soc*, 131, 611, 2861–2885.

Thorncroft, C. D. and M. Blackburn (1999): Maintenance of the African easterly jet. *Quart. J. Roy. Meteor. Soc.*, 125, 763–786.

Thorncroft, C. D., D. J. Parker, R. R. Burton, M. Diop, J. H. Ayers, H. Bariat, S. Devereau, A. Diongue, R. Dumelow, D. R. Kindred, N. M. Price, M. Saloum, C. M. Tayor, and A. M. Tompkins (2003): The JET2000 project: Aircraft observations of the African easterly jet and African easterly waves, *Bull. Amer. Meteor. Soc.*, 84, 337–351.

Thorpe, A. J. and Guymer, T. H. (1977): The nocturnal jet, *Quart. J. Roy. Meteor. Soc*, 103, 633–653, doi: 10.1002/qj.49710343809.

Trenberth, K. E., and D. J. Shea (2005): Relationships between precipitation and surface temperature, *Geophys. Res. Lett.*, 32, L14703, doi:10.1029/2005GL022760.

Trigo, I. F., I. T. Monteiro, F. Olesen, and E. Kabsch (2008), An assessment of remotely sensed land surface temperature, J. Geophys. Res., 113, D17108, doi:10.1029/2008JD010035.

Van Heerwaarden, Vil` -Guerau de Arellano, Gounou, Guichard and Couvreux (2010): Understanding the daily cycle of surface evapotranspiration: a new method to quantify the influence of forcings and feedbacks, Journal of Hydrology

Wai, M. M. K., E. A. Smith, P. Bessemoulin, A. D. Culfc, A. J. Dolmand, and T. Lebele (1997): Variability in boundary layer structure during hapex-sahel wet-dry season transition, *Journal of Hydrology*, 188-189, 965–997.

Wang, J., F. J. F. Chagnon, E. Williams, A. K. Betts, N. O. Renno, L. A. T. Machado, G. Bisht, R. Knox and R. L. Bras (2009), Impact of deforestation in the Amazon basin on cloud climatology. PNAS, www.pnas.org/cgi/doi/10.1073/pnas.0810156106.

Wan. Z., J. Dozier, (1996): A generalised split-window algorithm for retrieving land-surface temperature from space, *IEEE Trans. Geosci. Remote Sens.*, 34, 34, 892-905.

Watson, R. T., and the Core Writing Team, Eds., (2001): Climate Change 2001: Synthesis Report, *Cambridge University Press*, 398.

Weaver, C. (2004a): Coupling between large-scale atmospherique processes and mesoscale land-atmosphere interactions in the u.s. southern great plains during summer: Part i: Case studies, *Journal of Hydrometeorology*, 5, 1223–1246.

Weaver, C. (2004b): Coupling between large-scale atmospherique processes and mesoscale land-atmosphere interactions in the u.s. southern great plains during summer: Part ii: Mean impacts of the mesoscale, *Journal of Hydrometeorology*, 5, 1247–1258.

Wild, M. (2009): How well do ipcc-ar4/cmip3 climate models simulate global dimming/brightening and twentieth-century daytime and nighttime warming, *J. Geophys. Res.*, 114.

Williams, E., N. Renno, (1993): An Analysis of the Conditional Instability of the Tropical Atmosphere, *Mon. Wea. Rev.*, 121, 21–36.

D.Wilks (1997): Statistical methods in the atmospheric sciences, *Academic press isbn,* 0-12-751965-3.

Yang, C.-Y. and J. Slingo (2001): The diurnal cycle in the tropics, *Mon. Wea. Rev.*, 129, 784–801.

Yang, S. and E. Smith (2006): Mechanisms for diurnal variability of global tropical rainfall observed from trmm, *J. Climatol.*, 19, 5190–5226.

Zipser, E. J., Chuntao Liu, Daniel J. Cecil, Stephen W. Nesbitt, David P. Yorty, (2006): Where are the most intenses thunderstorms on earth?, *Bull. Amer. Meteor. Soc.*, 87, 1057–1071.

Zhang, C., P. Woodworth, and G. Gu (2006): The seasonal cycle in the lower troposphere over West Africa from sounding observations. *Quart. J. Roy. Meteor. Soc.,* 132, 2259–2582.

Zheng, X. and E. A. B. Eltahir (1998): The role of vegetation in the dynamics of West African monsoons, *J. Climate*, 11, 2078–2096.

Zhu, P. and A. B. (2002): A theoretical and observational analysis on the formation of fair-weather cumuli, *J. Atmos. Sci.*, 59, 1983–2006.

Appendix A:

Understanding the daily cycle of evapotranspiration: a method to quantify the influence of forcings and feedbacks

Chiel C. van Heerwaarden[1] **and Jordi Vilà-Guerau de Arellano**[1]
Amanda Gounou [2]**, Françoise Guichard**[2] **and Fleur Couvreux**[2]

[1] Meteorology and Air Quality Section, Wageningen University, The Netherlands

[2] CNRM-GAME, Météo-France and CNRS, Toulouse, France

Journal of Hydrometeorology, **11**, 1405–1422.

Abstract

A method to analyze the daily cycle of evapotranspiration over land is presented. It quantifies the influence of external forcings, such as radiation and advection, and of internal feedbacks induced by boundary-layer, surface-layer and land surface processes on evapotranspiration. It consists of a budget equation for evapotranspiration that is derived by combining a time derivative of the Penman-Monteith equation with a mixed-layer model for the convective boundary-layer.

Measurements and model results of days in two contrasting locations are analyzed using the method: mid-latitudes (Cabauw, The Netherlands) and semi-arid (Niamey, Niger). The analysis shows that the time evolution of evapotranspiration is a complex interplay of forcings and feedbacks. Although evapotranspiration is initiated by radiation, it is significantly regulated by the atmospheric boundary-layer and the land surface throughout the day. Boundary-layer feedbacks enhance in both cases the evapotranspiration up to 20 W m^{-2} h^{-1}. However, in the case of Niamey this is offset by the land surface feedbacks, since the soil drying reaches −30 W m^{-2} h^{-1}. Remarkably, surface-layer feedbacks are of negligible importance in a fully coupled system.

Analysis of the boundary-layer feedbacks hints the existence of two regimes in this feedback depending on atmospheric temperature, with a gradual transition region in between the two. In the low-temperature regime specific humidity variations induced by evapotran-spiration and dry-air entrainment have a strong impact on the evapotranspiration. In the high-temperature regime the impact of humidity variations is less pronounced and the effects of boundary-layer feedbacks are mostly determined by temperature variations.

Appendix B: Atmospheric contexts of the SOPs

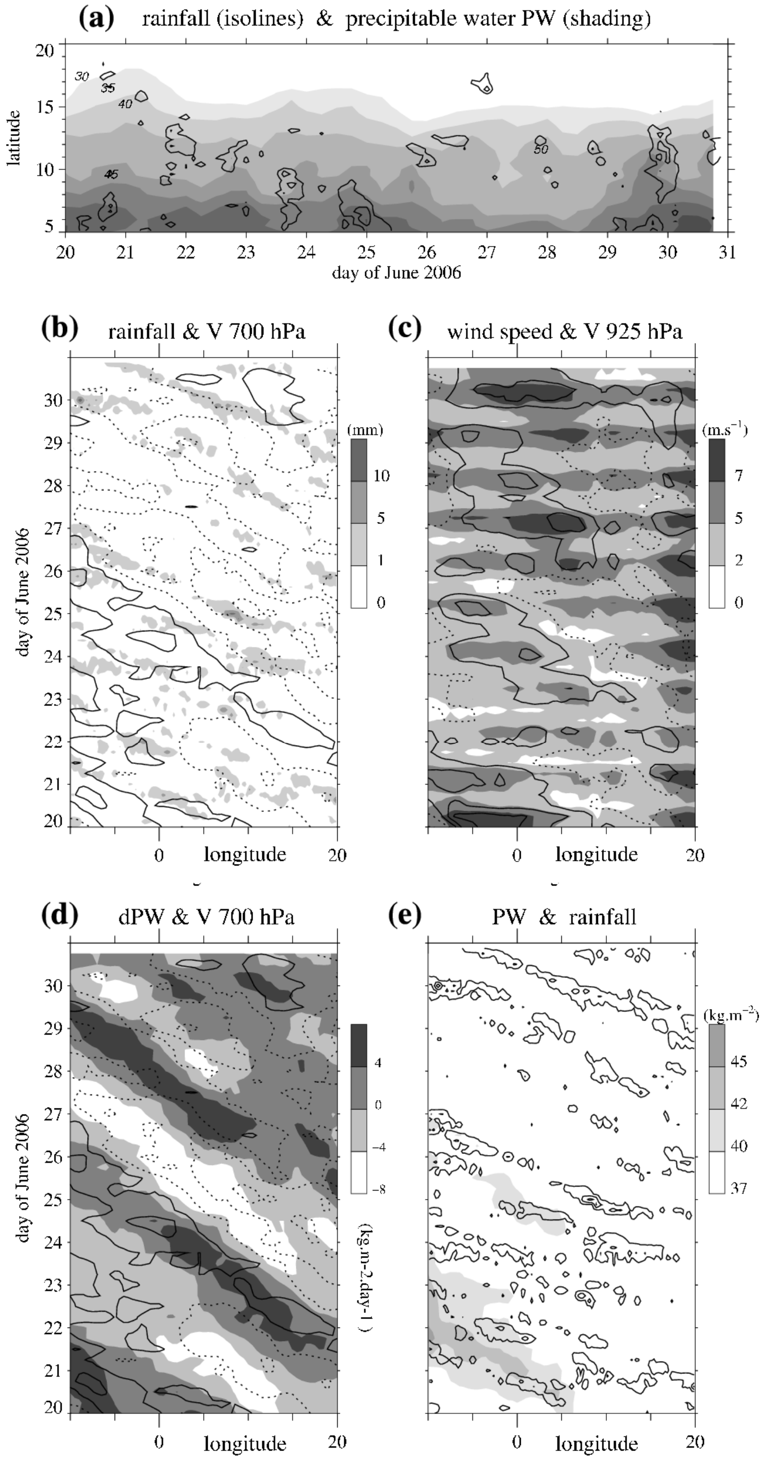

(a) Time-latitude diagram of precipitable water (shaded) and 3-hourly cumulative rainfall (isolines, 2 and 5 mm) averaged over [10°W,10°E] for a 7-day period centered on the 28th of August 2005, and average longitude-time Hovmoeller diagrams of (b) rainfall (shaded) and meridional wind at 700 hPa (interval of 2.5 m.s-1 between isolines), (c) wind speed (shaded) and meridional wind at 925 hPa (interval of 2.5 m.s-1 between isolines, note that the 0 m.s-1 isocountour is dotted), (d) precipitable water tendency (shaded) and meridional wind at 700 hPa and (e) precipitable water and rainfall (isolines). In (b) to (e) an average over [7°N,16°N] is shown. PW and wind fields are from the 6-hourly ECMWF analysis and rainfall corresponds to the 3-hourly TRMM product. In (d), the PW tendency at time t corresponds to PW(t+12h)-PW(t-12h), this allows filtering out diurnal fluctuations of PW which are expected to be unreliable.

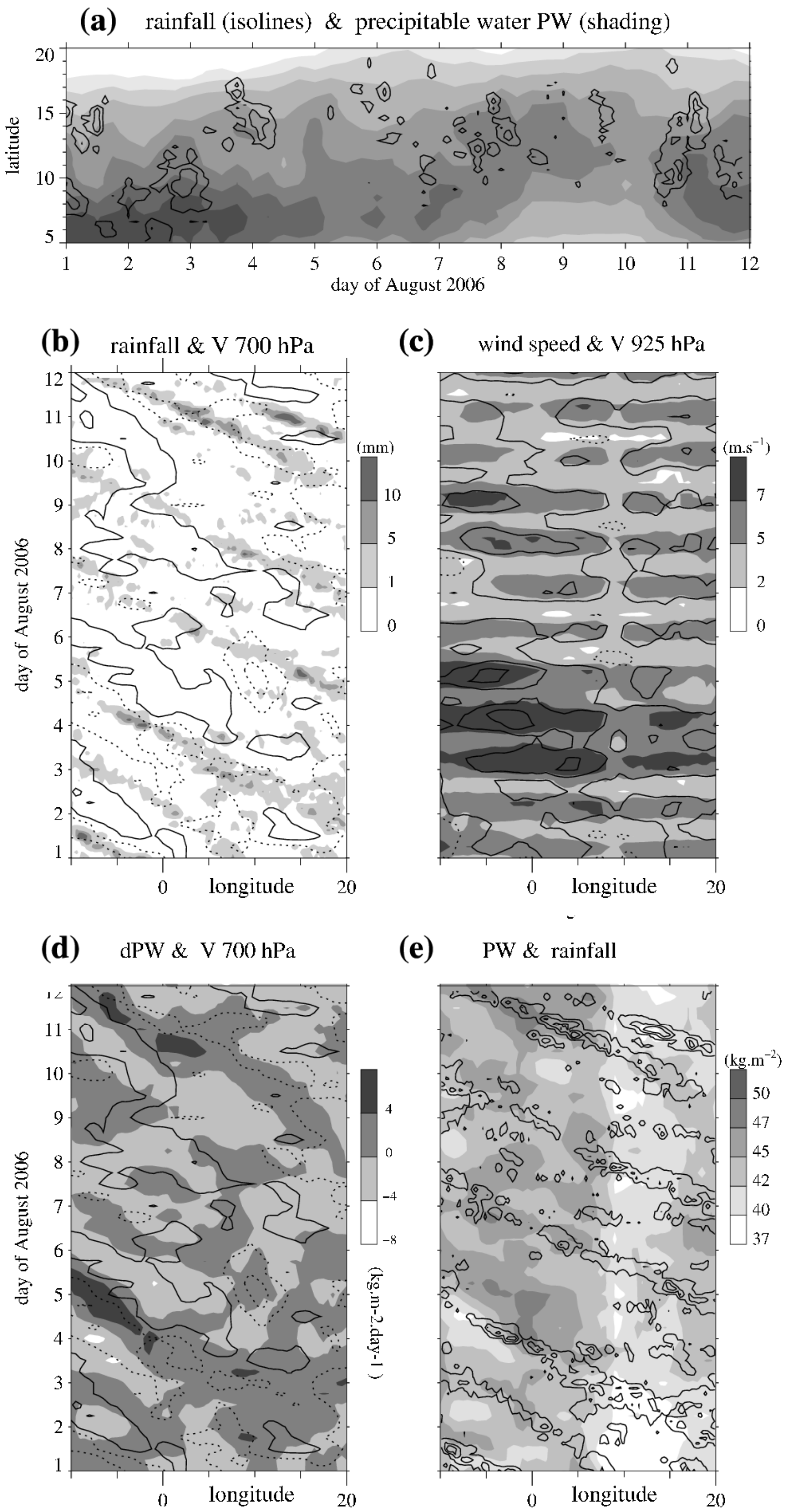

Figure 3: Same as Fig. 2 except for 1-12 August 2006.

APPENDIX C
Results of daily REF simulations - Chapter 4

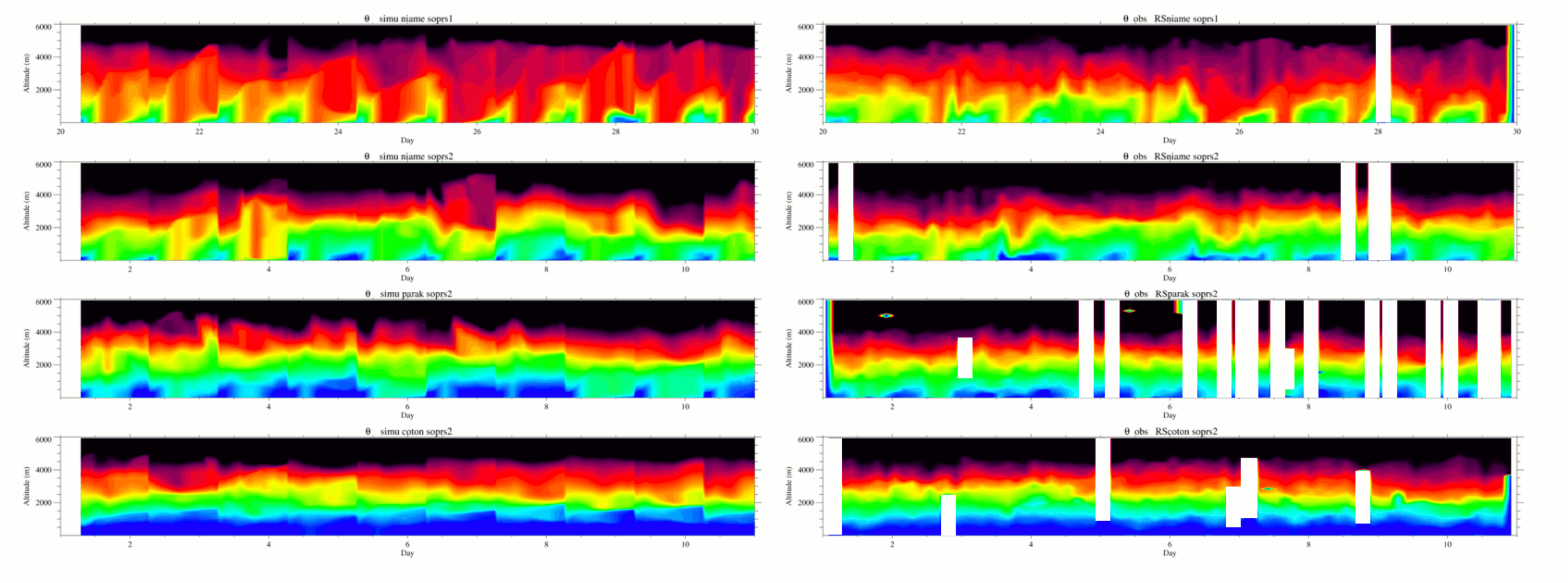

Time series of potential temperature at Niamey-SOP1, Niamey SOP2, Parakou SOP2 and Cotonou SOP2 in the simulations reinitialised every 24hrs(left column) and in the radiosoundings (right column).

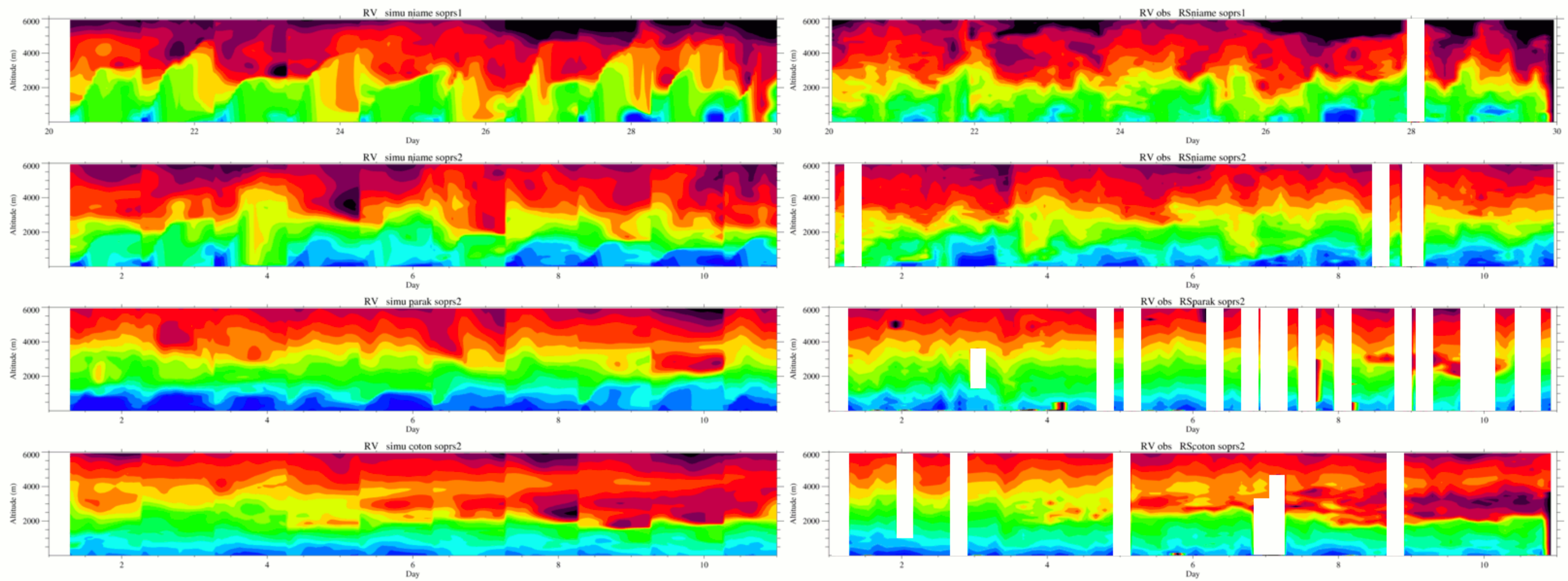

Time series of specific humidity in the REF simulations reinitialised (left column) and in the radiosoundings (right column) at Niamey-SOP1 (top plots), Niamey SOP2 (top middle plots), Parakou SOP2 (bottom middle plots) and Cotonou SOP2 (bottom plots).

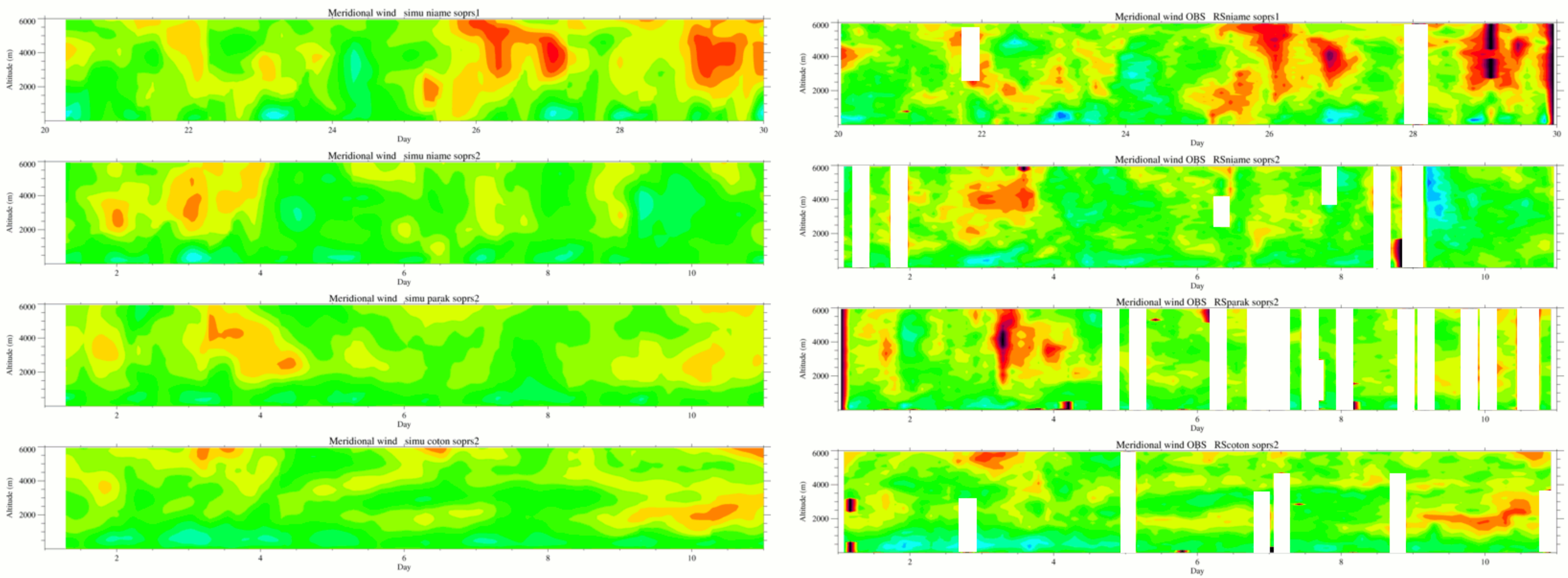

Time series of meridional wind at Niamey-SOP1, Niamey SOP2, Parakou SOP2 and Cotonou SOP2 in the simulations reinitialised every 24hrs(left column) and in the radiosoundings (right column).

Appendix D:

Frequency of Sahelian storm initiation enhanced over mesoscale soil-moisture patterns

Christopher M. Taylor[(1)], Amanda Gounou[(2)], Françoise Guichard[(2)], Phil P. Harris[(1)], Richard J. Ellis[(1)], Fleur Couvreux[(2)] and Martin De Kauwe[(1)]

[(1)] Centre of Ecology and Hydrology, Wallingford, United Kingdom
[(2)] CNRM-GAME, Météo-France and CNRS, Toulouse, France

Nature Geoscience, DOI: 10.1038/NGEO1173

Abstract

Evapotranspiration of soil moisture can affect temperature and humidity in the lower atmosphere, and thereby the development of convective rain storms. Climate models have illustrated the importance of soil-moisture–precipitation feedbacks for weekly rainfall totals in semi-arid regions, such as the Sahel1. However, large variations exist between model feedbacks, and the mechanisms governing the strength and sign of the feedback are uncertain. Here, we use satellite observations of land surface temperatures and convective cloud cover overWestAfrica—collected during thewet seasons between 2006 and 2010—to determine the impact of soil moisture on rainfall in the Sahel. We show that variations in soil moisture on length scales of approximately 10–40 km exert a strong control on storm initiation—as evidenced by the appearance of convective cloud. The probability of convective initiation is doubled over strong soil-moisture gradients compared with that over uniform soil-moisture conditions. We find that 37% of all storm initiations analysed occurred over the steepest 25% of soil-moisture gradients. We conclude that heterogeneities in soil moisture on scales of tens of kilometres have a pronounced impact on rainfall in the Sahel, and suggest that similar processes may be important throughout the semi-arid tropics.

Appendix E:

Observations of Diurnal Cycles Over a West African Meridional Transect: Pre-Monsoon and Full-Monsoon Seasons

Amanda Gounou, Françoise Guichard and Fleur Couvreux

CNRM-GAME, Météo-France and CNRS, Toulouse, France

published in Boundary Layer Meteorology, DOI 10.1007/s10546-012-9723-8

Abstract

We document and characterize the climatology of the diurnal cycles encountered along aWest African transect during the pre-monsoon and full-monsoon periods. The meridional gradient in low-level properties is fundamental for the monsoon dynamics and here, for the first time, it is studied based on a large set of observations from the African Monsoon Multidisciplinary Analysis (AMMA) campaign.

A detailed analysis of surface energy budget, boundary-layer structures and cloud occurrence is carried out to investigate the diurnal cycles of the low levels. A relatively weak meridional gradient of net radiation is observed during the pre-monsoon period, and a large gradient in sensible heat flux is found over the transect with values increasing from south to north. This, as well as the boundary-layer structures, partly explains the large contrasts in the diurnal amplitude of potential temperature and specific humidity along the transect. During the monsoon period, the atmospheric regimes drastically change involving strong interactions between the surface, atmosphere and clouds. The maximum in net radiation is shifted northwards, towards the Sahel, which potentially has a significant impact on the monsoon circulation. The sensible heat flux is considerably reduced and the diurnal amplitude is strongly damped, while the daytime boundary-layer growth decreases significantly in the Sahel related to changes in the balance of boundarylayer processes.

These results highlight the contrasted diurnal cycle regimes encountered over West Africa under dry, moist and wet conditions. They provide observationally-based diagnostics to investigate the ability of models to handle the representation of the diurnal cycle over land.

ETUDE DES PROCESSUS PILOTANT LES CYCLES DIURNES DE LA MOUSSON OUEST-AFRICAINE

Le cycle diurne est un mode de variabilité fondamental de la mousson Ouest-Africaine. Il est notamment observé à l'échelle locale sur l'évolution des propriétés de la couche limites atmosphériques mais aussi à des échelles plus importante sur la circulation de mousson et le développement de la convection profonde. En Afrique de l'ouest, ce mode de variabilité est peu documenté et encore mal représenté par les modèles numériques.

Ainsi, ces travaux de thèse se basent tout d'abord sur l'analyse d'observations collectées pendant la campagne de mesures AMMA pour caractériser les cycles diurnes le long d'un transect méridien allant de la côte Guinéenne jusqu'au Nord du Sahel. On se focalise ici sur les basses couches atmosphériques et les structures verticales pendant les phases d'humidification et de mousson.

Sur la base de cette étude, un cadre de modélisation a été développé pour analyser la représentation des cycles diurnes observés le long du transect méridien. Cette partie a permis de mettre en évidence des biais systématiques du modèle faisant entre autres intervenir les nuages et leur impact radiatif à la surface.

Enfin, les mécanismes de déclenchement diurne de la convection ont été étudiés, plus précisément les couplages à méso-échelle entre l'initiation de convection profonde et les propriétés de surface. Cette étude, basée sur l'analyse combinée de données satellites documentant plus de 2000 initiations d'orages montre l'importance des gradients de propriétés de surface sur le déclenchement des systèmes convectifs au Sahel.

Mots clés : Mousson d'Afrique de l'Ouest, cycle diurne, couche limite atmosphérique, interactions surface-atmosphère, modélisation méso-échelle

AMANDA GOUNOU
CNRM-GAME (CNRS/Météo-France)

FRANCOISE GUICHARD	CNRM-GAME	Directrice
FLEUR COUVREUX	CNRM-GAME	Co-Directrice
SERGE CHAUZY	LA	Président du Jury
CYRILLE FLAMANT	LATMOS	Rapporteur
MIGUEL GAERTNER	Université de Castille	Rapporteur
JON PETCH	MetOffice	Examinateur
CHRISTOPHER TAYLOR	CEH	Examinateur
JEAN-LUC REDELSPERGER	CNRM-GAME	Invité

THE DRIVING PROCESSES BEHIND THE DIURNAL CYCLE OF THE WEST AFRICAN MONSOON

The diurnal cycle is a fundamental mode of variability of the West African monsoon. It is particularly observed locally on the evolution properties of the atmospheric boundary layer but also at larger scales on the monsoon circulation and the development of deep convection. In West Africa, this mode of variability is poorly documented and not well represented by numerical models.

Thus, this thesis is based firstly on the analysis of observations collected during the AMMA measurement campaign to characterize the diurnal cycles along a transect meridian Guinean coast to northern Sahel. The focus here is on the lower atmospheric layers and vertical structures for phases of pre-monsoon and full monsoon periods.

Based on this study, a modeling framework was developed to analyze the representation of diurnal cycles observed along the meridional transect . This work has highlighted systematic biases of the model involving clouds and their radiative impact at the surface.

Finally, the triggering mechanisms of the diurnal convection were studied, specifically mesoscale couplings between initiation of deep convection and surface properties. This study, based on the combined analysis of satellite data documenting over 2000 initiation of storms shows the importance of gradients of surface properties on the onset of convective systems in the Sahel.

Keywords : West African monsoon, diurnal cycle, atmospheric boundary layer, surface-atmosphere interactions, mesoscale modelling

AMANDA GOUNOU
CNRM-GAME (CNRS/Météo-France)

FRANCOISE GUICHARD	CNRM-GAME	Supervisor
FLEUR COUVREUX	CNRM-GAME	Co-Supervisor
SERGE CHAUZY	LA	President of the Jury
CYRILLE FLAMANT	LATMOS	Reviewer
MIGUEL GAERTNER	Université de Castille	Reviewer
JON PETCH	MetOffice	Referee
CHRISTOPHER TAYLOR	CEH	Referee
JEAN-LUC REDELSPERGER	CNRM-GAME	Invited